

UNIVERSITY OF ALBERTA

**THE CHARACTERIZATION OF DIAMONDS AND THEIR MINERAL
INCLUSIONS FROM THE DIAVIK DIAMOND MINE, LAC DE GRAS,
NORTHWEST TERRITORIES, CANADA**

by

Cara Donnelly



A thesis submitted to the Faculty of Graduate Studies and Research in partial
fulfillment of the requirements for the degree of
Master of Science

DEPARTMENT OF EARTH AND ATMOSPHERIC SCIENCES

EDMONTON, ALBERTA

SPRING 2006



Library and
Archives Canada

Bibliothèque et
Archives Canada

Published Heritage
Branch

Direction du
Patrimoine de l'édition

395 Wellington Street
Ottawa ON K1A 0N4
Canada

395, rue Wellington
Ottawa ON K1A 0N4
Canada

Your file *Votre référence*

ISBN: 0-494-13810-6

Our file *Notre référence*

ISBN: 0-494-13810-6

NOTICE:

The author has granted a non-exclusive license allowing Library and Archives Canada to reproduce, publish, archive, preserve, conserve, communicate to the public by telecommunication or on the Internet, loan, distribute and sell theses worldwide, for commercial or non-commercial purposes, in microform, paper, electronic and/or any other formats.

The author retains copyright ownership and moral rights in this thesis. Neither the thesis nor substantial extracts from it may be printed or otherwise reproduced without the author's permission.

AVIS:

L'auteur a accordé une licence non exclusive permettant à la Bibliothèque et Archives Canada de reproduire, publier, archiver, sauvegarder, conserver, transmettre au public par télécommunication ou par l'Internet, prêter, distribuer et vendre des thèses partout dans le monde, à des fins commerciales ou autres, sur support microforme, papier, électronique et/ou autres formats.

L'auteur conserve la propriété du droit d'auteur et des droits moraux qui protègent cette thèse. Ni la thèse ni des extraits substantiels de celle-ci ne doivent être imprimés ou autrement reproduits sans son autorisation.

In compliance with the Canadian Privacy Act some supporting forms may have been removed from this thesis.

Conformément à la loi canadienne sur la protection de la vie privée, quelques formulaires secondaires ont été enlevés de cette thèse.

While these forms may be included in the document page count, their removal does not represent any loss of content from the thesis.

Bien que ces formulaires aient inclus dans la pagination, il n'y aura aucun contenu manquant.


Canada

ABSTRACT

This thesis consists of a study of the diamonds and their mineral inclusions from the A154 South pipe of the Diavik Diamond Mine, Northwest Territories, Canada. This study incorporated the characterization of the diamonds based on morphology, carbon isotopic composition, nitrogen concentration and aggregation state, and the inclusion mineral chemistry. The results are intended to provide additional insight into the characteristics of the diamond source regions beneath the central Slave craton.

Results show that diamond formation at Diavik occurred in a moderately-depleted, dominantly peridotitic mantle, under lithospheric conditions. Trace element studies have revealed a history of depletion and subsequent re-enrichment of the peridotitic diamond source regions. The obtained narrow distribution of the carbon isotopes may indicate that diamond formation resulted from an unfractionated fluid/melt carrying primordial carbon. The low aggregation states obtained for the diamonds further suggest mantle residence at fairly low temperatures.

ACKNOWLEDGEMENTS

First and foremost I would like to thank my supervisor, Thomas Stachel, not only for providing me with the opportunity to work on such a fantastic project but also for introducing me to the field of diamond geology.

I am very grateful to Sean Whiteford and Diavik Diamond Mines for allowing me to work on their exquisite samples and for providing funding for this project.

I would also like to thank my examining committee Thomas Stachel, Larry Heaman and Martyn Unsworth who took the time to read the thesis, sit through the exam and for their valuable comments which greatly improved the thesis.

For allowing me access to his laboratory facilities and for his enthusiasm, support and encouragement, I would like to thank Karlis Muehlenbachs. I am also grateful to Nobu Shimizu for his help with the ionprobe at Woods Hole and to Sergei Matveev for all of his instruction and assistance during microprobe analysis at the University of Alberta.

I would also thank Steve Creighton, Ralf Tappert, Anetta Banas and Dana Verigeanu of the Diamond Research Group, and pseudo-DRG members Shannon Zurevinski and Andrew Fagan for their helpful suggestions and insightful discussions.

TABLE OF CONTENTS

Chapter 1: Introduction

1.1. Introduction.....	1
1.2. Petrological and Geochemical Background.....	2
1.2.1. Inclusion Petrology.....	2
1.2.1.1. Lithospheric Diamonds.....	2
1.2.1.2. Asthenosphere and Transition Zone Diamonds.....	3
1.2.1.3. Lower Mantle Diamonds.....	4
1.2.2. Diamond Geochemistry.....	4
1.3. Thesis Intent.....	7
References.....	8
Figures.....	12

Chapter 2: Geologic Background

2.1. The Archean Slave Province.....	14
2.1.1. Introduction.....	14
2.1.2. Generalized Geology of the Slave Province.....	14
2.1.3. Plutonism and Deformation.....	16
2.1.4. Proterozoic Diabase Dykes.....	17
2.1.5. Formation Models for the Slave Province.....	18
2.2. The Lithospheric Mantle Beneath the Slave Craton.....	19
2.2.1. Overview.....	19
2.2.2. The Lithospheric Domains of the Slave.....	20
2.2.2.1. The Northern Slave.....	20
2.2.2.2. The Central Slave and Lac de Gras Area.....	21
2.2.2.3. The Southern Slave.....	22
2.3. Kimberlites of the Slave Craton.....	23
2.4. The Lac De Gras Area.....	25
2.4.1. The Lac Des Gras Kimberlite Field.....	25
2.4.2. Diavik Exploration History.....	26
References.....	27
Figures.....	33

Chapter 3: Diamonds and their Mineral Inclusions from the Diavik Diamond Mine, Northwest Territories, Canada

3.1. Introduction.....	39
3.2. Analytical Methods.....	40
3.3. Database.....	43
3.4. Major Element Compositions.....	43
3.4.1. Peridotitic Paragenesis.....	43
3.4.1.1. Garnet.....	43

3.4.1.2. Olivine.....	44
3.4.1.3. Clinopyroxene.....	44
3.4.1.4. Mg-chromite.....	45
3.4.1.5. Fe-Ni Sulphides.....	45
3.4.2. Eclogitic Paragenesis	45
3.4.2.1. Garnet.....	46
3.4.2.2. Clinopyroxene.....	46
3.4.2.3. SiO ₂	46
3.4.2.4. Fe Sulphides.....	47
3.4.3. Uncertain Paragenesis	47
3.4.3.1. Diamond.....	47
3.4.3.2. Ferropericlase.....	47
3.5. Trace Element Compositions	48
3.6. Geothermobarometry	49
3.7. Physical and Geochemical Characteristics of the Host Diamonds	50
3.7.1. Morphology and Colour.....	50
3.7.2. Carbon Isotopes.....	51
3.7.3. Nitrogen Contents and Aggregation Levels.....	52
3.8. Discussions and Conclusions	53
3.8.1. The Diamond Source Region at A154 South.....	53
3.8.2. Ferropericlase-bearing Diamonds: An Uncertain Paragenesis	56
3.8.3. Models for Diamond Sources in the Slave.....	58
References	60
Tables	67
Figures.....	73

Chapter 4: Discussion and Conclusions

4.1. Introduction.....	88
4.2. The Diamonds from A154 South	88
4.3. Diamond sources beneath the Diavik Mine and the central Slave.....	90
References	93

Appendix A: Analytical Methods

A.1. Diamond Cleaning.....	96
A.2. Diamond Crushing and Polishing	97
A.3. Electron-Probe Microanalysis (EMPA)	97
A.3.1. Introduction	97
A.3.2. Instrumentation.....	98
A.3.3. Sample Preparation	99
A.3.4. Analytical Settings	99
A.4. Secondary Ion Mass Spectrometry (SIMS).....	100
A.4.1. Introduction	100
A.4.2. Sample Preparation	100
A.4.3. Analytical Settings	101

A.5. Carbon Stable Isotope Analysis	101
A.5.1. Sample Preparation	101
A.5.2. Sample Analysis.....	102
A.6. Fourier Transform Infrared (FTIR) Spectrometry	102
A.6.1. Introduction	103
A.6.2. Sample Preparation	103
A.6.3. Analytical Settings	103
References	105

Appendix B: Diamond Photographs

B.1. Morphology	115
B.2. Colour.....	122
B.3. Surface Features	126
B.4. Inclusion Content	138

Appendix C: Supplementary Data

C.1. Microprobe Data.....	148
C.2. Ion Probe Data.....	171
C.3. Diamond Characteristics	173
C.4. Carbon Isotope Data.....	176
C.5. Nitrogen Data	177
C.6. Inventory	182

LIST OF TABLES

Table 3-1: Summary of the physical and geochemical characteristics of the A154 South diamonds and their mineral inclusions	67
Table 3-2: Major and trace element compositions of selected inclusions from A154 South diamonds.....	70
Table 3-3: Major element composition (EMPA-analyses, wt%) of selected sulphide inclusions	71
Table 3-4: Major element compositions (EPMA-analyses, wt%) of ferropericlase inclusions of uncertain paragenetic association	72

LIST OF FIGURES

Figure 1-1: Map showing the locations of cratons worldwide and their associated diamond deposits.....	12
Figure 1-2: Histogram showing the distribution of the carbon isotopic data for diamonds worldwide.....	13
Figure 2-1: Map showing the generalized geology of the Slave craton.....	33
Figure 2-2: Map illustrating the boundaries of the Anton Terrane, the Sleepy Dragon Terrane (SDT), the Contwoyto Terrane and the Hackett River Arc Terrane.....	34
Figure 2-3: Subdivisions of the lithospheric domains of the Slave, based on differing compositions, mantle stratigraphy and thermal state.....	35
Figure 2-4: Mantle cross-section of the Slave Craton.....	36
Figure 2-5: The distribution of kimberlites and subdivisions based on kimberlite emplacement ages of the Slave craton	37
Figure 2-6: Map of the central and southern Slave domains showing the location of diamond exploration projects.....	38
Figure 3-1: Map of the Slave craton and the central Slave craton	73
Figure 3-2: CaO vs Cr ₂ O ₃ (wt %) for garnet inclusions from A154 South diamonds, other Slave localities and worldwide sources	74
Figure 3-3: CaO (wt%) versus molar Mg number for A154 South olivine inclusions, compared to olivines from the Slave craton and worldwide sources.....	75
Figure 3-4: NiO (wt%) versus molar Mg number for A154 South olivine inclusions	76
Figure 3-5: Cation ratios (based on 6 oxygens) for clinopyroxenes from A154 South, the Slave craton and worldwide sources	77
Figure 3-6: Cr number versus FeO _{total} for magnesio-chromite inclusions from A154 South, Panda, Snap Lake and worldwide sources.....	78
Figure 3-7: Composition diagram showing seven eclogitic Fe-monosulphide inclusions and eight peridotitic Fe-Ni sulphides from A154 South diamonds	79
Figure 3-8: Photograph of diamond ddmi-200, a colourless triangular macle containing a colourless, octahedral diamond inclusion.....	80

Figure 3-9: NiO (wt%) versus Mg# for ferropericlasite inclusions from A154 South, the Slave craton, and worldwide localities.....	81
Figure 3-10: Rare earth element (REE _N) concentrations of peridotitic garnet inclusions from A154 South	82
Figure 3-11: Rare earth element (REE _N) concentrations of eclogitic garnet inclusions from A154 South and the worldwide average	83
Figure 3-12: Histogram showing the calculated equilibration temperatures (at assumed pressures of 5 GPa for coexisting garnet and olivine inclusions from A154 South, the Slave craton and worldwide sources.....	84
Figure 3-13: Histograms showing the carbon isotopic composition ($\delta^{13}\text{C}_{\text{PDB}}$) of diamonds from worldwide sources (Figure 3.13a) and from A154 South (Figure 3.13b)	85
Figure 3-14: Aggregation level (percentage of aggregation into the B-centre) versus the log of the total nitrogen concentration (atomic ppm).....	86
Figure 3-15: Illustration of the metasomatic re-enrichment event affecting harzburgitic garnets ddmi-216a and ddmi-216c from A154 South	87

LIST OF ABBREVIATIONS

‰	per mille
BSE	Backscatter Electrons
CSBS	Central Slave Basement Complex
DDMI	Diavik Diamond Mines Inc.
EDS	Energy Dispersive Spectrometer
fO_2	Oxygen fugacity
FTIRS	Fourier Transform Infrared Spectrometry
HREE	Heavy Rare Earth Elements
HREE _N	Heavy Rare Earth Elements normalized to C1 chondrite
IR	Infrared
LREE	Light Rare Earth Elements
LREE _N	Light Rare Earth Elements normalized to C1 chondrite
MORB	Mid Ocean Ridge Basalt
MREE	Middle Rare Earth Elements
MREE _N	Middle Rare Earth Elements normalized to C1 chondrite
PBD	Pee-Dee belemnite
PGE	Platinum Group Elements
ppm	parts per million
PSF	Product Splitting Facility
REE	Rare Earth Elements
REE _N	Rare Earth Elements normalized to C1 chondrite
SIMS	Secondary Ion Mass Spectrometry
SDT	Sleepy Dragon Terrane
TAPP	Tetragonal almandine pyrope phase
TTG	Tonalite-trondhjemite-granodiorite
VMS	Volcanogenic massive sulphide
WDS	Wavelength dispersive X-ray spectrometers
wt %	weight percent

In Tables:

A	aggregate
D	dodecahedroid
I	irregular
O	octahedra
TM	triangular macel
-	touching inclusion pair
,	non-touching inclusion pair
alt	altered inclusion

chr	chromite
coe	coesite
cpx	clinopyroxene
dia	diamond
E	eclogitic
exp	exposed 'inclusion'
fper	ferropericlaste
gnt	garnet
H	harzburgitic
L	lherzolitic
ol	olivine
P	peridotitic
s	sulphide

Chapter 1: Introduction

1.1. Introduction

Diamonds have typically been sought as gemstones, or for their physical properties (i.e. hardness, heat conductivity and capacity) utilized for industrial purposes. Beyond these conventional uses, diamonds represent pristine samples of the Earth's mantle. An abundance of information can be obtained from in depth studies of diamonds. They provide information regarding diamond formation processes, regional, chemical and thermal conditions of the diamond source region and they aid in our understanding of the composition and evolution of the subcratonic lithospheric mantle. However, limited information regarding these conditions can be gained from the direct study of diamonds themselves owing to the fact that diamonds are composed of essentially pure carbon with minimal impurities. Fortunately, some diamonds contain inclusions of mantle minerals that can be used to ascertain additional information regarding the origin of the diamond. These inclusions are isolated within the diamond matrix and are unable to interact with the inert diamond, or its host rock. The diamond serves to protect the inclusion from re-equilibration and metasomatic influences. The inclusions, therefore, represent chemically unaltered samples, and may be used to obtain considerable information regarding the composition and evolution of the mantle.

Diamonds are typically associated with kimberlite or lamproite diatremes, dikes and sills and the distribution of these intrusions are, for the most part, confined to old, stable cratonic areas (Figure 1.1). It is important to note that there is no genetic link between the diamond and the host rock. The kimberlite or lamproite is simply the transport mechanism of the diamond to the surface of the Earth. Compilations of the eruption ages of the host rocks have shown that diamond has intermittently been transported to the surface throughout extended periods of geologic time (Meyer, 1987). It can be reasonably inferred that both young and old diamonds must exist in the mantle. The most convincing evidence for the antiquity, of at least some diamonds, is the presence of diamonds in volcanics that erupted 2.7 Ga ago (i.e.

Wawa, Ontario; Stott et al., 2002). Furthermore, since diamonds are xenocrysts in the kimberlite, some diamonds must have remained behind in the mantle, available for later sampling. The most commanding evidence for the young age of some other diamonds is illustrated by the occurrence of Type Ib diamonds, with single nitrogen centres, and the young ages obtained for inclusions in such diamonds. For example, a Type Ib diamond from Koffiefontein, South Africa was found to have a Re-Os age of 68 ± 30 Ma, which is within error of the pipe emplacement age of 90 Ma (Pearson et al., 1998). Peridotitic diamonds, for the most part, appear to have older ages (>2 Ga), while eclogitic diamonds span a broader range from young ages, within the error of pipe emplacement ages, up to approximately 2.4 Ga (Pearson and Shirey, 1999).

1.2. Petrological and Geochemical Background

1.2.1. Inclusion Petrology

Mineral inclusions within diamond are not uncommon. There are approximately twenty minerals that have been identified as proto- or syngenetic inclusions, with an additional ten or so other minerals occurring as epigenetic (i.e. secondary or altered) inclusions (Meyer, 1987). If inclusions are syngenetic, they can be analyzed for their major, minor and trace element compositions to provide information regarding the chemical and mineralogical characteristics of source region at the time of diamond genesis. Assuming diamond formation is rapid, when certain pairs of non-touching (chemically isolated) inclusions occur within a stone, calculations can be made regarding the pressure and temperature conditions during diamond formation (Harris, 1992). Polyminerallic inclusions of touching minerals, also exist in diamond and they may have re-equilibrated to changing pressure and temperature conditions (Harris, 1992).

Three major diamond source regions have been identified in the mantle: (1) the lithospheric upper mantle, (2) the asthenosphere and transition zone, and (3) the lower mantle (Harris, 1992).

1.2.1.1. Lithospheric Diamonds

Diamond inclusion studies have shown that most diamonds form within the

lithospheric mantle beneath Archean cratons at depths of 150 to 200 km (Boyd and Gurney, 1986; Meyer, 1987), up to a maximum depth of approximately 250 km (Stachel et al., 1997). These diamonds have been classified into two suites, peridotitic and eclogitic, on the basis of the mineralogy and chemistry of their mineral inclusions (Meyer and Boyd, 1972; Meyer, 1987; Gurney, 1989). A third paragenesis, the websteritic suite, has been suggested as an intermediate between the peridotitic and eclogitic suites and is comprised of orthopyroxene, clinopyroxene and garnet (Gurney et al., 1984). Inclusion studies have shown that the majority of diamonds are sourced from peridotite, which is the most common rock in the Earth's upper mantle. Eclogitic source material appears to be more heterogeneously distributed in the mantle and is chemically similar to basaltic compositions (Kirkley, 1991).

The inclusion minerals of the peridotitic suite include olivine, Cr-rich garnet, orthopyroxene, Mg-chromite, and Cr-rich clinopyroxene. The peridotitic suite can be further subdivided into the lherzolitic and harzburgitic parageneses, based in the presence of Cr-diopside in lherzolitic mineralogies (Meyer, 1987). The eclogitic suite contains inclusions of Cr-poor grossular-almandine-pyrope garnet, omphacitic clinopyroxene (Na-rich) and rare kyanite, rutile, sanidine and/or coesite (Meyer, 1987). Sulphides are common inclusions in diamond and are not restricted in terms of paragenesis, however, they may be distinguished based of their Ni content, which is significantly higher for peridotitic sulphides (Yefimova et al., 1983).

1.2.1.2. Asthenosphere and Transition Zone Diamonds

Sublithospheric diamond formation in the asthenosphere (upper mantle) and transition zone has been recognized based on the presence of majoritic garnet inclusions in diamond. Experimental studies have found that the dissolution of pyroxene into the garnet structure, forming the majoritic garnet end-member, begins at depths greater than 250 km (Ringwood, 1967; Akaogi and Akimoto, 1977; Irifune, 1987), reaching completion at about 450 km depth (Irifune, 1987) for a pyrolitic bulk composition. At depths exceeding 550 to 600 km, majoritic garnet will begin to exsolve CaSi-perovskite (Irifune and Ringwood, 1987b; Wood, 2000). Stachel

(2001) has noted that nearly all majoritic diamond inclusions are eclogitic and have basaltic source chemistry. Different models have been proposed to explain the eclogitic source rock of majoritic garnets at depth, and include (1) formation in subducting oceanic slabs (Ringwood 1991; Stachel et al., 2000a; Stachel 2001; Tappert et al., 2005), (2) in plumes ascending from the core-mantle boundary (Hoffman and White, 1982) or the lower mantle (Griffin, 1999a), (3) precipitation from alkaline melts at depth (Moore et al., 1991), and (4) formation from 200 km thick eclogite layer in the Earth's upper mantle (Gasparik, 2002). Stachel (2001) used MORB-like trace element signatures and occasionally observed negative Eu anomalies (Kankan; Stachel et al., 2000a, Jagersfontein; Tappert et al., 2005) in majoritic garnets as evidence for a subduction related formation.

1.2.1.3. Lower Mantle Diamonds

A second group of sublithospheric diamonds exists, being sourced from the lower mantle at depths exceeding 660 km (Ringwood, 1982; Harris, 1992). Recognition of ferropericlase inclusions in diamonds led to the suggestion that diamonds may form at great depths in the lower mantle (Scott-Smith et al., 1984). However, the occurrence of ferropericlase is not sufficient evidence to indicate a lower mantle origin (Stachel et al., 2000b; Brey et al., 2004). The ferropericlase stability field also extends into the upper mantle where it could form if Si activity and f_{O_2} is low (Stachel et al., 2000b). Later studies have identified inclusions of ferropericlase coexisting with inclusions of tetragonal almandine pyrope phase (TAPP), MgSi-perovskite, CaSi-perovskite and SiO_2 which indicates a lower mantle origin (Stachel et al., 2000b and references therein). Ringwood (1991) and Stachel et al. (2000b) again employ a subduction related formation for lower mantle diamonds to explain extreme enrichment in LREE (200 to 2000 times chondritic) and Sr (70 to 1000 times chondritic) and positive and negative Eu anomalies in $CaSiO_3$.

1.2.2. Diamond Geochemistry

The host diamond can be analyzed to ascertain its carbon isotope composition and nitrogen concentration and aggregation. The worldwide distribution of carbon isotope values ($\delta^{13}C_{PDB}$) covers a broad range from -34.4 to + 2.7‰ (Kirkley et al.,

1991). There are marked differences, as shown in Figure 1.2, in the $\delta^{13}\text{C}$ values between the peridotitic and eclogitic parageneses. Generally, most peridotitic diamonds have a restricted range of $\delta^{13}\text{C}$ values, ranging between -10 to -1‰ with a mean of -5‰ (Kirkley et al., 1991). This range also correlates to the peak in the $\delta^{13}\text{C}$ distribution of diamonds worldwide, which is not surprising as the majority of diamonds belong to the peridotitic suite. It is the diamonds of the eclogitic paragenesis that are responsible for the broad range in $\delta^{13}\text{C}$ values observed. Eclogitic diamonds have a similar mode at -5‰ but they cover the entire range of $\delta^{13}\text{C}$ values and are skewed significantly towards the isotopically lighter values. As pointed out by Kirkley et al. (1991), there is no single deposit that has been found to contain the entire range of $\delta^{13}\text{C}$ values, and the $\delta^{13}\text{C}$ distribution has been found to be unique for each individual locality.

Whereas the relatively limited ranges in $\delta^{13}\text{C}$ values of the peridotitic suite, which represent normal mantle values, have been interpreted as indicating a primordial source of carbon, debate exists regarding the explanation of the variance observed in the eclogitic values. The typical composition of organic matter ($\delta^{13}\text{C}$ of approximately -35 to -20‰) and marine carbonates ($\delta^{13}\text{C}$ of approximately -2 to +2‰) fall within the range of the $\delta^{13}\text{C}$ values of the eclogitic paragenesis (Kirkley et al., 1991). This has resulted in models that postulate that the genesis of eclogitic diamonds is related to the subduction of oceanic crust that contains organic matter and marine carbonates. The models imply that the oceanic crust would recrystallize to eclogite upon subduction and the formation of eclogitic diamonds would occur from the conversion of the carbonaceous material from the subducting slab (Kirkley et al., 1991). However, nitrogen isotope data has been shown to be inconsistent with a model of diamond formation from subducted biogenic carbon, based on a study of combined $\delta^{13}\text{C}$ - $\delta^{15}\text{N}$ variations in eclogitic diamonds by Cartigny et al. (1998a). Alternate models have attributed the variations seen in the $\delta^{13}\text{C}$ values to isotopic fractionation within the mantle. Cartigny et al. (1998a) suggested that carbonatitic fluids/melts percolating through eclogite may release CO_2 and that this degassing causes isotopic fractionation that is sufficiently strong to explain the observed range in $\delta^{13}\text{C}$.

Nitrogen is the most common substitutional impurity in diamond and is typically present in concentrations ranging from <10 ppm to 2500 ppm (Bibby, 1992), but may, in some instances, exceed 0.5 wt% (Sellechopp et al., 1980). The presence or absence of nitrogen in diamond has been shown to have effects on diamond colour (Harris, 1987). The kinetics of the nitrogen aggregation may also be used to determine the residence time or the residence temperature of the diamond in the Earth's mantle.

Nitrogen is present in most diamonds, but the aggregation of the nitrogen has been found to vary. The nitrogen content has been used to classify diamonds into two groups: Type I diamonds where nitrogen is present and Type II diamonds where nitrogen is absent, or below the level of detection (approximately 10 ppm) for infrared spectroscopy (Gurney, 1989). These classifications can be further subdivided on the basis of the nitrogen aggregation state of the diamond into: Type *Ib* where diamonds contain nitrogen in a single substitution and Type *Ia*, where aggregated nitrogen is in the form of pairs (Type *IaA*), rings of four nitrogens surrounding a vacancy (Type *IaB*) or both (Type *IaAB*) (Evans and Qi, 1982).

Nitrogen occurs in most natural diamonds. When nitrogen is initially incorporated into the diamond lattice, it occurs as dispersed, single substitutional atoms (Type *Ib*) (Evans and Qi, 1982). However, only in rare cases is nitrogen observed as a single substitutional atom. In most occurrences, the nitrogen forms aggregates of two or more nitrogen atoms. This is attributed to the formation of more complex types of nitrogen aggregation due to the slow migration of the single nitrogen atoms during the long residence time of the diamond, at elevated temperatures, in the Earth's mantle (Evans, 1992).

Due to the fact that the aggregation characteristics of a diamond are temperature controlled, the thermal history of the diamonds studied can be constrained. Under normal geothermal gradients, after 200 to 2000 Ma in the mantle a diamond will be a Type *IaB* diamond, with all of its nitrogen in the B-centre (Gurney, 1989). A diamond may retain nitrogen in the non-aggregated, single substitution state (Type *Ib*) only if the residence time in the mantle, at temperatures of

1000 - 1400°C, after crystallization but prior to kimberlitic eruption, was less than 50 years (Gurney, 1989).

1.3. Thesis Intent

This study of the diamonds from the Diavik Diamond Mine will provide additional information regarding the thermal and chemical evolution of the lithospheric mantle beneath the central Slave Craton. This information would predate, by billions of years, the kimberlite emplacement events and the time-slices represented by the xenoliths and xenocrysts. Most importantly, the study will also clarify what the principal diamond source rock in the Earth's mantle is in the case of the Diavik Mine. So far the question if the A154 South diatreme contains a predominantly peridotitic or eclogitic diamond population has not been addressed.

One hundred inclusion-bearing diamonds from the A154 South pipe were examined and classified based on diamond morphology, carbon isotopic composition, nitrogen concentration and aggregation state, and inclusion mineral chemistry. These results are intended to provide further insight into the characteristics of the diamond source region in the central Slave craton.

References:

- Akaogi, M., and Akimoto, S. 1977. Pyroxene-garnet solid-solution equilibria in the systems $Mg_4Si_4O_{12}$ - $Mg_3Al_2Si_3O_{12}$ and $Fe_4Si_4O_{12}$ - $Fe_3Al_2Si_3O_{12}$ at high pressures and temperatures. *Physics of the Earth and Planetary Interiors*, 15, 90-106.
- Bibby, D.M. 1982. Impurities in natural diamond. *Chemistry and Physics of Carbon*, 18, 3-91. As cited in Gurney (1989).
- Boyd, F.R., and Gurney, J.J. 1986. Diamonds and the African lithosphere. *Science*, 232, 472-477.
- Cartigny, P., Harris, J.W., Phillips, D., Girard, M., and Javoy, M. (1998a) Subduction-related diamonds? The evidence for a mantle derived origin from coupled $\delta^{13}C$ - $\delta^{15}N$ determinations. *Chemical Geology*, 147, 147-159.
- Davies, R.M., Griffin, W.L., O'Reilly, S.Y., and Doyle, B.J. 2004. Mineral inclusions and geochemical characteristics of microdiamonds from the D027, A154, A21, A418, D018, DD17 and Ranch Lake kimberlites at Lac de Gras, Slave Craton, Canada. *Lithos*, 77, 39-55.
- Evans, T., and Qi, Z. 1982. The kinetics of nitrogen in diamond. In: *Proceedings of the Royal Society of London, Series A, Mathematical and Physical Sciences*, A381, 159-178.
- Gasparik, T. 2002. Experimental investigation of the origin of majoritic garnet inclusions in diamonds. *Physics and Chemistry of Minerals*, 29, 170-180.
- Gurney, J.J. 1989. Diamonds. In: *Kimberlites and related rocks, Proceedings of the IVth International Kimberlite Conference*, Ross, J., Jaques A.L., Ferguson, J., Green, D.H., O'Reilly, S.Y., Danchin, R.V., and Janse, A.J.A. (eds), Geological Society of Australia, Sydney, 935-965.
- Gurney, J.J., Harris, J.W., and Rickard, R.S. 1984. Minerals associated with diamonds from the Roberts Victor Mine. In: *Kimberlites II: the mantle and crust-mantle relationships*, Kornprobst, J. (ed), Elsevier, Amsterdam, 25- 32.
- Harris, J.W. 1992. Diamond Geology. In: *The properties of natural and synthetic diamond*, Field, A.C. (ed), Academic Press, London, 345-393.
- Harris, J.W. 1987. Recent physical, chemical and isotopic research of diamond. In: *Mantle Xenoliths*, Nixon, P.H. (ed), John Wiley & Sons, Chichester, 478-500.

- Heaman, L.M., Kjarsgaard, B.A., and Creaser, R.A. 2003. The timing of kimberlite magmatism in North America: implications for global kimberlite genesis and diamond exploration. *Lithos*, 71, 153-184.
- Hoffman, A.W., and White, W.M. 1982. Mantle plumes from ancient oceanic crust. *Earth and Planetary Science Letters*, 57, 421-436.
- Irifune, T. 1987. An experimental investigation of the pyroxene-garnet transformation in a pyrolite composition and its bearing on the constitution of the mantle. *Physics of the Earth and Planetary Interiors*, 45, 324-336.
- Irifune, T., and Ringwood, A.E. 1987b. Phase transformations in a harzburgite composition to 26 GPa: implications for dynamical behavior of subducting slab. *Earth and Planetary Science Letters*, 86, 365-376.
- Kirkley, M.B., Gurney, J.J., Otter, M.L., Hill, S.J., and Daniels, L.R. 1991. The application of C isotope measurements to the identification of the source of C in diamonds: a review. *Applied Geochemistry*, 6, 477-494.
- Meyer, H.O.A. and Boyd, F.R. 1972. Composition and origin of crystalline inclusions in natural diamonds. *Geochimica et Cosmochimica Acta*, 36, 1255-1273.
- Meyer, H.O.A. 1987. Inclusions in diamond. In: *Mantle xenoliths*, Nixon, P.H. (ed), John Wiley and Sons, Chichester, 501-522.
- Moore, R.O., Gurney, J.J., Griffin, W.L., and Shimizu, N. 1991. Ultra-high pressure garnet inclusions from Monastery diamonds – trace element abundance patterns and conditions of origin. *European Journal of Mineralogy*, 3, 213-230.
- Pearson D. G., Shirey S. B., Harris J. W., and Carlson R. W. 1998. Sulphide inclusions in diamonds from the Koffiefontein kimberlite, S. Africa: Constraints on diamond ages and mantle Re-Os systematics. *Earth and Planetary Science Letters*, 160, 311–326.
- Pearson, D.G., and Shirey, S.B. 1999. Isotopic dating of diamonds. In: *Application of Radiogenic Isotopes to Ore Deposit Research and Exploration. Reviews in Economic Geology*, vol.12. Society of Economic Geologists, Denver, 143-172.
- Ringwood, A.E. 1967. The pyroxene garnet transformation in the earth's mantle. *Earth and Planetary Science Letters*, 2, 255-263.
- Ringwood, A.E. 1982. Phase-Transformations and differentiation in subducted lithosphere-implications for mantle dynamics, basalt petrogenesis, and crustal evolution. *Journal of Geology*, 90, 611-643.

- Ringwood, A.E., 1991. Phase transformations and their bearing on the constitution and dynamics of the mantle. *Geochimica et Cosmochimica Acta*, 55, 2083–2110.
- Scott-Smith, B.H., Danchin, R.V., Harris, J.W., and Stracke, K.J. 1984. Kimberlites near Orroroo, South Australia. In: *Kimberlites I: kimberlites and related rocks*, Kornprobst, J., (ed), Elsevier, Amsterdam, 121-142.
- Sellschopp, J.P.F., Madiba, C.C.P., and Annegarn, H.J. 1980. Light volatiles in diamonds: physical interpretation and genetic significance. *Nuclear Instruments and Methods*, 168, 529-534. As cited in Harris (1987) and Gurney (1989).
- Stachel, T. 2001. Diamonds from the asthenosphere and transition zone. *European Journal of Mineralogy*, 13, 883-892.
- Stachel, T., and Harris, J.W. 1997. Syngenetic inclusions in diamond from the Birim field (Ghana) - A deep peridotitic profile with a history of depletion and re-enrichment. *Contributions to Mineralogy and Petrology*, 127, 336-352.
- Stachel, T., Brey, G.P., and Harris, J.W. 2000a. Kankan diamonds (Guinea) I: from the lithosphere down to the transition zone. *Contributions to Mineralogy and Petrology*, 140, 1-15.
- Stachel, T., Harris, J.W., Brey, G.P., and Joswig, W. 2000b. Kankan diamonds (Guinea) II: lower mantle inclusion parageneses. *Contributions to Mineralogy and Petrology*, 140, 16-27.
- Stott, G.M., Ayer, J.A., Wilson, A.C., and Grabowski, G.P.B. 2002. Are the Neoproterozoic diamond-bearing breccias in the Wawa area related to late-orogenic alkalic and “sanukitoid” intrusions?. Ontario Geological Survey. Open File Report 6100, 9-1 to 9-10.
- Tappert, R., Stachel, T., Harris, J.W., Shimizu, N., and Brey, G.P. 2004. Mineral inclusions in diamonds from the Panda kimberlite, Slave Province, Canada. *European Journal of Mineralogy*, 17, 423-440.
- Tappert, R., Stachel, T., Harris, J.W., Muehlenbachs, K., Ludwig, T., and Brey, G.P. 2005. Subducting the crust: the source of deep diamonds. *Geology*, 33, 565-568.
- Wood, B.J. 2000. Phase transformations and partitioning relations in peridotite under lower mantle conditions. *Earth and Planetary Science Letters*, 174, 341– 354.

Yefimova, E.S., Sobolev, N.V., and Pospelova, L.N. 1983. Sulphide inclusions in diamonds and specific features of their paragenesis. *Zapiski Vsesoyuznogo Mineralogicheskogo Obshchestva*, 112, 300-310. As cited in Harris, 1992.

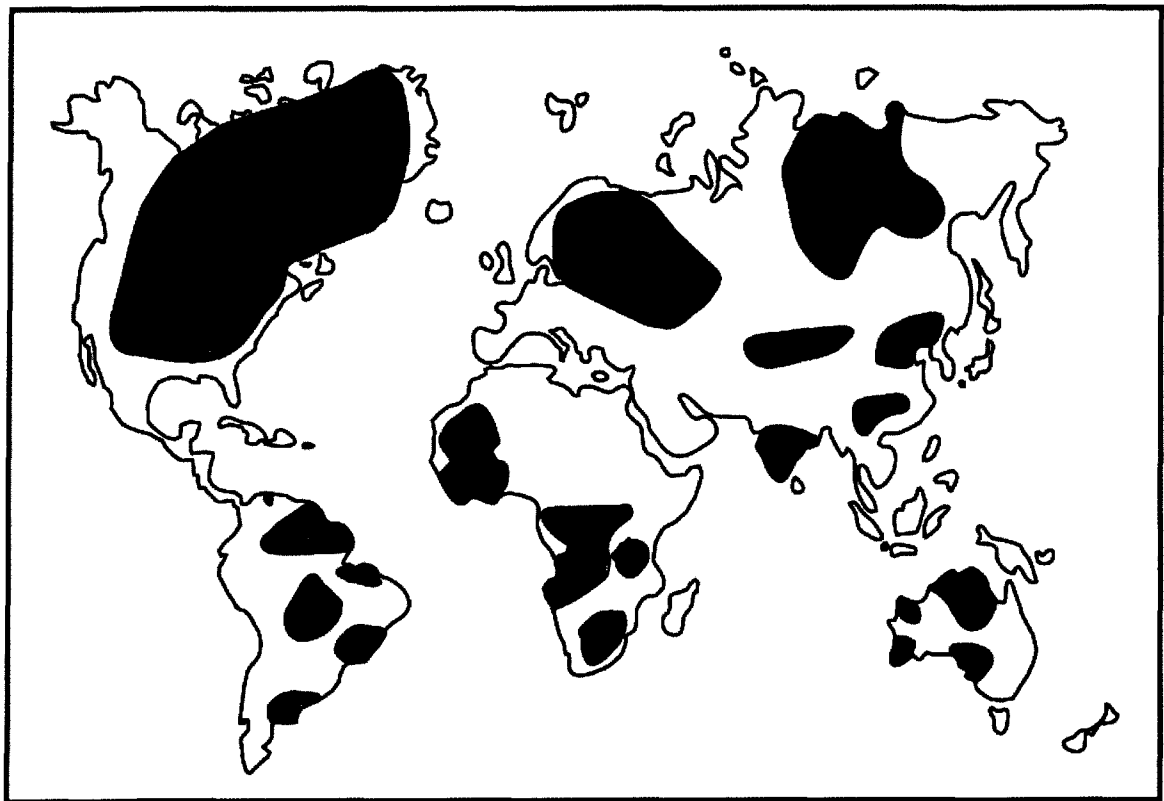


Figure 1.1. Map showing the locations of cratons worldwide (red outline) and their associated diamond deposits (blue diamonds). Modified from Gurney (1989).

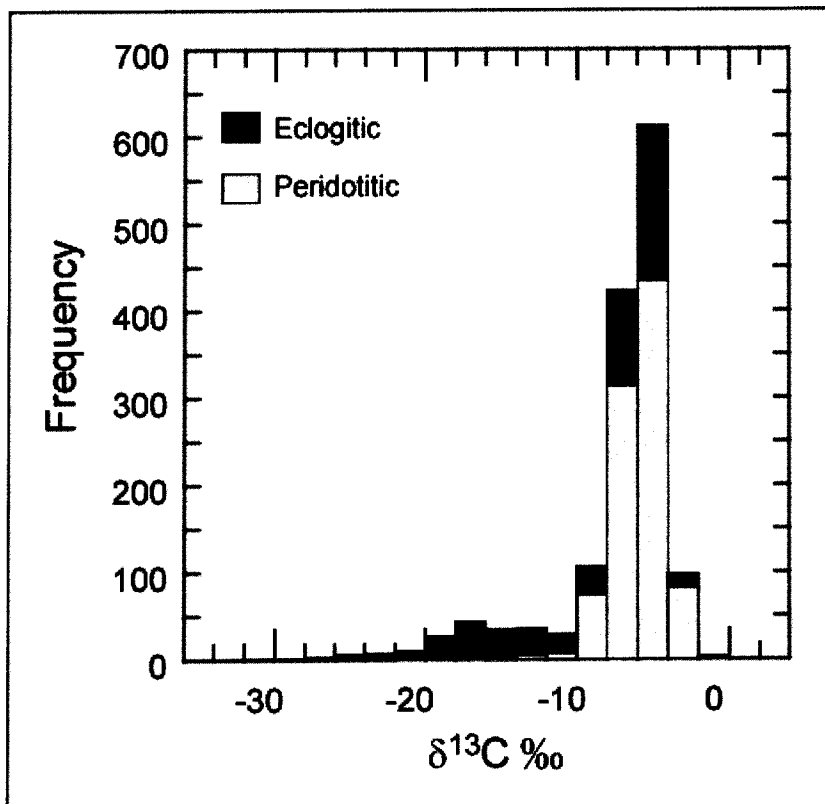


Figure 1.2. Histogram showing the distribution of the carbon isotopic data for diamonds worldwide. The data is subdivided based on inclusion mineralogy into the peridotitic and eclogitic suites.

Chapter 2: Geologic Background

2.1. The Archean Slave Province

2.1.1. Introduction

The Slave Province (Figure 2.1) is a small (~190,000 km²) Archean craton, located within the larger North American craton, and is comprised of rock assemblages ranging from 4.05 to 2.55 Ga (Armstrong and Kjarsgaard, 2003). The Slave craton contains granite-greenstone terranes that are comprised of volcano-sedimentary successions which overly older sialic basement and juvenile basement rocks (Armstrong and Kjarsgaard, 2003). The Slave craton has been intruded by granitoid rocks and the Archean assemblages are frequently cut by Proterozoic mafic dykes (Armstrong and Kjarsgaard, 2003).

The Slave craton is structurally bounded by Thelon Tectonic Zone (2.02 to 1.91 Ga) to the east and the Wopmay Orogen (1.91 to 1.84 Ga) to the west. In the south the Slave is bounded by the Taltson Magmatic Zone (1.99 to 1.91 Ga), the Great Slave Lake Shear Zone (1.98 to 1.93 Ga), and in the southeast, the McDonald Fault (Armstrong and Kjarsgaard, 2003). The Slave craton extends northward to Victoria Island, where it is, in part, bounded by the Bathurst Fault (Armstrong and Kjarsgaard, 2003).

2.1.2. Generalized Geology of the Slave Province

The Slave craton has been divided into eastern and western terranes, based on the presence of Mesoarchean basement in the west and the absence of this basement in the east (Kusky, 1989; Davis and Hegner, 1992; Thorpe et al., 1992; Bleeker et al., 1999b). This boundary broadly agrees with the Pb isotopic boundary (Figure 2.1) of Thorpe et al., (1992), which was defined using Pb-isotope data from volcanogenic massive sulphide (VMS) deposits within the Yellowknife Supergroup. To the west of this boundary, Pb from VMS deposits and galena from later gold deposits shows a significantly more radiogenic signature, indicating derivation from older felsic crust. To the east of the boundary, the Pb compositions show more juvenile isotopic

signatures. Davis and Hegner (1992) have reported a similar Nd isotopic boundary, seen in granites, approximately 100 km to the east (Figure 2.1) of the Pb line.

Kusky (1989) further subdivided the Slave into four terranes; the Anton Terrane, the Sleepy Dragon Terrane, the Contwoyto Terrane and the Hackett Rive Arc, shown in Figure 2.2. Bleeker et al. (1999b) has proposed a new basement terrane, the Central Slave Basement Complex (CSBC), which incorporates the Anton Terrane, the Sleepy Dragon Terrane and the Jolly Lake Complex (Thompson et al., 1995), stating that these terranes merely represent different parts of the CSBC.

The western Slave terrane, which basically consists of the Central Slave Basement Complex of Bleeker et al. (1999b), is dominantly underlain by Mesoarchean basement gneisses that are older than ca. 2.8 Ga (Armstrong and Kjarsgaard, 2003). The rocks of the CSBC show evidence of multiple stages of crustal growth, deformation and plutonism from 4.05 to 2.85 Ga (Armstrong and Kjarsgaard, 2003). The Anton terrane is generally comprised of metamorphosed granodiorite and quartz diorite (Henderson, 1985). In the west, the Anton terrane dips under the Proterozoic rocks of the Wopmay orogen (King, 1986) and to the east it is marked by a thick, near-vertical mylonite zone (Kusky, 1989). The Sleepy Dragon Terrane is comprised of intermediate to mafic quartzofeldspathic gneiss complexes (i.e. the 2.8 to 2.7 Ga Sleepy Dragon Complex of Henderson, 1985), banded and magmatic gneisses near Beniah Lake (Covello et al., 1988) and a 3152 ± 2 Ma (Krogh and Gibbins, 1978) chloritic granite on Point Lake (Easton, 1985). Isolated dioritic to gabbroic bodies are also observed in the Sleepy Dragon Terrane (Kusky, 1989).

The eastern terrane, defined based on the lack of Mesoarchean basement, is primarily comprised of intermediate to felsic, calc-alkaline volcanic rocks, greenstone belts and turbidite sequences or shelf assemblages (Armstrong and Kjarsgaard, 2003). The Contwoyto terrane and the Hackett River Arc of Kusky (1989) make up the eastern terrane. The Contwoyto terrane is dominantly composed of laterally continuous greywacke-mudstone turbidites but also contains tectonic slivers of ophiolite-like rocks and oceanic sedimentary rocks (i.e. shales and iron formations) that are exposed in a series of westward-verging folds and thrusts (Kusky, 1989).

This sequence of rocks was later intruded by a series of granitoids (Kusky et al., 1989). The Hackett River Arc is dominated by felsic volcanic rocks observed as a series of northwest-striking volcanic piles and syn-volcanic granitoid rocks to the south (Kusky, 1989). These volcanic piles are distinctly different from the greenstone belts further to the west which are dominantly mafic volcanic and plutonic rocks (Padgham, 1985).

The Central Slave Basement Complex is unconformably overlain by a thin (generally <200m thick), discontinuous, locally deformed sequence that is comprised of ultramafic, mafic and minor felsic volcanic rocks, conglomerates, quartzites and banded iron formations. Bleeker et al. (1999a) have grouped these rocks into a single lithostratigraphic group, namely, the Central Slave Cover Group (2.90-2.93 Ga; Bleeker, 1999a). The Central Slave Cover Group is the lowermost member of the Neoproterozoic supracrustal rocks of the Yellowknife Supergroup which dominate the surface geology in the Slave craton (Bleeker, 2003).

2.1.3. Plutonism and Deformation

The final stabilization of the craton is marked by intrusions of voluminous plutonic rocks. Davis et al. (1994) has divided the plutonism into three groups: Group 1 is comprised of 2689 – 2650 Ma trondhjemites and diorites. Group 2 consists of 2610 – 2600 Ma syn-to-late deformational monzodiorite-granodiorite and trondhjemite, while Group 3 is marked by 2599 – 2580 Ma post-deformational micaceous granites. Davis et al. (1994) note that Groups 1 and 2 typically have calc-alkaline chemistries, and trace element patterns similar to that of modern subduction-related igneous rocks. The Group 3 rocks are comparable to many Phanerozoic post-orogenic K-U-Th-rich granite suites (Davis et al., 1994).

A more detailed summary of plutonism and deformation in the Slave is provided by Bleeker (2003). Bleeker (2003) notes that the overall stratigraphy and granitoid geochronology is similar across the Slave craton, and summarized these events as follows: Widespread basaltic volcanism, along with minor komatiitic rocks, occurred at 2730 to 2700 Ma across the basement complex. Towards the top of the pile, local intercalations of rhyolite, tuff and reworked volcanoclastic rocks occur.

This was followed by a transition to more intermediate, felsic, or bimodal volcanism around 2700 to 2660 Ma. These volcanics are characterized by dacite-rhyolite complexes, abundant volcanoclastic material and widespread tonalite-trondhjemite-granodiorite (TTG) plutons. Widespread turbidite sedimentation occurred across the craton from 2670 to 2650 Ma. The first major folding event occurred within the Burwash Formation turbidites at 2645 – 2635 Ma, resulting in a northwest-southwest trending F_1 fold belt. Abundant tonalite-granodiorite \pm diorite plutons intruded from 2630 to 2610 Ma. From 2605 to 2590 Ma the more evolved two-mica granites (Group 3 of Davis et al., 1994) intruded in areas of downfolded turbidite sedimentary rocks. These intrusions were coeval with the craton-wide deformation that resulted in the north to northwest trending F_2 fold, which also refolded the F_1 fold belt. The stabilization of the Slave craton occurred after the termination of the 2590 to 2580 Ma “granite bloom” which is observed across the entire craton.

2.1.4. Proterozoic Diabase Dykes

At least six Proterozoic diabase dyke swarms are recognized in the Slave province (Kjarsgaard, 2001) with LeCheminant and van Breeman (1994) listing a seventh, the Hearne swarm. The oldest dykes in the Slave are the Malley dykes at 2.23 Ga (LeCheminant et al., 1996). These dykes, which have a 45° strike, intrude the Archean basement but do not crosscut Goulburn Supergroup (1.97 to 1.90 Ga) sediments (LeCheminant et al., 1996). Both the MacKay and Dogrib dykes have a similar orientation of $080\text{-}110^\circ$, but were found to have different petrological characteristics and different ages of 2.21 Ga and 2.19 Ga, respectively (Kjarsgaard, 2001). The ca. 2038 Ma Hearne swarm dykes are northeast striking dykes (LeCheminant et al., 1996), while the 2023 – 2030 Ma Lac de Gras dyke swarm has an overall trend of approximately 10° (LeCheminant and van Breeman, 1994). The later Mesoproterozoic dyke swarms include the Mackenzie and ‘305’ dykes. The Mackenzie dyke swarm (1.27 Ga) is the largest known radiating dyke swarm and trends north-northwest (LeCheminant and Heaman, 1989). The ‘305’- trending dykes, which are believed to be related to the Mackenzie dyke swarm, are observed in the central and north-central Slave (Armstrong and Kjarsgaard, 2003). It has been suggested that the Paleoproterozoic Malley, MacKay, Dogrib, Lac de Gras and

Hearne diabase dykes may indicate the progressive breakup of a larger Archean craton (LeCheminant and van Breeman, 1994; Bleeker, 2003).

2.1.5. Formation Models for the Slave Province

Tectonic models for the formation of the Slave Province can be divided into two main types, (1) intracratonic rift models, and (2) subduction and accretionary models. Intracratonic rifting models propose that the Slave Province developed within an extensional basin in an older craton (Davis et al., 1994, and references therein). The models invoking formation via subduction and accretionary processes include those of Kusky (1989) and references therein. Bleeker (2003) proposes a third model whereby accretion and collisional tectonics led to the formation of a late Archean supercontinent “Sclavia”, which included the Slave craton. Sclavia later experienced subsequent rifting and breakup in the Paleoproterozoic, resulting in multiple distinct cratons.

Intracratonic extension models for the Slave province included those of Henderson (1981) and Easton (1985) whereby volcanics and sediments filled normal fault-bounded linear troughs formed on pre-existing sialic crust during continental extension. Alternately, Helmstaedt et al. (1986) and Fyson and Helmstaedt (1988) have proposed models whereby volcanics and sediments were deposited in backarc basins that subsequently closed.

In the accretionary tectonic model of Kusky (1989), high strain zones separate four distinct terranes, namely the Anton terrane, the Sleepy Dragon terrane, the Contwoyto terrane and the Hackett River volcanic terrane. Kusky’s model hypothesized that the four terranes were then juxtaposed during collisional orogenesis. The Anton terrane has been interpreted as an Archean microcontinent, while it is believed that the Sleepy Dragon terrane may represent an exhumed, more eastern part of the Anton terrane (Kusky, 1989). The Contwoyto terrane has been interpreted as a westward-verging fold and thrust belt that contains slivers of greenstone volcanics and the Hackett River volcanic terrane has been interpreted as an Archean island arc (Kusky, 1989). The Contwoyto and Hackett River terranes are believed to represent a paired accretionary prism and island-arc system that was formed above a subduction

zone dipping to the east (Kusky, 1989). These terranes then collided with the Anton microcontinent during the main accretion event in the Slave, producing a basement nappe, the Sleepy Dragon terrane (Kusky, 1989). The resultant tectonic assemblage was later intruded by granitoid bodies during the final stages of cratonic stabilization.

In the more recent model of Bleeker (2003) the presence of three to four rifted margins was taken to indicate that the current Slave craton is only a small fragment of a much larger ancestral supercraton Sclavia. Along with the Slave, Bleeker (2003) groups the Dharwar craton, the Zimbabwe craton and the Wyoming craton into the supercontinent Sclavia based on their similar basement complexes, Meso- to Neoproterozoic successions, and similar progressions of late Archean granitoid suites, all culminating at 2.6 Ga or shortly thereafter. Sclavia is believed to have amalgamated at ca. 2.6 Ga. The breakup of Sclavia is believed to have occurred between 2.2 and 2.0 Ga based on ages of marginal dyke (i.e. the Malley, Mackay and Dogrib) swarms (LeCheminant et al., 1997) and marginal sedimentary sequences (Bleeker, 2003). The Slave craton then drifted individually for approximately 200 Ma before it was amalgamated by 2.0 to 1.8 Ga into Laurentia, the present day core of North America.

2.2. The Lithospheric Mantle Beneath the Slave Craton

2.2.1. Overview

The Slave craton has been subdivided into three compositionally distinct northeast-trending lithospheric domains (Figure 2.3) by Grütter et al. (1999) based on compositional data from more than 13,000 till sampled garnets. The southern Slave garnets are dominated by ilmenitic and eclogitic compositions (Grütter et al., 1999). The southern Slave also contains a high-Cr₂O₃ garnet population that have CaO contents of >1.8 wt%. The southern domain has been further subdivided by Carbno and Canil (2002) into a southwest and southeast terrane. Carbno and Canil (2002) note that the till samples used by Grütter et al. (1999) to define the southern lithospheric domain only contained garnets from the southeastern portion of the domain. The southeast garnets have a high proportion of high-Cr harzburgitic garnets, these garnets are absent from the southwest portion (Carbno and Canil,

2002). The north-trending Pb isotopic line of Thorpe et al. (1992) is used by Carbone and Canil (2002) to separate the southwest garnet populations from those in the southeast (Figure 2.3). The ~ 150 km wide central Slave domain, which includes the Lac de Gras area, contains evidence for an ultradepleted lithosphere, as indicated by the high proportion of subcalcic garnets with CaO contents <1.8 wt% (Grütter et al., 1999). The northern Slave domain is dominated by a moderately depleted lithosphere with a garnet population derived from lherzolitic and eclogitic lithologies (Grütter et al., 1999). Occurrences of sub-calcic garnets are rare in the northern Slave (Grütter et al., 1999).

2.2.2. The Lithospheric Domains of the Slave

Mantle xenolith studies are commonly used to investigate the composition, structure and thermal state of the lithosphere. These samples are transported to the surface within kimberlitic magmas. Mineral compositions within these xenoliths provide data for models that combine rock type, ambient temperature and pressure conditions at the time of entrainment and petrophysical properties (Pearson et al., 1999). All three of the lithospheric domains of the Slave show evidence of chemical stratification. However, the composition, depth and geothermal gradients have been found to vary across the three domains (Figure 2.4).

2.2.2.1. The Northern Slave

Mantle xenoliths from the Jericho kimberlite have been used to characterize the northern Slave domain. The Jericho pipe xenoliths are chiefly comprised of peridotite (67%), with lesser eclogite (25%) and pyroxenites (8%) (Kopylova et al., 1999b). Peridotites from the northern Slave have the most undepleted, lherzolite rich compositions in the Slave craton (Kopylova and Caro, 2004).

Kopylova et al. (2001 and 2003) using analyses of Re-Os isotopic compositions and chondrite-normalized PGE patterns have noted that the mantle of the northern Slave is also stratified with respect to age (Figure 2.4). The shallow layer represents Archean mantle and the deeper layer is Archean-Proterozoic mantle (Kopylova et al., 2001). Additionally, a thin layer of fertile peridotite enriched in

clinopyroxene and garnet and an underlying magmatic pyroxenite layer are believed to have formed later during the Phanerozoic (Kopylova et al., 2001). Kopylova et al. (1999b) also note a major petrological boundary at depths of 160-190 km which they infer to be the lithosphere-asthenosphere boundary. Geothermal gradients at the time of kimberlite eruption have been determined to be 37-38 mW/m² for the Jericho kimberlite (Kopylova et al., 1999b).

2.2.2.2. *The Central Slave and Lac de Gras Area*

A two-layered lithosphere has been recognized beneath the central Slave craton (Griffin et al., 1999a; Griffin et al., 1999b; Pearson et al., 1999; O'Reilly et al., 2001, Menzies et al., 2004) which consists of a shallow "ultra-depleted" harzburgite-rich layer and a deeper, less-depleted layer (Figure 2.4). Garnet compositions and xenolith data have revealed that the shallow layer is more magnesian, having olivine with forsterite contents of 92-94, while the deeper layer has forsterite contents of 91-92 (O'Reilly et al., 2001). Garnet compositions indicate that the shallow layer is comprised of approximately 60% harzburgite and 40% highly depleted lherzolite (O'Reilly et al., 2001). The lower layer is dominated by 80-85 % comparatively less depleted lherzolite and 15-20 % harzburgite (O'Reilly et al., 2001). The eclogites are concentrated near the bottom of the section (O'Reilly et al., 2001). A sharp boundary between the two layers occurs at depths of 140 to 150 km and this boundary is geochemically reflected in both olivine compositions (see above) and Zr, Y and Ti contents of concentrate garnets (O'Reilly et al., 2001). The thickness and depth of the two-layered structure has been found to vary across the central Slave domain. The maximum thicknesses and depth occur in the central part of the central Slave, while in the southern, northern and western parts of the craton the deeper more fertile layer raises to depths of ≤ 100 km and the shallower ultra-depleted layer is thinned or absent (O'Reilly et al., 2001).

Griffin et al. (1999a) defined the base of the lithosphere in the Slave as the temperature above which depleted garnets are no longer present. These "depleted" garnets are defined by Griffin et al. (1999a) as containing <10 ppm Y. At higher temperatures the garnets have undepleted trace-element signatures that are attributed to the interaction with asthenosphere-derived melts (Griffin et al., 1999a, and

references therein). As such, the depth of the lithosphere-asthenosphere boundary in the central Slave has been estimated to lie at depths of 200-220 km, which is in agreement with seismic data of Cook et al. (1999).

The xenolith and xenocryst studies have indicated the occurrence of two different paleogeotherms in the central Slave and the Lac de Gras area. A cooler paleogeotherm of 35-37 mW/m² exists for the upper layer of the lithosphere, compared to a 40 mW/m² paleogeotherm for the lower layer. Pearson et al. (1999) and Griffin et al. (1999b) have proposed a stepped paleogeotherm with a low geothermal gradient below temperatures of 900°C and an abrupt boundary at ~900 to 1000°C, with a higher geothermal gradient at greater depth coinciding with the more fertile layer. More recent studies (Doyle et al., 2003; Grütter and Moore, 2003; Menzies et al., 2004) report a continuous transition, rather than an abrupt stepped transition, from the lower geotherm in the upper layer to the higher geotherm in the deeper layer.

2.2.2.3. *The Southern Slave*

In a xenolith study of the Gahcho Kué kimberlite cluster, Kopylova and Caro (2004) revealed that the southeastern Slave is dominated by coarse peridotite (61%), eclogite (18%), deformed peridotite (17%), and orthopyroxenite (4%). The Cr-pyropes from the peridotitic xenoliths plot along the lherzolitic trend on a Ca-Cr diagram (Kopylova and Caro, 2004), reflecting the common presence of clinopyroxene in southern Slave peridotites, which is in agreement with the till sample analyses of Grütter et al. (1999).

Kopylova and Caro (2004) concluded that peridotite from the Gahcho Kué kimberlite cluster in the southeastern Slave formed within a deep, cold cratonic mantle at temperatures of 600-1300°C and pressures of 25-80 Kb. The minimum lithospheric thickness was determined to be 220-250 km, which is greater than that of the central Slave (~200 km; Pearson et al., 1999) and the northern Slave (160-190 km; Kopylova et al., 1999b).

The southwestern Slave domain was characterized by Carbno and Canil (2002) using garnet xenolith geochemistry from the Drybones Bay kimberlite. The high-Cr harzburgitic garnets seen in the southeastern domain are absent in the

southwestern domain (Carbno and Canil, 2002). The southwestern domain is characterized by ultra-depleted harzburgite at shallow depths which is then underlain by a moderately depleted mantle (Carbno and Canil, 2002). The ultradepleted Drybones Bay garnets show geochemical similarities (Cr_2O_3 , Zr, Y and Ti) to that observed for the shallow “harzburgite” layer from the central Slave domain, but the Drybones Bay garnets are much more calcic (Carbno and Canil, 2002). This led Carbno and Canil (2002) to hypothesize that the layered structure of the central Slave mantle lithosphere extends into the southwestern Slave domain where it has been severely overprinted due to subsequent heating and metasomatic events as suggested by the Drybones Bay garnet chemistries (i.e. elevated Ca, Zr and LREE). Another contrasting feature between the southwestern and southeastern domain is the thickness of the mantle lithosphere, at the time of kimberlite emplacement. For the 539 Ma (Heaman et al., 1997) 5034-Kennedy pipe of the Gahcho Kué kimberlite cluster, Kopylova and Caro (2004) have reported a minimum of thickness of 220-250 km, while the ~ 450 Ma Drybones Bay kimberlite recorded a thickness of 160 km (Carbno and Canil, 2002).

2.3. Kimberlites of the Slave Craton

Kimberlite age determinations have revealed that within the Slave craton, over relatively small distances, kimberlite fields of Eocene, Cretaceous, Jurassic, Permian, Siluro-Ordovician and Cambrian age exist (Davis and Kjarsgaard, 1997; Heaman et al., 2003). The oldest pipes in the Slave are the Precambrian (613 Ma) Anuri kimberlite located in the northern Slave (Masun et al., 2003) and the Cambrian (542 Ma) Kennedy Lake 5034 pipe in the southeastern Slave (Heaman et al., 2003; Masun et al., 2003). The youngest pipes occur in the Lac de Gras kimberlite field and are Eocene (47.0 to 56.0 Ma) in age (Davis and Kjarsgaard, 1997; Graham et al., 1999; Creaser et al., 2004). Heaman et al. (2004) also note that, excluding the northern Slave kimberlites, many kimberlite clusters proximal (~150 km) to Lac de Gras have emplacement ages which span most of the Phanerozoic. Heaman et al. (2004) have compiled age determinations for 58 Slave kimberlites, which at the time

represented approximately 17% of the known kimberlites from the Slave. From these age determinations, they have subdivided the Slave craton into four domains, which are shown on Figure 2.5. Domain I is located in the southwestern Slave and is characterized by Siluro-Ordovician kimberlite ages. Included within this domain are the Orion (435 Ma), Drybones Bay (441 Ma), Cross (450 Ma) and Ursa (459 Ma) kimberlites (Figure 2.6) (Heaman et al., 2004). Domain II is located in the southwestern Slave craton and contains Cambrian kimberlite magmatism. The 542 Ma Kennady Lake 5034 kimberlite and the 523-535 Ma Snap Lake dyke (Agashev et al., 2001) are located in this domain (Figure 2.6). Domain III is located within the central Slave and it is comprised primarily of Cretaceous and Eocene aged kimberlites. The 48 to 74 Ma kimberlites of the Lac de Gras area are included within this region. Domain IV is a mixed domain having Jurassic kimberlites in the Contwoyto field, including the ~ 173 Ma Jericho pipe (Heaman et al., 2002), a Permian kimberlite field located on Victoria Island having ages of ~256 to 286 Ma (as reported in Heaman et al., 2004), and the Precambrian Anuri kimberlite.

From the resulting domain distribution, Heaman et al. (2004) found no simple explanation for the observed pattern. They do, however, note that the N-S trending boundary that separates Domain I from the other domains is broadly coincident with the boundary used to separate the east and west terranes of the Slave Province, namely the exposed eastern margin of the Anton terrane or the Central Slave Basement Complex. This boundary was based on the occurrence of pre-2.8 Ga basement rocks (Bleeker, et al., 1999b, and references therein) and broadly coincides with the Pb isotopic boundary of Thorpe et al. (1992), as previously discussed.

Within the central Slave (Domain III), the Eocene to Cretaceous kimberlite magmatism has occurred within a relatively small area of 50 km² around Lac de Gras. Emplacement ages range between 45.2 and 74.7 Ma, based on 47 age determinations (Heaman et al., 2004). The large number of age determinations from this one domain is due to the observation that within the Slave the most economically significant pipes are Eocene in age. Heaman et al. (2004) also point out that although less than 5 km separate the ~55 Ma A154 pipes and the 74 Ma C13 pipes, it is only A154 that has a

high diamond grade. Creaser et al. (2004) further report that the highest diamond grades for the Lac de Gras kimberlites are restricted to narrow periods of kimberlite magmatism from 51 to 53 and 55 to 56 Ma.

2.4. The Lac De Gras Area

2.4.1. The Lac Des Gras Kimberlite Field

The Lac de Gras kimberlite field, which hosts >236 kimberlites (Kjarsgaard, 2001), is part of an assemblage of Archean and Proterozoic rocks of the Slave Province. The Diavik project pipes are located immediately to the east of East Island, on the eastern edge of Lac de Gras, adjacent to the Ekati Island shoreline (Figure 2.6). The geology of the project area is described by Bryan and Bonner (2003). The pipes are associated with the three main Archean rock units of East Island, a greywacke-mudstone metaturbidite, tonalite-quartz diorite, and a two-mica granite. The greywacke-mudstone turbidites are steeply dipping, trending northwest-southeast, through the centre of East Island. These metaturbidites have been intruded by the ca. 2610 – 2600 Ma tonalite –quartz diorite that dominates the southern portion of the island and hosts the A21 kimberlite. Much of the northern part of East Island is underlain by a ca. 2590 – 2580 Ma two-mica granite that forms a dyke and sheet complex and hosts the A154 South, A154 North and A418 kimberlites. Three Proterozoic diabase dyke sets, the Malley (ca. 2.23 Ga), Lac de Gras (ca. 2.02 Ga) and the Mackenzie (1.27 Ga), cut the Archean stratigraphy. The area is variably covered by Quaternary till, glaciofluvial and glaciolacustrine deposits which, in some places, exceed 30 m. The Diavik kimberlite diatremes are small (<2 ha), steep-sided pipes that appear circular in plan view. The kimberlites contain crater and hypabyssal facies rocks, with pyroclastic and re-sedimented volcanoclastic rocks being the dominant lithologies. The kimberlites are roughly aligned, having an approximate trend of 30 degrees.

The ages of the pipes in the Lac de Gras kimberlite field range from Eocene (47 Ma) to Cretaceous (86 Ma) (Heaman et al., 1997). The Diavik pipes have been dated, using Rb-Sr in mica, to obtain isochron ages of pipe emplacement of 55.5 ± 0.5

Ma for A154 South, 56.0 ± 0.7 Ma for A154 North, 55.2 ± 0.3 Ma for A418 and 55.7 ± 2.1 Ma for A21 (Amelin, 1996).

2.4.2. Diavik Exploration History

The Diavik Diamond Mine is an unincorporated joint venture between Aber Diamond Mines Ltd. and Diavik Diamond Mines Inc. (DDMI, a wholly owned subsidiary of Rio Tinto plc). The Diavik Mine is located 295 km northeast of Yellowknife, NWT on the eastern end of Lac de Gras (Figure 2.4).

Project kimberlites in the Lac de Gras area were staked in late 1991, during the early stages of the Canadian diamond rush that eventually encompassed much of the Slave Province. Exploration at Diavik involved the integration of remote sensing and airborne geophysical techniques, combined with the results of kimberlite indicator mineral analyses from glacial till collected down ice from the more prospective targets. These methods were then followed by ground surveys and further geophysical studies, with targets still remaining prospective being confirmed by drill testing. By the spring of 1995 the current Diavik resource, kimberlites A154 South, A154 North, A418, and A21, had been discovered. As of June 2003, the Diavik project included sixty-three kimberlite occurrences, with approximately 50% of them being diamondiferous (Bryan and Bonner, 2003).

References

- Agashev, A.M., Pokhilenko, N.P., McDonald, J.A., Takazawa, E., Vavilov, M.A., Sobolev, N.V., and Watanabe, T. 2001. A unique kimberlite – carbonatite primary association in the Snap Lake dyke system, Slave craton: evidence from geochemical and isotopic studies. The Slave-Kaapvaal Workshop, Program with Abstract, 42–44.
- Amelin, Y. 1996. Report on Rb-Sr and U-Pb study of kimberlite samples VR44444A through VR44465A. Confidential Reports for Kennecott Canada Inc., 7. As cited in Graham et al. (1990).
- Armstrong, J.P., and Kjarsgaard, B.A. 2003. Geological setting of kimberlites on the Archean Slave Province. VIIIth International Kimberlite Conference, Slave Province and Northern Alberta Field Trip Guidebook, 31-38.
- Bleeker, W. 2003. The late Archean record: a puzzle in ca. 35 pieces. *Lithos*, 71, 99-134.
- Bleeker, W., Ketchum, J.W.F., Jackson, V.A., and Villeneuve, M.E. 1999a. The Central Slave Basement Complex, Part I: its structural topology and autochthonous cover. *Canadian Journal of Earth Sciences*, 36, 1083-1109.
- Bleeker, W., and Davis, W.J. 1999b. Time and plutonism, deformation, and metamorphism in the Yellowknife Domain, Slave Province, Canada. *Canadian Journal of Earth Sciences*, 36, 1169-1187.
- Bryan, D., and Bonner, R. 2003. The Diavik Diamond Mine, Lac de Gras, Northwest Territories, Canada. VIIIth International Kimberlite Conference, Slave Province and Northern Alberta Field Trip Guidebook, 61-65.
- Carbno, G.B., and Canil, D. 2002. Mantle structure beneath the SW Slave craton, Canada: constraints from garnet geochemistry in the Drybones Bay kimberlite. *Journal of Petrology*, 43, 129-142.
- Carins, S.R., and Goff, S.P. 2005. Northwest Territories mineral exploration overview, November 2005. Northwest Territories Geoscience Office, 20p.
- Cook, F.A., van der Velden, A.J., Hall, K.W., and Roberts, B.J. 1999. Frozen subduction in Canada's Northwest territories: Lithoprobe deep lithospheric reflection profiling of the western Canadian shield. *Tectonics*, 18, 1-24.
- Covello, L., Roscoe, S.M., Donaldson, J.A., Roach, D., and Fyson, W.K. 1988. Archean quartz arenite and ultramafic rocks at Beniah Lake, Slave structural province, N.W.T. In Current research, part C. Geological Survey of Canada, Paper 88-1C, 223–232. As cited in Bleeker et al. (1999b).

- Creaser, R.A., Grütter, H., Carlson, J.A., and Crawford, B. 2004. Macrocrystal phlogopite Rb–Sr dates for the Ekati property kimberlites, Slave Province, Canada: evidence for multiple intrusive episodes in the Paleocene and Eocene. *Lithos*, 76, 399-414.
- Davis, W.J., and Hegner, E. 1992. Neodymium isotopic evidence for the tectonic assembly of Late Archean crust in the Slave province, northwest Canada. *Contributions to Mineralogy and Petrology*, 111, 493–504.
- Davis, W.J., Fryer, B.J., and King, J.E. 1994. Geochemistry and evolution of Late Archean plutonism and its significance to the tectonic development of the Slave craton. *Precambrian Research*, 67, 207 – 241.
- Davis, W.D., and Kjarsgaard, B.A. 1997. A Rb–Sr isochron age for a kimberlite from the recently discovered Lac de Gras field, Slave Province, Northwest Territories, Canada. *Journal of Geology*, 105, 503-509.
- Davis, W.J., and Bleeker, W. 1999. Timing of plutonism, deformation, and metamorphism in the Yellowknife Domain, Slave Province, Canada. *Canadian Journal of Earth Sciences*, 36, 1169-1187.
- Doyle, P.M., Gurney, J.J., and Le Roex, A. 2003. Xenoliths from the Arnie, Misery and Pigeon kimberlites, Ekati mine, NWT, Canada. VIIIth International Kimberlite Conference, Victoria, Canada, Extended Abstracts, 5p (CD not paginated).
- Easton, R.M. 1985. The nature and significance of pre-Yellowknife Supergroup rocks in the Point Lake area, Slave structural province, Canada. In: *Evolution of Archean supracrustal sequences*. Geological Association of Canada, Special Paper 28, 153-167. As cited in Bleeker and Davis, (1999a).
- Fyson, W.K., and Helmstaedt, H. 1988. Structural patterns and tectonic evolution of supracrustal domains in the Archean Slave province, Canada. *Canadian Journal of Earth Sciences*, 25, 301-315.
- Graham, I., Burgess, J.L., Bryan, D., Ravenscroft, P.J., Thomas, E., Doyle, B.J., Hopkins, R., and Armstrong, K.A. 1999. Exploration History and Geology of the Diavik Kimberlites, Lac de Gras, Northwest Territories, Canada. In: *Proceedings of the VIIth International Kimberlite Conference*, The J.B. Dawson Volume, Gurney, J.J., Gurney, J.L., Pascoe, M.D., and Richardson, S.H. (eds), Red Roof Design, Cape Town, 262-279.
- Griffin, W.L., Doyle, B.J., Ryan, C.G., Pearson, N.J., O'Reilly, S.Y., Davies, R., Kivi, K., van Acherbergh, E., and Natapov, L.M. 1999a. Layered mantle lithosphere in the Lac de Gras area, Slave craton: composition, structure and origin. *Journal of Petrology*, 40, 705– 727.

- Griffin, W.L., Doyle, B.J., Ryan, C.G., Pearson, N.J., O'Reilly, S.Y., Natapov, L., Kivi, K., Kretschmar, U., and Ward, J. 1999b. Lithosphere structure and mantle terranes: Slave craton, Canada. In: Proceedings of the VIIth International Kimberlite Conference, The J.B. Dawson Volume, Gurney, J.J., Gurney, J.L., Pascoe, M.D., and Richardson, S.H. (eds), Red Roof Design, Cape Town, 299–306.
- Grütter, H.S., Apter, D.B., and Kong, J. 1999. Crust– mantle coupling: evidence from mantle-derived xenocrystic garnets. In: Proceedings of the VIIth International Kimberlite Conference, The J.B. Dawson Volume, Gurney, J.J., Gurney, J.L., Pascoe, M.D., and Richardson, S.H. (eds), Red Roof Design, Cape Town, 307–313.
- Grütter, H.S., and Moore, R.O. 2003. Pyroxene geotherms revisited - an empirical approach based on Canadian xenoliths. VIIIth International Kimberlite Conference, Victoria, Canada, Extended Abstracts, 4p (CD, not paginated).
- Heaman, L.M., Kjarsgaard, B.A., Creaser, R.A., Cookenboo, H.O., and Kretschmar, U. 1997. Multiple episodes of kimberlite magmatism in the Slave Province, North America. Lithoprobe Workshop Report, 56, 14-17.
- Heaman, L.M., Creaser, R.A., and Cookenboo, H.O. 2002. Extreme high-field-strength element enrichment in Jericho eclogite xenoliths: a cryptic record of Paleoproterozoic subduction, partial melting and metasomatism beneath the Slave craton, Canada. *Geology*, 30, 507-510.
- Heaman, L.M., Kjarsgaard, B.A., and Creaser, R.A. 2003. The timing of kimberlite magmatism in North America: implications for global kimberlite genesis and diamond exploration. *Lithos*, 71, 153-184
- Heaman, L.M., Kjarsgaard, B.A., and Creaser, R.A. 2004. The temporal evolution of North American Kimberlites. *Lithos*, 76, 377-397.
- Helmstaedt, H., Padgham, W.A., and Brophy, J. 1986. Multiple dykes in the lower Kam Group, Yellowknife Greenstone Belt: Evidence for Archean sea-floor spreading? *Geology*, 14, 562-566.
- Henderson, J.B. 1981. Archean basin evolution in the Slave Province, Canada, In: Precambrian plate tectonics; Amsterdam, Elsevier, p. 213-235. As cited in Kusky (1989).
- Henderson, J.B. 1985. Geology of the Yellowknife – Hearne Lake area, District of MacKenzie: a segment across an Archean basin. Geological Survey of Canada, Memoir 414. As cited in Bleeker et al. (1999b).

- Hoffman, P., and Hall, L. 1993. Geology, Slave craton and environs, District of Mackenzie, Northwest Territories: Ottawa, Geological Survey of Canada Open File 2559.
- Jones, A.G., and Craven, J.A. 2004. Area selection for diamond exploration using deep-probing electromagnetic surveying. *Lithos*, 77, 765-782.
- King, J.E. 1986. The metamorphic internal zone of Wopmay orogen (Early Proterozoic), Canada: 30 km of structural relief in a composite section based on plunge projection. *Tectonics*, 5, 973–994. As cited Bleeker et al. (1999b).
- Kjarsgaard, B.A. 2001. Geology of the Lac de Gras Kimberlite Field, Central Slave Province, Canada. The Slave-Kapvaal Workshop, Merrickville, Ontario, Extended Abstracts, 2p (CD, not paginated).
- Kopylova, M.G., Russel, J.K., and Cookenboo, H. 1999b. Mapping the lithosphere beneath the north central Slave craton. In: Proceedings of the VIIth International Kimberlite Conference, The J.B. Dawson Volume, Gurney, J.J., Gurney, J.L., Pascoe, M.D., and Richardson, S.H. (eds), Red Roof Design, Cape Town, 468-479.
- Kopylova, M.G., and Caro, G. 2004. Mantle xenoliths from the southeastern Slave craton: evidence for chemical zonation in a thick, cold lithosphere. *Journal of Petrology*, 45, 1045-1067.
- Krogh, T.E., and Gibbins, W. 1978. U–Pb isotopic ages of basement and supracrustal rocks in the Point Lake area of the Slave structural province, Canada. Geological Association of Canada, Program with Abstracts, 7, 61. As cited in Bleeker et al. (1999b).
- Kusky, T.M., 1989. Accretion of the Archean Slave province. *Geology*, 17: 63-67.
- LeCheminant, A.N., and Heaman, L.M. (1989). Mackenzie igneous events, Canada: Middle Proterozoic hotspot magnetism associated with ocean opening. *Earth and Planetary Science Letters*, 96, 38-48.
- LeCheminant, A.N., and van Breeman, O. 1994. U-Pb ages of Proterozoic dyke swarms, Lac de Gras area, NWT: Evidence for progressive breakup of an Archean supercontinent. Geological Association of Canada/Mineralogical Association of Canada, Program with Abstracts, v.19. A26.

- LeCheminant, A.N., Heaman, L.M., van Breeman, O., Ernst, R.E., Baragar, W.R.A., and Buchan, K.L. 1996b. Mafic magnetism, mantle roots and kimberlites in the Slave craton. In: Searching for Diamonds in Canada, A.N. LeCheminant, D.G. Richardson, R.N.W. Dilabio, and K.A. Richardson (ed); Geological Survey of Canada, Open File 3228, p 161-169. As cited in Armstrong and Kjarsgaard (2003).
- LeCheminant, A.N. Buchan, A.N., van Breeman, O., and Heaman, L.M. 1997. Paleoproterozoic continental break-up and reassembly: evidence from 2.19 Ga diabase dyke swarms in the Slave and western Churchill provinces. Abstract Volume, Geological Association of Canada, v.22, A86.
- MacKenzie, J.M. and Canil, D. 1999. Composition and thermal evolution of cratonic mantle beneath the central Archean Slave Province, NWT, Canada. Contributions to Mineralogy and Petrology, 134, 313-324.
- Masun, K.M., Doyle, B.J., Ball, S.A., and Walker, S. 2003. The geology and mineralogy of the Anuri kimberlite, Nunavut, Canada. VIIIth International Kimberlite Conference, Victoria, Canada, Extended Abstracts, 6p (CD, not paginated).
- Menzies, A., Westerlund, K., Grütter, H., Gurney, J., Carlson, J., Fung, A., and Nowicki, T. 2004. Peridotitic mantle xenoliths from kimberlites on the Ekati Diamond Mine property, N.W.T., Canada: major element compositions and implications for the lithosphere beneath the central Slave craton. Lithos 77, 395-412.
- O'Reilly, S.Y., Griffin, W.L., Djomani, Y.P., Natapov, L.M., Pearson, N.J., Davies, R.M., Doyle, B.J., and Kivi, K. 2001. The mantle beneath the Slave Craton (Canada): Composition and Architecture. The Slave-Kapvaal Workshop, Merrickville, Ontario, Extended Abstracts, 5p (CD, not paginated).
- Padgham, W.A. 1985. Observations and speculations of supracrustal successions in the Slave Structural Province, in Ayres, L.D., Thurston, P.C., Card, K.D., and Weber, W., eds., Geological Association of Canada Special Paper 28, 133-151. As cited in Kusky (1989).
- Pearson, N.J., Griffin, W.L., Doyle, B.J., O'Reilly, S.Y., Van Achtenberg, E., Kivi, K. 1999. Xenoliths from kimberlite pipes of the Lac de Gras area, Slave Craton, Canada. In: Proceedings of the VIIth International Kimberlite Conference, The P.H. Nixon Volume, Gurney, J.J., Gurney, J.L., Pascoe, M.D., and Richardson, S.H. (eds), Red Roof Design, Cape Town, 644-658.

Thompson, P.H., Russel, I., Paul, D., Kerswill, J.A., and Froese, E. 1995. Regional geology and mineral potential of the Winter Lake – Lac de Gras area, central Slave Province, Northwest Territories. In Current research, part C. Geological Survey of Canada, Paper 1995-C, pp. 107–119. As cited in Bleeker and Davis (1999a).

Thorpe, R.I., Cumming, G.L. and Mortensen, J.K., 1992. A significant Pb isotope boundary in the Slave Province and its probable relation to ancient basement in the western Slave Province. In: Project Summaries, Canada-Northwest Territories Mineral Development Agreement 1987-91. Geol. Surv. Can. Open File Rep., 2484:179-184. As cited in Armstrong and Kjarsgaard (2003) and Griffin et al. (1999b).

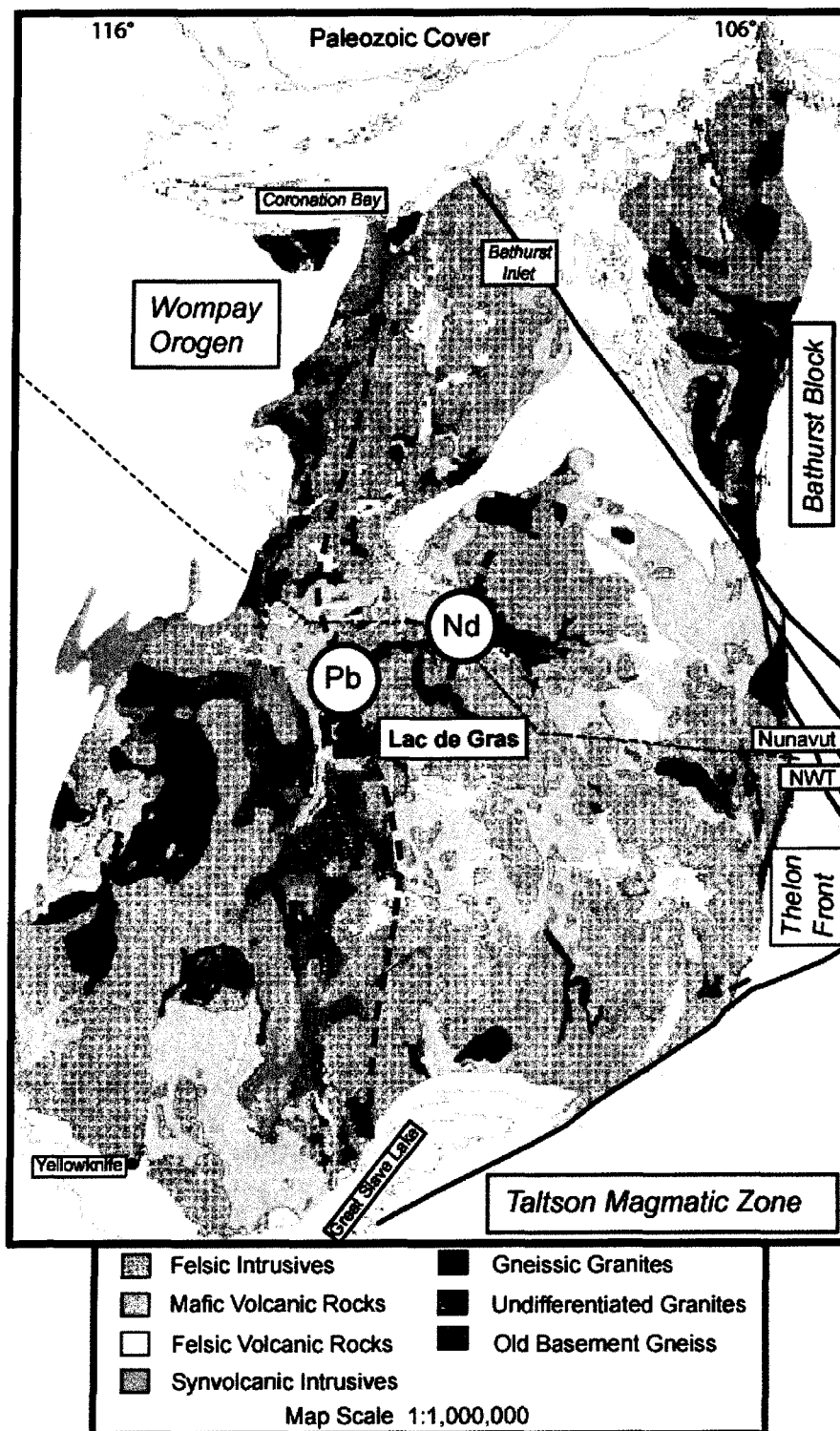


Figure 2.1. Map showing the generalized geology of the Slave craton, the Pb isotopic boundary of Thorpe et al. (1992) and the Nd isotopic boundary of Davis and Hegner (1992). Map is from Hoffman and Hall (1993).

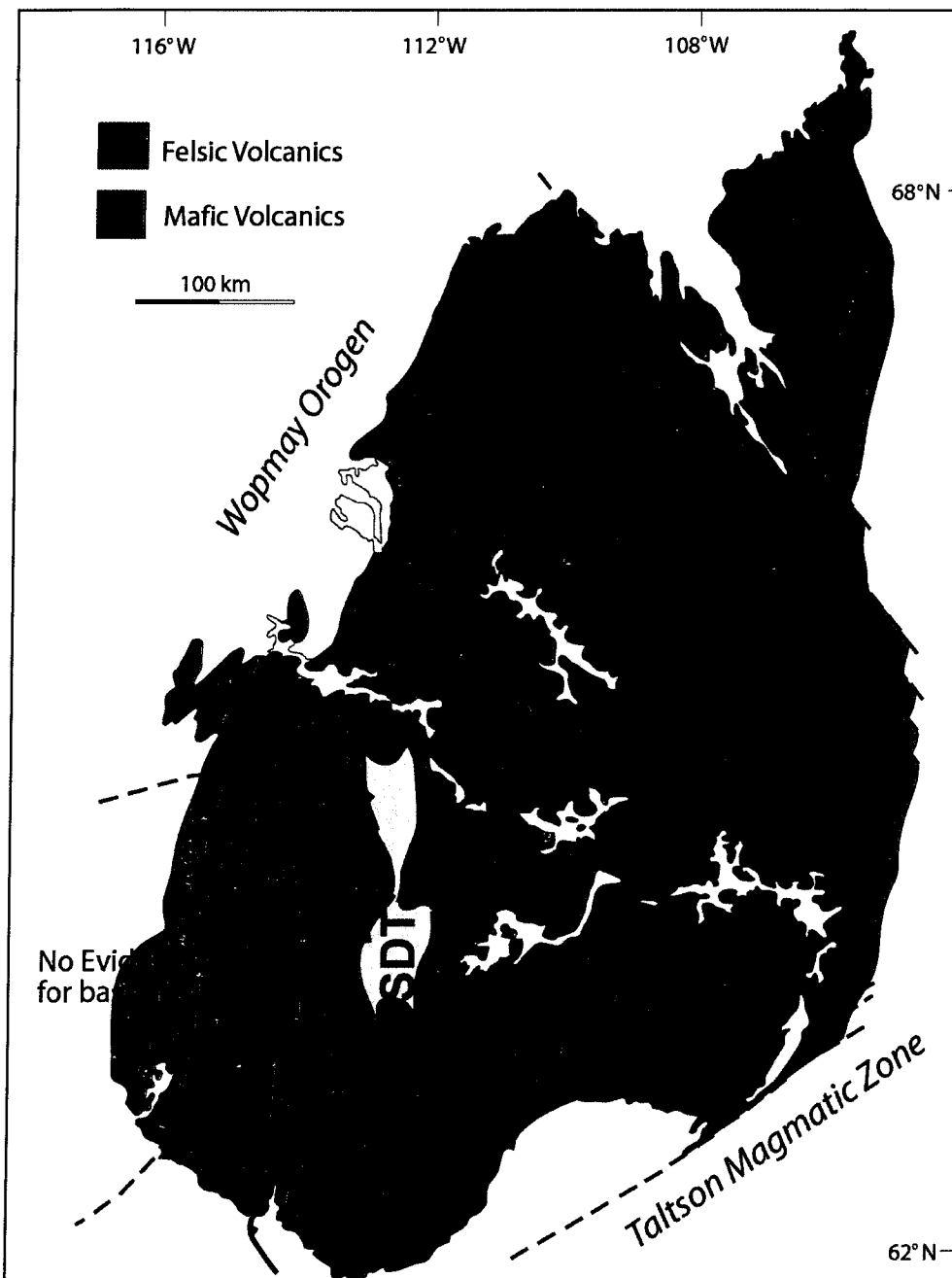


Figure 2.2. Map illustrating the boundaries of the Anton Terrane, the Sleepy Dragon Terrane (SDT), the Contwoyto Terrane and the Hackett River Arc Terrane. Map from Kusky (1989).

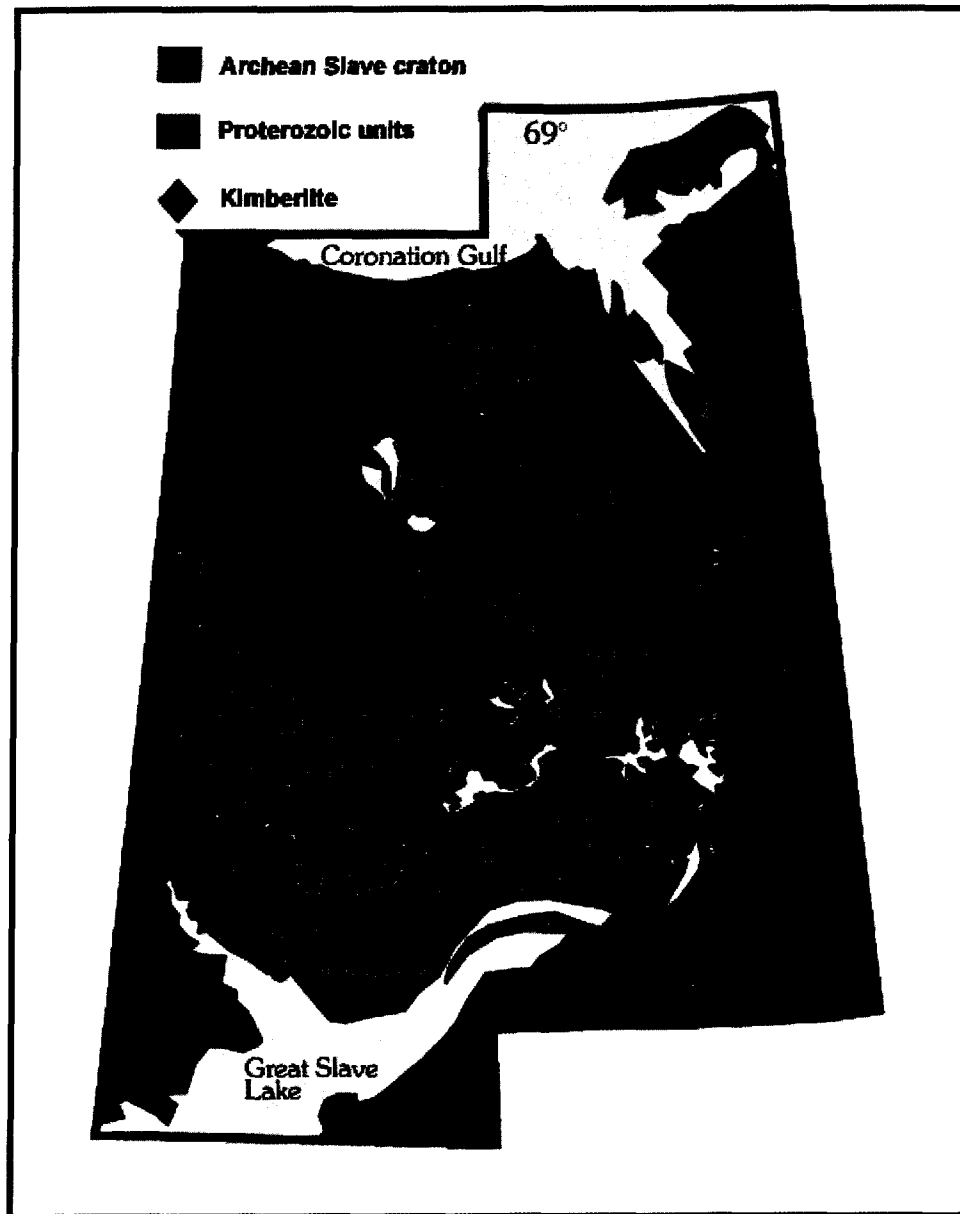


Figure 2.3. Subdivisions of the lithospheric domains of the Slave, based on differing compositions, mantle stratigraphy and thermal state. Map from Grütter et al. (1999). Southeast and southwest subdivisions are from Carbno and Canil (2002).

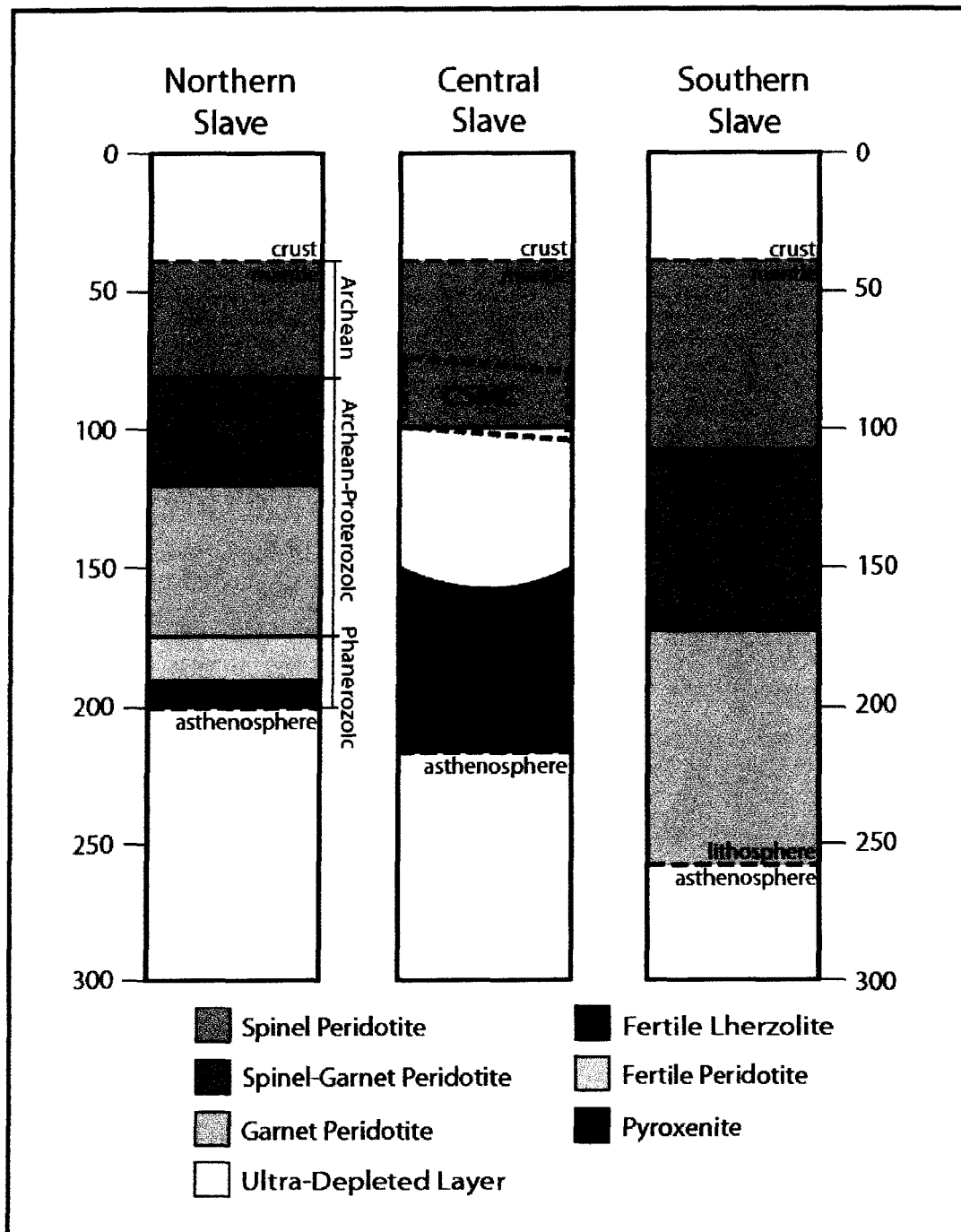


Figure 2.4. Mantle cross-section across the Slave craton. The depth of the crust-mantle boundary and the depth and extent of the CSMC (Central Slave Mantle Conductor) are estimated from the magnetotellurics data of Jones and Craven (2004). Depths from the southern, central and northern Slave are inferred from the data of Kopylova and Caro (2004), O'Reilly et al. (2001) and Kopylova et al. (1999b). Depths to the lithosphere-asthenosphere boundary represent maximum estimates.

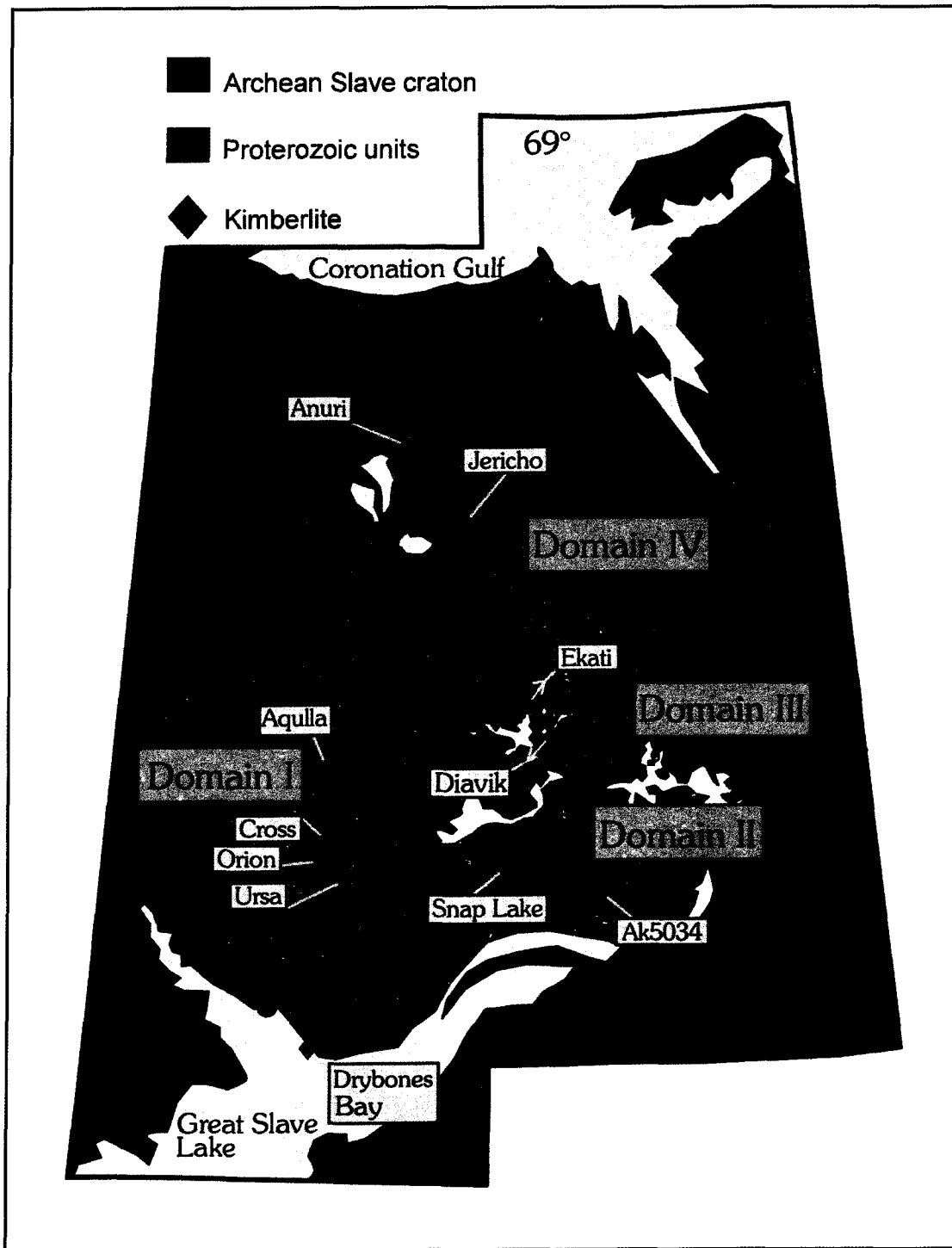


Figure 2.5. The distribution of kimberlites and subdivisions based on kimberlite emplacement ages of the Slave craton (after Heaman et al., 2003).

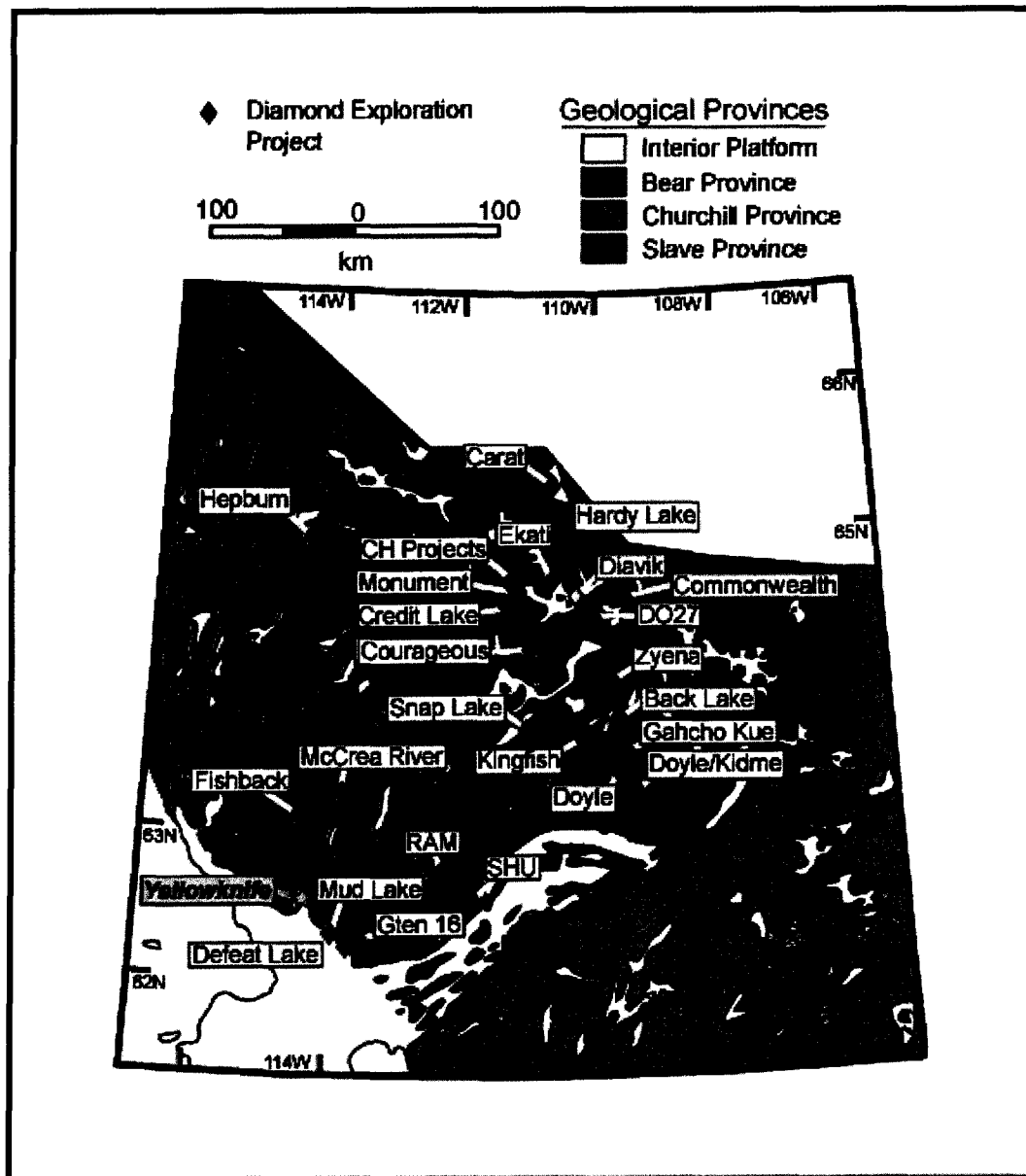


Figure 2.6. Map of the central and southern Slave domains in the Northwest Territories showing the location of diamond exploration projects. Map after Carins and Goff (2005).

Chapter 3: Diamonds and their Mineral Inclusions from the Diavik Diamond Mine, Northwest Territories, Canada

3.1. Introduction

Mineral inclusions in diamonds are generally regarded as representing pristine samples of the Earth's mantle, as they are protected from metasomatic influences and re-equilibration with the surrounding environment inside the diamond. As such, they have commonly been used as a means to investigate the lithospheric mantle. The majority of inclusion-based studies have been performed on diamonds from the Kalahari and Siberian cratons. However, in the early 1990's, diamondiferous kimberlites were discovered on the Slave craton and this has since led to the availability of inclusion-bearing diamond samples from Canada. Studies by Chinn et al. (1998), Stachel et al. (2003) and Tappert et al. (2004) have shown that diamonds from the Ekati kimberlites in the central Slave craton (Figure 3.1) were dominantly derived from peridotitic sources with a minor eclogitic component. An investigation of the diamonds from the Snap Lake/King Lake kimberlite dyke, in the southern part of the Slave Craton, also yielded an abundance of peridotitic inclusions (Pokhilenko et al., 2001 and 2004). However, a study from pipe DO27 (Davies et al., 1999), located in the Tli Kwi Cho kimberlite cluster on the south-eastern side of Lac de Gras, revealed a dominance of eclogitic diamonds (~50%) and a significant number of "ultradeep" inclusions (~25%) with a sublithospheric origin. A later study by Davies et al. (2004a) on microdiamonds from seven kimberlites, from the Lac de Gras region, including DO27, reported similarly high abundances of eclogitic and sublithospheric diamonds. Recently, Stachel et al. (2003) completed a comparison study of major element data for peridotitic inclusions from the Slave and Kaapvaal cratons, from which they concluded that the diamondiferous subcratonic lithospheric mantle beneath the Slave was chemically less depleted.

The present paper examines 100 inclusion-bearing diamonds from the A154 South pipe of the Diavik Diamond Mine. The Diavik Mine is located 295 km

northeast of Yellowknife, NWT on the eastern end of Lac de Gras (Figure 3.1, insert). The current Diavik property in the Lac de Gras area was staked in late 1991, during the early stages of the Canadian diamond rush that eventually encompassed much of the Slave Province. The Diavik pipes are located immediately to the east of East Island, on the eastern edge of Lac de Gras, adjacent to the Ekati Island shoreline. The Lac de Gras kimberlite field, which hosts >236 kimberlites (Kjarsgaard, 2001), is part of an assemblage of Archean and Proterozoic rocks of the Slave Province. By the spring of 1995 the current Diavik resource, comprising kimberlites A154 South, A154 North, A418, and A21, had been discovered. As of June 2003, the Diavik project included sixty-three kimberlite occurrences, with approximately 50% of them being diamondiferous (Bryan and Bonner, 2003). The ages of the pipes in the Lac de Gras kimberlite field range from Cretaceous (86Ma) to Eocene (47 Ma) (Heaman et al., 1997). The Diavik pipes have been dated, using Rb-Sr in mica, to obtain isochron ages of pipe emplacement of 55.5 ± 0.5 Ma for A154 South, 56.0 ± 0.7 Ma for A154 North, 55.2 ± 0.3 Ma for A418 and 55.7 ± 2.1 Ma for A21 (Amelin, 1996).

For the A154 South pipe we examined the major and trace element compositions of syngenetic mineral inclusions. Further studies were performed on the host diamonds to determine the carbon isotopic composition ($\delta^{13}\text{C}$) and the nitrogen content and aggregation characteristics. The results of this study will clarify what the principal diamond source rock is in the case of the Diavik mine and these results will be compared to previous inclusion studies from other Slave kimberlites. As well this study will provide additional information regarding the thermal and chemical evolution of the lithospheric mantle beneath the central Slave Craton.

3.2. Analytical Methods

For this study, 100 inclusion-bearing diamonds have been selected from more than 10,000 carats (+9 to -11 and +11 sieve sizes) from the A154 South pipe of the Lac de Gras kimberlites. The diamond characteristics including morphology, colour, surface features and evidence of plastic deformation were documented and are summarized in Table 3.1.

The diamonds were cracked to release the inclusions using a steel crusher. Initially, 157 inclusions were recovered from 100 diamonds, subsequently one inclusion was lost during sample preparation. The inclusion size ranged from 20-375 μm , with an average size of about 70 μm . Three magnesio-chromite “inclusions” were not completely enclosed within the host diamond, which may have allowed for re-equilibration at depth in the mantle, or by metasomatism from the kimberlitic magma upon kimberlite ascent. However, these exposed inclusions showed no compositional differences when compared to inclusions completely encapsulated by the diamond, and have been included within the data set.

The recovered inclusions were embedded in brass rings using Araldite[®] resin and were polished for microprobe analysis on a JOEL 8900 Electron Microprobe at the University of Alberta. An accelerating voltage of 20 kV and a beam current of 20 nA (30 nA for spinels) was used. Natural and synthetic silicate, oxide and metal standards were used. Count times ranged from 20 to 100 seconds for the elemental peaks and 20 to 100 seconds for the background. Between three and five analytical points were measured on each sample and then averaged. Detection limits were less than 200 ppm for all silicates, oxides and metals, excepting TiO_2 (207 ppm) for silicate analyses, TiO_2 (231 ppm), and Cr_2O_3 (643 ppm) for spinel analyses, and Cr (575 ppm) and Zn (257 ppm) for sulphide analyses.

Inclusions from all twelve garnet-bearing diamonds from this study were analyzed to determine selected rare earth element (REE: La, Ce, Nd, Sm, Eu, Dy, Er and Yb) and additional trace element (Ti, Y, Zr and Sr) concentrations using Secondary Ion Mass Spectrometry (SIMS). Measurements were performed on a Cameca IMS 3f Ion Microprobe at Woods Hole Oceanographic Institute. For analysis, the inclusions were coated with a thin layer of gold to obtain electrical conductivity. The samples were bombarded with a beam of negatively charged oxygen ions with a focused spot size (diameter of the primary ion beam) of approximately 20 μm for REE analyses and 3-5 μm for other trace elements. To suppress molecular interferences, an energy offset of 60 V and 90 V for REE and other trace elements, respectively, was applied (Shimizu and Hart, 1982). Elemental abundances were calculated using empirical relationships between concentration and

secondary ion yields for well-established standards (working curves) and normalization to silicon as internal standard. The results were further verified by comparative analyses of secondary mineral standards. Analytical uncertainties based on counting statistics range from 10-25 % (relative) for the REE and 5-15% for other trace elements.

The carbon isotopic composition of the diamonds was determined at the University of Alberta using a Finnigan Mat 252 Mass Spectrometer. For carbon isotopic analysis 0.5-1.5 mg of inclusion-free diamond fragments were combined with 1-2 g of purified copper oxide and combusted for ~12 h at 980°C. The CO₂ gas was extracted under vacuum using nitrogen traps and a mixture of dry ice and ethanol to remove impurities. The data are reported with respect to the Peedee belemnite standard.

The nitrogen concentration and aggregation characteristics of the host diamonds were determined on transparent, inclusion-free cleavage chips by Fourier transform infrared spectroscopy (FTIRS) using a Thermo-Nicolet Fourier Transform Infrared Spectrometer combined with an infrared microscope. Background measurements were performed approximately every three hours. Sample spectra were collected for 200 seconds. A pure Type II diamond spectrum was subtracted, removing the diamond two phonon absorbance, and simultaneously the sample spectrum was converted to absorption coefficient (i.e. normalized to a sample thickness of 1 cm). Spectra were then deconvoluted into A, B and D components using deconvolution software provided by David Fischer (Research Laboratories of the Diamond Trading Company, Maidenhead, UK). The concentrations of nitrogen, in atomic ppm, were calculated from absorption coefficient values at 1282 cm⁻¹ for the A-centre and B-centre, using the factors derived by Boyd et al. (1994) and Boyd et al. (1995). The detection limits were typically on the order of 10-20 ppm and were largely dependent on the quality of the sample. Concentration and aggregation state errors were generally between 10-20% relative.

3.3. Database

A reference database of inclusion analyses from worldwide sources was compared to the results of this study. The database is comprised of published and unpublished analyses referenced in Stachel and Harris (1997) and Stachel et al. (1998a, 2000a). The database was later expanded in Tappert et al. (2004). To this, the results of Davies et al. (2004a and 2004b), Deines & Harris (2004), Appleyard et al. (2004), McKenna et al. (2004), Promprated et al. (2004), Sobolev et al. (2004) and Tappert et al. (2004) have also been added.

3.4. Major Element Compositions

3.4.1. Peridotitic Paragenesis

The major element composition of diamond inclusions from A154 South indicate most diamonds are peridotitic, consisting of 83% of the diamonds from this study (Table 3.1). Chromite and olivine were, by far, the most commonly occurring peridotitic inclusions, followed by garnet, Fe-Ni sulphides and clinopyroxene.

3.4.1.1. *Garnet*

Peridotitic garnets occur in seven A154 South diamonds. Six garnet-bearing diamonds contain nine garnets of harzburgitic composition, while one diamond contains two garnets plotting in the Ca-saturated field in a Ca-Cr diagram, indicative of a lherzolitic paragenesis (Figure 3.2). The garnet inclusions range in Cr₂O₃ content from 7.0 wt% up to relatively high values of 15.7 wt% (Table 3.2). The CaO content ranges from 2.6 wt% to 6.0 wt%, with an average value of 4.2 wt%. Most harzburgitic garnets from the Slave craton are chemically less depleted than the worldwide average plotting close to the lherzolitic trend. The A154 South garnets have slightly lower CaO contents than the average for the Slave, with two garnets showing Ca contents less than 3 wt%. The Mg-number of the garnet inclusions ranged from 86–88, with a mean of 87. This distribution is similar to that observed for other Slave localities, as described by Stachel et al. (2003, their Figure 3).

3.4.1.2. Olivine

Fifty-four olivine inclusions were recovered from thirty-two diamonds. Additionally, one touching olivine-clinopyroxene pair was found. The forsterite contents range from 90.6 to 93.6 and excluding one diamond (ddmi-49a) this range is narrowed to 91.8 to 93.6 (Figure 3.3). These values coincide with the lower half of the Mg-numbers of the worldwide database. The CaO content of the olivine inclusions range from 0.02 to 0.07 wt% (Table 2.2 and Figure 3.3). The compositions of the A154 South olivines are similar to those of the Slave, which completely overlap with the worldwide database. However, the A154 South diamonds show less compositional variation than that seen for the rest of the Slave.

Stachel et al. (2003) noted a chemical distinction between Panda and DO27 olivine inclusions where Panda had high Ni contents and DO27 was low in Ni. This Ni discrepancy was not observed for orthopyroxene inclusions from these localities, which led Stachel et al. (2003) to propose that the low Ni in olivine was reflecting the modal olivine/orthopyroxene ratio of the source regions. In olivine inclusions from A154 South, this Ni discrepancy is not observed (Figure 3.4), as olivine Ni compositions overlap both those of Panda and DO27. No orthopyroxene inclusions were found in this study.

3.4.1.3. Clinopyroxene

Two diamonds were found to contain peridotitic clinopyroxene inclusions, one of which was an olivine-clinopyroxene touching inclusion pair. The distinction between peridotitic and eclogitic clinopyroxene (Figure 3.5) was determined after Meyer (1987) using Na₂O, Al₂O₃, and Cr₂O₃ contents. The clinopyroxene inclusion (ddmi-140) and touching inclusion pair (ddmi-141) had Mg-numbers of 93.8 and 91.2 and Ca-numbers $[100\text{Ca}/[\text{Ca}+\text{Mg}+\text{Fe}^{\text{total}}]]$ of 43.3 and 44.8 (Table 3.2). Both inclusions had similar Cr₂O₃ contents of 1.1 wt%. The Mg-numbers are typical for peridotitic clinopyroxenes but they are slightly more Ca rich than the worldwide average.

3.4.1.4. *Mg-chromite*

Mg-chromite is the most commonly occurring inclusion at A154 South, with fifty-six inclusions recovered from thirty-five diamonds. Some diamonds contained as many as fifteen individual chromite inclusions. One diamond contained a chromite and olivine inclusion pair (see Table 3.2) and another contained a chromite and sulphide inclusion pair (Table 3.3). Fe-contents range from 13.8 to 15.8 wt% ($\text{FeO}_{\text{total}}$). A154 South, along with most of the Slave is characterized by overall high ferric iron in Mg-chromites when compared to worldwide sources (Figure 3.6). The Cr-number [$100\text{Cr}/(\text{Cr}+\text{Al})$] is generally about 87, but reaches up to 91.5. An additional chromite inclusion from an A154 South microdiamond was studied by Davies et al. (2004a) and they report a comparatively low Cr-number of 72. Six diamonds had exposed chromite inclusions on the diamond surface. When analyzed, these inclusions revealed no compositional differences (Figure 3.6) when compared to true inclusions that were completely enclosed within the same diamond, which may indicate diamond breakage during production, rather than prior to, or during, kimberlite eruption.

3.4.1.5. *Fe-Ni Sulphides*

Eight diamonds were found to contain peridotitic Fe-Ni sulphides (Table 3.3). The designation to the peridotitic suite is based on the high Ni contents of the inclusion, but for three diamonds the paragenetic distinction was further confirmed based on the presence of co-existing inclusions of Mg-chromite (ddmi-150), olivine (ddmi-179) and lherzolitic garnet (ddmi-199). The Fe contents of peridotitic sulphides range widely from 23.59 to 47.61 wt% and Ni contents also show a wide range from 9.97 to 55.99 wt%, but were typically on the order of 20 wt% (Figure 3.7). Cu is present in these inclusions in relatively minor amounts (0.2 to 1.99 wt%), as is Co (0.37 to 0.96 wt%) and Cr (≤ 0.06 to 0.68 wt%).

3.4.2. Eclogitic Paragenesis

Eclogitic inclusions were found in 12 diamonds which contained sulphide (six diamonds), garnet (three), clinopyroxene (two) and “coesite” (one).

3.4.2.1. Garnet

Seven garnet inclusions, released from three diamonds, plot within the eclogitic field, having Cr_2O_3 contents of less than 2 wt% (Gurney, 1984). Two diamonds (ddmi-166 and ddmi-208) contained >10 individual garnet inclusions per stone. No significant compositional variations were found to exist between garnets from the same stone. The Mg-number of the eclogitic garnets varies from 63.2 to 69.5 and the CaO content from 13.7 to 14.6 wt%. These values fall towards the upper limit of the worldwide database and existing data for the Slave craton (Figure 3.2). Compositionally, the eclogitic garnets from the A154 South (Table 3.2) range from 0.05 to 0.08 wt% Cr_2O_3 , 0.12 to 0.16 wt% Na_2O and 0.30 to 0.36 wt% TiO_2 .

3.4.2.2. Clinopyroxene

Four eclogitic clinopyroxene inclusions were recovered from two diamonds. The clinopyroxene compositions differ between the two diamonds (ddmi-48 and ddmi-186), but are homogenous within the individual host. Inclusions from one diamond have Mg-numbers of 83 (ddmi-48), while for the other, Mg-numbers of 90 (ddmi-186) are observed. The high Mg-numbers obtained from ddmi-186 are atypical of eclogitic clinopyroxenes, as normal basaltic bulk rock compositions have Mg-numbers closer to 80. The low Mg-number inclusions contained higher CaO contents relative to the high Mg-number group, but were lower in Na_2O and Al_2O_3 (Figure 3.5).

3.4.2.3. SiO_2

A SiO_2 inclusion was found as a single phase inclusion in one diamond (ddmi-193). No visible fractures or alteration were associated with the inclusion, as such the SiO_2 inclusion was likely included as coesite. Analysis of the inclusion revealed no notable elemental impurities.

3.4.2.4. *Fe Sulphides*

Eight eclogitic sulphide inclusions were recovered from six diamonds and were found to be Fe-monosulphides (Table 3.3). Two sulphides (ddmi-37 and ddmi-93) had slightly elevated Cu (~2 wt% and 5 wt%) contents. The Fe contents ranged from approximately 54 to 60 wt%, with minor amounts of Ni (0.35 to 1.6 wt%) and Co (0.17 to 0.37 wt%) and variable amounts of Cu (0.49 to 5.0 wt%).

3.4.3. Uncertain Paragenesis

3.4.3.1. *Diamond*

A colourless octahedral diamond inclusion, showing no surface features or evidence of deformation, was found within a colourless triangular macle (spinel twin) (Figure 3.8). The included diamond was of sufficient size to allow for a comparative carbon isotope and nitrogen concentration and aggregation study to be performed on both the host and included diamond. The host diamond had a $\delta^{13}\text{C}$ value of -4.6 ‰, while the included diamond was isotopically lighter at -6.1 ‰. The host diamond was a Type IaA diamond with nitrogen concentrations of 863 ppm. The included diamond was also a Type IaA diamond, but had lower nitrogen concentrations of 334 ppm. Diamond inclusions from other Slave localities were reported by Davis et al. (2004a) and they observed inclusions with cubo-octahedral morphologies and variable colours, relative to their host diamond. Diamond can occur as an inclusion in either the peridotitic or eclogitic paragenesis.

3.4.3.2. *Ferropericlase*

Six ferropericlase inclusions were found in three faintly brown diamonds, having either irregular or high resorbed octahedral morphologies. A fourth diamond (ddmi-2) including ferropericlase was found to contain an additional mineral phase, pyrite (Table 3.3), which was determined to be eclogitic based on a very low Ni content. The ferropericlase inclusions are characterized by relatively high Mg numbers (81.3 to 87.0) and high NiO contents (0.98 to 2.03 wt%), when compared to the worldwide database, as shown in Table 3.4 and Figure 3.9. Notable impurities

include Cr₂O₃ (0.36 to 0.60 wt%), Na₂O (0.13 wt% to 0.34 wt%) and MnO (0.15 wt% to 0.22 wt%), which are normal ranges for ferropericlasite inclusions.

The occurrence of ferropericlasite is not restricted to a lower mantle origin as the ferropericlasite stability field also extends into the upper mantle (Stachel et al., 2000b; Brey et al., 2004). In the absence of additional inclusion phases such as tetragonal almandine pyrope phase (TAPP), MgSi-perovskite, CaSi-perovskite or SiO₂, which would indicate formation in lower mantle, the paragenetic designation of the four diamonds containing ferropericlasite remains uncertain.

3.5. Trace Element Compositions

Nine peridotitic garnets and three eclogitic garnets have been analyzed for rare earth elements (REE), Ti, Zr, Y and Sr. Eight of the peridotitic garnets belong to the harzburgitic suite and one to the lherzolitic suite. The rare earth element concentrations are normalized (REE_N) to the C1-chondrite composition of McDonough and Sun (1995).

Six of the harzburgitic garnets are characterized by sinusoidal REE_N patterns with a crest in the light REE (LREE_N) and a trough in the middle REE (MREE_N) (Figure 3.10). Such patterns are typical for harzburgitic garnets worldwide (see Stachel et al., 2004, for a recent review). Two harzburgitic garnets released from the same diamond (ddmi-216) have REE_N patterns that are only slightly sinusoidal, having depleted LREE_N, a positive slope in the LREE_N and enrichment in the MREE_N and HREE_N (Figure 3.9), with a peak at Eu. Such “normal” REE_N patterns are more commonly observed for lherzolitic garnets. The two ddmi-216 garnets have low Sr contents of <2 ppm whereas the remaining harzburgitic garnets have Sr contents that range from 3 ppm to 11 ppm with an average of 5 ppm. The Y contents of the harzburgitic garnets range between 1 ppm and 7 ppm with an average of 3 ppm, values which are typical for harzburgitic garnets worldwide. The Zr contents for the harzburgitic garnets range from 5 ppm to 66 ppm with an average of 35 ppm, which is double the worldwide average. The lherzolitic garnet has Sr and Zr of 1 ppm and 9 ppm, respectively, which are similar to lherzolitic garnets worldwide. However, the lherzolitic garnets have low Y and Ti contents at 1 ppm and 473 ppm.

The three A154 South eclogitic garnets analyzed have REE_N patterns that are similar to other eclogitic garnets worldwide, but the MREE and HREE concentrations are considerably lower (Figure 3.11). One eclogitic garnet inclusion (ddmi-205) has a positive Eu anomaly, another (ddmi-208) shows a negative anomaly. In the absence of Gd data the significance of these small anomalies cannot be assessed and may relate to analytical uncertainty in the determination of Sm and Eu. Eclogitic garnet inclusions typically have REE_N patterns with LREE_N about 1 times and HREE_N at about 30 times chondritic abundances (Stachel et al., 2004). The A154 South eclogitic garnets have about 0.5 times chondritic abundances of LREE_N and 5 times chondritic abundances of HREE_N. The trace elements Ti, Y and Zr of the A154 South eclogitic garnets also show lower concentrations than those observed for eclogitic garnets worldwide. The Ti contents range from 1568 to 2169 ppm with an average value of 1920 ppm, which is less than half the worldwide average of 4330 ppm. Similarly, the Y (11 to 12 ppm) and the Zr contents (8 to 27 ppm) are considerably lower than the worldwide averages of 38 and 53 ppm, respectively. Sr contents are comparable to those observed worldwide and range from 3 to 6 ppm. Beard et al. (1996) have suggested that eclogitic garnets with high CaO and the low REE contents may be related to a protolith having a significant plagioclase or clinopyroxene cumulate component.

3.6. Geothermometry

The composition (see Table 3.2) of two olivine-garnet pairs (ddmi-154 and ddmi-167) was used to estimate the temperatures of diamond formation using the Fe-Mg exchange between these two minerals (O'Neill and Wood, 1979; O'Neill, 1980). Temperatures of 1220 and 1230°C were calculated at an assumed pressure of 5 GPa (Figure 3.12). Additionally, one olivine-magnesio-chromite inclusion (Table 3.2) pair yielded a temperature of 1170°C based on the Fe-Mg exchange thermometer of O'Neill and Wall (1987). The non-touching inclusion pairs have an average temperature of 1200°C, which is slightly higher than the average garnet-olivine temperatures of 1180°C from DO27 (Davies et al., 2004a), 1180°C from Ekati (Chinn

et al., 1998), 1140°C from Panda (Stachel et al., 2003), and 1130°C from Snap Lake (calculated by Stachel et al., 2003, using the data of Pokhilenko et al., 2001).

The inclusion temperatures for the 56 magnesio-chromite inclusions analyzed in this study produced an uncommonly low range of values from 790 to 1020°C, yielding an average temperature of 940°C, using the empirical thermometer of Ryan et al. (1996) for Zn in spinel. A huge discrepancy (250°C), well beyond the errors of both thermometers, was observed for diamond ddmi-183 where temperatures of 920°C (Zn in spinel) and 1170°C (olivine-magnesio-chromite inclusion pair) were obtained for the same diamond. Possible explanations for this variance include that possibility that the chromites are sourced from a zone in the mantle that has a low modal abundance of olivine, such that the assumption that there is an inexhaustible reservoir of olivine does not apply. Another possibility is that the assumed constant Zn composition of mantle olivine of $\sim 52 \pm 14$ ppm from Ryan et al. (1996) does not hold true for Diavik.

3.7. Physical and Geochemical Characteristics of the Host Diamonds

3.7.1. Morphology and Colour

Four separate population surveys were conducted on Diavik diamonds in the +9 to -11 and the +11 size range, with samples ranging from 520 to 1020 stones. These surveys characterized the diamonds based on colour, morphology, presence/absence of coating and inclusion content. Diamond descriptions and preliminary classification of the included minerals was conducted based on the methodology outlined in Robinson (1979). The Diavik population in the +9 to -11 and the +11 size range is dominated by resorbed forms, particularly resorbed octahedral or dodecahedral morphologies. The Diavik production also contains an unusually high percentage ($\sim 12\%$) of diamonds having cubic morphologies, when compared to the estimate of $<1\%$ cubic diamonds (Harris, 1992) for southern African diamonds. These cubic stones are dominantly re-entrant cubes, but some flat-faced cubes and rounded cubes were also observed. Relatively sharp-edged octahedra, spinel twin triangular macles, and aggregates of three or more stones were also present. A high proportion of diamond fragments is attributed to breakage during production. It was noted that with increasing diamond size (1, 3 and 5 carat stones),

the quality of the production greatly improved, yielding more octahedral stones at the expense of cubes and dodecahedral morphologies.

The dominant body colour of diamonds from Diavik is colourless. Brown stones are relatively abundant and yellow, pink and grey stones were observed, but are rare. In addition, fibrous coats, ranging from thin, nearly transparent layers to partial or complete opaque cover of the diamond, occur throughout all size ranges. The fibrous coats range from grey to dark grey-black and in several cases, this coating is almost completely covered with triangular etch pits.

The suite of 100 inclusion-bearing diamonds for this study is comprised of octahedra (39%), dodecahedroids (23%), irregular/fragments (21%), macles (10%) and aggregates (7%). The sample suite is dominated by brown stones (58%), followed by colourless (34%), pink (4%), yellow (2%) and grey (2%) stones. Plastic deformation lines were observed, but were not common. However, the high proportion of brown diamonds indicates the plastic deformation has occurred (Robinson et al., 1979).

3.7.2. Carbon Isotopes

The carbon isotopic values ($\delta^{13}\text{C}$) of the 100 A154 South diamonds, summarized in Table 3.1 and shown in Figure 3.13, ranged from -10.5‰ to +0.7‰, with an average value of -5.1‰. The observed mode of -5.0‰ is consistent with that observed for diamonds worldwide of both the eclogitic and peridotitic suite. When a few outliers are removed, a narrow distribution with 94% of the diamonds having $\delta^{13}\text{C}$ values between -6.3‰ and -4.0‰ becomes apparent. Such a narrow distribution of carbon isotopic values is rarely observed for diamonds from other localities (Kirkley et al., 1991). The two isotopically heaviest values are from ferropericlase-bearing diamonds, while the two isotopically lightest values represent diamonds with eclogitic inclusions. There is no correlation between the carbon isotopic composition of the diamonds and the inclusion chemistry as was shown e.g. for Snap Lake by Pokhilenko et al. (2004). No correlations were observed with respect to diamond colour, morphology, or nitrogen content.

3.7.3. Nitrogen Contents and Aggregation Levels

Nitrogen is a common substitutional impurity in diamond and is present in most natural diamonds. The nitrogen content has been used to classify diamonds into two groups: Type I diamonds where nitrogen is present and Type II diamonds where nitrogen is absent, i.e., below the level of detection (approximately 10 ppm) for infrared spectroscopy (Gurney, 1989). These classifications can be further subdivided on the basis of the nitrogen aggregation state of the diamond into: Type *Ib* where diamonds contain nitrogen in a single substitution and Type *Ia* diamonds where nitrogen is aggregated in the form of pairs (Type *IaA*), rings of four nitrogens surrounding a vacancy (Type *IaB*) or both (Type *IaAB*) (Evans and Qi, 1982). Only in rare cases does nitrogen occur as a single substitutional atom, as the aggregation into pairs occurs rapidly at mantle temperatures (Evans and Harris, 1989 and references therein). The aggregation from Type *IaA* to Type *IaB* occurs at a much slower rate. The experimentally determined kinetics of the nitrogen aggregation (Evans and Harris, 1989; Taylor et al., 1990) can be used to constrain either the residence time or the time averaged residence temperature of the diamond in the mantle and is useful in characterizing diamond population groups.

The concentration and aggregation of the nitrogen impurities in the A154 South diamonds was determined using micro-FTIR spectroscopy (Table 3.1 and Figure 3.14). The nitrogen contents range typically range from <10 ppm (detection limit) to ~1200 ppm. Two Type *IaA* diamonds were found to have slightly elevated nitrogen contents at ~1800 ppm and two yellow, unresorbed octahedral Type *IaAB* diamonds, each containing >10 eclogitic garnet inclusions, had elevated nitrogen contents of 1800 and 3800 ppm. The nitrogen aggregation levels of the A154 South diamonds reflect predominantly (65%) poorly aggregated Type *IaA* diamonds (<10% B-centre aggregation), but also range to fully aggregated Type *IaB* (>90% B-centre aggregation) diamonds (5%). The intermediate Type *IaAB* diamonds comprise 25% of the population, with the remaining 5% being Type II nitrogen-free diamonds. When all diamonds showing evidence of plastic deformation (brown body colour or presence of deformation lines) are removed, this scatter greatly reduced, with all but

seven of the remaining diamonds having less than 25% of the nitrogen aggregated to B-centres.

3.8. Discussion and Conclusions

3.8.1. The Diamond Source Region at A154 South

The relatively high CaO content of the harzburgitic garnets and the comparatively low Mg numbers of the olivine inclusions indicate that diamond formation at A154 South occurred in a moderately depleted peridotitic environment. This is in agreement with that observed for the nearby Ekati (Chinn et al., 1998; Stachel et al., 2003; Tappert et al., 2004) and the Snap Lake/King Lake (Pokhilenko et al., 2004; Promprated et al., 2004) kimberlites, which are also dominated by peridotitic diamond populations. Pipe DO27 in the Lac de Gras area appears to be an exception in the central Slave as eclogitic diamonds dominate (Davies et al., 1999 and 2004a).

Trace element data from this study of A154 South, as well as Panda (Tappert et al., 2004) and Snap Lake/King Lake (Promprated et al., 2004) indicate that the diamond source rock has experienced an early depletion event, followed by a later metasomatic enrichment event characterized by high LREE/HREE in the re-enriching agent. The A154 South harzburgitic garnets typically have sinusoidal REE_N patterns, while the lherzolitic garnet has a normal REE_N pattern, consistent with worldwide data (Stachel et al., 2004). Two harzburgitic garnet inclusions from diamond ddmi-216 have low Sr contents and normal REE_N patterns more typical of lherzolitic garnets. Stachel et al. (2004) attribute the transition from sinusoidal towards more normal REE_N patterns in harzburgitic garnets to be a result of a shift from fluid dominated to melt dominated metasomatism (Figure 3.15). Stachel et al. (2004) note that harzburgitic garnets that have undergone “lherzolitic style” metasomatism (i.e., showing normal REE_N patterns) also have refertilized major element compositions, as seen by the low molar Cr-numbers [$100\text{Cr}/(\text{Cr} + \text{Al})$] of less than 30. This observation holds true for the two harzburgitic garnets with normal REE_N patterns released from diamond ddmi-216 which have Cr-numbers of less than 25.

Xenolith and xenocryst studies (Griffin et al., 1999b; Pearson et al., 1999; MacKenzie and Canil, 1999; Doyle et al., 2003; Grütter and Moore, 2003; Menzies et al., 2004) from the Lac de Gras area also agree with the inclusion data from this study, indicating a moderately-depleted, dominantly harzburgitic source rock composition. These studies also indicate that the lithosphere in the central Slave craton is stratified, consisting of two layers. The xenolith studies investigating the thermal regime of the lithosphere at Lac de Gras have revealed that the shallow lithospheric layer has a lower geothermal gradient corresponding to 35-37 mW/m² surface heat flow while the deeper layer is higher at 40 mW/m². Stachel et al. (2003) obtained a geothermal gradient of 37 mW/m² from two touching garnet-orthopyroxene inclusion pairs whereas a higher geotherm of 40 mW/m² was obtained for two non-touching garnet-orthopyroxene pairs from Snap Lake (calculated by Stachel et al., 2003, using the data of Pokhilenko et al., 2001). The A154 South diamonds have an average estimated formation temperature of ~1200°C (Figure 3.12), as determined from non-touching inclusion pairs. These temperatures are slightly higher than the average of 1180°C from Ekati (Chinn et al., 1998) and from DO27 (Davies et al., 2004a), 1140°C from Panda (Stachel et al., 2003), and 1130°C from Snap Lake (calculated by Stachel et al., 2003, using the data of Pokhilenko et al., 2001). These temperatures correspond to formation along a 40-42 mW/m² geotherm, which is consistent with estimates worldwide (Stachel et al., 2003, and references therein).

Nitrogen aggregation can be used to constrain either the residence time or the residence temperature of diamonds in the mantle. Time averaged mantle residence temperature estimates are relatively insensitive to the choice of mantle residence time. Under normal geothermal gradients, after 200 to 2000 Ma in the mantle a diamond will be a Type IaB diamond, with all of its nitrogen aggregated into the B-centre (Gurney, 1989). A diamond may retain nitrogen in the non-aggregated, single substitution state (Type *Ib*) only if the residence time at normal mantle temperatures, after crystallization but prior to kimberlitic eruption, was less than 50 years (Gurney, 1989). It has been noted that plastic deformation enhances the aggregation of nitrogen in diamond (Evans, 1992). When diamonds showing evidence of plastic

deformation, recognized by brown body colour or the occurrence of plastic deformation lines on the diamond surface, are excluded the overall number of diamonds with higher aggregation levels (Type IaAB or Type IaB) is significantly reduced. The high proportion of diamonds with poorly aggregated nitrogen is not unique to A154 South but appears to be common feature in the central Slave, being recognized at Ekati (Westerlund et al., 2001; Stachel et al., 2003; Westerlund, 2003a; Tappert et al., 2004) and DO27 (Davies et al., 1999; Davies et al., 2004a).

Low nitrogen aggregation levels as observed at A154 South have conventionally been taken to indicate a young age for the diamond population. Alternatively, if the diamonds are older, the abundance of Type IaA diamonds may indicate storage in the mantle at low temperatures, approximately between 1000-1100°C (Figure 3.14). To date, the only published diamond inclusion age from A154 is a Re-Os sulphide inclusion age from an eclogitic diamond which yielded a Re-depletion age of 3.03 ± 0.18 Ga and a model age of 3.35 ± 0.40 Ga (Pearson et al., 2002). Additionally, peridotitic sulphide inclusions from a Panda diamond yielded a similar isochron age 3.41 ± 0.28 Ga (Westerlund et al., 2003b). Combining old inclusion ages and low nitrogen aggregation states would argue for shallow storage in the mantle at lower temperatures.

A possible sub-population is indicated by two A154 South diamonds (ddmi-166 and ddmi-208). Both diamonds are unresorbed octahedra, each containing >10 eclogitic garnet inclusions and are the only yellow stones in this study. They have elevated nitrogen contents of 1800 and 3800 ppm and similar aggregation levels of 34 and 36 %B, respectively. Additionally, some of the A154 South diamonds have very high aggregation levels (Figure 3.14), which for the typical diamond formation temperatures calculated for the Slave (Figure 3.12), would yield unreasonably long residence times in the mantle. This suggests that these diamonds have experienced more intense plastic deformation or were exposed to higher temperature conditions, perhaps forming at greater depth, or proximal to a magmatic intrusion.

The diamond formation temperatures for A154 South diamonds (~1200°C based on non-touching inclusions) are inconsistent with the observed low temperatures of diamond residence in the mantle obtained from the nitrogen

aggregation levels. However, these aggregation temperature estimations are in agreement with touching inclusion pairs from Panda (see Stachel et al., 2003). To explain the observed nitrogen aggregation distribution, Stachel et al. (2003) and Tappert et al. (2004) have proposed rapid cooling of about 100-150°C of the diamond source region following diamond formation. They propose that the elevated temperatures (40-42 mW/m² geotherm) during diamond formation represent only a short-lived event, possibly related to magmatic intrusions, and that during the Archean a stable 35-37mW/m² geotherm was already established. Such a model is in agreement with the data from A154 South which would require cooling of the diamond source region on the order of 100-200°C to reconcile inclusion and nitrogen based thermometry.

Further information regarding the diamond source region can be gained from an investigation into the carbon isotopic composition of the diamonds. The bulk of the A154 South diamonds (94%) fall within a narrow range of typical mantle values of -6.3‰ and -4.0‰, irrespective of paragenesis. Such a narrow distribution is uncommon for most diamond localities worldwide (with few exception such as the Akwatia diamonds in Ghana, Stachel et al., 1997) but appears to be a commonality in the Slave craton with Snap Lake (Pokhilenko et al., 2004) and Panda (Westerlund et al., 2001 and 2003a) each having a limited range in $\delta^{13}\text{C}$ values. In a study of diamonds from the Ekati pipes Misery, Jay and Sable, Chinn et al. (1998) found a similarly narrow distribution for peridotitic diamonds, but eclogitic diamonds from these locations covered a wide range of isotopically lighter compositions (up to -27.4‰). At DO27 a large range in $\delta^{13}\text{C}$ values was observed (-35.8‰ to +0.2‰) reflecting the dominance of eclogitic diamonds (Davies et al., 2004). The narrow distribution seen at A154 South may be suggestive of diamond formation, irrespective of paragenesis, from an unfractionated fluid/melt carrying primordial carbon.

3.8.2. Ferropericlae-bearing Diamonds: An Uncertain Paragenesis

The presence of lower mantle diamonds in the Lac de Gras area has been identified by Davies et al. (1999 and 2004a) and Tappert et al. (2004) based on the assemblage of ferropericlae inclusions coexisting with MgSiO₃, CaSiO₃, and/or SiO₂. Four A154 South diamonds contained inclusions of ferropericlae but lacked

sufficient inclusions pairs (with pyrite present as the only co-existing inclusion pair) to confidently assign them to a lower mantle paragenesis. More than half of the ultradeep microdiamonds from the study of Davies et al. (2004a) were assigned a lower mantle origin based on inclusions of ferropericlase alone. However, the occurrence of ferropericlase as an inclusion in diamond is not conclusive evidence for a lower mantle origin (Stachel et al., 1998 and 2000b; Brey et al., 2004).

Ferropericlase can form as an inclusion in diamond in the upper mantle if Si activity and fO_2 are sufficiently low, conditions that would be met in a reduced dunitic source (Stachel et al., 1998). Hence, besides the lower mantle, ferropericlase-bearing diamonds at Lac de Gras could also be sourced in lithospheric dunites identified in several xenolith studies in the central Slave (Griffin et al., 1999a; Pearson et al., 1999; O'Reilly et al., 2001; Menzies et al., 2004).

It has been noted by Hutchinson et al. (1999) that diamonds from the lower mantle typically have irregular or dodecahedral morphologies and are dominantly Type II diamonds, or when nitrogen is present it is highly aggregated >94 %B. This observation holds true for the lower mantle diamonds from Panda, where all lower mantle diamonds were Type II diamonds having irregular morphologies. While Davies et al. (2004) reported that >80% of the ferropericlase-bearing diamonds from DO27 were Type II diamonds, resorbed octahedral morphologies were observed. The ferropericlase-bearing diamonds from A154 South had either resorbed octahedral or irregular morphologies. Two of the A154 South ferropericlase-bearing diamonds were Type II diamonds, while the other two were highly aggregated (59 and 82 %B) Type IaAB diamonds that had low nitrogen concentrations (<110 ppm). In addition to the lack of lower mantle inclusion pairs, the observed octahedral morphologies and nitrogen content may provide supporting evidence of a lithospheric origin for the ferropericlase-bearing diamonds.

If diamond ddmi-2 containing ferropericlase and a sulphide of eclogitic paragenesis was in fact formed in the lower mantle, this basaltic association would be in agreement with the observations of Stachel et al. (2000a and 2000b) where the bulk of diamonds from the asthenosphere/transition zone (majoritic garnet-bearing) and some lower mantle diamonds (Eu anomalies, high LREE and Sr contents) are linked

to some form of recycled oceanic crust. While the carbon isotope distribution of the A154 South diamonds is, on a whole, exceptionally narrow, the ferropericlasite-bearing diamonds typically are outliers of this distribution. The ferropericlasite-bearing diamonds are isotopically heavier (average -2.8‰) with two diamonds ddmi-114 and ddmi-2 having $\delta^{13}\text{C}$ values of -2.9 and +0.7‰, respectively. These heavy carbon isotopic compositions may indicate a genetic link to subducted marine carbonate (Kirkley et al., 1991), which has $\delta^{13}\text{C}$ values near zero, supporting models involving subducted oceanic crust.

3.8.3. Models for Diamond Sources in the Slave

As more age determinations become available for the subcratonic lithospheric mantle beneath the central Slave (Aulbach et al., 2001; Pearson et al., 2002; Gurney et al., 2003; Westerlund et al., 2003b; Aulbach et al., 2004) they provide mounting evidence for the existence of an Archean (>2.6 Ga) diamondiferous mantle keel.

A two-layered lithosphere has been proposed for the central Slave craton (Griffin et al., 1999a; Griffin et al., 1999b; Kopylova et al., 1999b; Pearson et al., 1999; O'Reilly et al., 2001, Carbno and Canil, 2002; Kopylova and Caro, 2004; Menzies et al., 2004) which consists of a shallow (<140-150 km) ultra-depleted olivine-rich layer and a deeper, less-depleted layer. Griffin et al. (1999a) proposed that the deeper layer represents accreted plume material and that this plume also provided the transport mechanism for the lower mantle diamonds in the central Slave (Davies et al., 2004a). However, the high Cr contents of the peridotitic garnet inclusions from Ekati, DO27, Snap Lake/King Lake, and those of this study at A154 South, cannot be explained by the model of Griffin et al. (1999a), which led Stachel et al. (2003) to propose an alternative model. Stachel et al. (2003) embrace the model of Kesson and Ringwood (1989), whereby both of the lithospheric layers in the Slave represent depleted, former oceanic lithosphere that was imbricated beneath the Slave during the subduction of hot, young slabs during the Archean. Stachel et al. (2003), cited experimental evidence in support of their model which shows that the bulk rock high Cr/Al ratio, implied by the high Cr garnets, could only be achieved by partial melting at relatively low pressures, in the spinel stability field. In their model,

Stachel et al. (2003) attribute the less depleted nature of the lower lithospheric layer to be the result of later metasomatic re-enrichment. The results of this study of the A154 South diamonds are more consistent with the latter model based on the high Cr contents observed in the harzburgitic garnets (Figure 3.2), as well as indications of metasomatic influences seen in the REE data.

References:

- Amelin, Y. 1996. Report on Rb-Sr and U-Pb study of kimberlite samples VR44444A through VR44465A. Confidential Reports for Kennecott Canada Inc., 7. As cited in Graham et al. (1999).
- Appleyard, C.M., Viljoen, K.S., and Dobbe, R. 2004. A study of eclogitic diamonds and their inclusions from the Finsch kimberlite pipe, South Africa. *Lithos*, 313-332.
- Aulbach, S., Griffin, W.L., Pearson, N.J., O'Reilly, S.Y., Doyle, B.J., and Kivi, K. 2001. Re-Os isotope evidence for Meso-Archaean mantle beneath 2.7 Ga Contwoyto Terrane, Slave Craton, Canada: Implications for the tectonic history of the Slave Craton. The Slave-Kapvaal Workshop, Merrickville, Ontario, Extended Abstracts, 5p (CD, not paginated).
- Aulbach, S., Griffin, W.L., Pearson, N.J., O'Reilly, S.Y., Kivi, K., and Doyle, B.J. 2004. Constraints on mantle formation and evolution from HSE abundances and Re-Os isotope systematics of sulfide inclusions in mantle xenocrysts. *Chemical Geology*, 208, 61-88.
- Beard, B.L., Fraracci, K.N., Taylor, L.A., Snyder, G.A., Clayton, R.A., Mayeda, T.K., and Sobolev, N.V. 1996. Petrography and geochemistry of eclogites from the Mir kimberlite, Yakutia, Russia. *Contributions to Mineralogy and Petrology*, 125, 293-310.
- Bleeker, W., and Davis, W.J. 1999b. Time and plutonism, deformation, and metamorphism in the Yellowknife Domain, Slave Province, Canada. *Canadian Journal of Earth Sciences*, 36, 1169-1187.
- Boyd, S.R., Kiflawi, I., and Woods, G.S. 1994. The relationship between infrared absorption and the A defect concentration in diamond. *Philosophical Magazine B*, 69, 1149-1153.
- Boyd, S.R., Kiflawi, I., and Woods, G.S. 1995. Infrared absorption by the B nitrogen aggregate in diamond. *Philosophical Magazine B*, 72, 351-361.
- Brey, G.P., Bulatov, V., Girnis, A., Harris, J.W., and Stachel, T. 2004. Ferropericlasite - a lower mantle phase in the upper mantle. *Lithos*, 77, 655-663.
- Bryan, D., and Bonner, R. 2003. The Diavik Diamond Mine, Lac de Gras, Northwest Territories, Canada. In: VIIIth International Kimberlite Conference, Slave Province and Northern Alberta Field Trip Guidebook, 61-65.

- Carbno, G.B., and Canil, D. 2002. Mantle structure beneath the SW Slave craton, Canada: constraints from garnet geochemistry in the Drybones Bay kimberlite. *Journal of Petrology*, 43, 129-142.
- Chinn, I.L., Gurney, J.J., and Kyser, K.T. 1998. Diamonds and mineral inclusions from the NWT, Canada. VIIth International Kimberlite Conference, Cape Town, Extended Abstracts. Addendum, 4p, not paginated.
- Davies, R.M., Griffin, W.L., Pearson, N.J., Andrew, A.S., Doyle, B.J., and O'Reilly, S.Y. 1999. Diamonds from the Deep: Pipe DO-27, Slave Craton, Canada. In: *Proceedings of the VIIth International Kimberlite Conference, The J.B. Dawson Volume*, Gurney, J.J., Gurney, J.L., Pascoe, M.D., and Richardson, S.H. (eds), Red Roof Design, Cape Town, 148-155.
- Davies, R.M., Griffin, W.L., O'Reilly, S.Y., and Doyle, B.J. 2004a. Mineral inclusions and geochemical characteristics of microdiamonds from the D027, A154, A21, A418, D018, DD17 and Ranch Lake kimberlites at Lac de Gras, Slave Craton, Canada. *Lithos*, 77, 39-55.
- Davies, R.M., Griffin, W.L., O'Reilly, S.Y., and McCandless, T.E. 2004b. Inclusions in diamonds from the K14 and K10 kimberlites, Buffalo Hills, Alberta, Canada: diamond growth in a plume? *Lithos*, 77, 99-111.
- Deines, P. and Harris, J.W. 2004. New insights into the occurrence of C-13-depleted carbon in the mantle from two closely associated kimberlites: Letlhakane and Orapa, Botswana. *Lithos*, 77, 125-142.
- Doyle, P.M., Gurney, J.J., and Le Roex, A. 2003. Xenoliths from the Arnie, Misery and Pigeon kimberlites, Ekati mine, NWT, Canada. VIIIth International Kimberlite Conference, Victoria, Canada, Extended Abstracts, 4p (CD, not paginated).
- Droop, G.T.R. 1987. A general equation for estimating Fe³⁺ concentrations in ferromagnesian silicates and oxides from microprobe analyses, using stoichiometric criteria. *Mineralogical Magazine*, 51, 431-435.
- Evans, T. 1992. Aggregation of nitrogen in diamonds. In: *The properties of natural and synthetic diamond*. Field, J.E., (ed), Academic Press, 259-290.
- Evans, T., and Qi, Z. 1982. The kinetics of nitrogen in diamond. *Proc. Roy. Soc. London*. A381, 159-178.
- Evans, T. and Harris, J. 1989. Nitrogen aggregation, inclusion equilibration temperatures and the age of diamonds. In: *Kimberlites and related rocks*. J. Ross et al. (eds) Blackwell, Carlton, 1001-1006.

- Graham, I., Burgess, J.L., Bryan, D., Ravenscroft, P.J., Thomas, E., Doyle, B.J., Hopkins, R., and Armstrong, K.A. 1999. Exploration History and Geology of the Diavik Kimberlites, Lac de Gras, Northwest Territories, Canada. In: Proceedings of the VIIth International Kimberlite Conference, The J.B. Dawson Volume, Gurney, J.J., Gurney, J.L., Pascoe, M.D., and Richardson, S.H. (eds), Red Roof Design, Cape Town, 262-279.
- Griffin, W.L., Doyle, B.J., Ryan, C.G., Pearson, N.J., O'Reilly, S.Y., Davies, R., Kivi, K., van Acherbergh, E., Natapov, L.M. 1999a. Layered mantle lithosphere in the Lac de Gras area, Slave craton: composition, structure and origin. *Journal of Petrology*, 40, 705– 727.
- Griffin, W.L., Doyle, B.J., Ryan, C.G., Pearson, N.J., O'Reilly, S.Y., Natapov, L., Kivi, K., Kretschmar, U., and Ward, J. 1999b. Lithosphere structure and mantle terranes: Slave craton, Canada. In: Proceedings of the VIIth International Kimberlite Conference, The J.B. Dawson Volume, Gurney, J.J., Gurney, J.L., Pascoe, M.D., and Richardson, S.H. (eds), Red Roof Design, Cape Town,, 299–306.
- Grütter, H.S., Apter, D.B., and Kong, J. 1999. Crust– mantle coupling: evidence from mantle-derived xenocrystic garnets. In: Proceedings of the VIIth International Kimberlite Conference, The J.B. Dawson Volume, Gurney, J.J., Gurney, J.L., Pascoe, M.D., and Richardson, S.H. (eds), Red Roof Design, Cape Town,, 307–313.
- Grütter, H.S. and Moore, R.O. 2003. Pyroxene geotherms revisited- an empirical approach based on Canadian xenoliths. VIIIth International Kimberlite Conference, Victoria, Canada, Extended Abstracts, 4p (CD, not paginated).
- Gurney, J.J. 1989. Diamonds. In: Kimberlites and related rocks. J. Ross et al. (eds) Blackwell, Carlton, 934-965.
- Gurney, J.J., Westerlund, K.J., Carlson, R.W., Shirey, S.B. 2003. Mineral compositions and Re-Os isotope systematics of harzburgitic nodules from the Panda kimberlite, Slave craton. VIIIth International Kimberlite Conference, Victoria, Canada, Extended Abstracts, 3p (CD, not paginated).
- Harris, J.W. 1992. Diamond Geology. In: The properties of natural and synthetic diamond, Field, A.C. (ed), Academic Press, London, 345-393.
- Heaman, L.M., Kjarsgaard, B.A., Creaser, R.A., Cookenboo, H.O., Kretschmar, U., 1997. Multiple episodes of kimberlite magmatism in the Slave Province, North America. *Lithoprobe Workshop Report*, 56, 14-17.

- Kesson, S.E., and Ringwood, A.E. 1989b. Slab mantle interactions 2. The formation of diamonds. *Chemical Geology*, 78, 97-118.
- Kirkley, M.B., Gurney, J.J., Otter, M.L., Hill, S.J., and Daniels, L.R. 1991. The application of C isotope measurements to the identification of the source of C in diamonds: a review. *Applied Geochemistry*, 6, 477-494.
- Kjarsgaard, B.A. 2001. Geology of the Lac de Gras Kimberlite Field, Central Slave Province, Canada. The Slave-Kapvaal Workshop, Merrickville, Ontario, Extended Abstracts, 2p (CD, not paginated).
- Kopylova, M.G., Russel, J.K., and Cookenboo, H. 1999b. Mapping the lithosphere beneath the north central Slave craton. In: Proceedings of the VIIth International Kimberlite Conference, The J.B. Dawson Volume, Gurney, J.J., Gurney, J.L., Pascoe, M.D., and Richardson, S.H. (eds), Red Roof Design, Cape Town, 468-479.
- Kopylova, M.G., and Caro, G. 2004. Mantle xenoliths from the southeastern Slave craton: evidence for chemical zonation in a thick, cold lithosphere. *Journal of Petrology*, 45, 1045-1067.
- Mc Kenna, N., Gurney, J.J., Klump, J., and Davidson, J.M. 2004. Aspects of diamond mineralisation and distribution at the Helam Mine, South Africa. *Lithos*, 77, 193-208.
- MacKenzie, J.M. and Canil, D. 1999. Composition and thermal evolution of cratonic mantle beneath the central Archean Slave Province, NWT, Canada. *Contributions to Mineralogy and Petrology*, 134, 313-324.
- McDonough, W. and Sun, S.S. 1995. The composition of the Earth. *Chemical Geology*, 120, 223-253.
- Menzies, A.H., Westerlund, K.J., Grütter, H.G., Gurney, J.J., Carlson, J.W., Fung, A., and Nowicki, T.E. 2004. Peridotitic mantle xenoliths from kimberlites on the Ekati Diamond Mine property, N.W.T., Canada: major element compositions and implications for the lithosphere beneath the central Slave craton. *Lithos* 77, 35-412.
- Meyer, H.O.A. 1987. Inclusions in diamond. In: *Mantle xenoliths*, Nixon, P.H. (ed), John Wiley and Sons, Chichester, 501-522.
- O'Neill, H.St.C. 1980. An experimental study of the iron-magnesium partitioning between garnet and olivine and its calibration as a geothermometer: corrections. *Contributions to Mineralogy and Petrology*, 72, 337.

- O'Neill, H.St.C. and Wood, B. 1979. An experimental study of the iron-magnesium partitioning between garnet and olivine and its calibration as a geothermometer. *Contributions to Mineralogy and Petrology*, 70, 59-70.
- O'Neill, H.St.C. and Wall, V.J. 1987. The olivine-orthopyroxene-spinel oxygen geobarometer, the nickel precipitation curve, and the oxygen fugacity of the earth's upper mantle. *Journal of Petrology*, 28, 1169- 1191.
- O'Reilly, S.Y., Griffin, W.L., Djomani, Y.P., Natapov, L.M., Pearson, N.J., Davies, R.M., Doyle, B.J., and Kivi, K. 2001. The mantle beneath the Slave Craton (Canada): Composition and Architecture. The Slave-Kapvaal Workshop, Merrickville, Ontario, Extended Abstracts, 5p (CD, not paginated).
- Pearson, N.J., Griffin, W.L., Doyle, B.J., O'Reilly, S.Y., Van Achtenberg, E., Kivi, K. 1999. Xenoliths from kimberlite pipes of the Lac de Gras area, Slave Craton, Canada. In: Proceedings of the VIIth International Kimberlite Conference, The P.H. Nixon Volume, Gurney, J.J., Gurney, J.L., Pascoe, M.D., and Richardson, S.H. (eds), Red Roof Design, Cape Town, 644-658.
- Pearson, N.J., Alard, O., Griffin, W.L., Jackson, S.E., and O'Reilly, S.Y. 2002. In situ measurements of Re–Os isotopes in mantle sulfides by laser ablation multicollector-inductively coupled mass spectrometry: analytical methods and preliminary results. *Geochimica et Cosmochimica Acta* 66, 1037– 1050.
- Pokhilenko, N.P. Sobolev, N.V., McDonald, J.A., Hall, A.E., Yefimova, E.S., Zedgenizov, D.A., Logvinova, A.M., and Reimers, L.F. 2001. Crystalline inclusions in diamonds from kimberlites of the Snap Lake area (Slave Craton, Canada): New evidences for the anomalous lithospheric structure. *Doklady Earth Science*, 380, 806-811.
- Pokhilenko, N.P., Sobolev, N.V., Reutsky, V.N., Hall, A.E., and Taylor, L.A. 2004. Crystalline inclusions and C isotope ratios in diamonds from the Snap Lake/King Lake kimberlite dyke system: evidence of ultradeep and enriched lithospheric mantle. *Lithos*, 77, 57-67.
- Promprated, P., Taylor, L.A., Anand, M., Floss, C., Sobolev, N.V., and Pokhilenko, N.P. 2004. Multiple-mineral inclusions in diamonds from the Snap Lake/King Lake kimberlite dike, Slave craton, Canada: a trace-element perspective. *Lithos*, 77, 69-81.
- Robinson, D. (1979). Surface textures and other features of diamonds. PhD Thesis, University of Cape Town, 220p.
- Ryan, C.G., Griffin, W.L., Pearson, N.J. 1996. Garnet geotherms - pressure-temperature data from Cr-pyrope garnet xenocrysts in volcanic rocks. *Journal of Geophysical Research*, 101, 5611-5625.

- Shimizu, N. and Hart, S.R. 1982. Applications of the ion microprobe to geochemistry and cosmochemistry. *Annual Review of Earth and Planetary Sciences*, 10, 483-526.
- Sobolev, N.V., Lavrentev, Y.G., Pokhilenko, N.P., Usova, L.V. 1973. Chrome-rich garnets from the kimberlites of Yakutia and their paragenesis. *Contributions to Mineralogy and Petrology*, 40, 39-52.
- Sobolev, N.V., Logvinova, A.M., Zedgenizov, D.A., and Seryotkin, Y.V. 2004. Mineral inclusions in microdiamonds and macrodiamonds from kimberlites of Yakutia: a comparative study. *Lithos*, 77, 225-242.
- Stachel, T., and Harris, J.W. 1997. Syngenetic inclusions in diamond from the Birim field (Ghana) - A deep peridotitic profile with a history of depletion and re-enrichment. *Contributions to Mineralogy and Petrology*, 127, 336-352.
- Stachel, T., Harris, J.W., and Brey, G.P. 1998a. Rare and unusual mineral inclusions in diamonds from Mwadui, Tanzania. *Contributions to Mineralogy and Petrology*, 132, 34-47.
- Stachel, T., Brey, G.P., Harris, J.W. 2000a. Kankan diamonds (Guinea) I: from the lithosphere down to the transition zone. *Contributions to Mineralogy and Petrology*, 140, 1-15.
- Stachel, T., Harris, J.W., Brey, G.P., and Joswig, W. 2000b. Kankan diamonds (Guinea) II: lower mantle inclusion parageneses. *Contributions to Mineralogy and Petrology*, 140, 16-27.
- Stachel, T., Harris, J.W., Tappert, R., and Brey, G.P. 2003. Peridotitic inclusions in diamonds from the Slave and the Kaapvaal cratons - similarities and differences based on a preliminary data set. *Lithos*, 71, 489-503.
- Stachel, T., Aulbach, S., Brey, G.P., Harris, J.W., Leost, I., Tappert, R., and Viljoen, K.S. 2004. The trace element composition of silicate inclusions in diamonds: a review. *Lithos*, 77, 1-19.
- Tappert, R., Stachel, T., Harris, J.W., Shimizu, N., and Brey, G.P. 2004. Mineral inclusions in diamonds from the Panda kimberlite, Slave Province, Canada. *European Journal of Mineralogy*, 17, 423-440.
- Taylor, W.R., Jaques, A.L., and Ridd, M. 1990. Nitrogen-defect aggregation characteristics of some Australasian diamonds: Time-temperature constraints on the source regions of pipe and alluvial diamonds. *American Mineralogist*, 75, 1290-1310.

- Westerlund, K.J., Gurney, J.J., Shirey, S.B., and Hauri, E. 2001. Nitrogen aggregation and stable nitrogen and carbon isotope characteristics of diamonds from the Panda kimberlite, Slave craton, Canada. The Slave-Kapvaal Workshop, Merrickville, Ontario, Extended Abstracts, 4p (CD not paginated).
- Westerlund, K.J., Hauri, E.H., and Gurney, J.J. 2003a. FTIR absorption and stable nitrogen and carbon isotope microanalysis of mid-Archean diamonds from the Panda kimberlite. VIIIth International Kimberlite Conference, Victoria, Canada, Extended Abstracts, 4p (CD, not paginated).
- Westerlund, K.J., Shirey, S.B., Richardson, S.H., Gurney, J.J., and Harris, J.W. 2003b. Re-Os systematics of diamond inclusion sulfides from the Panda kimberlite, Slave craton. VIIIth International Kimberlite Conference, Victoria, Canada, Extended Abstracts, 5p (CD, not paginated).

Table 3.1. Summary of the physical and geochemical characteristics of the A154 South diamonds and their mineral inclusions.

Sample	Assemblage	Paragenesis	Shape	Colour	Deformation	d13C	Type	NT (at. ppm)	Aggregation (%B)
ddmi-001	2chr	Peridotitic	D	Brown	No	-4.5	IaAB	526	15
ddmi-002	fper,s	Uncertain	O	Brown	No	0.7	IaAB	125	69
ddmi-003	ol	Peridotitic	O	Brown	No	-5.5	IaA	49	4
ddmi-004	2chr	Peridotitic	I	Grey	No	-5.0	IaAB	377	12
ddmi-005	ol	Peridotitic	D	Colourless	No	-5.3	IaAB	86	65
ddmi-006	chr	Peridotitic	O	Colourless	No	-5.0	IaAB	344	76
ddmi-008	gnt	Peridotitic	TM	Brown	No	-5.7	IaA	250	4
ddmi-013	ol	Peridotitic	O	Brown	Yes	-3.9	IaA	44	0
ddmi-014	ol	Peridotitic	O	Brown	No	-4.6	IaAB	55	38
ddmi-025	2chr	Peridotitic	O	Colourless	No	-5.1	IaA	232	0
ddmi-034	2chr,s	Peridotitic	I	Brown	No	-4.5	IaA	333	3
ddmi-036	chr,3chr(exp)	Peridotitic	I	Brown	No	-4.5	IaA	247	0
ddmi-037	5s	Eclogitic	D	Colourless	No	-8.6	IaA	270	9
ddmi-040	2chr	Peridotitic	O	Brown	No	-4.3	IaAB	142	80
ddmi-043	2chr	Peridotitic	O	Colourless	No	-4.8	IaAB	179	22
ddmi-044	3chr	Peridotitic	D	Brown	No	-5.0	IaA	245	0
ddmi-046	chr	Peridotitic	O	Colourless	No	-4.0	IaAB	385	65
ddmi-047	chr	Peridotitic	I	Brown	No	-4.6	IaA	435	2
ddmi-048	4cpx	Eclogitic	D	Colourless	No	-10.5	IaAB	165	81
ddmi-049	ol	Peridotitic	D	Brown	No	-4.2	IaB	118	97
ddmi-058	chr	Peridotitic	I	Colourless	No	-5.1	IaA	511	2
ddmi-078	2s	Eclogitic	D	Colourless	No	-5.2	IaA	560	0
ddmi-093	s	Eclogitic	D	Colourless	No	-5.1	IaA	724	0
ddmi-098	2chr	Peridotitic	O	Colourless	No	-4.3	IaA	318	0
ddmi-100	chr,3chr(exp)	Peridotitic	D	Brown	No	-4.4	IaA	19.5	0
ddmi-101	ol	Peridotitic	I	Brown	No	-6.0	IaB	410	98
ddmi-103	chr	Peridotitic	I	Colourless	No	-5.1	IaAB	178	48
ddmi-108	chr	Peridotitic	I	Colourless	No	-5.3	IaA	432	4
ddmi-110	ol	Peridotitic	I	Brown	No	-4.8	IaA	481	3
ddmi-111	3ol	Peridotitic	O	Colourless	No	-6.3	IaA	195	8
ddmi-112	s	Peridotitic	O	Brown	Yes	-5.4	IaA	366	0
ddmi-114	fper	Uncertain	I	Brown	No	-2.9	II	-	-

Abbreviations Shape – O: octahedra, D: dodecahedroid, I: irregular, TM: triangular macel, A: aggregate.

Abbreviations Assemblage – gnt: garnet, ol: olivine, chr: magnesio-chromite, fper: ferropericlase, s: sulphide, cpx: clinopyroxene, coe: coesite, dia: diamond, (exp): exposed mineral on surface, (alt): altered mineral, *comma*: non-touching inclusion pair, *hyphen*: touching-inclusion pair, *number*: number of inclusions.

Table 3.1. (cont.)

Sample	Assemblage	Paragenesis	Shape	Colour	Deformation	d13C	Type	NT (at. ppm)	Aggregation (%B)
ddmi-115	s	Peridotitic	O	Brown	No	-5.5	laA	48	0
ddmi-119	13chr,2chr(exp)	Peridotitic	I	Colourless	No	-4.9	laA	257	0
ddmi-120	chr	Peridotitic	D	Colourless	No	-4.5	laA	557	3
ddmi-123	ol	Peridotitic	D	Brown	Yes	-6.3	laAB	99	39
ddmi-124	ol	Peridotitic	OA	Pink	Yes	-5.5	laA	661	0
ddmi-126	2chr,chr(exp)	Peridotitic	D	Brown	No	-5.0	laA	193	1
ddmi-127	s	Eclogitic	D	Colourless	No	-5.3	laA	711	0
ddmi-129	ol	Peridotitic	TM	Brown	No	-5.8	laB	1051	100
ddmi-130	s	Peridotitic	TM	Colourless	No	-5.4	laA	1873	0
ddmi-133	2 gnt	Peridotitic	OA	Brown	No	-5.4	laA	418	0
ddmi-135	3ol	Peridotitic	OA	Brown	No	-4.4	laA	549	4
ddmi-139	3ol	Peridotitic	TM	Pink	No	-6.2	laA	458	2
ddmi-140	cpx	Peridotitic	O	Brown	No	-4.6	laA	21	0
ddmi-141	ol-cpx	Peridotitic	O	Colourless	No	-5.1	laA	29	0
ddmi-142	ol	Peridotitic	O	Brown	No	-4.6	laA	424	0
ddmi-144	2ol	Peridotitic	O	Brown	No	-4.5	laA	149	0
ddmi-145	2chr	Peridotitic	I	Colourless	No	-5.2	laA	185	0
ddmi-146	chr	Peridotitic	I	Brown	No	-4.4	laA	66	0
ddmi-147	12chr	Peridotitic	O	Brown	No	-5.2	laA	182	0
ddmi-148	2ol	Peridotitic	O	Brown	No	-6.1	laA	89	6
ddmi-150	2chr,s	Peridotitic	D	Brown	No	-4.8	laB	294	98
ddmi-151	2ol	Peridotitic	TM	Pink	No	-6.3	laAB	384	19
ddmi-152	3chr,chr(exp)	Peridotitic	D	Brown	No	-5.0	laA	119	0
ddmi-153	3/per	Uncertain	I	Brown	No	-4.2	laAB	58	57
ddmi-154	gnt,2ol	Peridotitic	O	Brown	No	-4.8	laAB	109	58
ddmi-155	ol	Peridotitic	O	Brown	No	-5.3	laAB	440	19
ddmi-156	s	Peridotitic	D	Brown	No	-4.9	laA	105	0
ddmi-159	gnt (alt)	Peridotitic	DA	Grey	No	-5.1	laA	1225	0
ddmi-161	ol	Peridotitic	O	Brown	No	-6.1	laA	315	6
ddmi-162	ol	Peridotitic	OA	Colourless	No	-8.6	laA	41	0
ddmi-165	3ol	Peridotitic	O	Brown	No	-5.2	laA	232	0
ddmi-166	10gnt	Eclogitic	O	Yellow	No	-4.8	laAB	3833	36
ddmi-167	gnt,2ol	Peridotitic	O	Brown	Yes	-4.8	laA	17	0
ddmi-168	ol	Peridotitic	Th	Brown	No	-5.6	laA	109	10

Table 3.1. (cont.)

Sample	Assemblage	Paragenesis	Shape	Colour	Deformation	d13C	Type	NT (at ppm)	Aggregation (%B)
ddm1-169	2chr	Peridotitic	O	Brown	No	-5.2	1aA	63	0
ddm1-170	2ol	Peridotitic	TM	Brown	No	-5.4	1aA	38	7
ddm1-172	2chr	Peridotitic	I	Colourless	No	-5.0	1aA	78	0
ddm1-173	fper	Uncertain	O	Brown	No	-4.8	II	-	-
ddm1-174	ol	Peridotitic	O	Colourless	No	-4.3	1aA	76	0
ddm1-175	6gnt	Peridotitic	O	Brown	No	-4.4	1aA	294	0
ddm1-176	chr	Peridotitic	I	Colourless	No	-5.2	1aA	63	0
ddm1-177	2ol	Peridotitic	OA	Brown	No	-5.2	II	-	-
ddm1-179	ol,s	Peridotitic	O	Brown	Yes	-5.6	1aAB	159	11
ddm1-180	2ol	Peridotitic	I	Brown	No	-6.3	1aAB	126	30
ddm1-182	chr	Peridotitic	TM	Brown	No	-5.1	II	-	-
ddm1-183	ol,chr	Peridotitic	O	Brown	No	-5.3	1aB	384	91
ddm1-184	ol	Peridotitic	I	Colourless	No	-5.4	1aA	414	6
ddm1-186	2cpx	Eclogitic	O	Colourless	No	-4.9	1aA	822	0
ddm1-187	6chr,chr(exp)	Peridotitic	D	Colourless	No	-4.6	1aA	373	0
ddm1-188	3chr	Peridotitic	O	Brown	Yes	-5.1	1aA	321	0
ddm1-190	2ol	Peridotitic	D	Brown	No	-5.6	1aAB	185	11
ddm1-193	coe	Eclogitic	D	Brown	No	-5.1	II	-	-
ddm1-195	ol	Peridotitic	D	Brown	No	-6.1	1aAB	61	84
ddm1-196	2s	Eclogitic	DA	Colourless	No	-5.1	1aA	904	0
ddm1-198	s	Eclogitic	DA	Colourless	No	-5.3	1aA	629	0
ddm1-199	2gnt,s	Peridotitic	O	Brown	No	-5.2	1aA	994	4
ddm1-200	dia	Uncertain	TM	Colourless	No	-4.6	1aA	863	2
ddm1-202	2s	Peridotitic	O	Brown	No	-5.0	1aA	502	4
ddm1-203	chr	Peridotitic	O	Colourless	No	-4.3	1aA	557	7
ddm1-205	2gnt	Eclogitic	O	Pink	No	-4.8	1aA	860	0
ddm1-206	ol	Peridotitic	O	Brown	No	-5.2	1aA	862	7
ddm1-207	2chr	Peridotitic	I	Colourless	Yes	-5.5	1aA	344	3
ddm1-208	12gnt	Eclogitic	O	Yellow	No	-5.0	1aAB	1791	34
ddm1-210	2ol	Peridotitic	O	Brown	No	-5.4	1aAB	134	49
ddm1-213	ol	Peridotitic	D	Brown	No	-5.2	1aAB	272	65
ddm1-214	2chr	Peridotitic	I	Colourless	No	-5.0	1aA	669	8
ddm1-215	3chr	Peridotitic	I	Colourless	No	-5.0	1aA	2636	0
ddm1-216	2gnt	Peridotitic	O	Brown	No	-5.7	1aAB	219	37

Table 3.2. Major and trace element compositions of selected inclusions from A154 South diamonds. Major element compositions (EPMA-analyses) are reported as wt%.

Mineral Sample Assemblage Suite	Garnet ddmi-8a gnt P	Garnet ddmi-154a gnt, 2ol P	olivine ddmi-154c gnt, 2ol P	Garnet ddmi-167a gnt, 2ol P	olivine ddmi-167b gnt, 2ol P	Garnet ddmi-199a 2gnt, s P (Iherz)	Garnet ddmi-216a 2gnt P	olivine ddmi-183a ol,chr P	chromite ddmi-183d ol,chr P	chromite ddmi-176 chr P	olivine ddmi-141b ol-cpx P	clinopyroxene ddmi-141a ol-cpx P	Garnet ddmi-166a 10gnt E	Garnet ddmi-206a 2gnt E
P ₂ O ₅	0.03	0.03	≤0.01	0.02	0.01	≤0.01	≤0.04	≤0.01	-	-	≤0.01	≤0.01	0.06	0.08
SiO ₂	41.33	41.04	41.60	42.07	41.20	41.45	41.32	40.86	0.22	0.10	41.07	54.60	41.17	39.72
TiO ₂	0.12	0.08	≤0.02	≤0.02	≤0.02	0.06	≤0.05	≤0.02	0.29	0.13	≤0.02	0.09	0.36	0.36
Al ₂ O ₃	14.17	11.53	≤0.02	18.47	≤0.02	17.69	17.50	≤0.02	4.84	5.87	≤0.02	1.02	22.77	22.17
Cr ₂ O ₃	10.85	15.68	0.04	6.97	0.04	7.15	7.99	0.05	65.57	64.20	≤0.02	1.14	0.08	0.05
V ₂ O ₅	0.05	0.05	≤0.01	0.04	≤0.01	0.05	0.05	≤0.01	0.25	0.26	≤0.01	0.02	0.02	0.02
FeO	5.85	5.82	7.34	5.50	6.47	6.95	5.94	7.31	16.13	15.44	6.78	2.87	9.75	11.20
MnO	0.23	0.26	0.11	0.21	0.10	0.29	0.25	0.11	0.09	0.11	0.09	0.10	0.21	0.19
NiO	≤0.01	≤0.01	0.31	≤0.01	0.03	≤0.01	≤0.03	0.31	0.08	0.09	0.32	0.06	≤0.01	≤0.01
MgO	22.91	19.88	49.93	22.70	50.50	19.52	21.80	50.93	13.72	13.50	50.45	16.80	11.94	10.79
CaO	2.89	5.91	0.04	3.73	0.04	6.03	4.34	0.03	-	-	0.03	20.80	14.08	13.63
Na ₂ O	≤0.01	0.02	≤0.01	0.02	0.02	0.02	0.02	0.02	-	-	≤0.01	1.29	0.14	0.12
K ₂ O	≤0.01	≤0.01	≤0.01	≤0.01	≤0.01	≤0.01	≤0.02	≤0.01	-	-	≤0.01	0.02	≤0.01	≤0.01
ZnO	-	-	-	-	-	-	-	-	0.09	0.08	-	-	-	-
Oxide Total	98.44	100.30	99.45	99.78	98.46	99.24	98.77	99.69	101.27	99.79	98.84	98.83	100.58	98.33
Ti (ppm)	988	680		210		473	311						2034	1568
Sr (ppm)	4.18	10.79		3.77		0.86	1.87						6.15	2.63
Y (ppm)	2.25	2.04		1.14		1.36	6.70						12.78	11.32
Zr (ppm)	29.02	49.88		4.59		8.52	65.54						27.05	8.41
La (ppm)	0.26	1.19		0.71		0.22	0.04						0.12	0.10
Ce (ppm)	4.40	9.81		3.62		0.81	0.24						0.91	0.83
Nd (ppm)	3.43	7.82		3.27		0.49	0.67						1.74	1.61
Sm (ppm)	0.70	1.44		0.34		0.15	0.44						1.10	1.05
Eu (ppm)	0.19	0.34		0.17		0.02	0.32						0.50	0.31
Dy (ppm)	0.44	0.40		0.13		0.09	0.98						1.88	1.15
Er (ppm)	0.22	0.31		0.07		0.07	0.43						1.19	0.99
Yb (ppm)	0.18	0.27		0.30		0.20	0.35						1.22	0.85

Table 3.3. Major element composition (EMPA-analyses, wt%) of selected sulphide inclusions.

Mineral Sample Assemblage Paragenesis	Fe-Ni Sulphide ddml-156 sulph Peridotitic	Fe-Ni Sulphide ddml-179 ol, sulph Peridotitic	Fe-Ni Sulphide ddml-199 2 gnt, sulph Peridotitic	Fe-Ni Sulphide ddml-202 2 sulph Peridotitic	Fe-Sulphide ddml-002 fper, sulph Eclogitic	Fe-Sulphide ddml-037 sulph Eclogitic	Fe-Sulphide ddml-093 sulph Eclogitic	Fe-Sulphide ddml-127 sulph Eclogitic
Si	0.03	0.02	0.02	0.02	0.04	0.05	0.03	0.03
Cr	0.28	0.68	≤0.06	0.22	<0.06	≤0.06	≤0.06	≤0.06
Fe	38.83	39.64	23.89	36.85	45.76	56.47	56.35	56.35
Mn	≤0.02	≤0.02	≤0.02	≤0.02	≤0.02	≤0.02	≤0.02	≤0.02
Ni	22.32	21.19	39.85	22.68	<0.01	1.10	1.56	1.56
Mg	≤0.01	≤0.01	≤0.01	≤0.01	≤0.01	≤0.01	≤0.01	≤0.01
Cu	0.57	0.31	0.20	0.96	0.36	2.33	1.33	1.33
Co	0.51	0.43	0.96	0.50	0.05	0.27	0.34	0.34
Zn	0.07	0.07	0.07	0.04	0.05	0.03	0.05	0.05
S	36.94	36.85	33.75	37.76	52.91	38.54	38.95	38.95
Total	99.54	99.19	98.74	99.03	99.18	98.80	98.60	98.60

Table 3.4. Major element composition (EPMA-analyses, wt%) of ferropericlase inclusions of uncertain paragenetic association.

Mineral Sample Assemblage	Ferropericlase ddmi-2 fper, s	Ferropericlase ddmi-114 fper	Ferropericlase ddmi-153 3fper	Ferropericlase ddmi-173 2fper
P ₂ O ₅	≤0.01	≤0.01	≤0.01	≤0.01
SiO ₂	0.10	0.02	0.13	0.10
TiO ₂	≤0.02	≤0.02	≤0.02	≤0.02
Al ₂ O ₃	≤0.02	≤0.02	≤0.02	≤0.02
Cr ₂ O ₃	0.60	0.36	0.46	0.45
V ₂ O ₃	≤0.01	≤0.01	≤0.01	≤0.01
FeO	21.56	28.53	26.41	20.79
MnO	0.15	0.16	0.20	0.15
NiO	1.09	2.03	1.02	1.11
MgO	77.22	69.44	71.47	78.26
CaO	≤0.01	≤0.01	≤0.01	≤0.01
Na ₂ O	0.33	0.34	0.22	0.22
K ₂ O	≤0.01	≤0.01	≤0.01	≤0.01
Total	101.13	100.96	99.99	101.17



Figure 3.1. Map of the Slave craton and the central Slave (inset), modified from Bleeker and Davis (1999b) and Davies et al. (2004a). North, central and south subdivisions for the Slave are from Grütter et al. (1999).

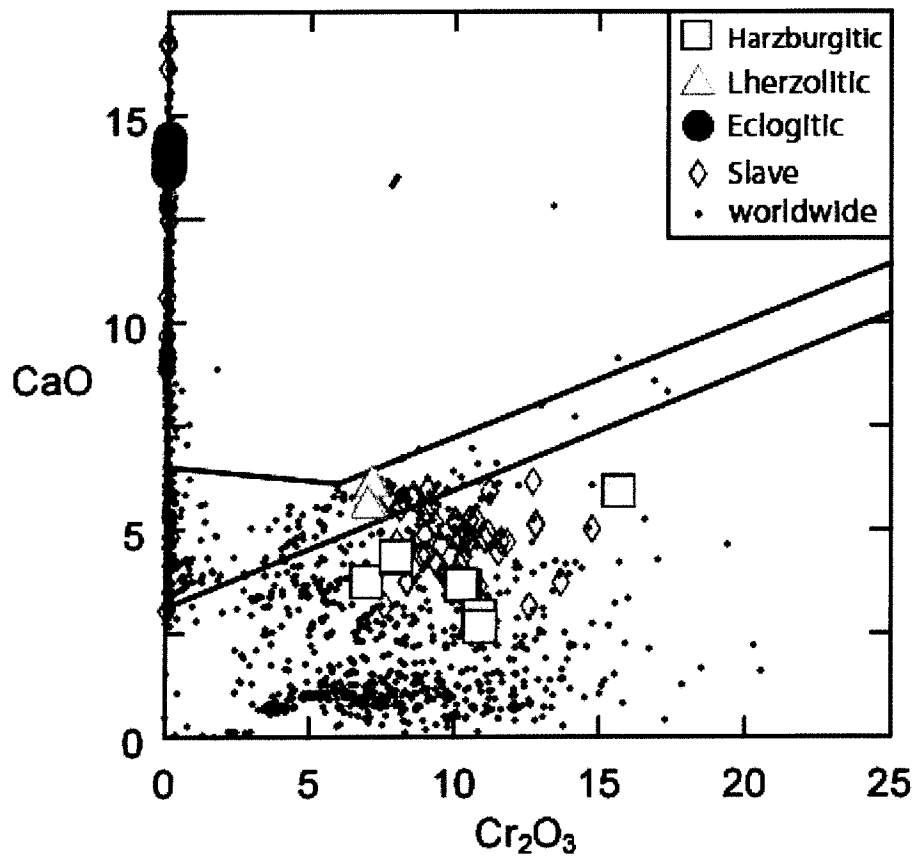


Figure 3.2. CaO vs Cr₂O₃ (wt%) for garnet inclusions from A154 South diamonds, other Slave localities and worldwide sources. The lherzollitic compositional field is taken from Sobelev et al. (1973).

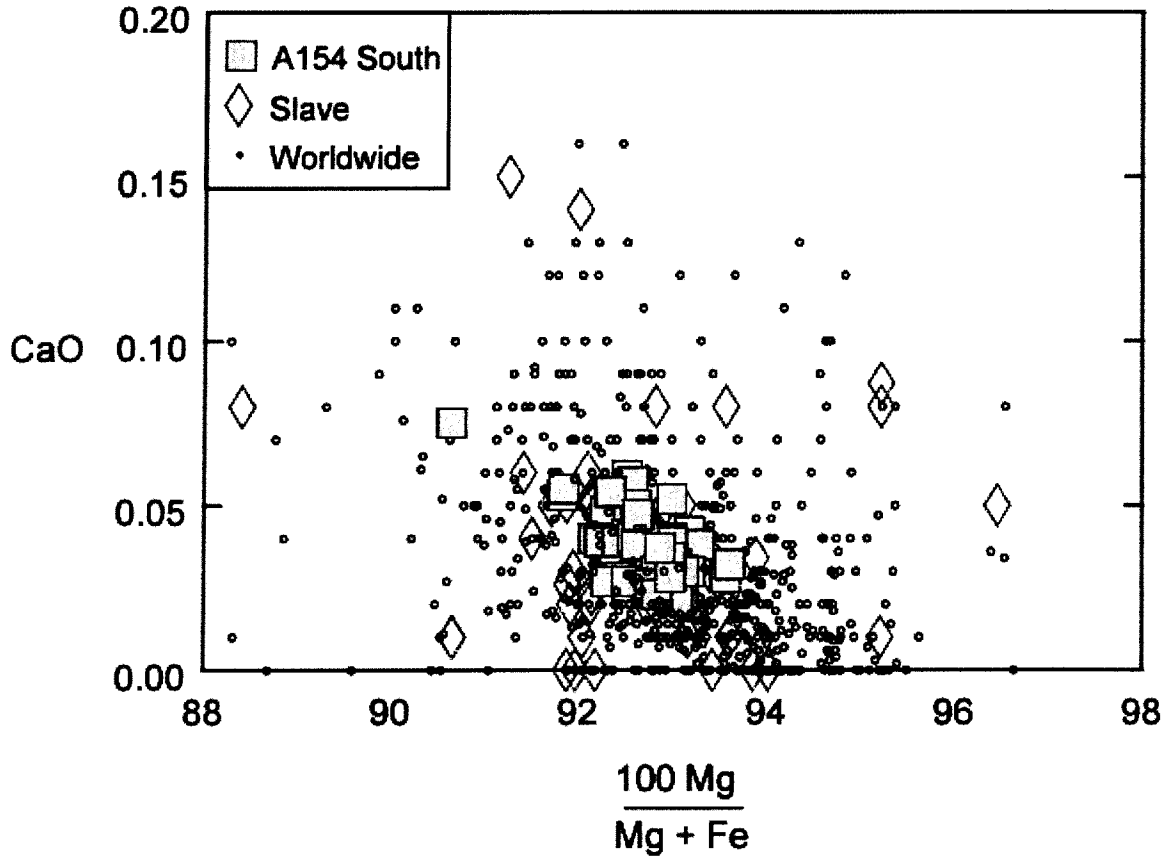


Figure 3.3. CaO (wt%) versus molar Mg number for A154 South olivine inclusions, compared to olivines from the Slave craton and worldwide sources.

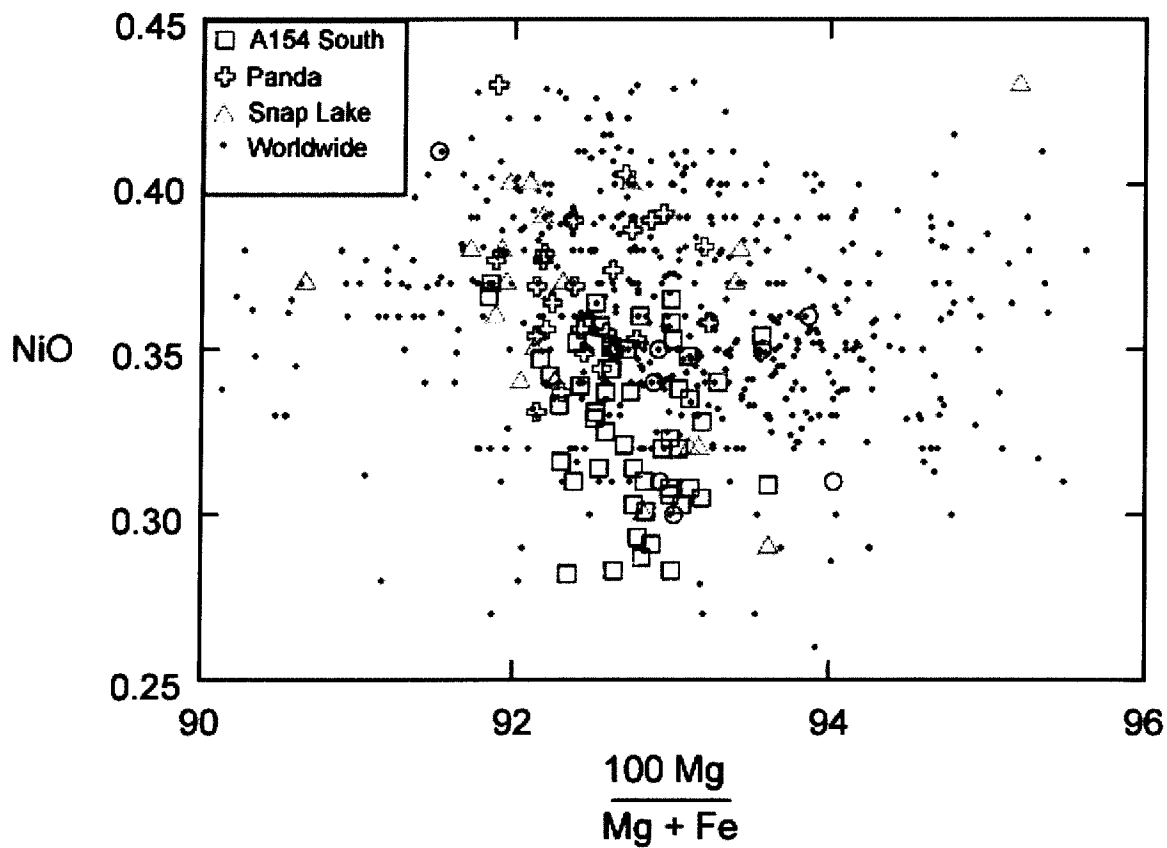


Figure 3.4. NiO (wt%) versus molar Mg number for A154 South olivine inclusions (squares). Note the distinct groupings for Panda and DO27. The A154 South diamonds, as well as Snap Lake, overlap both groupings.

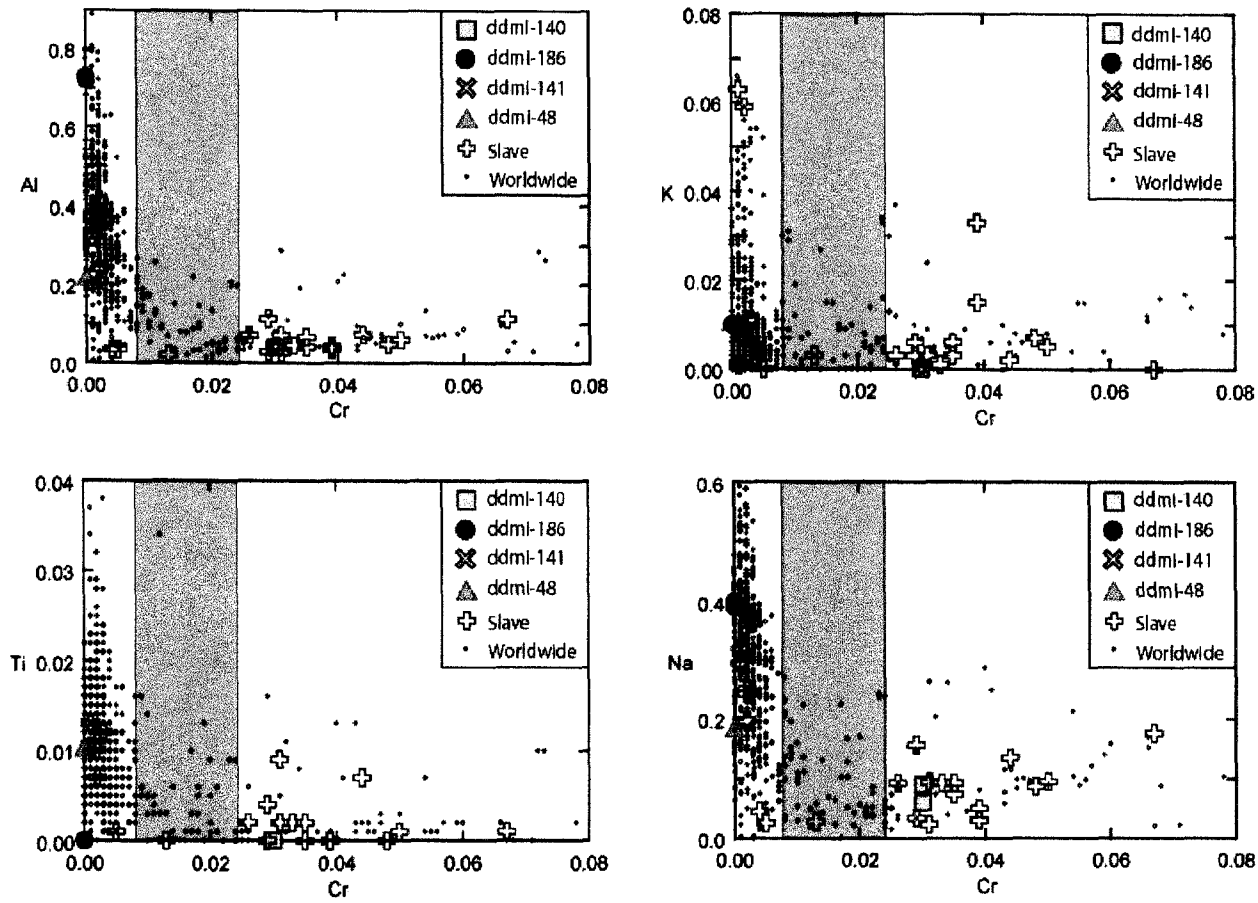


Figure 3.5. Cation proportions (based on 6 oxygens) for clinopyroxenes from A154 South, the Slave craton and worldwide sources. The shaded area represents clinopyroxenes of websteritic paragenesis (after Davies et al., 2004b) and separates Cr poor eclogitic clinopyroxenes from the worldwide less abundant, peridotitic Cr-diopsides.

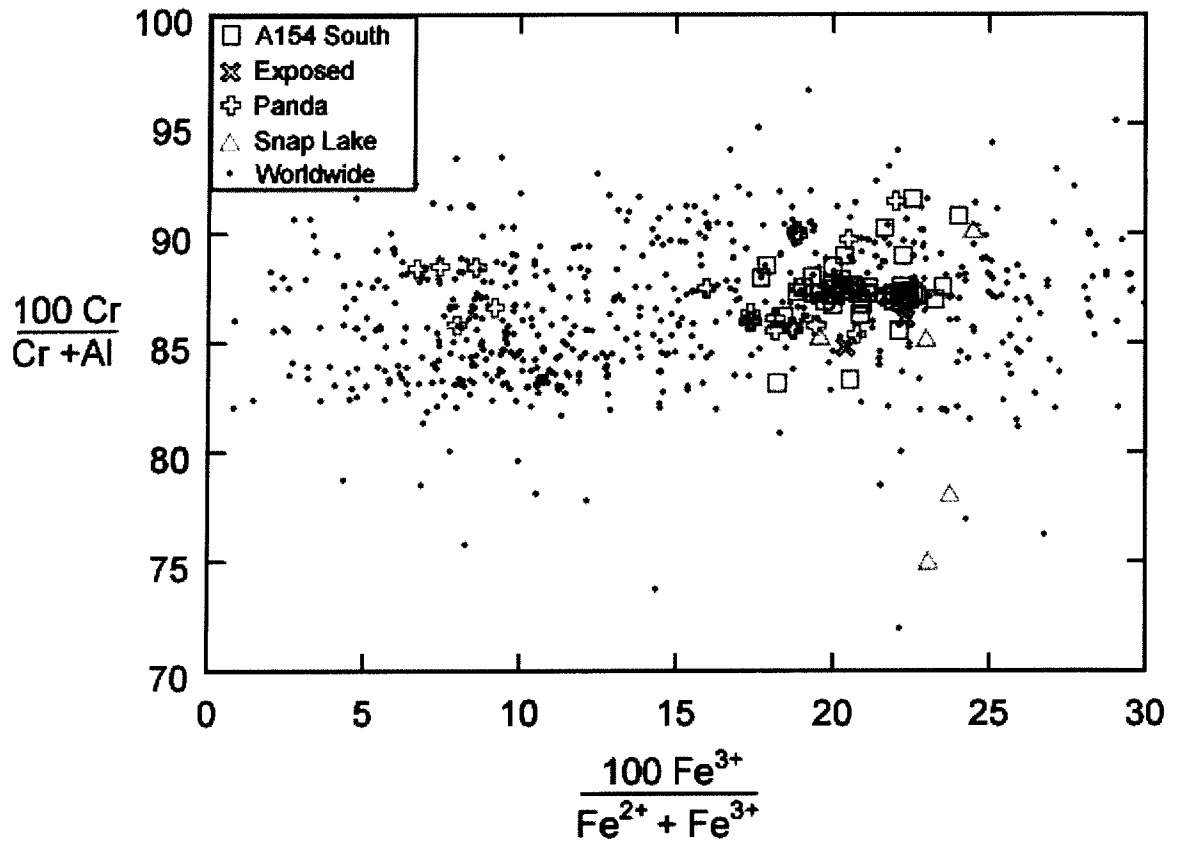


Figure 3.6. Cr number versus ferric iron ratio for magnesiochromite inclusions from A154 South, Panda, Snap Lake and worldwide sources. Fe^{3+} calculated after Droop (1987).

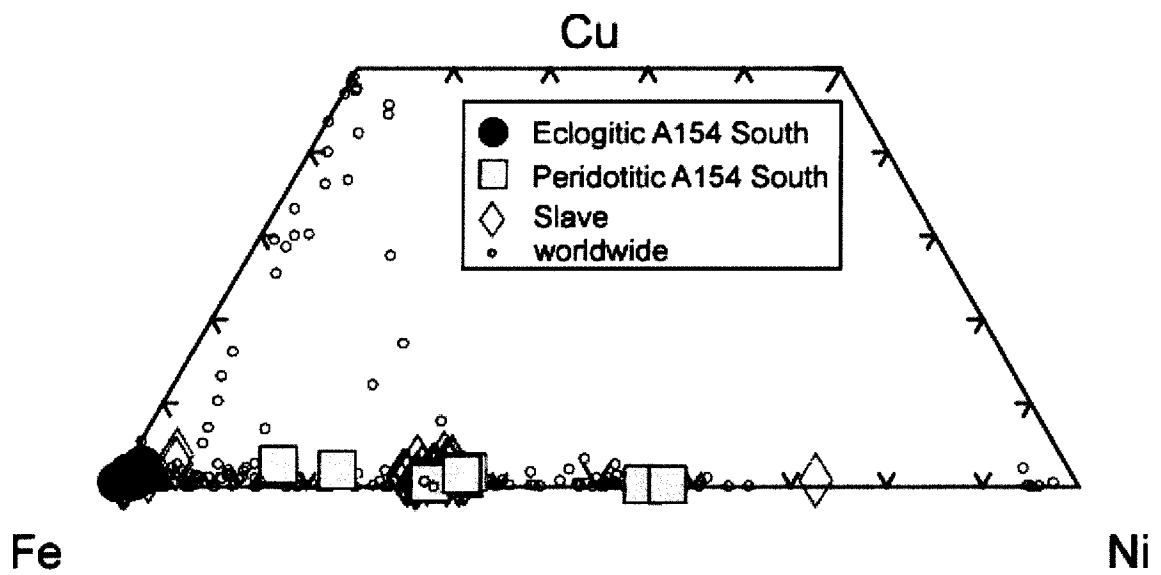


Figure 3.7. Composition diagram showing eight eclogitic Fe-monosulphide inclusions and eight peridotitic Fe-Ni sulphides from A154 South diamonds, the Slave craton and worldwide sources in the Fe-Ni-Cu system in elemental wt%.

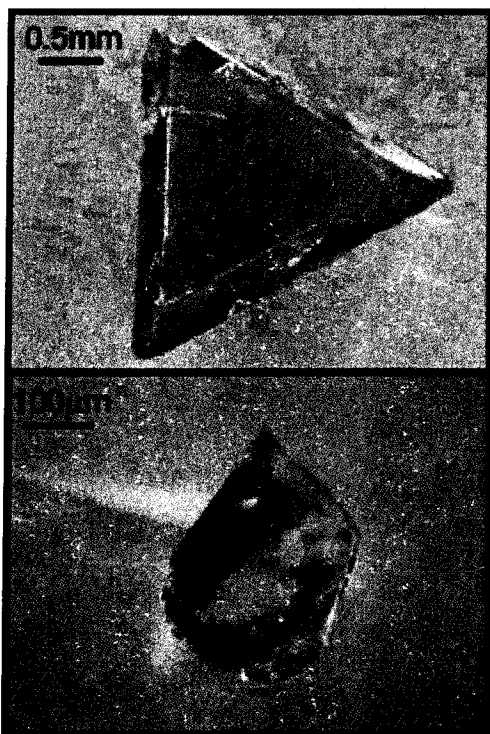


Figure 3.8. Photograph of diamond ddmi-200, a colourless triangular macle (top) containing a colourless, octahedral diamond inclusion (bottom).

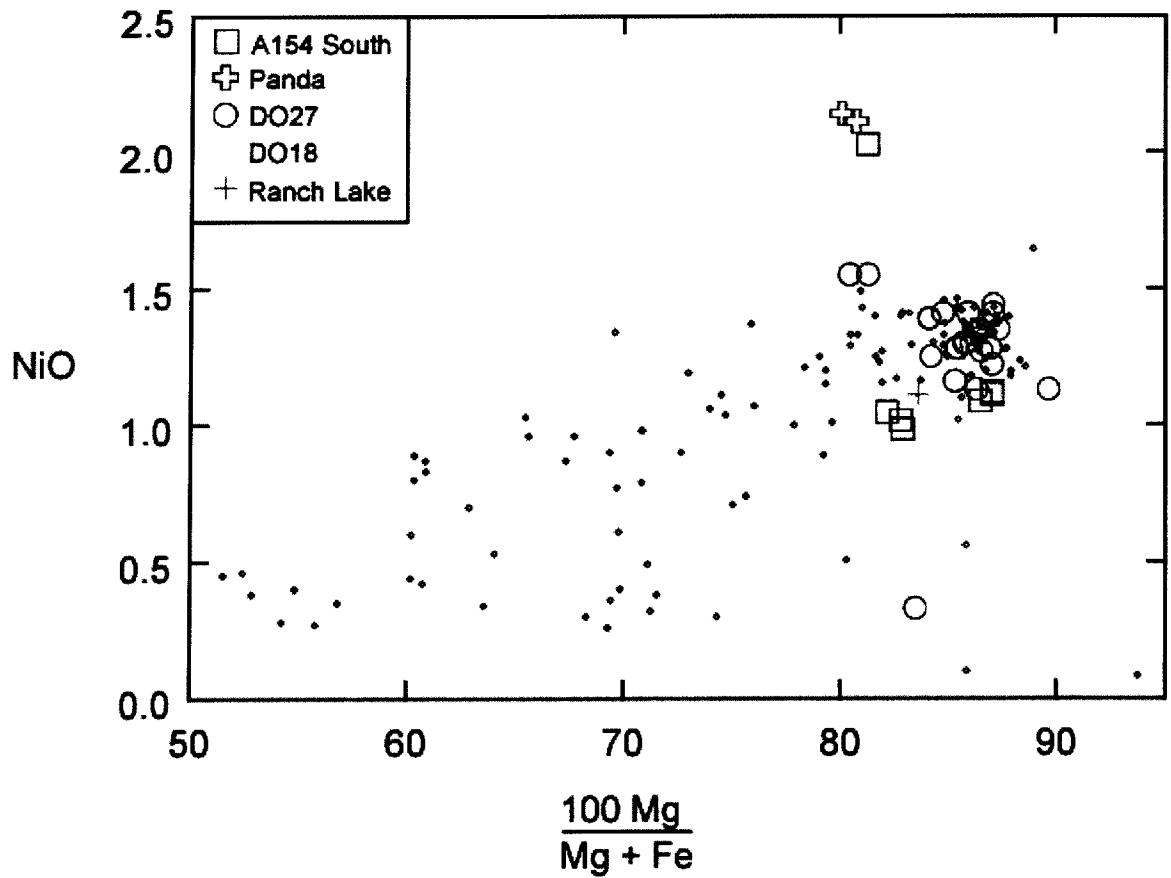


Figure 3.9. NiO (wt%) versus Mg# for ferropericlase inclusions from A154 South, the Slave craton, and worldwide localities.

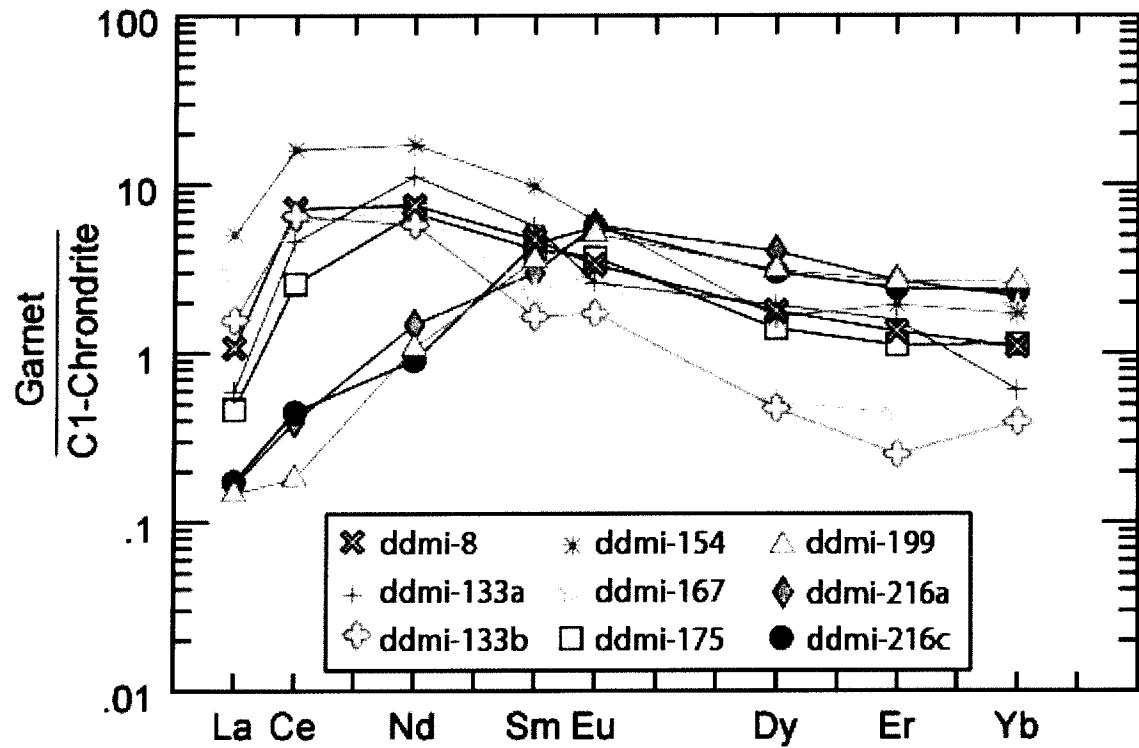


Figure 3.10. Rare earth element (REE_N) concentrations of peridotitic garnet inclusions from A154 South normalized to C1 after McDonough and Sun (1995). Diamond ddm-199 is of lherzolitic paragenesis.

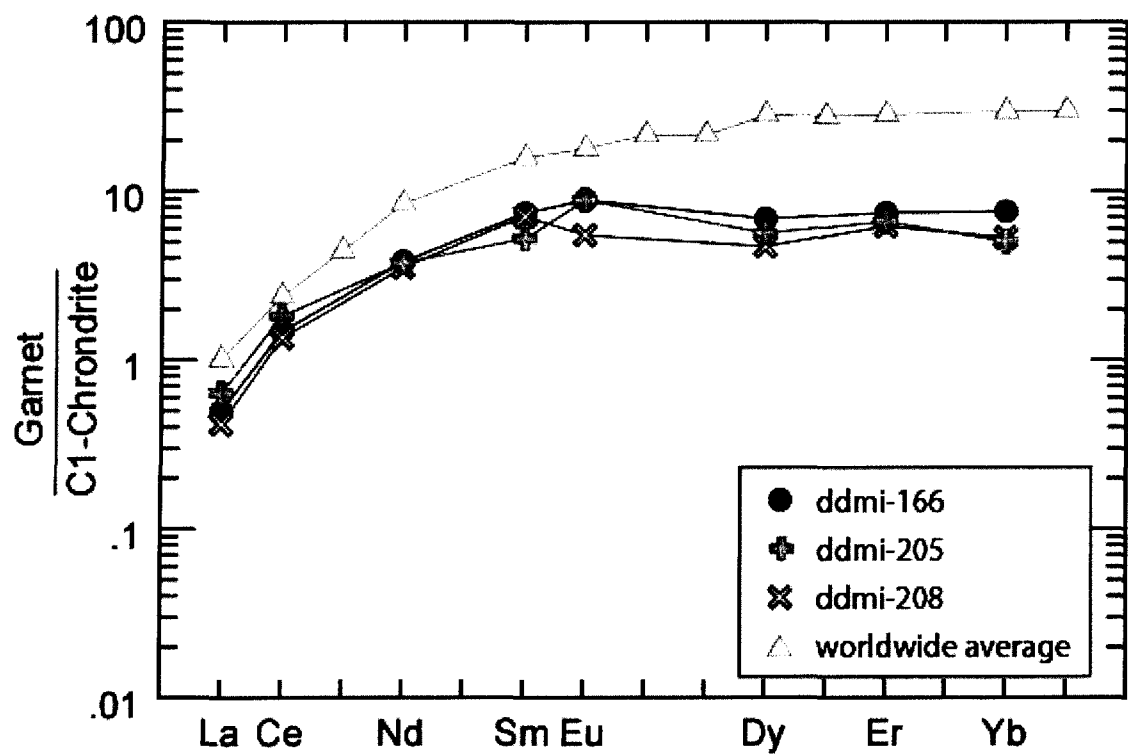


Figure 3.11. Rare earth element (REE_N) concentrations of eclogitic garnet inclusions from A154 South and the worldwide average normalized to C1 after McDonough and Sun (1995).

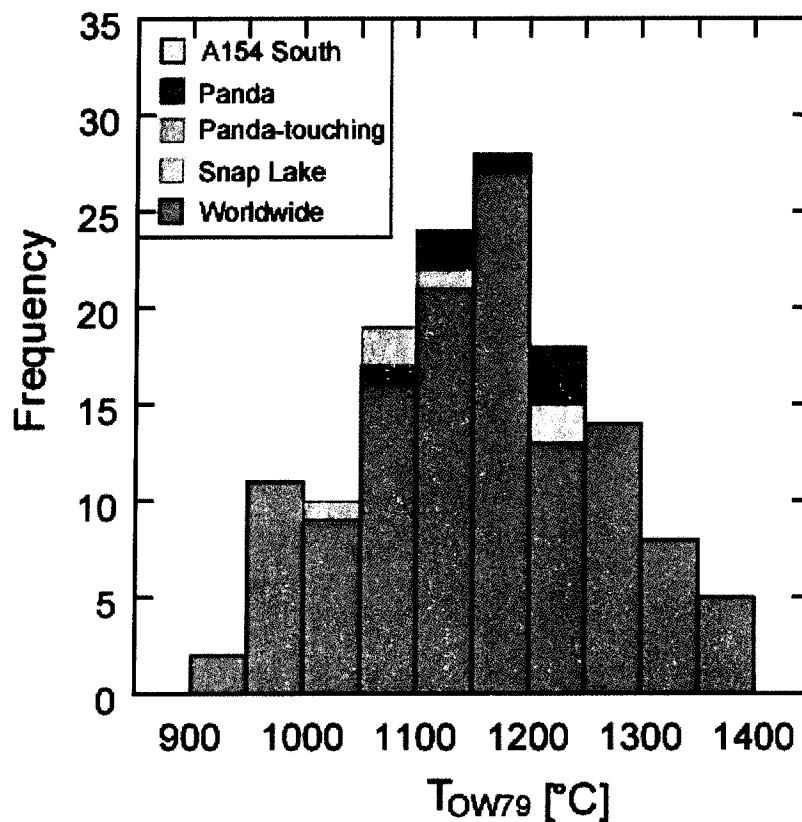


Figure 3.12. Histogram showing the calculated equilibration temperatures (at assumed pressures of 5 GPa) for coexisting garnet and olivine inclusions (O'Neill and Wood, 1979; O'Neill, 1980) from A154 South, the Slave craton and worldwide sources. Touching olivine-garnet inclusions from Panda yielded equilibration temperatures of 1000 to 1100°C (Stachel et al., 2003; Tappert et al., 2004).

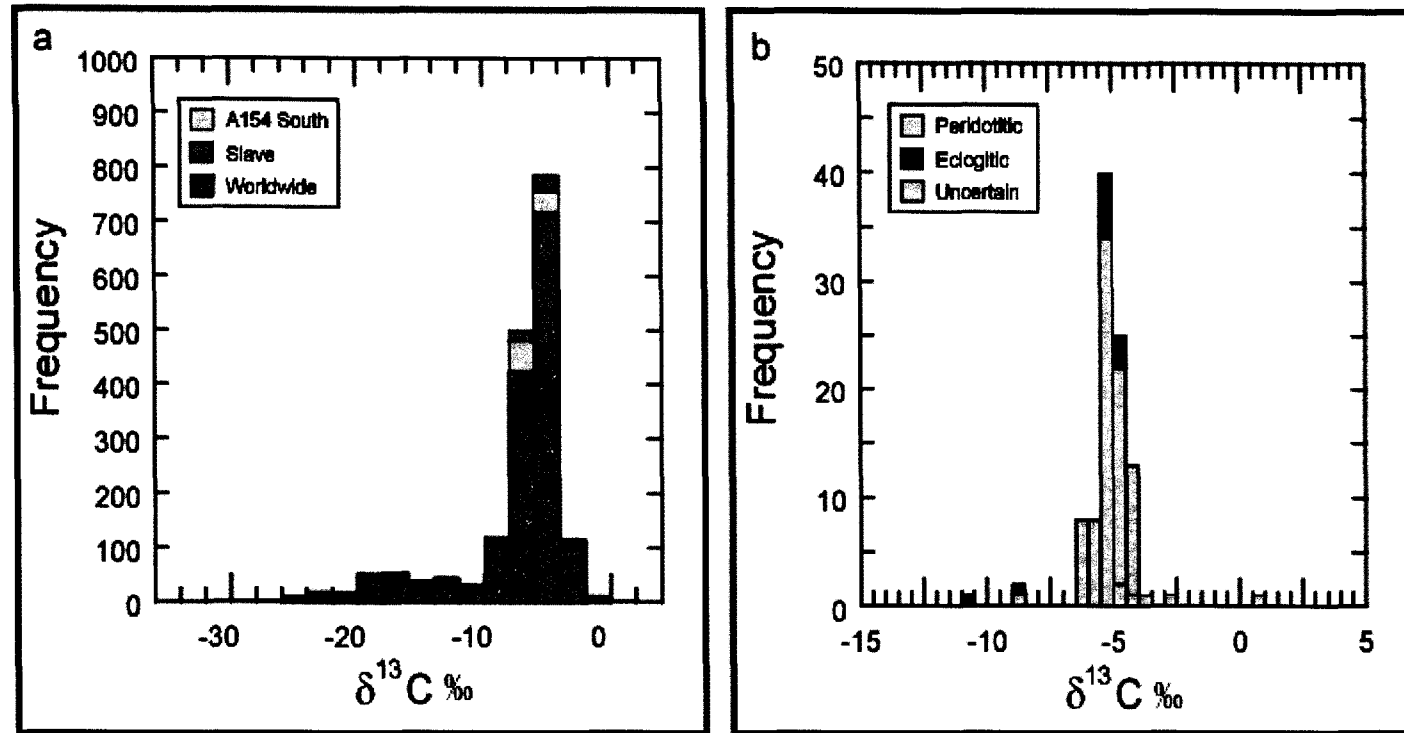


Figure 3.13. Histograms showing the carbon isotopic composition ($\delta^{13}\text{C}_{\text{PDB}}$) of diamonds from worldwide sources (Figure 3.13a) and from A154 South (Figure 3.13b, shown on a more detailed scale). Figure 3.13a shows diamonds from this study (blue), other Slave kimberlites and worldwide sources. Most of the isotopically light values observed for the Slave craton are from the dominantly eclogitic DO27 pipe (Davies et al., 1999 and 2004a). When the DO27 diamonds are removed, the $\delta^{13}\text{C}$ values for the Slave range from -16.8 to -2.1 ‰. The carbon isotopic distribution seen for the A154 South pipe is comparatively narrow, with 94% of diamonds having $\delta^{13}\text{C}$ values between -6.3‰ and -4.0‰.

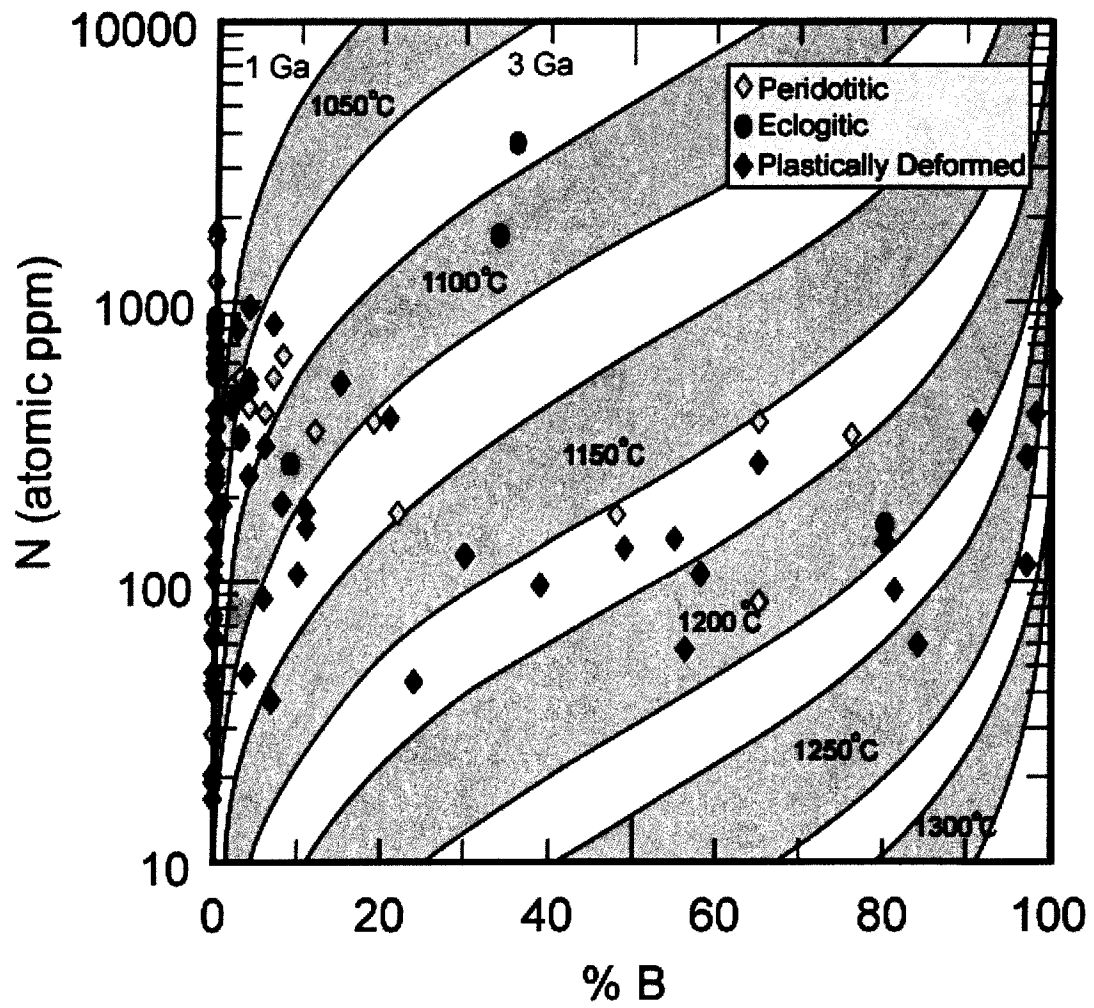


Figure 3.14. The log of the total nitrogen concentration (atomic ppm) versus the aggregation level (percentage of aggregation into the B-centre). Isotherms for time averaged (1 and 3 Ga) residence temperature after Taylor et al. (1990).

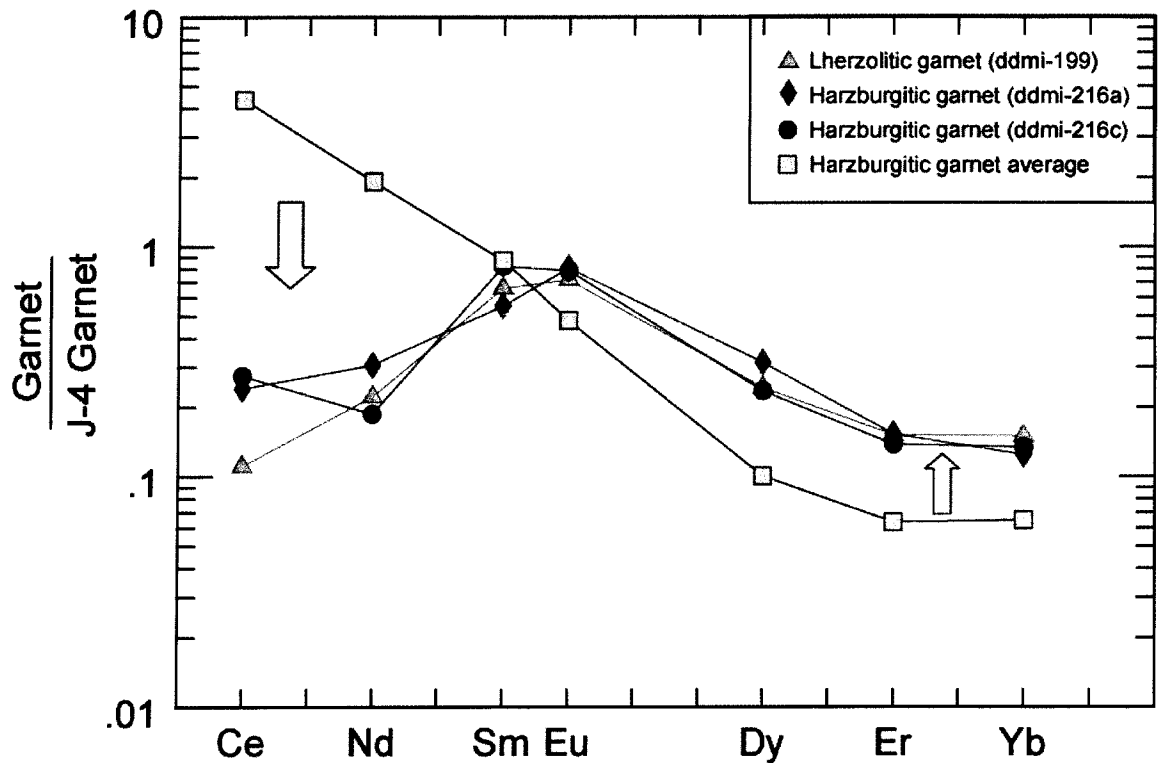


Figure 3.15. Illustration of the metasomatic re-enrichment event affecting harzburgitic garnets ddmi-216a and ddmi-216c from A154 South. Most harzburgitic garnets from A154 South have sinusoidal REE_N patterns typical for harzburgitic garnets worldwide. The single lherzolitic garnet from this study has a positive slope in the LREE_N and enrichment in the MREE_N and HREE_N. Two harzburgitic garnets from diamond ddmi-216 show evidence of metasomatic re-enrichment event with refertilization towards “normal” REE_N patterns typically observed among lherzolitic garnets. Stachel et al. (2004) attribute this style of re-enrichment as resulting from melt metasomatism, since it involves an agent with only moderately fractionated LREE/HREE. The rare earth element concentrations are normalized to a garnet from a primitive mantle bulk rock composition (J-4 garnet peridotite xenoliths from Jagersfontein) studied by Jagoutz and Spettel.

Chapter 4: Discussion and Conclusion

4.1. Introduction

Diamonds from the A154 South pipe of the Diavik Diamond mine in the central Slave craton have been characterized by combined studies of the morphological characteristics, carbon isotopic composition, nitrogen impurities, and mineral inclusion chemistry. This provides information for characterizing the diamond source regions and mantle storage environments, as well as the timing of diamond growth relative to kimberlite emplacement.

Until recent years, the bulk of information regarding diamond formation processes has come from diamond inclusion studies mainly from southern Africa and Siberia. The discovery of high-grade diamondiferous kimberlite pipes on the Slave craton in Canada has since led to a surge in diamond exploration. Canada's first diamond mine, Ekati, began production in 1998 and was followed by Diavik in 2003. The Jericho pipe in the northern Slave craton is on track to be the Slave's next diamond mine with production scheduled to begin in 2006 and Snap Lake is expected to start production in 2007. With increased exploration and the opening of new mines, comes the availability of research samples and the opportunity to study the lithospheric mantle of a comparatively uncharacterized craton. While limited diamond inclusion studies have been conducted in the Slave craton i.e. Chinn et al. (1998), Davies et al. (1999), Pokhilenko et al. (2001), Stachel et al. (2003), Davies et al. (2004a), Pokhilenko et al. (2004), and Tappert et al. (2004), similar studies are ongoing.

4.2. The Diamonds from A154 South

The diamonds discussed in this study were selected from the +9 to -11 and +11 sieve-size fraction of the run-of-mine production from A154 South at the Diavik Production Splitting Facility (PSF) in Yellowknife, Northwest Territories. This allowed for an opportunity to compare and contrast the inclusion-bearing diamond population with the remaining A154 South production in these size ranges. While the

Diavik mine is well known for producing high quality colourless, octahedral stones, it was found that the Diavik population, within the smaller diamond sizes studied, was actually dominated by resorbed morphologies. The dominant morphology observed was dodecahedral, while octahedral stones comprised 14% of the population and sharp-edged octahedra accounted for only 5% of the diamonds (see pages 162-164). Cubic morphologies (14%), twins (11%) and aggregates (3%) were also observed. A large proportion of the diamonds (30%) were found to have irregular shapes, or were partial diamond fragments that lacked distinguishing crystal faces. At larger diamond sizes (1, 3 and 5 carat stones), it was noted that the quality of the production greatly improved, yielding more octahedral stones at the expense of cubes and dodecahedral morphologies.

However, this morphological distribution was not observed within the inclusion-bearing diamond population. Inclusion-bearing stones were dominated by octahedra (39%), followed by dodecahedroids (23%) and irregular/fragmented (21%) stones. Twins (10%) and aggregates (8%) were also found to contain inclusions, however, the cubic stones were inclusion-free. Inclusion-bearing diamonds comprised <5% of the production within the +9 and +11 size range, and at larger diamond sizes the proportion of inclusion-bearing stones was found to be even considerably lower.

The dominant body colour of the Diavik production was colourless (63%), followed by brown (23%) (see page 163). Yellow, pink and grey stones were observed, but were rare. Conversely, the inclusion-bearing diamonds were dominated by brown stones (58%), followed by colourless (34%), pink (4%), yellow (2%) and grey (2%) stones.

While clear differences between the inclusion-bearing and non-inclusion-bearing populations were observed, there were no distinct correlations between the inclusion content, colour and morphology of the inclusion-bearing stones, excepting the observation that all ferropericlase-bearing diamonds were all faint brown in colour.

4.3. Diamond sources beneath the Diavik Mine and the central Slave

Davies et al. (1999) reported in their initial study of diamonds from pipe DO27 that the majority of diamonds were eclogitic (50%), with less abundant peridotitic (25%) diamonds and an abnormally large proportion (25%) of diamonds from super-deep sources. Mineral inclusions from DO27 revealed high Mg-numbers for olivine inclusions (average of 93.3) and a sole harzburgitic garnet showed high Cr₂O₃ and CaO contents of 14.76 and 5.00 wt%, compared to the worldwide averages of about 8 and 2 wt%, respectively (Davies et al., 1999). Subsequent studies (Chinn et al., 1998; Pokhilenko et al., 2001; Stachel et al., 2003; Pokhilenko et al., 2004; Tappert et al., 2004) have revealed that the diamond source regions in the Slave are not as anomalous as was initially indicated by the study of DO27. These later studies, as well as the data presented in this study of A154 South, found that the diamonds were dominantly (around 80%) peridotitic, with lesser eclogitic and rare sublithospheric diamonds.

The relatively high CaO content of the harzburgitic garnets and the comparatively low Mg numbers of the olivine inclusions from A154 South, as well as other Slave localities (Chinn et al., 1998; Davies et al., 1999; Pokhilenko et al., 2001; Stachel et al., 2003; Davies et al., 2004a; Pokhilenko et al., 2004; Tappert et al., 2004) indicate that diamond formation in the central Slave occurred in a moderately depleted peridotitic environment, compared to that of the Kaapvaal (Stachel et al., 2003, and references therein) or Siberian cratons (Griffin et al., 1993). The REE data from garnet inclusions in diamonds from A154 South, Panda (Tappert et al., 2004) and Snap Lake (Promprated et al., 2004) indicate that this less depleted nature of the diamond source regions may, in part, reflect metasomatic influences. The harzburgitic garnets in the Slave typically have sinusoidal REE_N patterns that are enriched in LREE, providing evidence for a depletion event followed by later re-enrichment in the Slave craton. This study also revealed that a more complex history is recorded by some of the A154 South garnets. The clear division in harzburgitic and lherzolitic REE_N patterns found at Panda (Tappert et al., 2004) and Snap Lake (Promprated et al., 2004) does not hold true for A154 South, as observed in the transitional harzburgitic garnets from diamond ddmi-216. Additionally, the eclogitic

garnets from A154 South are also anomalous, having REE_N concentrations and Ti, Y and Zr contents that are considerably lower than that observed for eclogitic garnets worldwide.

Inclusion based pressure-temperature estimates from the Slave craton indicate that diamond formation in the Slave occurred along a 40-42 mW/m² geotherm which is similar to diamond formation from other cratons (Stachel et al., 2003, and references therein). Touching-inclusion estimates reveal equilibration at lower temperatures, plotting closer to the 37 mW/m² geotherm (Stachel et al., 2003). Diamond formation temperature estimates from the A154 South diamonds, as determined from non-touching inclusion pairs, support these observations as the obtained temperatures of ~1200°C for A154 South correspond to formation along a 40-42 mW/m² geotherm.

Given the Archean Re-Os ages obtained for sulphide inclusions in diamonds from the Lac de Gras area (Pearson et al., 2002 and Westerlund et al., 2003b), the dominance of diamonds having low nitrogen aggregation states (Davies et al., 1999; Westerlund et al., 2001; Stachel et al., 2003; Westerland, 2003a; Davies et al., 2004a; Tappert et al., 2004 and this study) would indicate that the temperature decrease indicated by the touching-inclusion pairs must have occurred shortly after diamond formation. For this study of the A154 South diamonds, 65% of the diamonds were Type IaA diamonds with less than 10% of the nitrogen aggregated into the B-centre. Inclusion-based formation temperatures indicate formation at ~1200°C would then require cooling of the diamond source region on the order of 100-200°C to reconcile the inclusion and nitrogen based temperatures.

The amount of diamonds of sublithospheric origin in the Slave also appears to be considerably less than initially thought. Tappert et al. (2004) reported that 5% of diamonds from Panda contained mineral inclusion pairs of definitive lower mantle origin and Pokhilenko et al. (2004) reported that four garnets from Snap Lake contained a majoritic component (but likely still represent lithospheric sources). All of the diamonds containing inclusions of ferropericlase in this study of A154 South and the bulk of the ferropericlase-bearing diamonds from DO27 (Davies et al., 1999 and Davies et al., 2004a) lack the necessary inclusion pairs to unequivocally confirm

a lower mantle origin. A possible lithospheric origin for the ferropericlase-bearing diamonds from this study of the A154 South diamonds is further supported by the observed resorbed octahedral morphologies of the host diamonds, and the Type IaAB ferropericlase-bearing diamonds.

The diamond source regions in the Slave are also characterized by an uncommonly narrow carbon isotopic distribution of the diamonds. Carbon isotopic analyses have revealed that all of the A154 South diamonds from this study fall within a narrow range of -10.5‰ to +0.7‰, with 94% of these diamonds having typical mantle values of -6.3‰ and -4.0‰, irrespective of paragenesis. Similar narrow $\delta^{13}\text{C}$ distributions are also observed at Snap Lake (Pokhilenko et al., 2001 and 2004) and Panda (Westerlund et al., 2001 and 2003a). However a small number of eclogitic diamonds from Ekati (Chinn et al., 1999) and the bulk of the eclogitic diamonds from DO27 (Davies et al., 2004a) have isotopically lighter values. The narrow $\delta^{13}\text{C}$ distribution corresponding to typical mantle values observed in the A154 South diamonds may indicate that diamond formation resulted from an unfractionated fluid/melt carrying primordial carbon.

It has been proposed that a two-layered lithospheric structure exists in the central Slave (Griffin et al., 1999a; Griffin et al., 1999b; Pearson et al., 1999; O'Reilly et al., 2001; Menzies et al., 2004) and it has also been suggested that this lithosphere may also extend into the southwestern Slave (Carbno and Canil, 2002). Locally, within the Lac de Gras area, xenolith studies have shown no significant compositional variability (Pearson et al., 1999; Griffin et al., 1999a; Griffin et al., 1999b, Menzies et al., 2004) between individual kimberlite pipes. This suggests that the dominantly eclogitic mantle sample contained in the DO27 pipe is an anomaly in the central Slave and that this variance may be related to sampling by the kimberlite. Similar paragenetic associations, inclusion mineral chemistry, estimated P-T conditions of formation, narrow ranges of carbon isotopic composition of the diamonds and comparable nitrogen characteristics are observed among diamonds from the pipes at Ekati, Snap Lake/King Lake and A154 South.

References:

- Carbno, G.B., and Canil, D. 2002. Mantle structure beneath the SW Slave craton, Canada: constraints from garnet geochemistry in the Drybones Bay kimberlite. *Journal of Petrology*, 43, 129-142.
- Chinn, I.L., Gurney, J.J., and Kyser, K.T. 1998. Diamonds and mineral inclusions from the NWT, Canada. VIIth International Kimberlite Conference, Cape Town. Addendum, not paginated.
- Davies, R.M., Griffin, W.L., Pearson, N.J., Andrew, A.S., Doyle, B.J., and O'Reilly, S.Y. 1999. Diamonds from the Deep: Pipe DO-27, Slave Craton, Canada. In *Proceedings of the VII International Kimberlite Conference*, 148-155.
- Davies, R.M., Griffin, W.L., O'Reilly, S.Y., and Doyle, B.J. 2004a. Mineral inclusions and geochemical characteristics of microdiamonds from the D027, A154, A21, A418, D018, DD17 and Ranch Lake kimberlites at Lac de Gras, Slave Craton, Canada. *Lithos*, 77, 39-55.
- Griffin, W.L., Sobolev, N.V., Ryand, C.G., Pokhilenko, N.P., Win, T.T., and Yefimoya, E.S. 1993. Trace elements in garnets and chromites: Diamond formation in the Siberian lithosphere. *Lithos*, 29, 235-256.
- Griffin, W.L., Doyle, B.J., Ryan, C.G., Pearson, N.J., O'Reilly, S.Y., Davies, R., Kivi, K., van Achterbergh, E., and Natapov, L.M. 1999a. Layered mantle lithosphere in the Lac de Gras area, Slave craton: composition, structure and origin. *Journal of Petrology*, 40, 705– 727.
- Griffin, W.L., Doyle, B.J., Ryan, C.G., Pearson, N.J., O'Reilly, S.Y., Natapov, L., Kivi, K., Kretschmar, U., and Ward, J. 1999b. Lithosphere structure and mantle terranes: Slave craton, Canada. In: *Proceedings of the VIIth International Kimberlite Conference, The J.B. Dawson Volume*, Gurney, J.J., Gurney, J.L., Pascoe, M.D., and Richardson, S.H. (eds), Red Roof Design, Cape Town, 299–306.
- Kopylova, M.G., Russel, J.K., and Cookenboo, H. 1999b. Mapping the lithosphere beneath the north central Slave craton. In: *Proceedings of the VIIth International Kimberlite Conference, The J.B. Dawson Volume*, Gurney, J.J., Gurney, J.L., Pascoe, M.D., and Richardson, S.H. (eds), Red Roof Design, Cape Town, 468-479.
- Kopylova, M.G., and Caro, G. 2004. Mantle xenoliths from the southeastern Slave craton: evidence for chemical zonation in a thick, cold lithosphere. *Journal of Petrology*, 45, 1045-1067.

- Menzies, A.H, Westerlund, K.J, Grütter, H.G, Gurney, J.J, Carlson, J.W, Fung, A., and Nowicki, T.E. 2004. Peridotitic mantle xenoliths from kimberlites on the Ekati Diamond Mine property, N.W.T., Canada: major element compositions and implications for the lithosphere beneath the central Slave craton. *Lithos* 77, 35-412.
- O'Reilly, S.Y., Griffin, W.L., Djomani, Y.P., Natapov, L.M., Pearson, N.J., Davies, R.M., Doyle, B.J., and Kivi, K. 2001. The mantle beneath the Slave Craton (Canada): Composition and Architecture. The Slave-Kapvaal Workshop, Merrickville, Ontario, Extended Abstracts, 5p (CD, not paginated).
- Pearson, N.J., Griffin, W.L., Doyle, B.J., O'Reilly, S.Y., Van Achtenberg, E., Kivi, K. 1999. Xenoliths from kimberlite pipes of the Lac de Gras area, Slave Craton, Canada. In: Proceedings of the VIIth International Kimberlite Conference, The P.H. Nixon Volume, Gurney, J.J., Gurney, J.L., Pascoe, M.D., and Richardson, S.H. (eds), Red Roof Design, Cape Town, 644-658.
- Pearson, N.J., Alard, O., Griffin, W.L., Jackson, S.E., and O'Reilly, S.Y. 2002. In situ measurements of Re–Os isotopes in mantle sulfides by laser ablation multicollector-inductively coupled mass spectrometry: analytical methods and preliminary results. *Geochimica et Cosmochimica Acta*, 66, 1037– 1050.
- Pokhilenko, N.P. Sobolev, N.V., McDonald, J.A., Hall, A.E., Yefimova, E.S., Zedgenizov, D.A., Logvinova, A.M., and Reimers, L.F. 2001. Crystalline inclusions in diamonds from kimberlites of the Snap Lake area (Slave Craton, Canada): New evidences for the anomalous lithospheric structure. *Dokl. Earth Sci.*, 380, 806-811.
- Pokhilenko, N.P., Sobolev, N.V., Reutsky, V.N., Hall, A.E., and Taylor, L.A. 2004. Crystalline inclusions and C isotope ratios in diamonds from the Snap Lake/King Lake kimberlite dyke system: evidence of ultradeep and enriched lithospheric mantle. *Lithos*, 77, 57-67.
- Promprated, P., Taylor, L.A., Anand, M., Floss, C., Sobolev, N.V., and Pokhilenko, N.P. 2004. Multiple-mineral inclusions in diamonds from the Snap Lake/King Lake kimberlite dike, Slave craton, Canada: a trace-element perspective. *Lithos*, 77, 69-81.
- Stachel, T., Harris, J.W., Tappert, R., and Brey, G.P. 2003. Peridotitic inclusions in diamonds from the Slave and the Kaapvaal cratons - similarities and differences based on a preliminary data set. *Lithos*, 71, 489-503.
- Tappert, R., Stachel, T., Harris, J.W., Shimizu, N., and Brey, G.P. 2004. Mineral inclusions in diamonds from the Panda kimberlite, Slave Province, Canada. *European Journal of Mineralogy*, 17, 423-440.

- Westerlund, K.J., Gurney, J.J., Shirey, S.B., and Hauri, E. 2001. Nitrogen aggregation and stable nitrogen and carbon isotope characteristics of diamonds from the Panda kimberlite, Slave craton, Canada. The Slave-Kapvaal Workshop, Merrickville, Ontario, Extended Abstracts, 5p (CD, not paginated).
- Westerlund, K.J., Hauri, E.H., and Gurney, J.J. 2003a. FTIR absorption and stable nitrogen and carbon isotope microanalysis of mid-Archean diamonds from the Panda kimberlite. VIIIth International Kimberlite Conference, Victoria, Canada, Extended Abstracts, 4p (CD, not paginated).
- Westerlund, K.J., Shirey, S.B., Richardson, S.H., Gurney, J.J., and Harris, J.W. 2003b. Re-Os systematics of diamond inclusion sulfides from the Panda kimberlite, Slave craton. VIIIth International Kimberlite Conference, Victoria, Canada, Extended Abstracts, 5p (CD, not paginated)

Appendix A: Analytical Methods

A.1. Diamond Cleaning

After receiving samples from the Diavik Product Splitting Facility (PSF) in Yellowknife, the diamonds were thoroughly cleaned in the laboratory of Dr. Larry Heaman. Samples were placed in 5mL PFA Teflon vials which were filled with ~4mL of 48% reagent grade hydrofluoric acid. The vials were placed on a hot plate and heated at ~70°C overnight. The vials were removed from the hotplate and placed in an ultrasonic bath for 5 minutes. The hydrofluoric acid was diluted and decanted using distilled water. The samples were then rinsed and decanted three times with distilled water and a further three times using ethanol. The diamonds were dried at room temperature on weigh paper and placed in their respective sample containers. Prior to analysis, each stone was cleaned using an ultrasonic bath with ethanol for ~10 minutes.

A.2. Diamond Crushing and Polishing

Following detailed microscopic examination to document inclusion content and all distinguishing features, the diamonds were cracked using a steel piston crusher. After breakage, the inclusions were recovered and individually mounted in ~5 mm long brass rings, having an inside diameter of 5 mm, using Araldite[®] epoxy resin. The brass rings were then placed on a hot plate at ~45°C and left to harden for 48 hours. After hardening of the resin, the samples were polished on 600 and 800 grit plates. A final polish was performed using a silk-screen plate and 1/4 µm diamond paste. The samples were then cleaned for ~5 minutes using an ultrasonic bath with purified ethanol.

A.3. Electron-Probe Microanalysis (EMPA)

A.3.1. Introduction

The concentrations of major and minor elements of the mineral inclusions in the A154 South diamonds were quantitatively determined using electron microprobe (EMPA) techniques. For analysis, a beam of electrons was used to bombard the sample, resulting in the emission of characteristic X-rays. When the incident electrons interact with the atoms of the sample they do not penetrate in a linear

fashion, but rather become scattered. Two different types of scattering occur, elastic and inelastic. During elastic scattering the kinetic energy and velocity remain constant, but the trajectory changes, resulting in a process known as *electron backscattering*. During inelastic scattering, there are only slight changes in the trajectory, however there is energy lost due to interactions with the orbital electrons of the sample. This inelastic interaction will result in the following phenomenon:

- a) photon excitement (heating)
- b) cathodoluminescence
- c) continuum radiation (bremsstrahlung radiation)
- d) production of secondary electrons
- e) production of backscattered electrons
- f) ejection of outer shell electrons (Auger electron production)
- g) emission of *characteristic x-rays* (WDS and EDS)

If electrons of sufficient energy strike the sample, each element present in the sample will emit characteristic X-rays having wavelengths unique to that particular element. The intensities of X-ray production at these wavelengths can then be detected and measured. A quantitative measure may then be obtained, after comparison to standards and matrix corrections are applied.

A.3.2. Instrumentation

The JXA-8900 SuperProbe at the University of Alberta is equipped with 5 wavelength dispersive X-ray spectrometers (WDS). In a WDS spectrometer, the X-rays impinge upon a diffracting crystal that is set at a particular angular position designed to diffract only the characteristic X-ray of interest. The diffracted X-rays will then enter a gas-filled proportional counter and are counted. Several elements can be measured on a single spectrometer, as the position of the diffracting crystal and the associated counter can be adjusted to accept a range of characteristic wavelengths.

The electron microprobe at the University of Alberta is also equipped with an energy dispersive spectrometer (EDS). For EDS, the entire X-ray spectrum is

acquired simultaneously, allowing for a prompt qualitative assessment of the sample. While EDS can be also be used for the analysis of some major elements, the WDS method used in this study provided precise measurement of major and minor elements.

The JXA-8900 SuperProbe also contains a backscatter electron detector (BSE) which is used for sample imaging during this study. The backscatter efficiency is a function of the atomic number of the sample, thus the image contrasts seen are due to the differences in the atomic number of the various phases in the sample.

A.3.3. Sample Preparation

Each sample was cleaned for ~5 minutes in an ultrasonic bath using ethanol, followed by an additional ~5 minutes in petroleum ether. Samples were then carbon coated, to attain electrical conductivity, by combusting carbon rods in a vacuum chamber.

A.3.4. Analytical Settings

Wavelength dispersive X-ray spectrometers (WDS) were used for quantitative analyses. Analyses were conducted using a 20 kV acceleration voltage and a 20 nA beam current with a beam size of 1-3 μm . Spectrometer settings for silicate phases, spinels and sulphides are summarized in Table B.1, showing (1) X-ray line, (2) detector crystal, (3) background measurement position relative to the peak position, (4) background and peak counting times, (5) measurement mode, and (6) secondary standards.

Natural and synthetic silicate, oxide and metal standards were used. Detection limits (Table B.2) were calculated at 99% confidence (exceeding 3 standard deviations of the background, $3\sigma_b$) using the following equation, where I_p and I_b are the peak and background count rates (cps), respectively, and t_b is the time of background counting.

$$DL = 3\sqrt{I_b t_b} / (I_p t_b - I_b t_b)$$

Detection limits were less than 200 ppm for all silicates, oxides and metals, excepting TiO₂ (207 ppm) for silicate analyzes, Ti (231 ppm), and Cr₂O₃ (643 ppm) for spinel analyses, and Cr (575 ppm) and Zn (257 ppm) for sulphide analyses.

A.4. Secondary Ion Mass Spectrometry (SIMS)

A.4.1. Introduction

The concentrations of selected rare earth elements (REE: La, Ce, Nd, Sm, Eu, Dy, Er and Yb) and additional trace elements (Ti, Sr, Y, and Zr) of 12 garnet inclusions were determined using Secondary Ion Mass Spectrometry (SIMS). Measurements were conducted at the Northwest National Ion Microprobe Facility (NENIMF) at the Woods Hole Oceanographic Institute by Dr. Nobumichi Shimizu using a CAMECA IMS-3f ion microprobe.

For analysis, negatively charged oxygen ions are accelerated onto a clean, gold coated surface (providing electrical conductivity). This energetic bombardment causes atoms of the sample to be ejected in a spluttering process. Thus, the surface of the sample becomes a source of secondary ions which represent the elements or isotopes found in the near surface region of the sample. The resulting secondary ions are accelerated into the mass spectrometer where they are separated according to their mass and are counted at the detector.

The SIMS technique is considered “destructive” as it generally creates a pit on the order of 10 to 20 μm in diameter, having a depth of a few microns. However, with large enough grains, or additional polishing, repeat analyses are possible. Another key advantage of the SIMS technique is that it can provide sensitivities near parts per billion.

A.4.2. Sample Preparation

Each polished sample was cleaned for ~5 minutes in an ultrasonic bath using ethanol, followed by an additional ~5 minutes in petroleum ether. Samples were then coated with gold to attain electrical conductivity.

A.4.3. Analytical Settings

Secondary ions were sputtered by bombardment of the sample with a beam of negatively charged oxygen ions. The nominal impact energy of the primary beam on the sample surface was 14.5 keV. The primary beam size used was 20 μm for the determination of the REE concentrations and $\sim 5 \mu\text{m}$ for the trace element determination of Ti, Sr, Y, and Zr. An energy offset of -60V for REE and -90V for trace elements (Ti, Sr, Y and Zr) was applied to suppress molecular interferences (Shimizu and Hart, 1982). Count rates for each element and the background were collected for 50 seconds. Elemental abundances were calculated using empirical relationships between concentration and secondary ion yields for well-established standards (working curves) and normalization to an internal silicon standard. The results were further verified by repeat analyses of secondary mineral standards (PN1 and PN2). Analytical uncertainties were on the order of 10-25% (relative) for REE and 5-15% for other trace elements.

A.5. Carbon Stable Isotope Analysis

A.5.1. Sample Preparation

For carbon isotope analysis, 1-2 g of purified copper oxide (CuO), as a oxygen source, was combined with 0.5-1.5 mg of diamond fragments (clear, transparent single fragments where available) in a ~ 25 cm long quartz glass tube, with a 5 mm diameter. The tube was evacuated overnight and was then cut and sealed using a blow torch to remove it from the vacuum line. The sealed tube was then heated for ~ 10 hours at 980°C to combust the diamond fragments and allow for the formation of CO_2 gas. After slow cooling (2-3 hours) the quartz tube was then broken under vacuum. The CO_2 gas was extracted under vacuum, using nitrogen traps and a mixture of dry ice and ethanol to remove impurities. The volume of sample gas was measured during the extraction to assure that there was complete combustion of the sample. The sample gas was transferred to glass sample tubes.

A.5.2. Sample Analyses

Measurements of the carbon isotopic composition of the diamonds were determined in the Stable Isotope Laboratory at the University of Alberta by Dr. Karlis Muehlenbachs, using a Finnigan Mat 252 Mass Spectrometer. Eight analytical cycles were performed for each sample to ensure high accuracy. For calibration, a laboratory-standard CO₂ gas was measured simultaneously.

The carbon isotopic composition is expressed using delta (δ) notation, where δ is the difference in the isotopic ratio between the sample and a standard, expressed in parts per thousand or per mille (‰). The $\delta^{13}\text{C}$ are reported relative to the PDB (belemnite from the Peedee Formation) standard.

$$\delta^{13}\text{C}_{\text{sample}} = \left[\frac{{}^{13}\text{C}/{}^{12}\text{C}_{\text{sample}} - {}^{13}\text{C}/{}^{12}\text{C}_{\text{standard}}}{{}^{13}\text{C}/{}^{12}\text{C}_{\text{standard}}} \right] \times 1000$$

Three diamonds were selected for a reproducibility study (Table B.3), whereby four separate measurements per stone revealed a maximum variation of 0.18‰. The observed variation may be related to slight differences in the combustion and/or extraction process, or to isotopic heterogeneities within the diamond. Analytical precision is on the order of $\pm 0.1\%$.

A.6. Fourier Transform Infrared (FTIR) Spectroscopy

A.6.1. Introduction

The concentration and aggregation state of the nitrogen impurities in the A154 South diamonds were determined using Fourier Transform Infrared (FTIR) Spectrometry. Nitrogen is the most frequently occurring impurity in diamond and can be present in concentrations exceeding 1000 ppm. Nitrogen is present in most diamonds, but the aggregation of the nitrogen has been found to vary. Diamonds are classified into the following categories, based on the presence or absence of nitrogen and its aggregation state:

- Type I: Diamonds that contain detectable nitrogen; subdivided into:
- Type Ia: Diamonds containing aggregated nitrogen (A-centres, B-centres, N3-centres and platelets), further subdivided into:
 - Type IaA: Diamonds having ($\geq 90\%$) of the nitrogen in A-centres
 - Type IaB: Diamonds having ($\geq 90\%$) of the nitrogen in B-centres
 - Type IaAB: Diamonds with nitrogen in both A- and B-centres
 - Type Ib: Diamonds with single substitutional nitrogen
- Type II: Diamonds that do not contain nitrogen, or concentrations of nitrogen below the level of detection; subdivided into:
- Type IIa: Nitrogen free diamonds
 - Type IIb: Diamonds with boron as the major impurity

A.6.2. Sample Preparation

Analyses were conducted on transparent, inclusion-free diamond cleavage chips recovered from the initial diamond breaking. Between two and five analyses were performed for each diamond, with reported concentrations representing an average. The cleavage chips were individually placed onto a sample holder under the IR microscope.

A.6.3. Analytical Settings

Measurements were conducted at the University of Alberta using a Thermo Nicolet Nexus 470 FT-IR spectrometer coupled with a Continuum IR microscope that was equipped with a KBr beam splitter.

The system was continuously purged with nitrogen gas to maintain a stable environment and prior to analysis a background measurement was performed. Additional background measurements were conducted every two to three hours. Measurements were collected in transmission mode using an aperture size ranging between 50 and 100 μm , as determined by sample size. Spectra were collected in the range of 650 to 4000 cm^{-1} for 200 seconds, at a spectral resolution of 4 cm^{-1} .

In order to determine the nitrogen concentration and aggregation state of a sample quantitatively, the spectra of the sample diamond were background corrected, normalized to a thickness of 1cm and the resulting spectra were then deconvoluted.

The normalization was accomplished by measuring the absorption spectrum of a Type II (nitrogen free) diamond standard and performing baseline correction. The absorbance at 1995 cm^{-1} was then determined and normalized to 11.94, the experimentally determined intrinsic absorbance in diamond.

During the measurement of an unknown sample, the sample spectra were baselined and then the normalized Type II spectrum was “subtracted” (involving a normalization process), removing the pure diamond spectrum from the nitrogen spectrum. Spectral deconvolution, using the deconvolution software *CAXBO87* developed by David Fischer (Research Laboratories of the Diamond Trading Company, Maidenhead, UK), was used to determine nitrogen contents and aggregation states. The deconvolution program separated the sample spectrum into A-, B- and D-components and calculated the absorption coefficient values for each component. Examples of Type IaA, IaB and IaAB spectra are shown in Figure B.1.

Nitrogen concentrations (atomic ppm) were calculated from absorption coefficient values at 1282 cm^{-1} using experimentally derived conversion factors for the A-centre (Boyd et al., 1994) and the B-centre (Boyd et al., 1995). Detection limits and analytical errors are variable as they are highly dependant on sample quality. Detection limits and analytical errors are typically on the order of 10 - 20 ppm.

References

- Boyd, S.R., Kiflawi, I., and Woods, G.S. 1995. Infrared absorption by the B nitrogen aggregate in diamond *Philosophical Magazine B*, 72, 351-361.
- Boyd, S.R., Kiflawi, I., and Woods, G.S. 1994. The relationship between infrared absorption and the A defect concentration in diamond. *Philosophical Magazine B*, 69, 1149-1153.
- Shimizu, N., and Hart, S.R. 1982. Applications of the ion microprobe to geochemistry and cosmochemistry. *Annual Review of Earth and Planetary Sciences*, 10, 483-526.

Table A.1. Settings for the quantitative electron microprobe analysis (EMPA) of major and minor elements using wavelength dispersive spectrometers (WDS).

Minerals: Silicates

Element	X-Ray	Crystal	Background Position		Count Times		PHA Mode	Standard
			Lower	Upper	Peak	Backgr.		
K	K α	PET	2.500	2.500	20	10	Differential	Orthoclase
V	K α	LIFH	3.000	3.000	30	15	Integral	V-metal
P	K α	PETH	1.800	1.500	20	10	Differential	Apatite
Na	K α	TAPJ		3.000	30	30	Differential	Albite
Ni	K α	LIFH	1.500	1.500	50	25	Integral	Ni-metal
Ti	K α	PET	2.000	2.000	50	25	Differential	Rutile
Al	K α	TAP	2.600	2.000	20	10	Differential	Pyrope
Ca	K α	PETH	2.000	2.000	20	10	Integral	Diopside
Si	K α	TAPJ		2.000	20	10	Differential	Diopside
Fe	K α	LIFH	2.600	1.500	20	10	Differential	Fayalite
Cr	K α	PET	1.931	2.000	20	10	Differential	Chromite
Mn	K α	LIFH	2.000	2.000	30	15	Integral	Mn ₂ O ₃
Mg	K α	TAP		3.000	30	30	Differential	FeO ₉₃

Table A.1. (cont.)

Minerals: Spinel

Element	X-Ray	Crystal	Background Position		Count Times	PHA Mode	Standard
			Lower	Upper			
Ti	K α	PET	2.000	2.000	50.0	Differential	Rutile
V	K α	LIFH	3.000	3.000	15.0	Intergral	V-metal
Si	K α	TAPJ		2.000	100.0	Differential	Diopside
Ni	K α	LIFH	1.500	1.500	15.0	Intergral	Ni-metal
Cr	K α	PET	1.931	2.000	50.0	Differential	Chromite
Al	K α	TAPJ	2.600	2.000	20.0	Differential	Pyrope
Fe	K α	LIFH	2.600	1.500	10.0	Differential	Fayalite
Zn	K α	LIFH	1.500	1.500	100.0	Differential	Gahnite
Mn	K α	LIFH	2.000	2.000	15.0	Intergral	Mn ₂ O ₃
Mg	K α	TAP		3.000	20.0	Differential	F _{0.93}

Table A.1. (cont.)

Minerals: Sulphides

Element	X-Ray	Crystal	Background Position		Count Times		PHA Mode	Standard
			Lower	Upper	Peak	Backgr.		
Cr	K α	PET	1.931	2.000	40.0	20.0	Differential	Chromite
Mn	K α	LIF	2.000	2.000	100.0	50.0	Differential	Mn-metal
Si	K α	TAPJ		2.000	30.0	15.0	Differential	Diopside
Fe	K α	LIFH	2.600	1.500	20.0	10.0	Differential	Fayalite
S	K α	PET	1.700	1.700	40.0	20.0	Differential	Pyrite
Co	K α	LIFH		1.500	30.0	15.0	Intergal	Co-metal
Zn	K α	LIFH	1.500	1.500	40.0	20.0	Intergal	sphalerite
Ni	K α	LIFH	1.500	1.500	50.0	25.0	Intergal	Ni-metal
Cu	K α	LIFH	1.500	1.500	40.0	20.0	Intergal	Cu-metal
As	L α	TAPJ	2.000	2.000	30.0	15.0	Differential	As ₂ Te ₅
Mg	K α	TAPJ		3.000	30.0	15.0	Differential	F ₀₉₃

Table A.2. Electron microprobe analyses (EMPA) detection limits calculated at 99% confidence.

Minerals: Silicates

Element	Peak Intensity (cps)	Background Intensity (cps)	Peak Time (s)	Background Time (s)	No. Averaged Analyses	Detection Limit (relative wt%)	Standard (wt %)	Detection Limit (wt %)	Detection Limit (ppm)
K ₂ O	2745.9	37.3	20	20	5	0.00068	14.920	0.0101	101
MgO	738.5	11.8	30	30	5	0.00116	8.600	0.0100	100
P ₂ O ₅	3875.5	50.5	35	35	5	0.00042	40.870	0.0172	172
Na ₂ O	1028.1	9.1	30	30	5	0.00073	11.590	0.0084	84
NiO	39015.6	286.3	25	25	5	0.00012	127.253	0.0149	149
TiO ₂	21573.8	268.85	25	25	5	0.00021	100.000	0.0207	207
Al ₂ O ₃	1872.3	72	20	20	5	0.00141	12.600	0.0178	178
CaO	9210.4	90.8	30	30	5	0.00026	25.740	0.0066	66
SiO ₂	11909	54.9	10	10	5	0.00027	55.370	0.0147	147
FeO	16743.7	102.6	15	15	5	0.00021	67.550	0.0142	142
Cr ₂ O ₃	7484.8	115.25	20	20	5	0.00044	40.700	0.0178	178
MnO	20327.4	97.45	15	15	5	0.00017	89.866	0.0152	152
V ₂ O ₃	49562.1	115.65	15	15	5	0.00008	147.114	0.0111	111

Table A.2. (cont.)

Minerals: Spinel

Oxide	Peak Intensity (cps)	Background Intensity (cps)	Peak Time (s)	Background Time (s)	No. Averaged Analyses	Detection Limit (relative wt%)	Standard (wt %)	Detection Limit (wt %)	Detection Limit (ppm)
MgO	7624.4	18.5	30	30	4	0.00015	51.630	0.0080	80
NiO	39015.6	286.0	50	25	4	0.00013	127.253	0.0167	167
TiO ₂	21573.8	268.9	50	25	4	0.00023	100.000	0.0231	231
ZnO	5261.4	128.85	100	100	4	0.00033	42.500	0.0141	141
Al ₂ O ₃	1951.9	35.7	20	10	4	0.00148	12.600	0.0186	186
SiO ₂	12512.0	42.3	20	10	4	0.00025	55.370	0.0137	137
FeO	16835.9	108.2	20	10	4	0.00029	67.550	0.0199	199
Cr ₂ O ₃	7554.4	544.7	20	10	4	0.00158	40.700	0.0643	643
MnO	20327.4	97.5	30	15	4	0.00019	89.866	0.0170	170
V ₂ O ₃	49562.1	115.7	30	15	4	0.00008	147.114	0.0124	124

Table A.2. (cont.)

Minerals: Sulphides

Element	Peak Intensity (cps)	Background Intensity (cps)	Peak Time (s)	Background Time (s)	No. Averaged Analyses	Detection Limit (relative wt%)	Standard (wt %)	Detection Limit (wt %)	Detection Limit (ppm)
Cr	7554.4	544.7	20	10	5	0.00141	40.700	0.0575	575
Mn	4555.5	16.2	100	50	5	0.00017	100.000	0.0168	168
Si	12512.0	16.2	30	15	5	0.00011	25.884	0.0029	29
Fe	16835.9	108.15	20	10	5	0.00026	52.508	0.0138	138
S	5439.9	37.6	40	20	5	0.00034	53.447	0.0182	182
Mg	8707.1	8.1	30	15	5	0.00011	31.137	0.0035	35
Co	36708.0	253.4	30	15	5	0.00015	100.000	0.0151	151
Ni	37822.6	290.7	50	25	5	0.00012	100.000	0.0122	122
Cu	34172.7	302.5	40	20	5	0.00015	100.000	0.0154	154
Zn	11154.9	198	40	20	5	0.00039	66.800	0.0257	257

Table A.3. Results of three reproducibility experiments used to examine the variability of the obtained carbon isotopic values.

Sample	No. Fragments	Weight (mg)	$\delta^{13}\text{C}$ (‰)
ddmi-269(1)	1	1.2	-5.420
ddmi-269(2)	1	0.8	-5.452
ddmi-269(3)	2	0.9	-5.471
ddmi-269(4)	1	1.6	-5.418

Average = -5.440
Standard Deviation = 0.026
Maximum Variability = 0.051

Sample	No. Fragments	Weight (mg)	$\delta^{13}\text{C}$ (‰)
ddmi-44(1)	1	1.0	-5.020
ddmi-44(2)	1	1.3	-4.923
ddmi-44(3)	1	0.9	-5.014
ddmi-44(4)	1	1.2	-4.971

Average = -4.982
Standard Deviation = 0.045
Maximum Variability = 0.097

Sample	No. Fragments	Weight (mg)	$\delta^{13}\text{C}$ (‰)
ddmi-1(1)	4	1.0	-4.480
ddmi-1(2)	4	0.8	-4.504
ddmi-1(3)	1	0.6	-4.435
ddmi-1(4)	3	0.7	-4.322

Average = -4.435
Standard Deviation = 0.081
Maximum Variability = 0.182

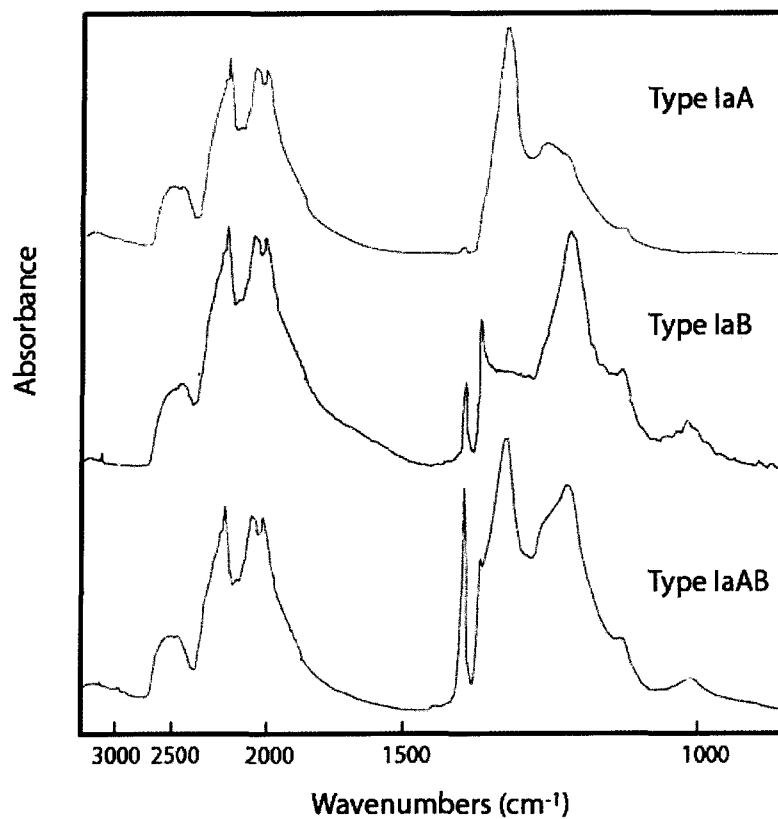


Figure A.1. Examples of infrared spectra of Type IaA, Type IaB, and Type IaAB diamonds collected from A154 South samples ddmi-7, ddmi-129, and ddmi-213, respectively.

Appendix B: Diamond Photographs

B.1. Morphologies

Octahedra

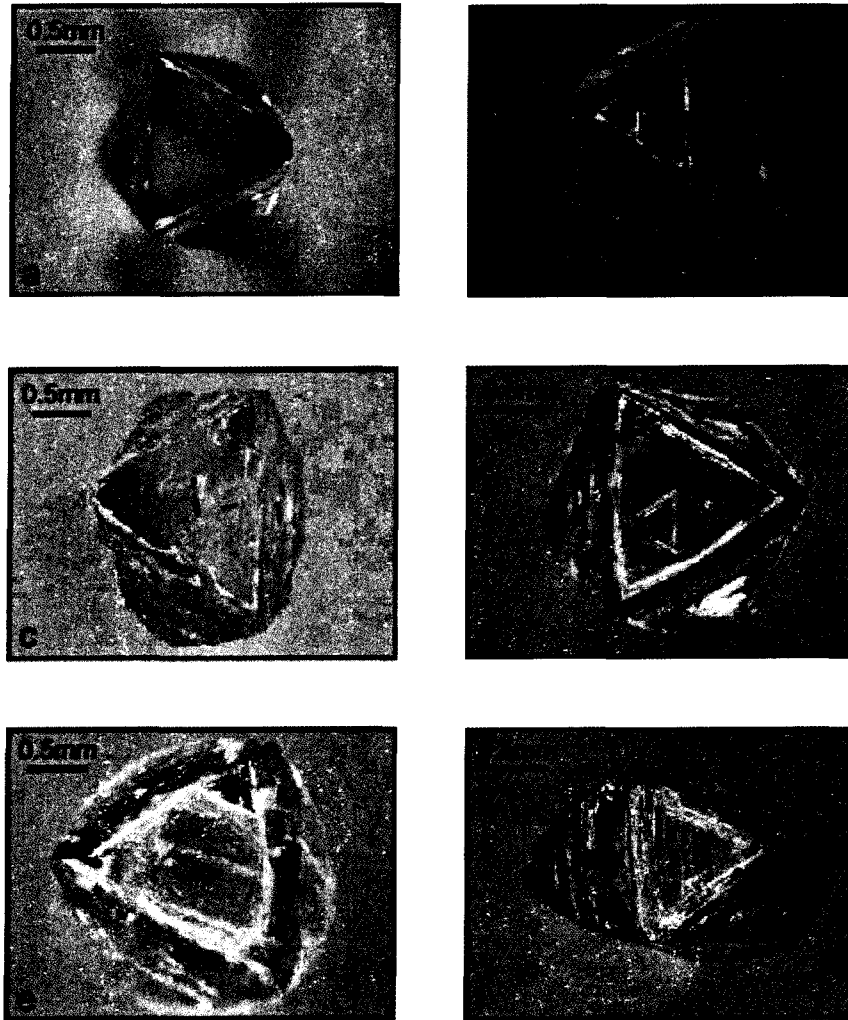


Figure B.1. Examples of representative octahedral crystals. (a) Flat-faced octahedron. (b) Tabular octahedron. (c-e) Slightly resorbed octahedron. (f) Elongated, slightly resorbed octahedron. Photographs (a-f) are from diamonds ddmi-157, ddmi-143, ddmi-202, ddmi-206, ddmi-141, and ddmi-46.

Cubes

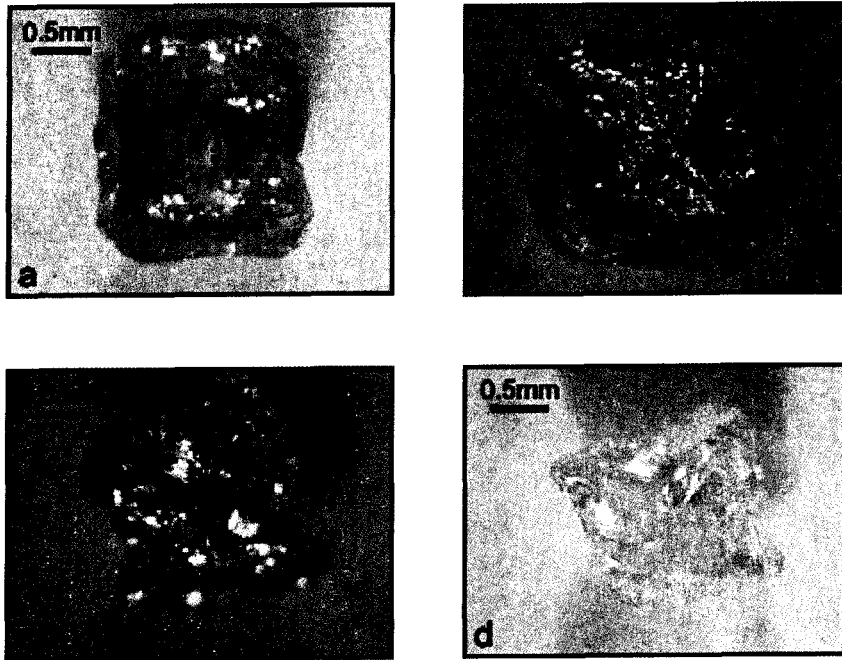


Figure B.2. Examples of cube morphologies. Photographs (a-d) are from diamonds ddmi-218, ddmi-178, ddmi-219, and ddmi-220.

Twins

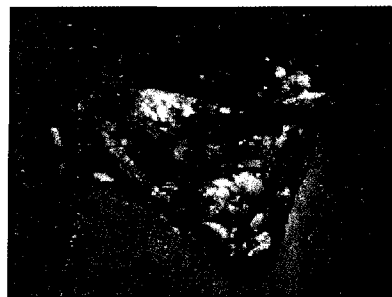
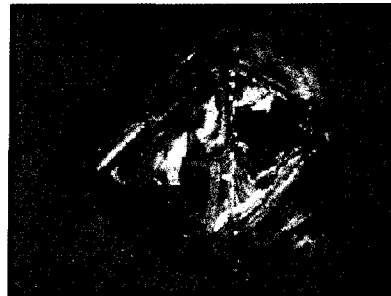


Figure B.3. (a) Octahedral macle (spinel twin). (b) Octahedral contact twin. (c) Tetrahedral twin. Photographs (a-c) are from diamonds ddmi-221, ddmi-129, and ddmi-189.

Tetrahexahedra

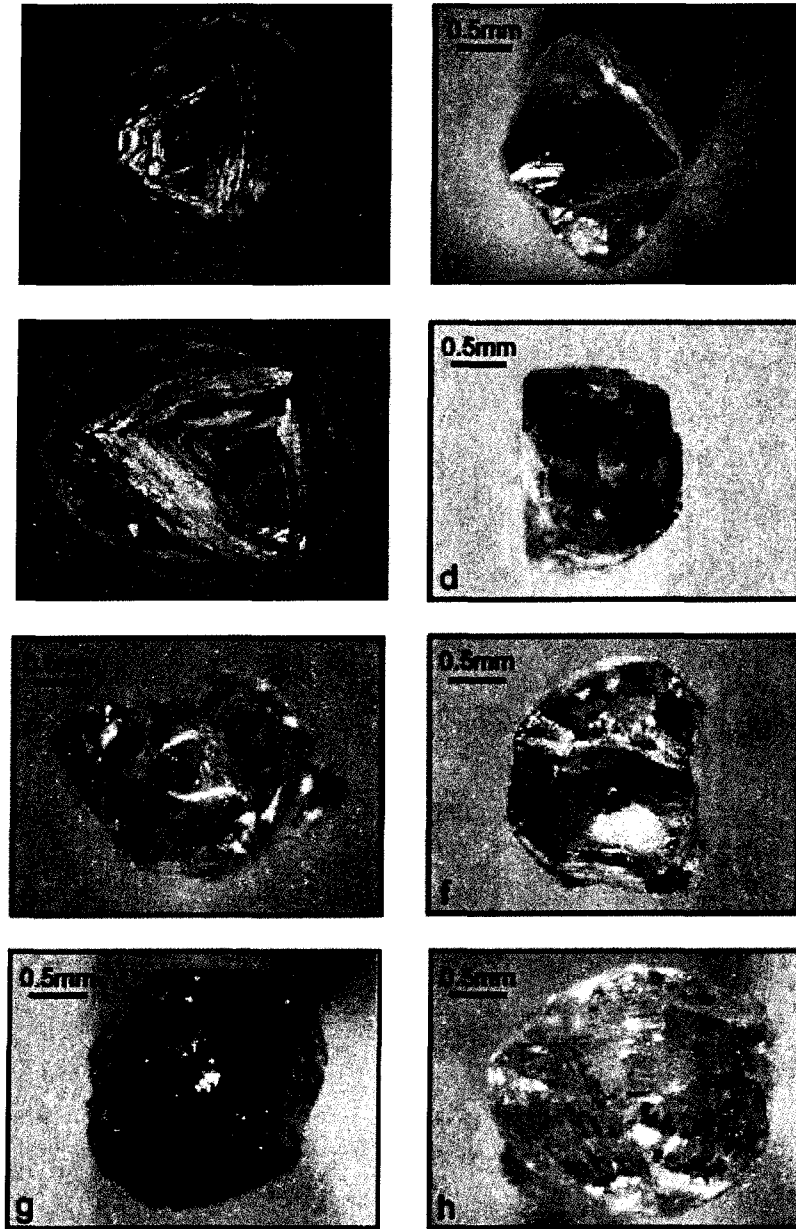


Figure C.B. Representative dodecahedroid shapes, classified based on >50% resorption to dodecahedral faces. (a-f) Scale of increasing degree of resorption, from 50% to 90%. (g-h) Fully resorbed dodecahedra crystals. Photographs (a-h) are from diamonds ddmi-134, ddmi-48, ddmi-201, ddmi-129, ddmi-136, ddmi-127, ddmi-222, and ddmi-223.

Aggregates

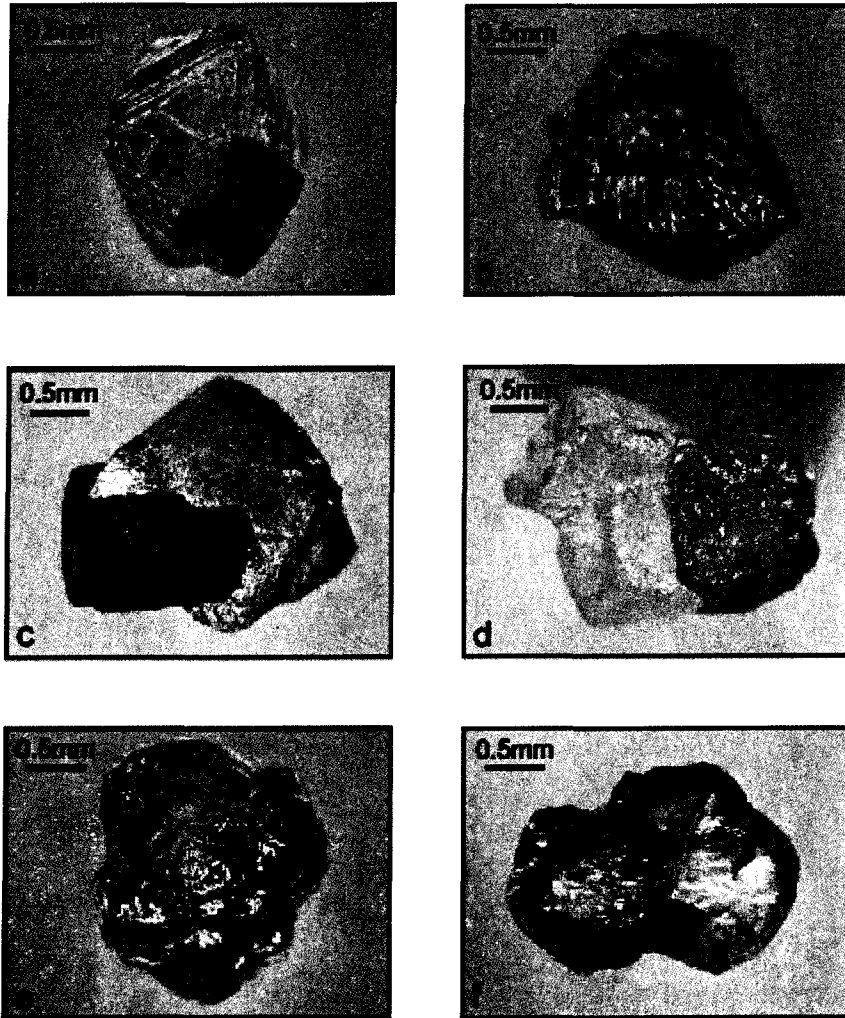


Figure B.5. Aggregates of three or more stones. (a-c) Octahedral aggregates. (d) Aggregate of three cubes. (e-f) Tetrahexahedra aggregates. Photographs (a-f) are from diamonds ddmi-162, ddmi-135, ddmi-177, ddmi-217, ddmi-198, and ddmi-189.

Irregular

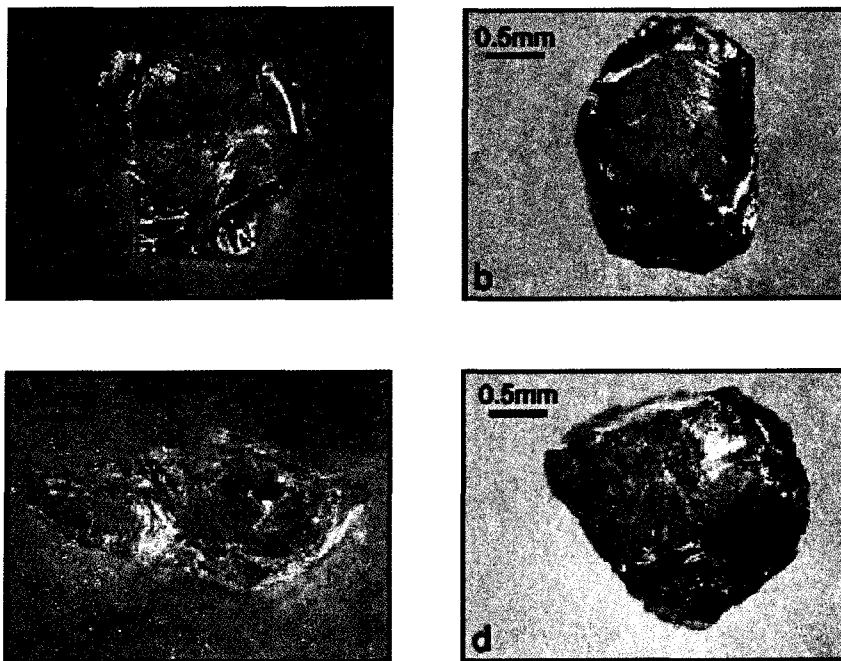


Figure B.6. Examples of diamonds having irregular shapes. These stones lack distinguishing crystal faces that would allow for the classification into one of the other morphological subdivisions. Photographs (a-d) are from diamonds ddmi-160, ddmi-47, ddmi-203, and ddmi-44.

Fragments

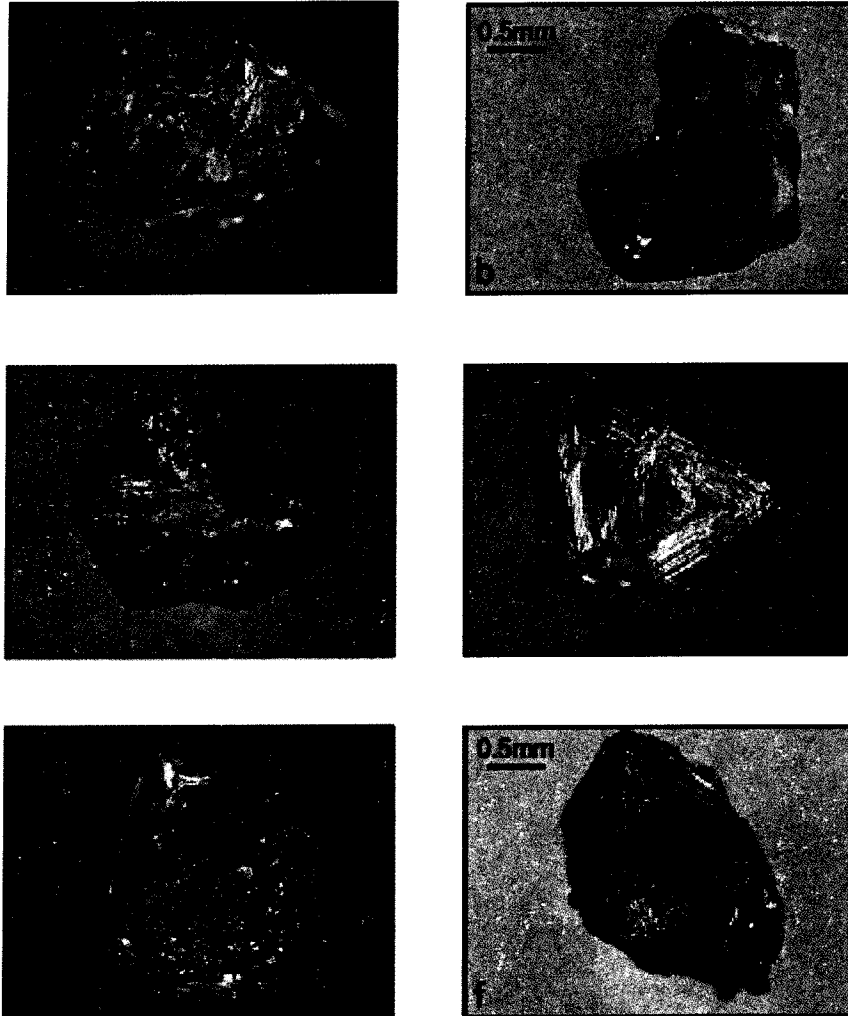


Figure B.7. Characteristic diamond fragments. (a-d) Show examples of diamonds with fresh breaks, having no evidence of etching or resorption. (e-f) Examples of old breaks (prior to kimberlite eruption), which have experienced resorption. Photographs (a-f) are from diamonds ddmi-125, ddmi-152, ddmi-130, ddmi-190, ddmi-158, and ddmi-161.

B.2. Colour

Colourless

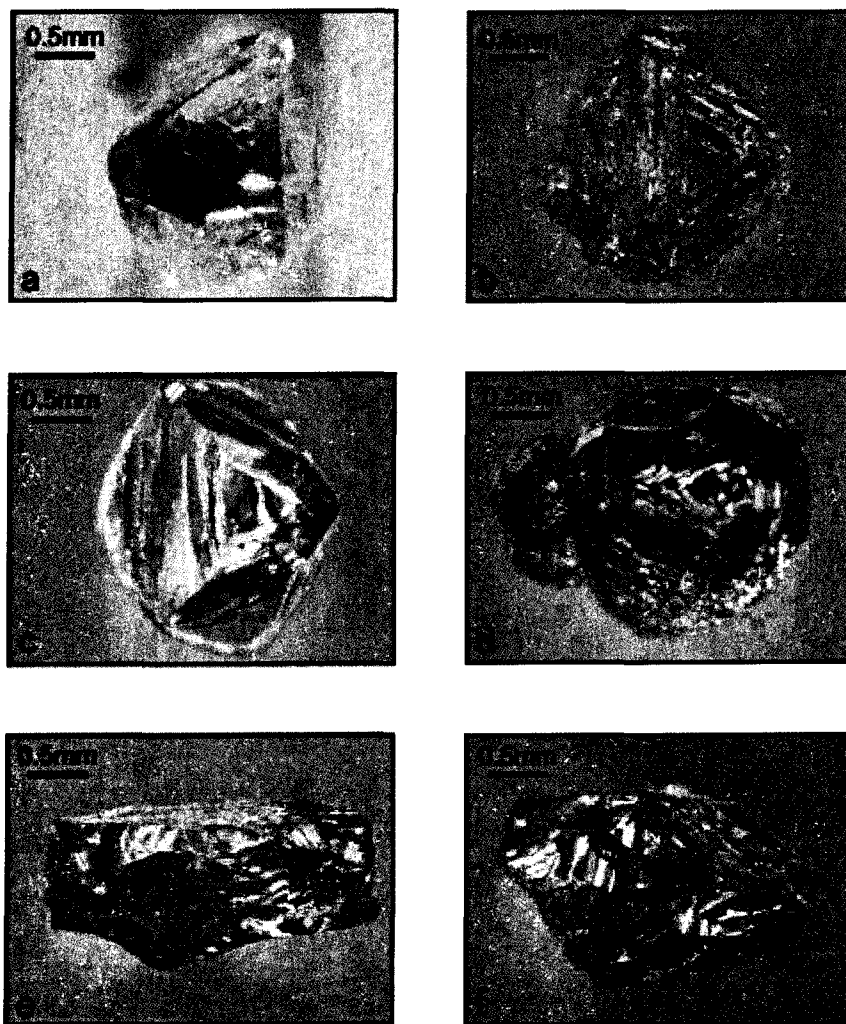


Figure B.8. Examples of colourless diamonds. Photographs (a-f) are diamonds ddmi-224, ddmi-98, ddm-141, ddmi-198, ddmi-103, and ddmi-108.

Brown

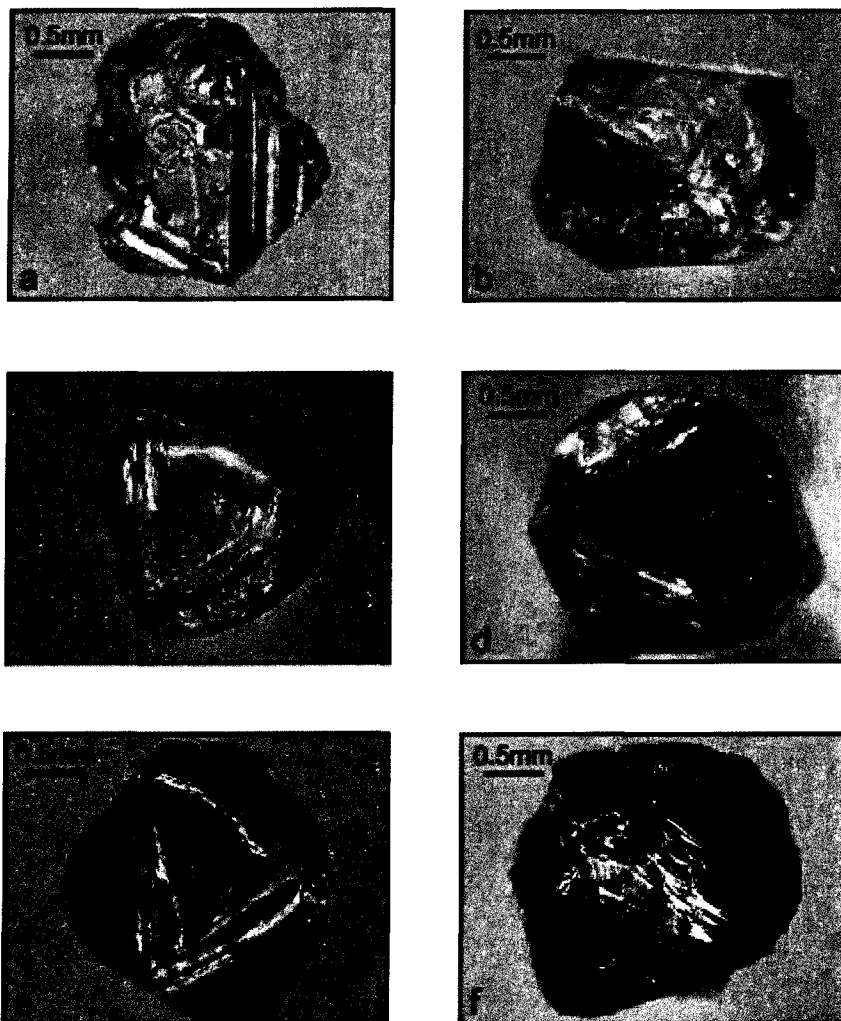


Figure B.9. Diamonds showing increasing intensity of brown body colours. (a-b) Faint brown body colours. (c-d) Intermediate brown body colours. (e-f) Strong brown body colours. Photographs (a-f) are from diamonds ddmi-147, ddmi-100, ddmi-170, ddmi-13, ddmi-123, and ddmi-107.

Pink

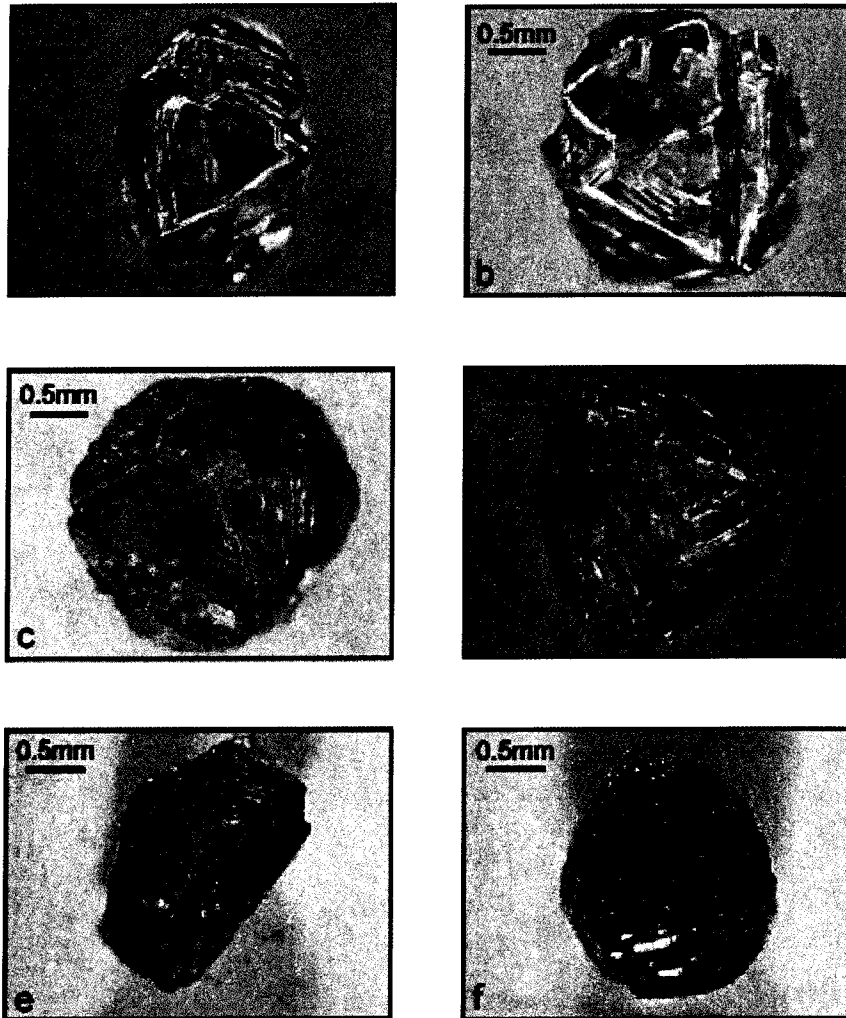


Figure B.10. Diamonds showing a range of pink body colours. (a-b) Faint pink body colours. (c-e) Intermediate pink body colours. (f) Strong pink body colour. Photographs (a-f) are from samples ddmi-205, ddmi-124, ddmi-117, ddmi-139, ddmi-226, and ddmi-225.

Yellow and Grey

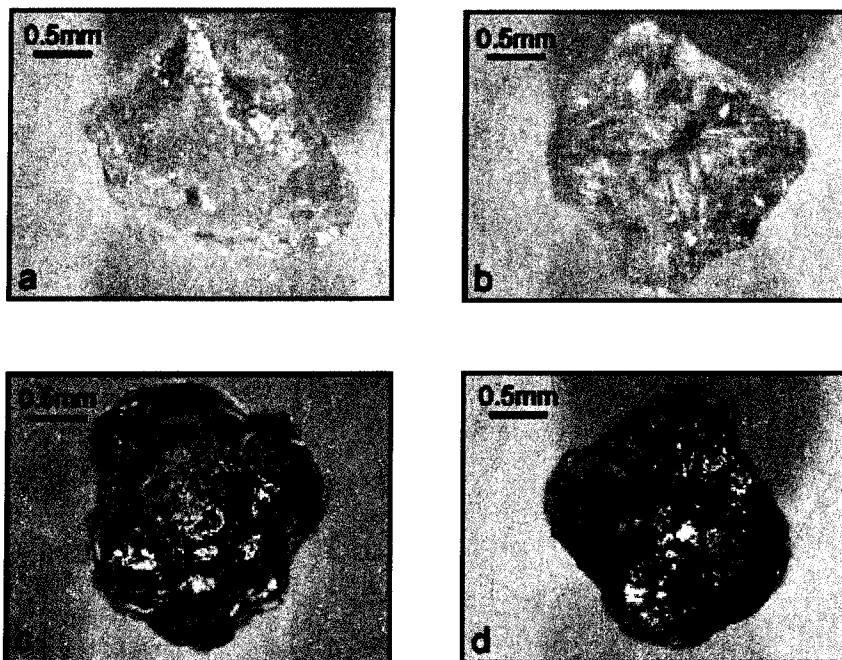


Figure B.11. (a-b) Diamonds with yellow body colours. (c-d) Diamonds with grey body colours. Photographs (a-d) are from diamonds ddmi-227, ddmi-228, ddmi-159, and ddmi-229.

B.3. Surface Features

Terraces

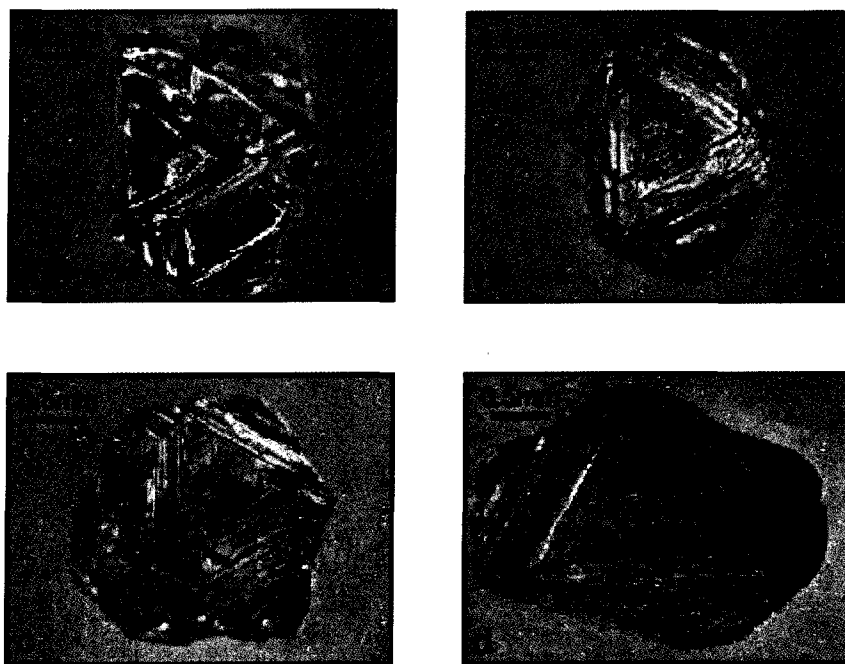


Figure B.12. Terraces are raised triangular plates/growth layers on octahedral crystal faces. Photographs (a-d) are diamonds ddmi-205, ddmi-6, ddmi-211, and ddmi-179.

Shield and Serrate Laminae

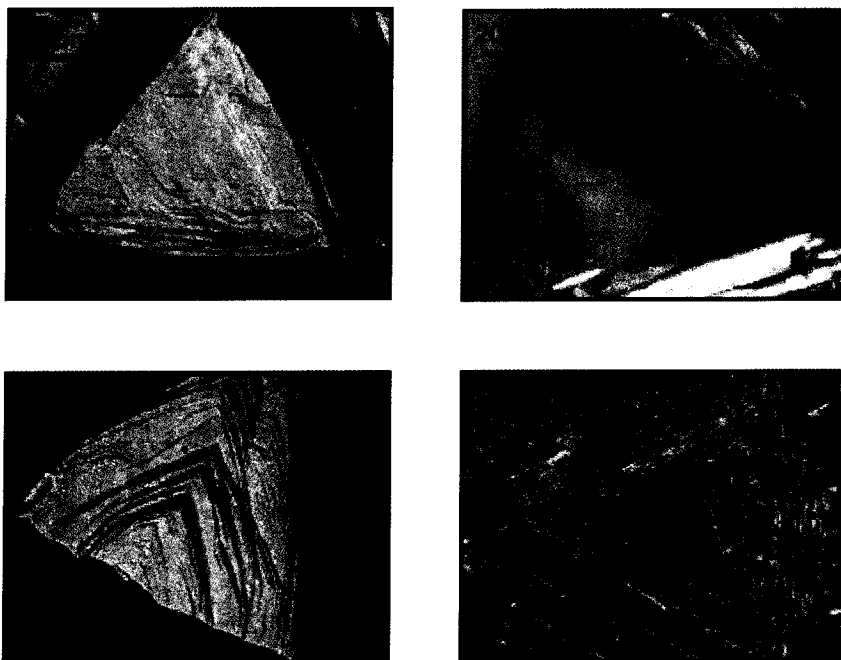


Figure B.13. Shield and serrate laminae are resorption features that are observed on the diamond surface as thin, raised lines that are parallel to octahedral growth. (a-c) Examples of shield laminae. (d) Example of serrate laminae. Photographs (a-d) are from diamonds ddmi-205, ddmi-10, ddmi-144, and ddmi-181.

Herringbone Line

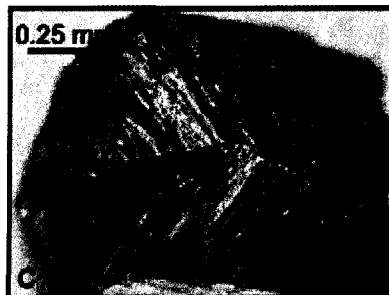
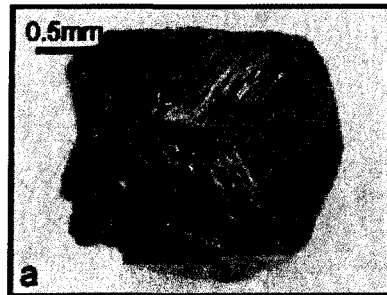


Figure B.14. Herringbone lines are planes of contact twinning where the "spine" marks the plane of twinning. Photographs (a-c) are from diamonds ddmi-117, ddmi-216, and ddmi-151.

Trigons

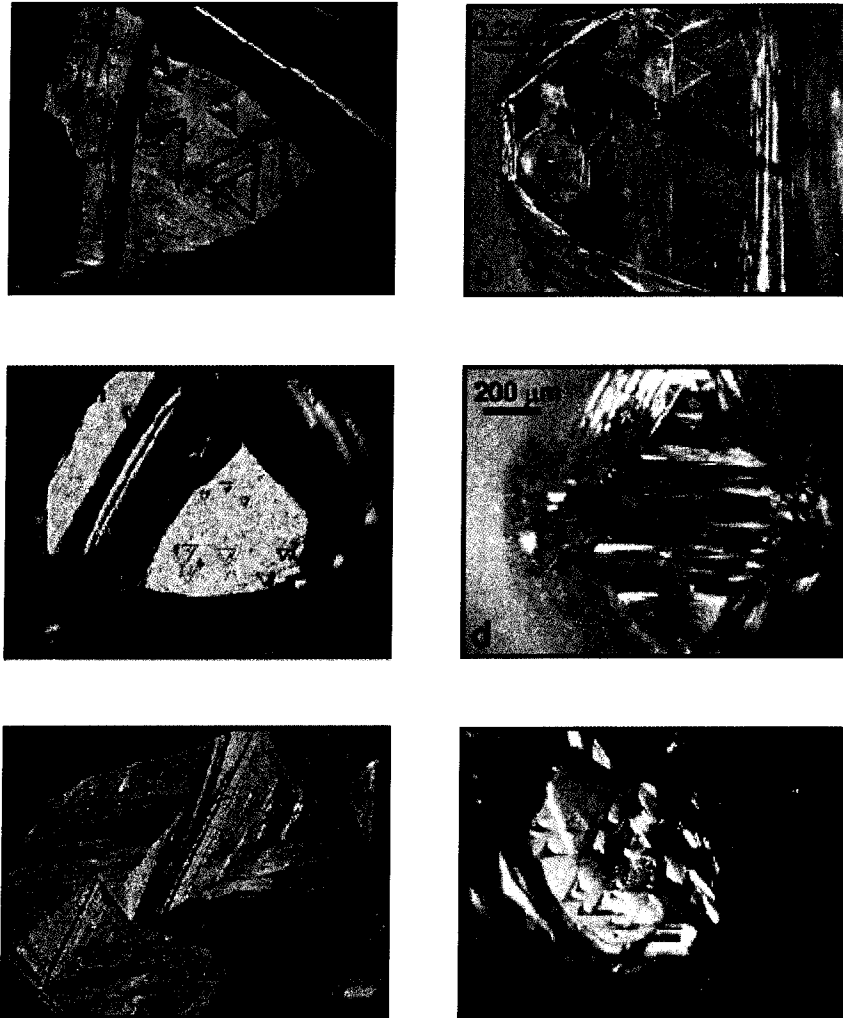


Figure B.15. Negatively-oriented trigonal etch pits (trigons). (a) Shows an example of pyramidal (pointed-bottomed) and terraced trigons. (b-c) Flat-bottomed trigons. (d-f) Examples of trigons with positive relief. Photographs (a-f) are from diamonds ddmi- ddmi-120, ddmi-167, ddmi-194, ddmi-27, ddmi-155, and ddmi-29.

Hexagons

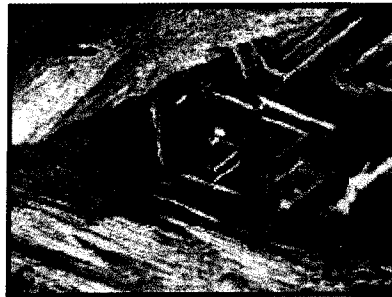
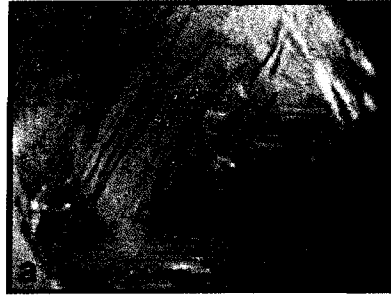


Figure B.16. Hexagonal pits (hexagons) are flat-bottomed etch pits which represent a combination of positive and negative trigons and are indicative of changing mantle conditions. (a-b) Fully developed hexagons. (c) Partly developed hexagons. Photographs (a-c) are from diamonds ddmi-14, ddmi-170, and ddmi-164.

Tetragons

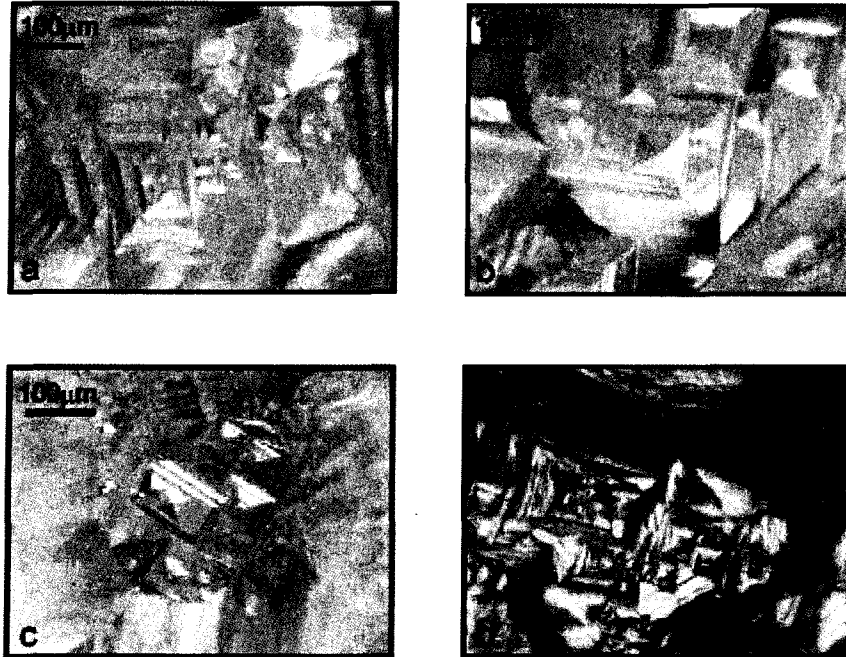


Figure B.17. Tetragonal etch pits (tetragons) on cube faces. (a-c) Examples of tetragons with positive relief. (d) Tetragons with negative relief. Photographs (a-d) are from diamonds dmi-151, dmi-230, dmi-231, and dmi-178.

Hillocks

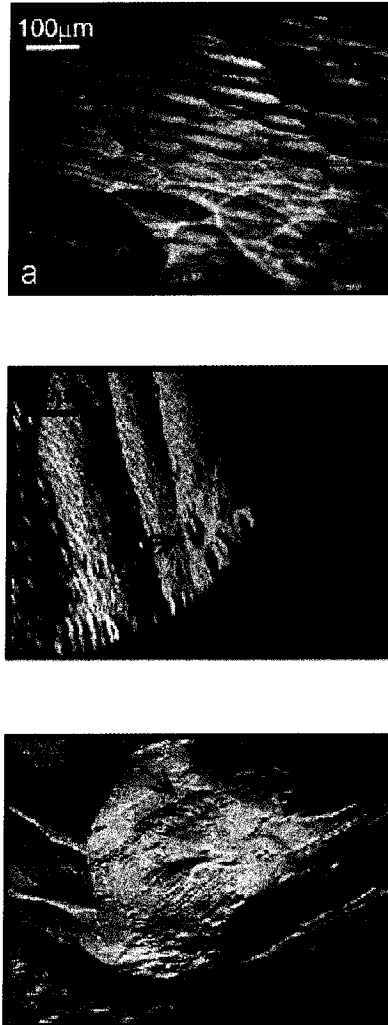


Figure B.18. Hillocks are resorption features observed on tetrahedral faces, often observed forming along octahedral growth planes. (a) Broad, rounded, high relief ellipsoidal hillocks. (b) Example of a pyramidal hillock having a rounded, triangular-pyramidal form. Pyramidal hillocks are typically isolated or scattered occurrences on tetrahedral faces. (c) Rounded ellipsoidal hillocks (blue arrow) and the most frequently observed type of hillock, fine, narrow, elongate hillocks (red arrow). Photographs (a-c) are from diamonds ddmi-37, ddmi-136, and ddmi-121.

Inclusion Voids



Figure B.19. Inclusion voids are the sites of pre-existing mineral inclusions that have fallen out, or have dissolved out of, their host diamond. (a) Inclusion void that has experienced resorption. (b) Inclusion void that experienced minor resorption but still preserves the inclusion shape. (c) Pristine, unresorbed inclusion void. Photographs (a-c) are from diamonds ddmi-208, ddmi-140, and ddmi-123.

Plastic Deformation

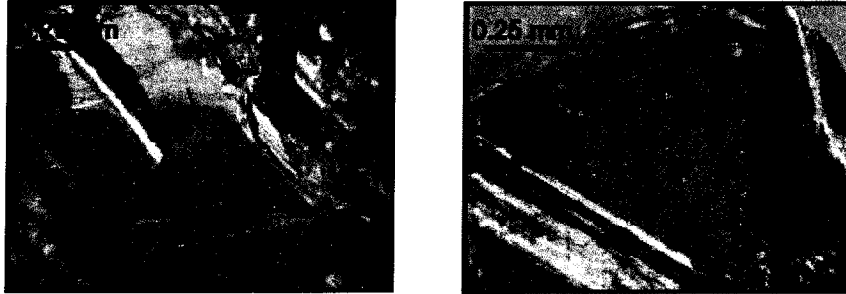


Figure B.20. Plastic deformation is observed as a series of fine, parallel, laminations on dodecahedral faces or as linear orientations of trigons on octahedral faces. (a) Shows plastic deformation in one direction. (b) Plastic deformation in two directions, with associated lines of trigons. Photographs (a) and (b) are from diamonds ddmi-207 and ddmi-188.

Frosting

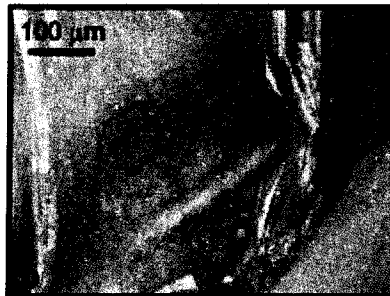
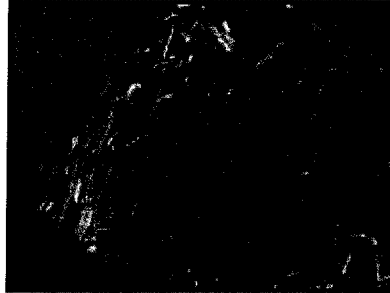


Figure B.21. Representative diamond frosting. (a-b) Fine frosting superimposed onto other surface features, including trigons. (c) Coarse frosting which typically has etch pits on the outer surface. The etch pits range from irregular to trigonal and hexagonal shapes, with negative relief. Photographs (a-c) are from diamonds ddmi-174, ddmi-46, and ddmi-47.

Coats

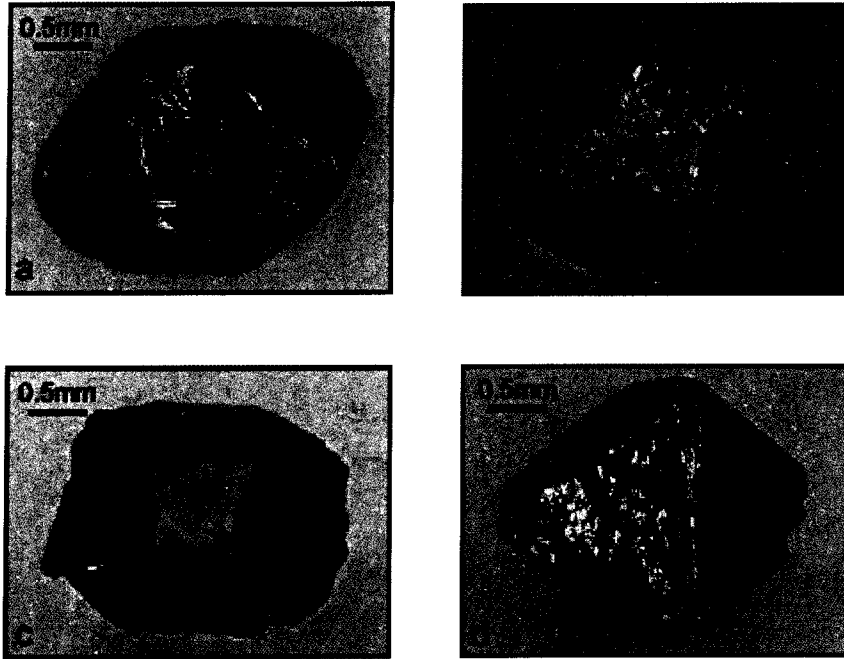


Figure B.22. Representative diamond coats. (a-c) Partially coated diamonds. (d) Fully coated diamond. Photographs (a-d) are from diamonds ddmi-267, ddmi-184, ddmi-257 and ddmi-266.

Internal Fractures

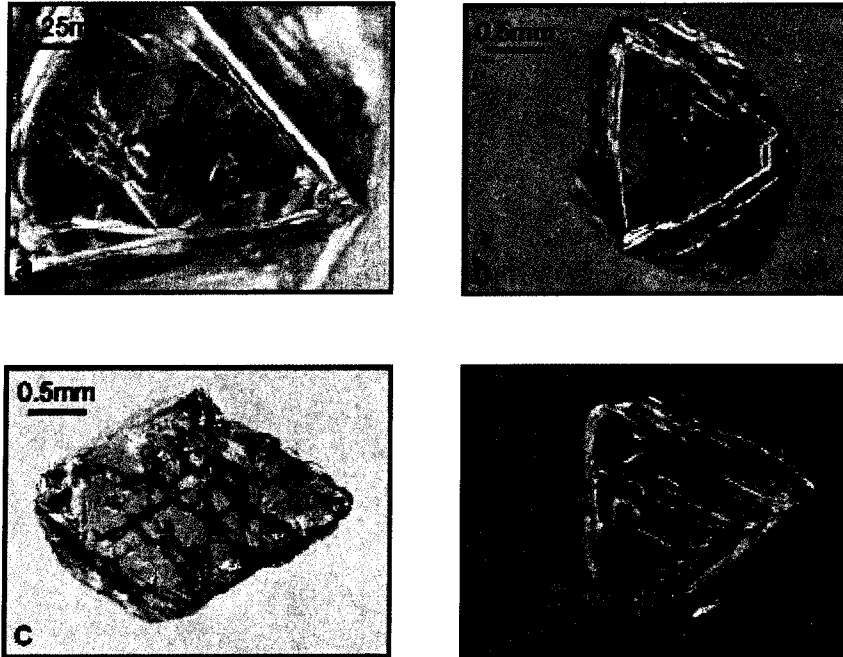


Figure B.23. Internal fractures in diamonds. (a-b) Examples of internal fractures. (c-d) Internal fractures that have been lined by graphite. Photographs (a-d) are from diamonds ddmi-206, ddmi-155, ddmi-106, and ddmi-132.

B.4. Inclusion Content

Peridotitic Garnet

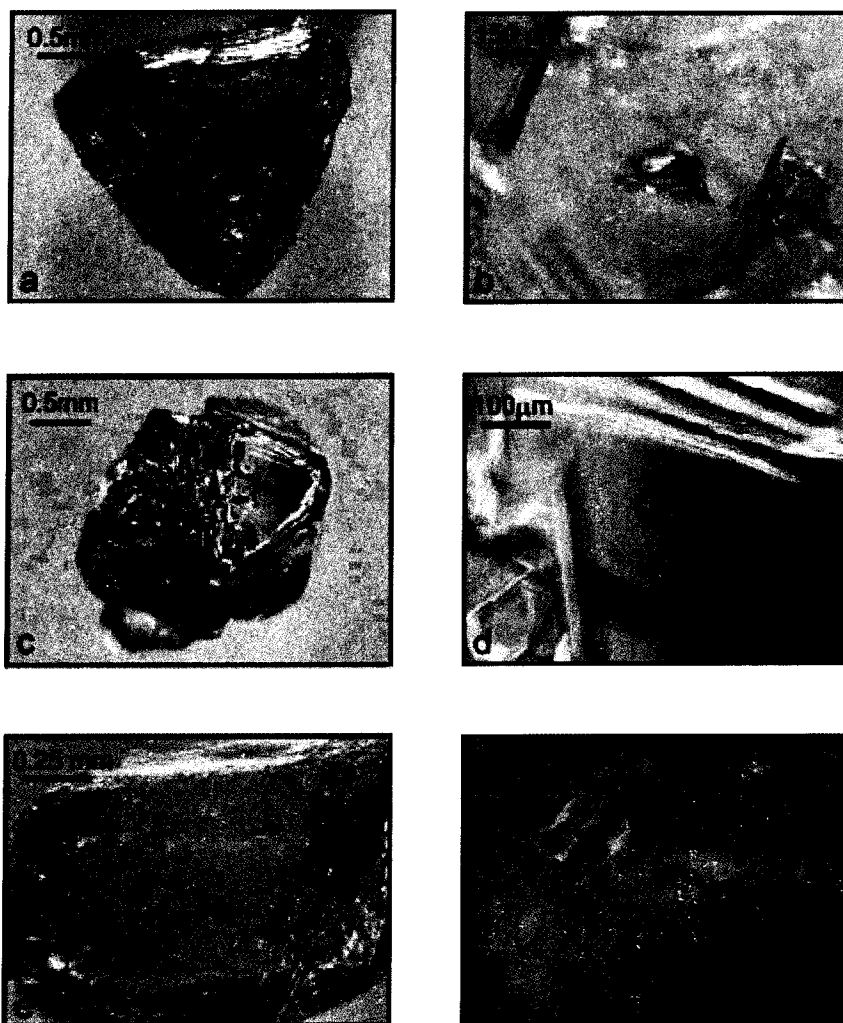


Figure B.24. Peridotitic garnet inclusions. (a-b) Diamond ddmi-8 contained one harzburgitic garnet inclusion. (c-d) Diamond ddmi-199 contained two lherzolitic garnet inclusions. (e) Six harzburgitic garnet inclusions in sample ddmi-175. (f) Harzburgitic garnet and olivine inclusion pair from ddmi-154.

Olivine

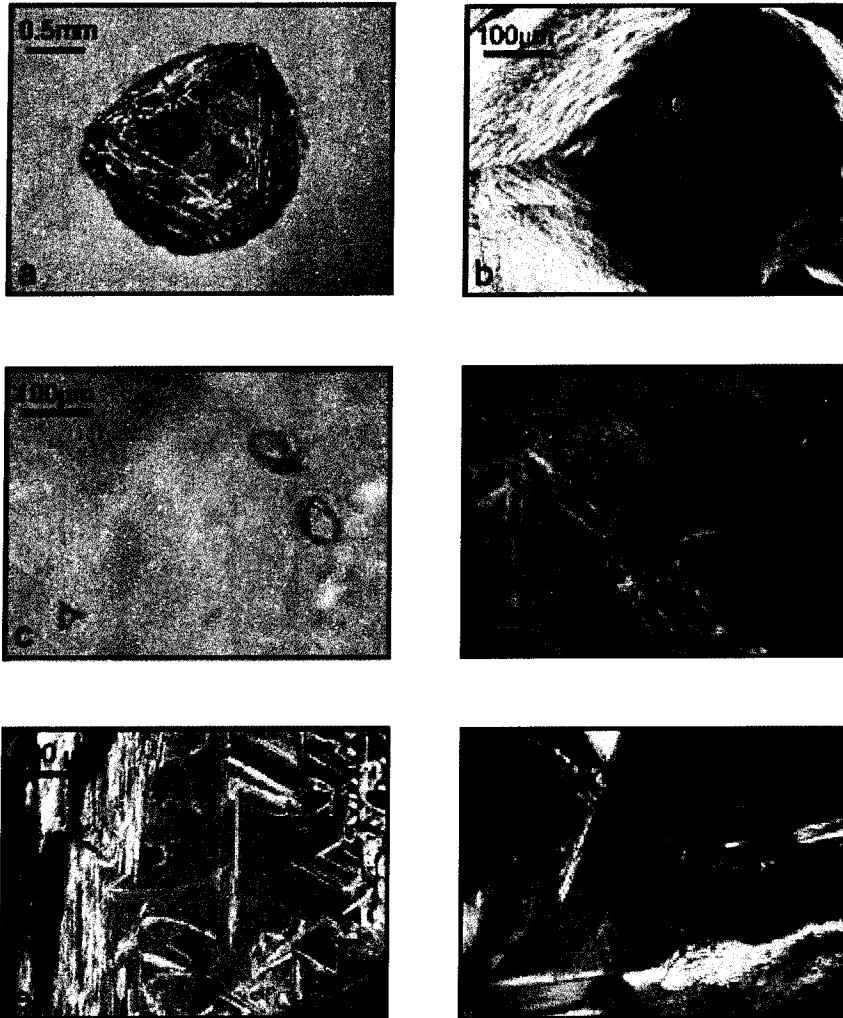


Figure B.25. Olivine inclusions in diamonds. Photographs (a-f) are from diamonds ddmi-165, ddmi-123, ddmi-174, ddmi-101, ddmi-210, and ddmi-187.

Chromite

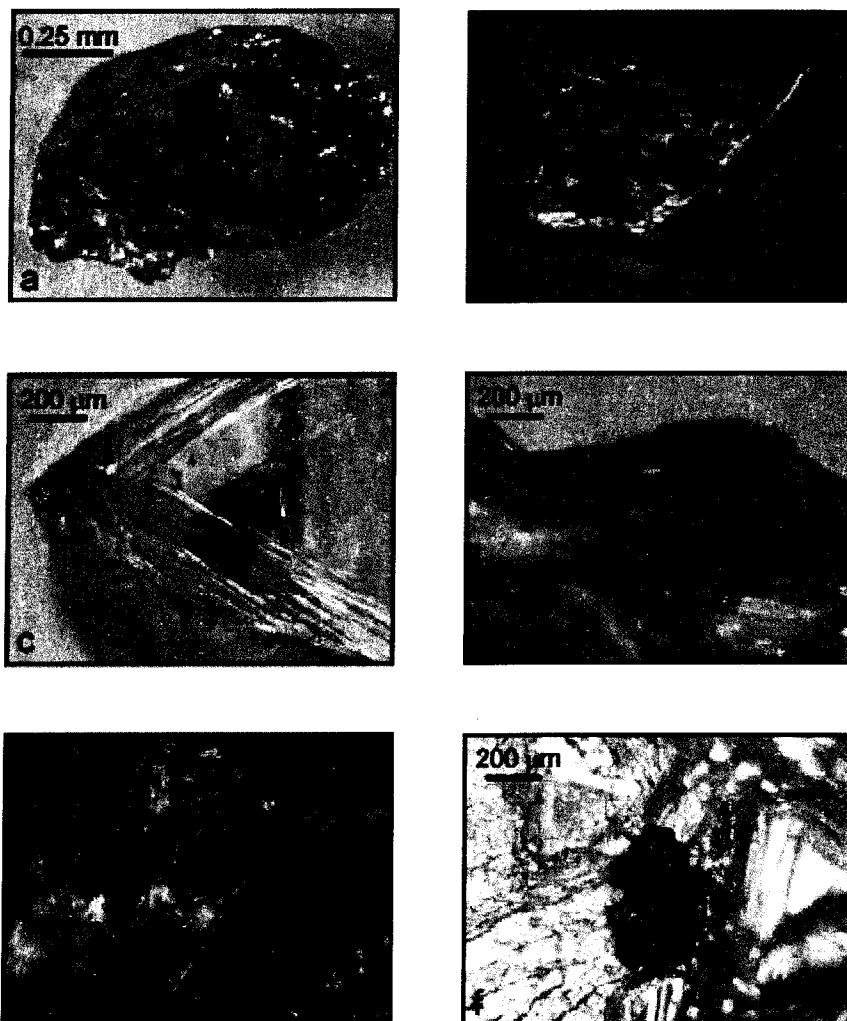


Figure B.26. (a-d) Chromite inclusions encapsulated in diamonds. (e-f) Exposed chromite inclusions on the diamond surface. Subsequent analyses revealed no compositional differences between enclosed and exposed inclusions. Photographs (a-f) are from diamonds ddmi-121, ddmi-169, ddmi-46, ddmi-119 (included), ddmi-119 (exposed) and ddmi-36.

Clinopyroxene

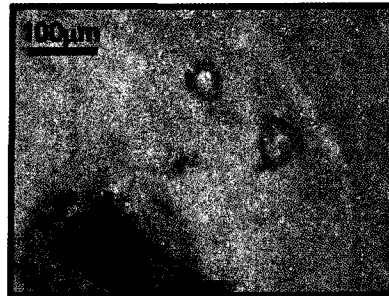


Figure B.27. (a) Four eclogitic clinopyroxene inclusions with faint green colouration. (b) Colourless peridotitic clinopyroxene inclusions and stacked graphite inclusions. (c) Touching peridotitic clinopyroxene-olivine inclusion pair. Photographs (a-c) are from diamonds ddmi-48, ddmi-186, and ddmi-141.

Sulphides

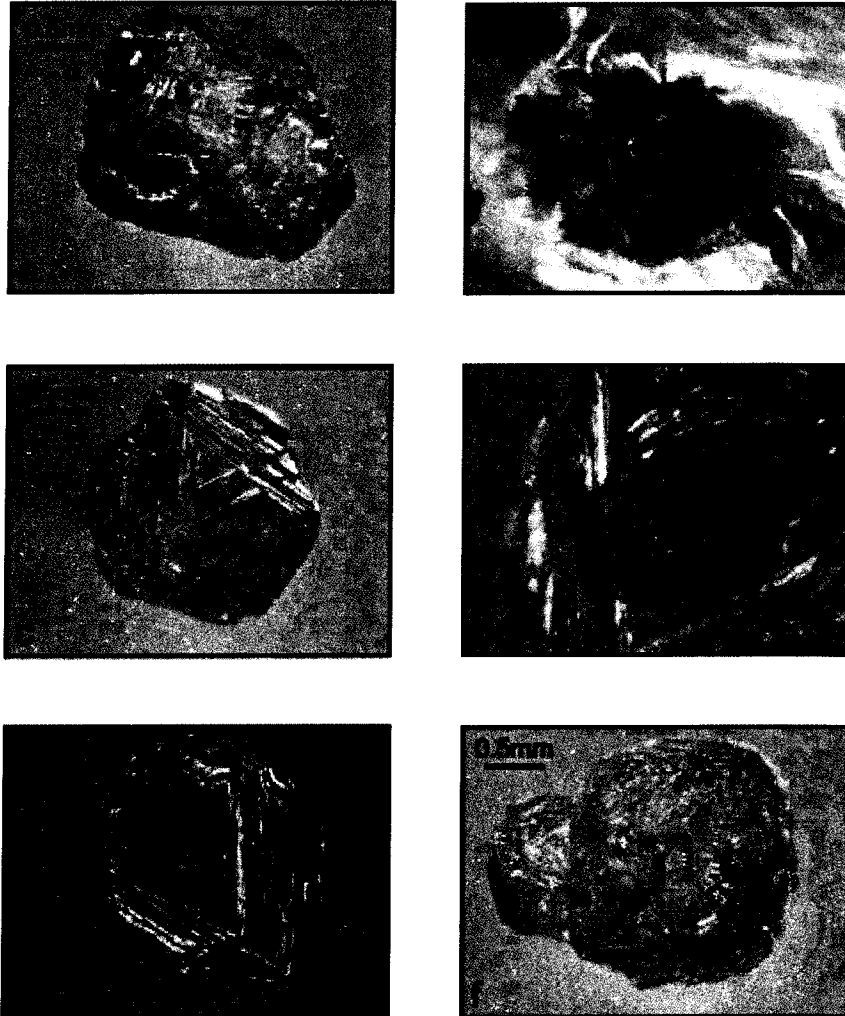


Figure B.28. Sulphide inclusions in A154 South diamonds typically occur as thin smears on internal cleavage surfaces which radiate out from distinct sulphide crystals. Photographs (a-f) are from ddmi-37 (diamond), ddmi-37 (inclusion), ddmi-211, ddmi-97, ddmi-122, and ddmi-198.

Eclogitic Garnet

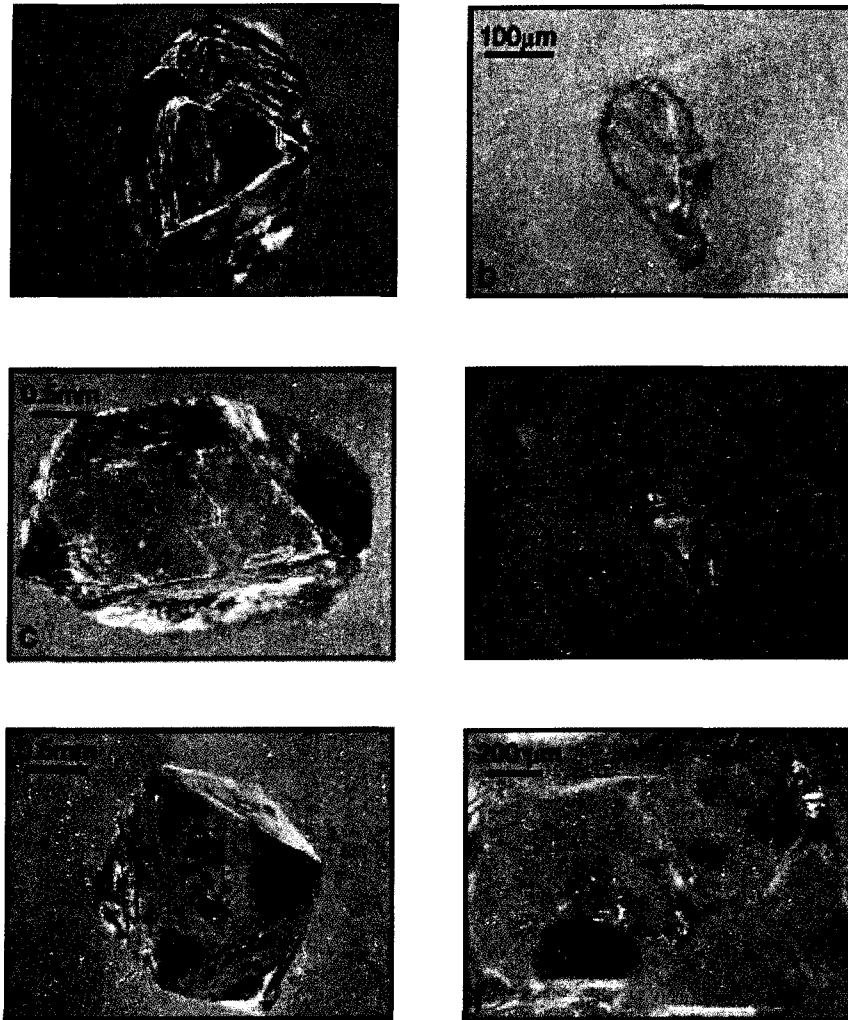


Figure B.29. Eclogitic garnet inclusions. Photographs (a-f) are from diamonds ddmi-205 (diamond), ddmi-205 (inclusion), ddmi-102 (diamond), ddmi-102 (inclusion), ddmi-208, and ddmi-166.

Other Inclusions

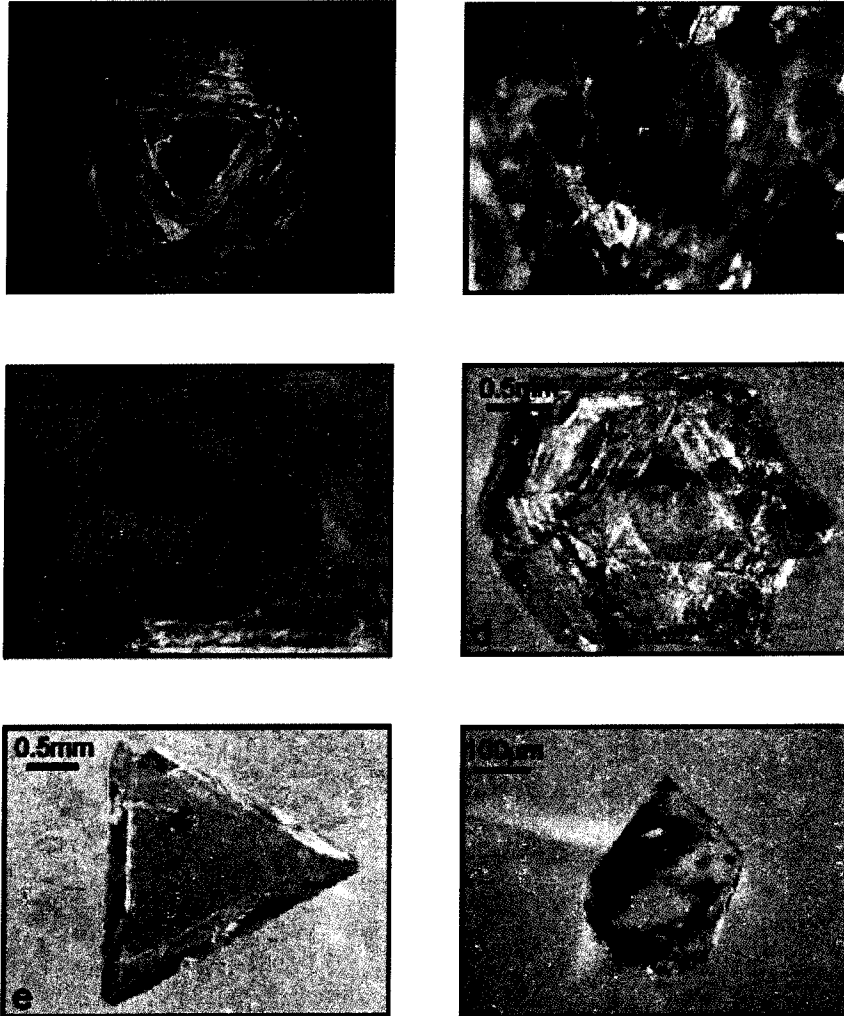


Figure B.30. Rare inclusions in A154 South diamonds. (a-c) Ferropericlase inclusions of uncertain paragenetic association. (d) Eclogitic coesite inclusion. (e-f) Octahedral diamond inclusion enclosed within a triangular macle. Photographs (a-f) are from diamonds ddmi-173, ddmi-114, ddmi-154, ddmi-193, ddmi-200 (diamond), and ddmi-200 (inclusion).

Graphite

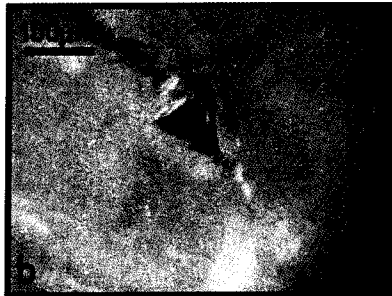
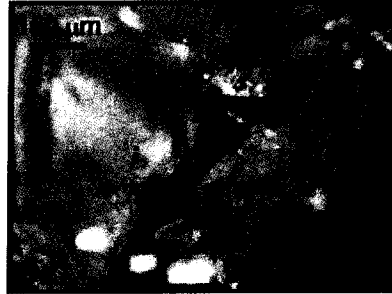


Figure B.31. Representative graphite inclusions. (a-b) Stacked graphite inclusions. (c) Wispy graphite inclusions. Photographs (a-c) are from diamonds ddmi-37, ddmi-63, and ddmi-98.

Altered Inclusion

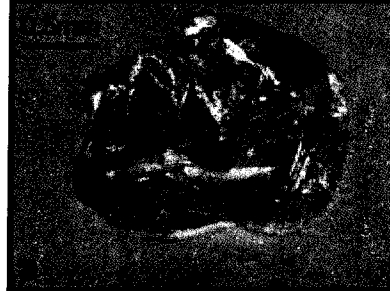


Figure B.32. Examples of altered inclusions from A154 South diamonds. Altered inclusions are typically orange or white in colour and are associated with fractures. Photographs (a-c) are from diamonds ddmi-213, ddmi-171, and ddmi-207.

Appendix C: Supplementary Data

C.1. Microprobe Data

Table C.1. Inclusion abundance table for the 100 diamonds (161 inclusions) from A154 South studied.

Peridotitic (83 Diamonds)	(133 inclusions)
Pyrope garnet	11
Olivine	54
Chromite	56
Cr-diopside	2
NiFe-sulphide	8
Altered pyrope garnet	2
Eclogitic (12 Diamonds)	(20 inclusions)
Pyrope-almandine garnet	7
Omphacitic clinopyroxene	4
Coesite	1
Fe-sulphide	8
Uncertain (5 Diamonds)	(8 inclusions)
Ferropericlase	7
Diamond	1

Table C.2. Electron microprobe analyses of *garnet* inclusions from A154 South diamonds. Major element compositions (EPMA-analyses) are given as wt%

Sample	ddmi-8a	ddmi-133a	ddmi-133b	ddmi-154a	ddmi-166a	ddmi-166b	ddmi-166c
Assemblage	gnt	2gnt	2gnt	gnt, 2ol	10gnt	10gnt	10gnt
Suite	P	P	P	P	E	E	E
P ₂ O ₅	0.03	0.03	0.02	0.03	0.06	0.04	0.04
SiO ₂	41.33	42.33	41.95	41.04	41.17	41.67	41.76
TiO ₂	0.12	0.11	0.12	0.08	0.36	0.30	0.30
Al ₂ O ₃	14.17	15.00	14.75	11.53	22.77	22.44	22.76
Cr ₂ O ₃	10.85	10.87	10.83	15.68	0.08	0.08	0.08
V ₂ O ₃	0.05	0.06	0.06	0.05	0.02	≤0.01	0.02
FeO	5.85	6.07	6.31	5.82	9.75	9.35	9.42
MnO	0.23	0.24	0.27	0.26	0.21	0.18	0.17
NiO	≤0.01	≤0.01	≤0.01	≤0.01	≤0.01	≤0.01	≤0.01
MgO	22.91	23.44	23.28	19.88	11.94	11.87	12.09
CaO	2.89	2.64	2.66	5.91	14.08	14.57	14.43
Na ₂ O	≤0.01	≤0.01	≤0.01	0.02	0.14	0.14	0.14
K ₂ O	≤0.01	≤0.01	≤0.01	≤0.01	≤0.01	≤0.01	≤0.01
Oxide Total	98.44	100.84	100.28	100.30	100.58	100.68	101.24
P	0.003	0.002	0.005	0.003	0.007	0.005	0.005
Si	6.078	6.067	6.056	6.066	5.999	6.058	6.035
Ti	0.013	0.012	0.013	0.009	0.039	0.033	0.033
Al	2.455	2.534	2.510	2.008	3.909	3.845	3.877
Cr	1.261	1.232	1.236	1.832	0.009	0.010	0.009
V³⁺	0.005	0.007	0.006	0.006	0.002	0.002	0.002
Fe²⁺	0.719	0.728	0.762	0.719	1.188	1.137	1.139
Mn	0.028	0.029	0.033	0.033	0.026	0.022	0.021
Ni	0.001	0.001	0.002	0.001	0.000	0.001	0.001
Mg	5.023	5.009	5.010	4.380	2.593	2.573	2.606
Ca	0.455	0.406	0.411	0.935	2.198	2.270	2.234
Na	0.004	0.002	0.000	0.005	0.039	0.040	0.039
K	0.000	0.002	0.002	0.001	0.001	0.000	0.000
Cation Total	16.045	16.032	16.047	15.999	16.010	15.994	16.000

Table C.2. (cont.)

Sample Assemblage Suite	ddmi-167a		ddmi-175a		ddmi-175b		ddmi-198a		ddmi-198b		ddmi-205a		ddmi-205b	
	gnt, 2ol P	6gnt P	6gnt P	6gnt P	2gnt, s P	2gnt, s P	2gnt, s P	2gnt, s P	2gnt E	2gnt E	2gnt E	2gnt E		
P ₂ O ₅	0.02	0.03	0.02	0.02	≤0.01	≤0.01	≤0.01	≤0.01	0.05	0.08	0.05	0.08		
SiO ₂	42.07	41.38	41.67	41.67	41.45	41.45	41.39	41.39	39.34	39.72	39.34	39.72		
TiO ₂	≤0.02	≤0.02	≤0.02	≤0.02	0.06	0.06	0.06	0.06	0.36	0.36	0.36	0.36		
Al ₂ O ₃	18.47	15.99	16.10	16.10	17.69	17.69	17.28	17.28	21.83	22.17	21.83	22.17		
Cr ₂ O ₃	6.97	10.34	10.25	10.25	7.15	7.15	7.02	7.02	0.06	0.05	0.06	0.05		
V ₂ O ₅	0.04	0.04	0.04	0.04	0.05	0.05	0.05	0.05	≤0.01	0.02	≤0.01	0.02		
FeO	5.50	6.26	6.19	6.19	6.95	6.95	6.87	6.87	11.16	11.20	11.16	11.20		
MnO	0.21	0.32	0.31	0.31	0.29	0.29	0.27	0.27	0.19	0.19	0.19	0.19		
NiO	≤0.01	≤0.01	≤0.01	≤0.01	≤0.01	≤0.01	≤0.01	≤0.01	≤0.01	≤0.01	≤0.01	≤0.01		
MgO	22.70	21.48	21.69	21.69	19.52	19.52	20.21	20.21	10.93	10.79	10.93	10.79		
CaO	3.73	3.64	3.65	3.65	6.03	6.03	5.52	5.52	14.20	13.63	14.20	13.63		
Na ₂ O	0.02	≤0.01	≤0.01	≤0.01	0.02	0.02	≤0.01	≤0.01	0.12	0.12	0.12	0.12		
K ₂ O	≤0.01	≤0.01	≤0.01	≤0.01	≤0.01	≤0.01	≤0.01	≤0.01	≤0.01	≤0.01	≤0.01	≤0.01		
Oxide Total	99.78	99.52	99.97	99.97	99.24	99.24	98.71	98.71	98.25	98.33	98.25	98.33		
P	0.003	0.003	0.003	0.003	0.001	0.001	0.002	0.002	0.006	0.010	0.006	0.010		
Si	6.016	6.024	6.032	6.032	6.048	6.048	6.062	6.062	5.934	5.967	5.934	5.967		
Ti	0.003	0.002	0.002	0.002	0.007	0.007	0.006	0.006	0.041	0.041	0.041	0.041		
Al	3.113	2.743	2.747	2.747	3.043	3.043	2.983	2.983	3.880	3.925	3.880	3.925		
Cr	0.788	1.190	1.173	1.173	0.825	0.825	0.813	0.813	0.007	0.006	0.007	0.006		
V ³⁺	0.005	0.005	0.005	0.005	0.006	0.006	0.006	0.006	0.001	0.002	0.001	0.002		
Fe ²⁺	0.658	0.762	0.750	0.750	0.848	0.848	0.842	0.842	1.408	1.407	1.408	1.407		
Mn	0.026	0.039	0.038	0.038	0.036	0.036	0.034	0.034	0.025	0.024	0.025	0.024		
Ni	0.001	0.001	0.001	0.001	0.000	0.000	0.001	0.001	0.000	0.001	0.000	0.001		
Mg	4.839	4.662	4.681	4.681	4.246	4.246	4.414	4.414	2.457	2.416	2.457	2.416		
Ca	0.572	0.568	0.566	0.566	0.942	0.942	0.866	0.866	2.295	2.195	2.295	2.195		
Na	0.004	0.004	0.004	0.004	0.006	0.006	0.004	0.004	0.034	0.035	0.034	0.035		
K	0.001	0.001	0.000	0.000	0.000	0.000	0.000	0.000	0.000	0.001	0.000	0.001		
Cation Total	16.027	16.004	16.001	16.001	16.009	16.009	16.031	16.031	16.089	16.029	16.089	16.029		

Table C.2. (cont.)

Sample Assemblage Suite	ddmi-208b 12gnt E	ddmi-208c 12gnt E	ddmi-216a 2gnt P	ddmi-216c 2gnt P
P ₂ O ₅	0.06	0.05	≤0.04	≤0.04
SiO ₂	39.92	40.31	41.32	41.61
TiO ₂	0.33	0.31	≤0.05	≤0.05
Al ₂ O ₃	22.01	22.02	17.50	16.24
Cr ₂ O ₃	0.06	0.07	7.99	8.00
V ₂ O ₃	≤0.02	≤0.02	0.05	0.05
FeO	9.50	9.48	5.94	6.33
MnO	0.19	0.18	0.25	0.25
NiO	≤0.03	≤0.03	≤0.03	≤0.03
MgO	12.02	12.11	21.80	21.86
CaO	14.06	13.83	4.34	4.30
Na ₂ O	0.16	0.14	0.02	0.03
K ₂ O	≤0.02	≤0.02	≤0.02	≤0.02
Oxide Total	98.52	98.33	98.77	98.28
P	0.007	0.006	0.003	0.004
Si	5.962	5.988	5.989	6.076
Ti	0.037	0.034	0.005	0.004
Al	3.873	3.862	2.989	2.795
Cr	0.007	0.008	0.916	0.924
V ³⁺	0.003	0.002	0.006	0.006
Fe ²⁺	1.187	1.180	0.720	0.773
Mn	0.024	0.022	0.030	0.031
Ni	0.001	0.000	0.001	0.002
Mg	2.676	2.686	4.711	4.759
Ca	2.250	2.204	0.674	0.673
Na	0.045	0.039	0.006	0.008
K	0.000	0.001	0.002	0.000
Cation Total	16.071	16.044	16.051	16.055

Table C.3. Electron microprobe analyses of *olivine* inclusions from A154 South diamonds. Major element compositions (EPMA analyses) are given as wt%.

Sample	ddmi-3a	ddmi-5b	ddmi-13a	ddmi-14a	ddmi-49a	ddmi-101a	ddmi-111a
Assemblage	ol	ol	ol	ol	ol	ol	3ol
Suite	P	P	P	P	P	P	P
P ₂ O ₅	0.02	0.02	≤0.01	≤0.01	0.02	≤0.01	≤0.01
SiO ₂	40.75	40.51	39.67	41.11	40.45	40.57	41.32
TiO ₂	≤0.02	≤0.02	≤0.02	≤0.02	≤0.02	≤0.02	≤0.02
Al ₂ O ₃	≤0.02	≤0.02	≤0.02	≤0.02	≤0.02	≤0.02	≤0.02
Cr ₂ O ₃	0.04	0.05	0.04	0.04	0.05	0.04	0.04
V ₂ O ₅	≤0.01	≤0.01	≤0.01	≤0.01	≤0.01	≤0.01	≤0.01
FeO	6.25	6.77	6.87	7.00	9.00	7.52	6.96
MnO	0.08	0.09	0.09	0.09	0.11	0.11	0.10
NiO	0.31	0.31	0.30	0.30	0.20	0.33	0.36
MgO	51.31	50.33	51.70	50.25	48.97	50.51	50.23
CaO	0.03	0.03	0.02	0.03	0.07	0.05	0.04
Na ₂ O	≤0.01	≤0.01	≤0.01	≤0.01	0.03	0.02	0.02
K ₂ O	≤0.01	≤0.01	≤0.01	≤0.01	0.02	≤0.01	≤0.01
Oxide Total	98.87	98.19	98.77	98.90	98.97	99.22	99.13
P	0.000	0.000	0.000	0.000	0.000	0.000	0.000
Si	0.996	0.999	0.976	1.006	0.999	0.994	1.009
Ti	0.000	0.000	0.000	0.000	0.000	0.000	0.000
Al	0.000	0.000	0.000	0.000	0.000	0.000	0.000
Cr	0.001	0.001	0.001	0.001	0.001	0.001	0.001
V³⁺	0.000	0.000	0.000	0.000	0.000	0.000	0.000
Fe²⁺	0.128	0.140	0.141	0.143	0.186	0.154	0.142
Mn	0.002	0.002	0.002	0.002	0.002	0.002	0.002
Ni	0.006	0.006	0.006	0.006	0.004	0.007	0.007
Mg	1.869	1.850	1.896	1.833	1.803	1.845	1.828
Ca	0.001	0.001	0.001	0.001	0.002	0.001	0.001
Na	0.001	0.000	0.001	0.000	0.002	0.001	0.001
K	0.000	0.000	0.000	0.000	0.001	0.000	0.000
Cation Total	3.003	3.000	3.024	2.993	3.001	3.005	2.991

Table C.3. (cont)

Sample Assemblage Suite	ddmi-111b		ddmi-111c		ddmi-123a		ddmi-124b		ddmi-129a		ddmi-135c		ddmi-135a	
	3ol	P	3ol	P	ol	P	ol	P	ol	P	3ol	P	3ol	P
P ₂ O ₅	≤0.01		≤0.01		0.017		≤0.01		≤0.01		0.021		≤0.01	
SiO ₂	40.976		41.230		41.910		41.308		41.945		41.220		40.776	
TiO ₂	≤0.02		≤0.02		≤0.02		≤0.02		≤0.02		≤0.02		≤0.02	
Al ₂ O ₃	≤0.02		≤0.02		≤0.02		≤0.02		≤0.02		0.030		≤0.02	
Cr ₂ O ₃	0.050		0.080		0.056		≤0.02		0.029		0.056		0.051	
V ₂ O ₃	≤0.01		≤0.01		≤0.01		≤0.01		≤0.01		≤0.01		≤0.01	
FeO	6.850		6.700		6.602		7.515		6.680		6.860		6.944	
MnO	0.093		0.088		0.088		0.091		0.087		0.087		0.096	
NiO	0.365		0.328		0.346		0.354		0.340		0.320		0.320	
MgO	50.970		51.428		49.958		50.353		52.090		51.477		51.254	
CaO	0.040		0.042		0.026		0.042		0.038		0.032		0.029	
Na ₂ O	≤0.01		≤0.01		0.015		0.021		≤0.01		≤0.01		≤0.01	
K ₂ O	≤0.01		≤0.01		≤0.01		≤0.01		≤0.01		≤0.01		≤0.01	
Oxide Total	99.424		99.975		99.080		99.753		101.289		100.153		99.549	
P	0.000		0.000		0.000		0.000		0.000		0.000		0.000	
Si	0.998		0.998		1.020		1.005		1.001		0.996		0.993	
Ti	0.000		0.000		0.000		0.000		0.000		0.000		0.000	
Al	0.000		0.000		0.000		0.000		0.000		0.001		0.000	
Cr	0.001		0.002		0.001		0.000		0.001		0.001		0.001	
V ³⁺	0.000		0.000		0.000		0.000		0.000		0.000		0.000	
Fe ²⁺	0.140		0.136		0.134		0.153		0.133		0.139		0.141	
Mn	0.002		0.002		0.002		0.002		0.002		0.002		0.002	
Ni	0.007		0.006		0.007		0.007		0.007		0.006		0.006	
Mg	1.851		1.855		1.813		1.826		1.853		1.855		1.861	
Ca	0.001		0.001		0.001		0.001		0.001		0.001		0.001	
Na	0.000		0.001		0.001		0.001		0.001		0.001		0.001	
K	0.000		0.000		0.000		0.000		0.000		0.000		0.000	
Cation Total	3.001		3.001		2.979		2.995		2.999		3.002		3.006	

Table C.3. (cont)

Sample Assemblage Suite	ddmi-135b 3ol P	ddmi-139a 3ol P	ddmi-139b 3ol P	ddmi-139c 3ol P	ddmi-141b ol-cpx P	ddmi-142a cl P	ddmi-144a 2ol P
P ₂ O ₅	≤0.01	≤0.01	≤0.01	≤0.01	≤0.01	≤0.01	≤0.01
SiO ₂	41.00	41.29	42.02	41.47	41.07	41.62	41.56
TiO ₂	≤0.02	≤0.02	≤0.02	≤0.02	≤0.02	≤0.02	≤0.02
Al ₂ O ₃	≤0.02	≤0.02	≤0.02	≤0.02	≤0.02	≤0.02	≤0.02
Cr ₂ O ₃	0.05	0.07	0.08	0.04	≤0.02	0.03	≤0.02
V ₂ O ₃	≤0.01	≤0.01	≤0.01	≤0.01	≤0.01	≤0.01	≤0.01
FeO	6.73	7.12	7.23	6.91	6.78	7.31	6.97
MnO	0.10	0.10	0.09	0.10	0.09	0.09	0.09
NiO	0.34	0.36	0.35	0.35	0.32	0.36	0.34
MgO	51.04	49.55	49.25	50.36	50.45	50.17	49.92
CaO	0.02	0.04	0.04	0.03	0.03	0.03	0.03
Na ₂ O	0.02	≤0.01	0.02	≤0.01	≤0.01	0.02	0.02
K ₂ O	≤0.01	≤0.01	≤0.01	≤0.01	≤0.01	≤0.01	≤0.01
Oxide Total	99.37	98.58	99.14	99.33	98.84	99.70	99.01
P	0.000	0.000	0.000	0.000	0.000	0.000	0.000
Si	0.999	1.014	1.024	1.010	1.005	1.011	1.015
Ti	0.000	0.000	0.000	0.000	0.000	0.000	0.000
Al	0.000	0.000	0.000	0.000	0.000	0.000	0.000
Cr	0.001	0.001	0.001	0.001	0.000	0.001	0.000
V ³⁺	0.000	0.000	0.000	0.000	0.000	0.000	0.000
Fe ²⁺	0.137	0.146	0.147	0.141	0.139	0.148	0.142
Mn	0.002	0.002	0.002	0.002	0.002	0.002	0.002
Ni	0.007	0.007	0.007	0.007	0.006	0.007	0.007
Mg	1.853	1.813	1.790	1.828	1.840	1.817	1.817
Ca	0.001	0.001	0.001	0.001	0.001	0.001	0.001
Na	0.001	0.000	0.001	0.001	0.001	0.001	0.001
K	0.000	0.000	0.000	0.000	0.000	0.000	0.000
Cation Total	3.001	2.986	2.975	2.990	2.995	2.989	2.985

Table C.3. (cont)

Sample Assemblage Suite	ddimi-144b		ddimi-148b		ddimi-148c		ddimi-151c		ddimi-154b		ddimi-154c		ddimi-155a	
	2 ol	P	2 ol	P	2 ol	P	2 ol	P	grt, 2 ol	P	grt, 2 ol	P	ol	P
P ₂ O ₅	≤0.01	≤0.01	≤0.01	≤0.01	0.02	0.02	≤0.01	≤0.01	≤0.01	≤0.01	≤0.01	≤0.01	≤0.01	≤0.01
SiO ₂	41.40	39.27	41.42	41.42	39.37	39.37	40.41	40.41	41.60	41.60	41.60	41.60	42.08	42.08
TiO ₂	≤0.02	≤0.02	≤0.02	≤0.02	≤0.02	≤0.02	≤0.02	≤0.02	≤0.02	≤0.02	≤0.02	≤0.02	≤0.02	≤0.02
Al ₂ O ₃	≤0.02	≤0.02	≤0.02	≤0.02	0.06	0.06	0.05	0.05	0.04	0.04	0.04	0.04	0.04	0.04
Cr ₂ O ₃	≤0.01	≤0.01	≤0.01	≤0.01	≤0.01	≤0.01	≤0.01	≤0.01	≤0.01	≤0.01	≤0.01	≤0.01	≤0.01	≤0.01
V ₂ O ₅	7.10	7.00	7.19	7.19	6.71	6.71	7.28	7.28	7.34	7.34	7.34	7.34	7.51	7.51
FeO	0.10	0.09	0.10	0.10	0.09	0.09	0.10	0.10	0.11	0.11	0.11	0.11	0.11	0.11
MnO	0.35	0.28	0.33	0.33	0.31	0.31	0.31	0.31	0.31	0.31	0.31	0.31	0.34	0.34
NiO	50.69	52.08	49.83	49.83	51.51	51.51	50.61	50.61	49.93	49.93	49.93	49.93	50.01	50.01
CaO	0.03	0.05	0.06	0.06	0.03	0.03	0.05	0.05	0.04	0.04	0.04	0.04	0.04	0.04
Na ₂ O	≤0.01	0.03	0.02	0.02	≤0.01	≤0.01	0.03	0.03	≤0.01	≤0.01	≤0.01	≤0.01	≤0.01	≤0.01
K ₂ O	≤0.01	≤0.01	≤0.01	≤0.01	≤0.01	≤0.01	≤0.01	≤0.01	≤0.01	≤0.01	≤0.01	≤0.01	≤0.01	≤0.01
Oxide Total	98.75	98.93	99.08	99.08	98.17	98.17	98.90	98.90	99.45	99.45	99.45	99.45	100.21	100.21
P	0.00	0.00	0.00	0.00	0.00	0.00	0.00	0.00	0.00	0.00	0.00	0.00	0.00	0.00
Si	1.01	0.97	1.01	1.01	0.97	0.97	0.99	0.99	1.01	1.01	1.01	1.01	1.02	1.02
Ti	0.00	0.00	0.00	0.00	0.00	0.00	0.00	0.00	0.00	0.00	0.00	0.00	0.00	0.00
Al	0.00	0.00	0.00	0.00	0.00	0.00	0.00	0.00	0.00	0.00	0.00	0.00	0.00	0.00
Cr	0.00	0.00	0.00	0.00	0.00	0.00	0.00	0.00	0.00	0.00	0.00	0.00	0.00	0.00
V ³⁺	0.00	0.00	0.00	0.00	0.00	0.00	0.00	0.00	0.00	0.00	0.00	0.00	0.00	0.00
Fe ²⁺	0.14	0.14	0.15	0.15	0.14	0.14	0.15	0.15	0.15	0.15	0.15	0.15	0.15	0.15
Mn	0.00	0.00	0.00	0.00	0.00	0.00	0.00	0.00	0.00	0.00	0.00	0.00	0.00	0.00
Ni	0.01	0.01	0.01	0.01	0.01	0.01	0.01	0.01	0.01	0.01	0.01	0.01	0.01	0.01
Mg	1.83	1.91	1.82	1.82	1.90	1.90	1.85	1.85	1.81	1.81	1.81	1.81	1.80	1.80
Ca	0.00	0.00	0.00	0.00	0.00	0.00	0.00	0.00	0.00	0.00	0.00	0.00	0.00	0.00
Na	0.00	0.00	0.00	0.00	0.00	0.00	0.00	0.00	0.00	0.00	0.00	0.00	0.00	0.00
K	0.00	0.00	0.00	0.00	0.00	0.00	0.00	0.00	0.00	0.00	0.00	0.00	0.00	0.00
Cation Total	2.99	3.03	2.99	2.99	3.02	3.02	3.01	3.01	2.99	2.99	2.99	2.99	2.98	2.98

Table C.3. (cont)

Sample Assemblage Suite	ddmi-161a ol P	ddmi-162a ol P	ddmi-165a 3 ol P	ddmi-165b 3 ol P	ddmi-165c 3 ol P	ddmi-167b gnt, 2 ol P	ddmi-167c gnt, 2 ol P
P ₂ O ₅	≤0.01	0.02	0.02	≤0.01	0.02	0.01	≤0.01
SiO ₂	40.87	41.33	41.49	41.07	41.01	41.20	40.75
TiO ₂	≤0.02	≤0.02	≤0.02	≤0.02	≤0.02	≤0.02	≤0.02
Al ₂ O ₃	≤0.02	≤0.02	≤0.02	≤0.02	≤0.02	≤0.02	≤0.02
Cr ₂ O ₃	0.03	0.05	0.08	0.05	0.04	0.04	0.04
V ₂ O ₅	≤0.01	≤0.01	≤0.01	≤0.01	≤0.01	≤0.01	≤0.01
FeO	7.17	7.21	7.33	7.43	7.18	6.47	7.05
MnO	0.10	0.09	0.10	0.10	0.10	0.10	0.09
NiO	0.34	0.35	0.33	0.34	0.32	0.03	0.29
MgO	50.13	50.68	50.79	50.77	51.12	50.50	50.84
CaO	0.06	0.05	0.04	0.04	0.04	0.04	0.04
Na ₂ O	0.02	0.02	0.02	0.02	≤0.01	0.02	0.02
K ₂ O	≤0.01	≤0.01	≤0.01	≤0.01	≤0.01	≤0.01	≤0.01
Oxide Total	98.77	99.87	100.26	99.88	99.89	98.46	99.19
P	0.00	0.00	0.00	0.00	0.00	0.00	0.00
Si	1.00	1.00	1.00	1.00	1.00	1.01	1.00
Ti	0.00	0.00	0.00	0.00	0.00	0.00	0.00
Al	0.00	0.00	0.00	0.00	0.00	0.00	0.00
Cr	0.00	0.00	0.00	0.00	0.00	0.00	0.00
V ³⁺	0.00	0.00	0.00	0.00	0.00	0.00	0.00
Fe ²⁺	0.15	0.15	0.15	0.15	0.15	0.13	0.14
Mn	0.00	0.00	0.00	0.00	0.00	0.00	0.00
Ni	0.01	0.01	0.01	0.01	0.01	0.01	0.01
Mg	1.83	1.83	1.83	1.84	1.85	1.84	1.85
Ca	0.00	0.00	0.00	0.00	0.00	0.00	0.00
Na	0.00	0.00	0.00	0.00	0.00	0.00	0.00
K	0.00	0.00	0.00	0.00	0.00	0.00	0.00
Cation Total	3.00	3.00	3.00	3.00	3.00	2.99	3.00

Table C.3. (cont)

Sample Assemblage Suite	ddmi-168a		ddmi-170a		ddmi-170b		ddmi-174b		ddmi-177a		ddmi-177b		ddmi-179a	
	ol	P	2 ol	P	2 ol	P	ol	P	2 ol	P	2 ol	P	ol	P
P ₂ O ₅	0.02		≤0.01		0.03		0.02		0.02		≤0.01		≤0.01	
SiO ₂	41.31		41.59		41.15		39.59		41.19		41.13		41.03	
TiO ₂	≤0.02		≤0.02		≤0.02		≤0.02		≤0.02		≤0.02		≤0.02	
Al ₂ O ₃	≤0.02		≤0.02		≤0.02		≤0.02		≤0.02		≤0.02		0.03	
Cr ₂ O ₃	0.05		0.06		0.05		0.03		0.06		0.05		0.06	
V ₂ O ₅	≤0.01		≤0.01		≤0.01		≤0.01		≤0.01		≤0.01		≤0.01	
FeO	6.81		8.08		8.04		6.71		7.02		6.66		6.71	
MnO	0.09		0.10		0.10		0.09		0.08		0.10		0.10	
NiO	0.36		0.37		0.37		0.35		0.35		0.35		0.31	
MgO	51.00		51.00		50.79		54.76		50.86		51.19		50.91	
CaO	0.03		0.05		0.06		0.03		0.04		0.04		0.03	
Na ₂ O	0.02		0.02		0.02		≤0.01		≤0.01		≤0.01		≤0.01	
K ₂ O	≤0.01		≤0.01		≤0.01		≤0.01		≤0.01		≤0.01		≤0.01	
Oxide Total	99.75		101.34		100.67		101.65		99.69		99.59		99.24	
P	0.00		0.00		0.00		0.00		0.00		0.00		0.00	
Si	1.00		1.00		1.00		0.95		1.00		1.00		1.00	
Ti	0.00		0.00		0.00		0.00		0.00		0.00		0.00	
Al	0.00		0.00		0.00		0.00		0.00		0.00		0.00	
Cr	0.00		0.00		0.00		0.00		0.00		0.00		0.00	
V ³⁺	0.00		0.00		0.00		0.00		0.00		0.00		0.00	
Fe ²⁺	0.14		0.16		0.16		0.13		0.14		0.14		0.14	
Mn	0.00		0.00		0.00		0.00		0.00		0.00		0.00	
Ni	0.01		0.01		0.01		0.01		0.01		0.01		0.01	
Mg	1.84		1.83		1.83		1.96		1.84		1.85		1.85	
Ca	0.00		0.00		0.00		0.00		0.00		0.00		0.00	
Na	0.00		0.00		0.00		0.00		0.00		0.00		0.00	
K	0.00		0.00		0.00		0.00		0.00		0.00		0.00	
Cation Total	3.00		3.00		3.00		3.05		3.00		3.00		3.00	

Table C.3. (cont)

Sample Assemblage Suite	ddmi-180a		ddmi-180b		ddmi-183a		ddmi-184b		ddmi-190a		ddmi-190b		ddmi-195b	
	2 ol	P	2 ol	P	ol, chr	P	ol	P	2 ol	P	2 ol	P	ol	P
P ₂ O ₅	≤0.01	≤0.01	≤0.01	≤0.01	≤0.01	≤0.01	≤0.01	≤0.01	≤0.01	≤0.01	≤0.01	≤0.01	≤0.01	≤0.01
SiO ₂	42.42	41.31	41.31	41.27	40.86	41.27	41.27	41.27	40.61	40.53	40.53	40.53	40.21	40.21
TiO ₂	≤0.02	≤0.02	≤0.02	≤0.02	≤0.02	≤0.02	≤0.02	≤0.02	≤0.02	≤0.02	≤0.02	≤0.02	≤0.02	≤0.02
Al ₂ O ₃	≤0.02	0.07	0.07	≤0.02	≤0.02	≤0.02	≤0.02	≤0.02	≤0.02	≤0.02	≤0.02	≤0.02	≤0.02	≤0.02
Cr ₂ O ₃	0.04	0.05	0.05	0.03	0.05	0.03	0.03	0.03	0.05	0.08	0.08	0.08	0.07	0.07
V ₂ O ₅	≤0.01	≤0.01	≤0.01	≤0.01	≤0.01	≤0.01	≤0.01	≤0.01	≤0.01	≤0.01	≤0.01	≤0.01	≤0.01	≤0.01
FeO	7.29	7.19	7.19	7.39	7.31	7.39	7.39	7.39	6.82	6.96	6.96	6.96	6.92	6.92
MnO	0.11	0.10	0.10	0.10	0.11	0.10	0.10	0.10	0.09	0.10	0.10	0.10	0.08	0.08
NiO	0.32	0.34	0.34	0.36	0.31	0.36	0.36	0.36	0.31	0.31	0.31	0.31	0.29	0.29
MgO	51.00	50.57	50.57	50.63	50.93	50.63	50.63	50.63	50.71	50.53	50.53	50.53	50.51	50.51
CaO	0.04	0.04	0.04	0.03	0.03	0.03	0.03	0.03	0.03	0.03	0.03	0.03	0.04	0.04
Na ₂ O	0.02	0.03	0.03	0.02	0.02	0.02	0.02	0.02	0.02	≤0.01	≤0.01	≤0.01	0.03	0.03
K ₂ O	≤0.01	≤0.01	≤0.01	≤0.01	≤0.01	≤0.01	≤0.01	≤0.01	≤0.01	≤0.01	≤0.01	≤0.01	≤0.01	≤0.01
Oxide Total	101.31	99.75	99.75	99.90	99.69	99.90	99.90	99.90	98.72	98.62	98.62	98.62	98.22	98.22
P	0.00	0.00	0.00	0.00	0.00	0.00	0.00	0.00	0.00	0.00	0.00	0.00	0.00	0.00
Si	1.01	1.00	1.00	1.00	1.02	1.00	1.00	1.00	1.00	1.00	1.00	1.00	0.99	0.99
Ti	0.00	0.00	0.00	0.00	0.00	0.00	0.00	0.00	0.00	0.00	0.00	0.00	0.00	0.00
Al	0.00	0.00	0.00	0.00	0.00	0.00	0.00	0.00	0.00	0.00	0.00	0.00	0.00	0.00
Cr	0.00	0.00	0.00	0.00	0.00	0.00	0.00	0.00	0.00	0.00	0.00	0.00	0.00	0.00
V ³⁺	0.00	0.00	0.00	0.00	0.00	0.00	0.00	0.00	0.00	0.00	0.00	0.00	0.00	0.00
Fe ²⁺	0.15	0.15	0.15	0.15	0.15	0.15	0.15	0.15	0.14	0.14	0.14	0.14	0.14	0.14
Mn	0.00	0.00	0.00	0.00	0.00	0.00	0.00	0.00	0.00	0.00	0.00	0.00	0.00	0.00
Ni	0.01	0.01	0.01	0.01	0.01	0.01	0.01	0.01	0.01	0.01	0.01	0.01	0.01	0.01
Mg	1.82	1.83	1.83	1.83	1.80	1.83	1.83	1.83	1.85	1.85	1.85	1.85	1.86	1.86
Ca	0.00	0.00	0.00	0.00	0.00	0.00	0.00	0.00	0.00	0.00	0.00	0.00	0.00	0.00
Na	0.00	0.00	0.00	0.00	0.00	0.00	0.00	0.00	0.00	0.00	0.00	0.00	0.00	0.00
K	0.00	0.00	0.00	0.00	0.00	0.00	0.00	0.00	0.00	0.00	0.00	0.00	0.00	0.00
Cation Total	2.99	3.00	3.00	3.00	2.98	3.00	3.00	3.00	3.00	3.00	3.00	3.00	3.01	3.01

Table C.3. (cont)

Sample Assemblage Suite	ddmi-206a		ddmi-210a		ddmi-210b		ddmi-213b	
	ol P	2 ol P	ol P	2 ol P	ol P	2 ol P	ol P	2 ol P
P ₂ O ₅	0.02	0.04	≤0.01	≤0.01	0.02	0.02	0.02	0.02
SiO ₂	40.73	39.80	39.81	39.81	40.86	40.86	40.86	40.86
TiO ₂	≤0.02	≤0.02	≤0.02	≤0.02	≤0.02	≤0.02	≤0.02	≤0.02
Al ₂ O ₃	≤0.02	0.03	0.03	0.03	0.06	0.06	0.06	0.06
Cr ₂ O ₃	≤0.02	0.06	0.03	0.03	0.03	0.03	0.06	0.06
V ₂ O ₅	≤0.01	≤0.01	≤0.01	≤0.01	≤0.01	≤0.01	≤0.01	≤0.01
FeO	7.21	7.58	7.36	7.36	6.91	6.91	6.91	6.91
MnO	0.08	0.09	0.08	0.08	0.09	0.09	0.09	0.09
NiO	0.31	0.28	0.28	0.28	0.30	0.30	0.30	0.30
MgO	51.80	51.23	51.89	51.89	50.20	50.20	50.20	50.20
CaO	0.03	0.05	0.05	0.05	0.02	0.02	0.02	0.02
Na ₂ O	0.03	0.03	0.03	0.03	0.03	0.03	0.03	0.03
K ₂ O	≤0.01	≤0.01	≤0.01	≤0.01	≤0.01	≤0.01	≤0.01	≤0.01
Oxide Total	100.25	99.24	99.61	99.61	98.54	98.54	98.54	98.54
P	0.00	0.00	0.00	0.00	0.00	0.00	0.00	0.00
Si	0.99	0.98	0.97	0.97	1.00	1.00	1.00	1.00
Ti	0.00	0.00	0.00	0.00	0.00	0.00	0.00	0.00
Al	0.00	0.00	0.00	0.00	0.00	0.00	0.00	0.00
Cr	0.00	0.00	0.00	0.00	0.00	0.00	0.00	0.00
V ³⁺	0.00	0.00	0.00	0.00	0.00	0.00	0.00	0.00
Fe ²⁺	0.15	0.16	0.15	0.15	0.14	0.14	0.14	0.14
Mn	0.00	0.00	0.00	0.00	0.00	0.00	0.00	0.00
Ni	0.01	0.01	0.01	0.01	0.01	0.01	0.01	0.01
Mg	1.87	1.88	1.89	1.89	1.84	1.84	1.84	1.84
Ca	0.00	0.00	0.00	0.00	0.00	0.00	0.00	0.00
Na	0.00	0.00	0.00	0.00	0.00	0.00	0.00	0.00
K	0.00	0.00	0.00	0.00	0.00	0.00	0.00	0.00
Cation Total	3.01	3.02	3.03	3.03	3.00	3.00	3.00	3.00

Table C.4. Electron microprobe analyses of *magnesio-chromite* inclusions from A154 South diamonds. Fe³⁺ is calculated after Droop (1987). Major element compositions (EPMA-analyses) are given as wt%.

Sample	ddmi-1a	ddmi-1c	ddmi-4a	ddmi-6a	ddmi-25b	ddmi-25c	ddmi-34a
Assemblage	2chr	2chr	2chr	chr	2chr	2chr	2chr
Suite	P	P	P	P	P	P	P
SiO ₂	0.12	0.45	0.21	0.36	0.11	0.09	0.38
TiO ₂	0.08	0.07	0.04	0.08	0.08	0.08	0.04
Al ₂ O ₃	6.29	7.08	6.79	4.08	6.25	6.13	8.36
Cr ₂ O ₃	63.75	62.64	63.24	66.04	63.74	63.68	61.45
V ₂ O ₃	0.29	0.24	0.24	0.21	0.26	0.28	0.22
Fe ₂ O ₃	3.78	4.74	2.96	3.56	3.47	3.33	2.83
FeO	11.87	10.08	11.78	10.99	11.66	11.95	11.40
MnO	0.11	0.10	0.11	0.11	0.11	0.11	0.10
NiO	0.08	0.10	0.09	0.10	0.09	0.09	0.09
MgO	13.86	15.54	13.83	14.31	13.86	13.57	14.38
ZnO	0.08	0.08	0.08	0.11	0.08	0.08	0.09
Oxide Total	100.31	101.11	99.40	99.95	99.71	99.40	99.33
Si	0.030	0.114	0.056	0.095	0.030	0.025	0.099
Ti	0.016	0.013	0.008	0.016	0.015	0.015	0.007
Al	1.937	2.133	2.103	1.267	1.936	1.908	2.560
Cr	13.166	12.653	13.132	13.762	13.234	13.291	12.628
V ³⁺	0.061	0.049	0.051	0.044	0.056	0.059	0.045
Fe ³⁺	0.743	0.910	0.586	0.705	0.685	0.662	0.554
Fe ²⁺	2.592	2.153	2.588	2.423	2.561	2.638	2.477
Mn	0.024	0.022	0.024	0.023	0.024	0.025	0.022
Ni	0.017	0.020	0.019	0.022	0.018	0.018	0.018
Mg	5.399	5.918	5.416	5.622	5.426	5.342	5.571
Zn	0.015	0.015	0.016	0.020	0.015	0.017	0.018
Cation Total	24.000	24.000	24.000	24.000	24.000	24.000	24.000
[O]	32.000	33.000	34.000	35.000	36.000	37.000	38.000

* denotes an exposed surface inclusion.

Table C.4. (cont.)

Sample Assemblage Suite	ddmi-34b		ddmi-36a		ddmi-36b*		ddmi-36c*		ddmi-40a		ddmi-43a		ddmi-43b	
	2chr	P	chr, 3chr(exp)	P	chr, 3chr(exp)	P	chr, 3chr(exp)	P	2chr	P	2chr	P	2chr	P
SiO ₂	0.20		0.13		0.11		0.23		0.21		0.16		0.12	
TiO ₂	0.04		0.05		0.06		0.08		0.04		0.08		0.04	
Al ₂ O ₃	8.30		8.36		5.36		6.44		7.49		5.89		7.63	
Cr ₂ O ₃	61.73		61.82		64.49		63.30		62.32		63.91		62.61	
V ₂ O ₅	0.22		0.20		0.26		0.26		0.22		0.27		0.23	
Fe ₂ O ₃	3.24		3.49		3.75		3.56		3.24		3.36		3.61	
FeO	11.20		11.03		11.96		11.41		11.40		12.80		11.04	
MnO	0.11		0.09		0.12		0.11		0.10		0.12		0.11	
NiO	0.10		0.12		0.08		0.10		0.09		0.08		0.09	
MgO	14.39		14.51		13.60		14.13		14.15		13.16		14.44	
ZnO	0.09		0.08		0.08		0.08		0.09		0.07		0.08	
Oxide Total	99.62		99.87		99.87		99.72		99.34		99.89		99.99	
Si	0.051		0.034		0.030		0.061		0.056		0.042		0.030	
Ti	0.008		0.009		0.013		0.016		0.008		0.015		0.008	
Al	2.540		2.549		1.666		1.988		2.309		1.831		2.332	
Cr	12.666		12.645		13.450		13.103		12.881		13.331		12.841	
V ³⁺	0.046		0.041		0.055		0.056		0.047		0.056		0.048	
Fe ³⁺	0.632		0.679		0.745		0.701		0.637		0.667		0.704	
Fe ²⁺	2.432		2.387		2.639		2.499		2.492		2.824		2.395	
Mn	0.024		0.020		0.026		0.025		0.021		0.028		0.025	
Ni	0.020		0.024		0.017		0.021		0.018		0.016		0.019	
Mg	5.565		5.596		5.346		5.516		5.515		5.176		5.584	
Zn	0.018		0.015		0.015		0.016		0.017		0.014		0.016	
Cation Total	24.000		24.000		24.000		24.000		24.000		24.000		24.000	
[O]	32.000		33.000		34.000		35.000		36.000		37.000		38.000	

Table C.4. (cont.)

Sample Assemblage Suite	ddmi-44a		ddmi-44b		ddmi-46a		ddmi-47a		ddmi-58a		ddmi-58b		ddmi-98b	
	3chr P		3chr P		chr P		chr P		2chr P		2chr P		2chr P	
SiO ₂	0.15		0.15		0.16		0.20		0.16		0.15		0.10	
TiO ₂	0.09		0.09		0.48		0.03		0.07		0.08		0.08	
Al ₂ O ₃	6.21		6.12		6.09		7.50		6.12		6.30		5.64	
Cr ₂ O ₃	63.39		63.41		64.14		62.47		63.53		63.63		64.87	
V ₂ O ₅	0.26		0.27		0.22		0.22		0.27		0.27		0.20	
Fe ₂ O ₃	3.40		2.94		2.98		3.44		2.89		3.57		3.02	
FeO	11.95		12.36		10.78		11.32		12.16		11.64		12.58	
MnO	0.11		0.11		0.10		0.11		0.10		0.11		0.11	
NiO	0.08		0.07		0.11		0.09		0.08		0.06		0.08	
MgO	13.64		13.27		14.71		14.24		13.39		13.94		13.27	
ZnO	0.08		0.09		0.10		0.11		0.09		0.09		0.08	
Oxide Total	99.37		98.87		99.86		99.73		98.87		99.85		100.02	
Si	0.040		0.040		0.041		0.052		0.043		0.039		0.028	
Ti	0.018		0.018		0.094		0.006		0.014		0.015		0.016	
Al	1.931		1.916		1.871		2.302		1.916		1.946		1.752	
Cr	13.222		13.322		13.227		12.862		13.335		13.184		13.521	
V ³⁺	0.056		0.057		0.046		0.045		0.058		0.058		0.042	
Fe ³⁺	0.675		0.588		0.585		0.675		0.578		0.705		0.599	
Fe ²⁺	2.636		2.746		2.351		2.466		2.699		2.552		2.773	
Mn	0.024		0.025		0.022		0.024		0.023		0.025		0.024	
Ni	0.017		0.015		0.023		0.019		0.017		0.013		0.016	
Mg	5.365		5.255		5.720		5.528		5.301		5.446		5.214	
Zn	0.016		0.017		0.020		0.021		0.017		0.018		0.016	
Cation Total	24.000		24.000		24.000		24.000		24.000		24.000		24.000	
[O]	32.000		32.000		32.000		32.000		32.000		32.000		32.000	

Table C.4. (cont.)

Sample Assemblage Suite	ddmi-98c		ddmi-100a		ddmi-100b*		ddmi-100c*		ddmi-103a		ddmi-108a		ddmi-119a	
	2chr	P	chr, 3chr(exp)	P	chr, 3chr(exp)	P	chr, 3chr(exp)	P	2chr	P	chr	P	13chr, 2chr(exp)	P
SiO ₂	0.13		0.17		0.15		0.14		0.15		0.12		0.17	
TiO ₂	0.07		0.04		0.06		0.06		0.11		0.06		0.07	
Al ₂ O ₃	5.60		6.85		6.35		6.20		6.49		6.03		6.04	
Cr ₂ O ₃	64.20		63.16		63.84		63.53		63.89		63.69		62.97	
V ₂ O ₅	0.19		0.24		0.23		0.25		0.29		0.28		0.31	
Fe ₂ O ₃	3.42		3.63		3.49		3.29		3.42		2.96		3.34	
FeO	12.42		11.43		11.39		11.63		11.56		11.70		11.93	
MnO	0.12		0.11		0.11		0.10		0.12		0.10		0.11	
NiO	0.08		0.09		0.10		0.09		0.09		0.08		0.08	
MgO	13.28		14.14		14.10		13.77		14.08		13.62		13.47	
ZnO	0.08		0.09		0.09		0.09		0.14		0.10		0.09	
Oxide Total	99.60		99.64		99.90		99.15		100.34		98.74		98.58	
Si	0.035		0.043		0.040		0.036		0.038		0.033		0.045	
Ti	0.014		0.008		0.012		0.013		0.021		0.013		0.014	
Al	1.747		2.106		1.957		1.929		1.992		1.886		1.895	
Cr	13.433		13.029		13.203		13.267		13.158		13.370		13.251	
V ³⁺	0.041		0.051		0.049		0.052		0.061		0.060		0.065	
Fe ³⁺	0.682		0.712		0.686		0.654		0.670		0.592		0.670	
Fe ²⁺	2.750		2.493		2.491		2.569		2.519		2.598		2.656	
Mn	0.027		0.024		0.024		0.022		0.027		0.022		0.025	
Ni	0.017		0.018		0.021		0.019		0.018		0.018		0.017	
Mg	5.239		5.498		5.499		5.421		5.468		5.390		5.345	
Zn	0.016		0.018		0.017		0.018		0.026		0.019		0.017	
Cation Total	24.000		24.000		24.000		24.000		24.000		24.000		24.000	
[O]	32.000		32.000		32.000		32.000		32.000		32.000		32.000	

Table C.4. (cont.)

Sample Assemblage Suite	ddmi-119b 13chr, 2chr(exp)		ddmi-119c* 13chr, 2chr(exp)		ddmi-120a chr		ddmi-126a 2chr, 1chr(exp)		ddmi-145a 2chr		ddmi-145b 2chr		ddmi-146a chr	
	P		P		chr	P		2chr	P		2chr	P	chr	P
SiO ₂	0.11		0.28		0.10	0.13		0.27		0.11		0.12		0.12
TiO ₂	0.08		0.07		0.20	0.11		0.16		0.16		0.11		0.11
Al ₂ O ₃	6.36		6.21		7.13	6.25		6.01		6.06		6.43		6.43
Cr ₂ O ₃	63.86		63.25		62.89	63.66		63.19		63.76		63.53		63.53
V ₂ O ₅	0.27		0.28		0.17	0.27		0.28		0.27		0.26		0.26
Fe ₂ O ₃	3.72		3.21		3.28	3.47		3.38		3.44		3.83		3.83
FeO	11.72		12.16		10.51	11.98		12.18		11.94		11.43		11.43
MnO	0.10		0.11		0.11	0.11		0.11		0.11		0.10		0.10
NiO	0.09		0.09		0.09	0.08		0.09		0.09		0.09		0.09
MgO	13.96		13.58		14.65	13.71		13.61		13.70		14.14		14.14
ZnO	0.08		0.09		0.09	0.10		0.09		0.09		0.08		0.08
Oxide Total	100.34		99.32		99.21	99.87		99.37		99.72		100.12		100.12
Si	0.028		0.073		0.025	0.035		0.073		0.029		0.032		0.032
Ti	0.015		0.014		0.039	0.022		0.032		0.032		0.021		0.021
Al	1.954		1.931		2.197	1.932		1.871		1.878		1.978		1.978
Cr	13.173		13.198		12.994	13.212		13.189		13.263		13.109		13.109
V ³⁺	0.057		0.059		0.036	0.057		0.059		0.057		0.054		0.054
Fe ³⁺	0.730		0.638		0.646	0.686		0.672		0.680		0.752		0.752
Fe ²⁺	2.558		2.684		2.298	2.629		2.688		2.626		2.495		2.495
Mn	0.023		0.024		0.024	0.024		0.024		0.025		0.022		0.022
Ni	0.018		0.018		0.019	0.017		0.019		0.019		0.020		0.020
Mg	5.429		5.343		5.706	5.366		5.357		5.373		5.501		5.501
Zn	0.015		0.018		0.018	0.020		0.017		0.017		0.016		0.016
Cation Total	24.000		24.000		24.000	24.000		24.000		24.000		24.000		24.000
[O]	32.000		32.000		32.000	32.000		32.000		32.000		32.000		32.000

Table C.4. (cont.)

Sample Assemblage Suite	ddmi-147a		ddmi-147b		ddmi-147c		ddmi-147d		ddmi-150b		ddmi-150c		ddmi-152b	
	12chr	P	12chr	P	12chr	P	12chr	P	2chr, s	P	2chr, s	P	3chr, 1chr(exp)	P
SiO ₂	0.10	0.11	0.11	0.11	0.11	0.18	0.18	0.21	0.20	0.20	0.11	0.11	0.11	0.11
TiO ₂	0.18	0.18	0.18	0.18	0.18	0.18	0.18	0.54	0.53	0.53	0.17	0.17	0.17	0.17
Al ₂ O ₃	6.27	6.05	6.22	6.13	6.22	6.13	5.88	5.88	6.07	6.07	6.48	6.48	6.48	6.48
Cr ₂ O ₃	63.44	63.24	63.41	63.37	63.41	63.37	63.97	63.97	63.57	63.57	63.19	63.19	63.19	63.19
V ₂ O ₅	0.26	0.26	0.26	0.27	0.26	0.27	0.20	0.20	0.19	0.19	0.29	0.29	0.29	0.29
Fe ₂ O ₃	3.75	3.15	3.49	3.43	3.49	3.43	2.74	2.74	3.63	3.63	3.53	3.53	3.53	3.53
FeO	11.58	12.20	11.83	12.05	11.83	12.05	11.41	11.41	10.63	10.63	12.04	12.04	12.04	12.04
MnO	0.11	0.11	0.11	0.10	0.11	0.10	0.09	0.09	0.09	0.09	0.11	0.11	0.11	0.11
NiO	0.09	0.09	0.09	0.09	0.09	0.09	0.09	0.09	0.09	0.09	0.08	0.08	0.08	0.08
MgO	13.99	13.36	13.76	13.68	13.76	13.68	14.31	14.31	14.92	14.92	13.70	13.70	13.70	13.70
ZnO	0.09	0.08	0.09	0.08	0.09	0.08	0.11	0.11	0.09	0.09	0.10	0.10	0.10	0.10
Oxide Total	99.87	98.82	99.54	99.56	99.54	99.56	99.54	99.54	99.99	99.99	99.79	99.79	99.79	99.79
Si	0.027	0.028	0.028	0.048	0.028	0.048	0.055	0.055	0.051	0.051	0.030	0.030	0.030	0.030
Ti	0.035	0.036	0.035	0.035	0.035	0.035	0.106	0.106	0.103	0.103	0.033	0.033	0.033	0.033
Al	1.937	1.895	1.931	1.901	1.931	1.901	1.818	1.818	1.862	1.862	2.005	2.005	2.005	2.005
Cr	13.143	13.291	13.197	13.195	13.197	13.195	13.275	13.275	13.079	13.079	13.113	13.113	13.113	13.113
V ³⁺	0.054	0.055	0.054	0.057	0.054	0.057	0.043	0.043	0.039	0.039	0.060	0.060	0.060	0.060
Fe ³⁺	0.740	0.631	0.691	0.681	0.691	0.681	0.541	0.541	0.711	0.711	0.696	0.696	0.696	0.696
Fe ²⁺	2.536	2.711	2.605	2.654	2.605	2.654	2.504	2.504	2.313	2.313	2.642	2.642	2.642	2.642
Mn	0.024	0.024	0.024	0.023	0.024	0.023	0.020	0.020	0.020	0.020	0.023	0.023	0.023	0.023
Ni	0.019	0.019	0.018	0.019	0.018	0.019	0.018	0.018	0.018	0.018	0.017	0.017	0.017	0.017
Mg	5.465	5.294	5.400	5.372	5.400	5.372	5.598	5.598	5.786	5.786	5.360	5.360	5.360	5.360
Zn	0.017	0.015	0.017	0.016	0.017	0.016	0.021	0.021	0.018	0.018	0.020	0.020	0.020	0.020
Cation Total	24.000	24.000	24.000	24.000	24.000	24.000	24.000	24.000	24.000	24.000	24.000	24.000	24.000	24.000
[O]	32.000	32.000	32.000	32.000	32.000	32.000	32.000	32.000	32.000	32.000	32.000	32.000	32.000	32.000

Table C.4. (cont.)

Sample Assemblage Suite	ddmi-152c		ddmi-169a		ddmi-172a		ddmi-176a		ddmi-182c		ddmi-183d		ddmi-187a	
	3chr, P	1chr(exp) P	2chr P	2chr P	2chr P	2chr P	chr P	chr P	chr P	chr, P	chr, P	6chr, P	chr(exp) P	
SiO ₂	0.11		0.13	0.13	0.10	0.10	0.22	0.22	0.22	0.22	0.22	0.13	0.13	
TiO ₂	0.16		0.16	0.09	0.13	0.13	0.20	0.20	0.20	0.20	0.29	0.05	0.05	
Al ₂ O ₃	6.38		6.39	6.37	5.87	5.87	4.46	4.46	4.46	4.84	4.84	6.40	6.40	
Cr ₂ O ₃	63.09		63.24	63.51	64.20	64.20	65.45	65.45	65.45	65.57	65.57	63.58	63.58	
V ₂ O ₃	0.28		0.26	0.28	0.26	0.26	0.24	0.24	0.24	0.25	0.25	0.27	0.27	
Fe ₂ O ₃	3.63		3.22	3.41	3.23	3.23	3.92	3.92	3.92	3.64	3.64	3.66	3.66	
FeO	11.75		11.88	11.84	12.22	12.22	11.26	11.26	11.26	12.48	12.48	11.45	11.45	
MnO	0.12		0.11	0.11	0.11	0.11	0.10	0.10	0.10	0.09	0.09	0.10	0.10	
NiO	0.09		0.08	0.09	0.09	0.09	0.09	0.09	0.09	0.08	0.08	0.09	0.09	
MgO	13.80		13.70	13.76	13.50	13.50	14.21	14.21	14.21	13.72	13.72	14.04	14.04	
ZnO	0.09		0.10	0.09	0.08	0.08	0.09	0.09	0.09	0.09	0.09	0.09	0.09	
Oxide Total	99.48		99.26	99.68	99.79	99.79	100.23	100.23	100.23	101.27	101.27	99.85	99.85	
Si	0.028		0.033	0.033	0.028	0.028	0.059	0.059	0.059	0.056	0.056	0.033	0.033	
Ti	0.033		0.032	0.017	0.027	0.027	0.040	0.040	0.040	0.056	0.056	0.011	0.011	
Al	1.978		1.988	1.973	1.821	1.821	1.380	1.380	1.380	1.488	1.488	1.973	1.973	
Cr	13.124		13.187	13.191	13.375	13.375	13.598	13.598	13.598	13.522	13.522	13.162	13.162	
V ³⁺	0.058		0.054	0.060	0.055	0.055	0.050	0.050	0.050	0.051	0.051	0.057	0.057	
Fe ³⁺	0.719		0.639	0.675	0.640	0.640	0.776	0.776	0.776	0.715	0.715	0.721	0.721	
Fe ²⁺	2.585		2.620	2.602	2.692	2.692	2.474	2.474	2.474	2.722	2.722	2.506	2.506	
Mn	0.027		0.025	0.025	0.025	0.025	0.022	0.022	0.022	0.020	0.020	0.023	0.023	
Ni	0.020		0.016	0.019	0.019	0.019	0.019	0.019	0.019	0.017	0.017	0.019	0.019	
Mg	5.412		5.385	5.388	5.303	5.303	5.566	5.566	5.566	5.335	5.335	5.478	5.478	
Zn	0.017		0.020	0.017	0.015	0.015	0.017	0.017	0.017	0.018	0.018	0.018	0.018	
Cation Total	24.000		24.000	24.000	24.000	24.000	24.000	24.000	24.000	24.000	24.000	24.000	24.000	
[O]	32.000		32.000	32.000	32.000	32.000	32.000	32.000	32.000	32.000	32.000	32.000	32.000	

Table C.4. (cont.)

Sample Assemblage Suite	ddmi-187b		ddmi-188b		ddmi-203a		ddmi-207a		ddmi-214a		ddmi-215a		ddmi-215b	
	6chr	chr(exp)	3chr	P	chr	P	2chr	P	2chr	P	3chr	P	chr	P
SiO ₂	0.15		0.40		0.13		0.37		0.12		0.12		0.14	
TiO ₂	0.06		0.08		0.07		0.08		0.07		0.04		0.04	
Al ₂ O ₃	6.14		6.96		5.36		6.29		6.21		6.31		5.96	
Cr ₂ O ₃	63.96		61.76		64.51		62.96		63.85		63.92		64.35	
V ₂ O ₃	0.30		0.28		0.27		0.26		0.24		0.26		0.26	
Fe ₂ O ₃	3.64		4.79		3.44		3.78		3.67		3.29		3.23	
FeO	11.66		10.53		12.30		11.86		11.37		11.71		11.62	
MnO	0.10		0.11		0.12		0.11		0.12		0.09		0.10	
NiO	0.09		0.09		0.08		0.07		0.08		0.09		0.09	
MgO	13.96		14.96		13.36		13.97		14.07		13.84		13.87	
ZnO	0.09		0.09		0.08		0.10		0.09		0.09		0.08	
Oxide Total	100.13		100.03		99.72		99.85		99.90		99.76		99.74	
Si	0.039		0.102		0.036		0.096		0.030		0.032		0.036	
Ti	0.011		0.015		0.013		0.015		0.015		0.008		0.007	
Al	1.893		2.124		1.671		1.941		1.917		1.952		1.847	
Cr	13.227		12.650		13.489		13.036		13.219		13.263		13.371	
V ³⁺	0.062		0.058		0.057		0.055		0.051		0.054		0.056	
Fe ³⁺	0.716		0.934		0.685		0.746		0.723		0.651		0.639	
Fe ²⁺	2.550		2.281		2.722		2.599		2.491		2.569		2.553	
Mn	0.022		0.023		0.026		0.025		0.026		0.020		0.022	
Ni	0.018		0.019		0.017		0.015		0.018		0.019		0.019	
Mg	5.444		5.778		5.268		5.454		5.492		5.415		5.434	
Zn	0.017		0.017		0.016		0.018		0.017		0.017		0.015	
Cation Total	24.000		24.000		24.000		24.000		24.000		24.000		24.000	
[O]	32.000		32.000		32.000		32.000		32.000		32.000		32.000	

Table C.5. Electron microprobe analyses of *clinopyroxene* inclusions from A154 South diamonds. Major element compositions (EMPA-analyses) are given as wt%.

Sample	ddmi-48a	ddmi-48b	ddmi-140c	ddmi-141a	ddmi-186a	ddmi-186b
Assemblage	4 cpx	4 cpx	cpx	ol-cpx	2 cpx	2 cpx
Suite	E	E	P	P	E	E
P ₂ O ₅	0.04	0.02	≤0.01	≤0.01	≤0.01	≤0.01
SiO ₂	55.06	54.62	55.47	54.60	54.78	55.23
TiO ₂	0.27	0.27	0.03	0.09	0.08	0.07
Al ₂ O ₃	4.98	4.91	1.04	1.02	17.71	17.51
Cr ₂ O ₃	0.12	0.12	1.14	1.14	0.04	0.03
V ₂ O ₃	0.04	0.03	0.02	0.02	<0.01	0.02
FeO	5.02	5.05	2.11	2.87	1.17	1.22
MnO	0.07	0.07	0.09	0.10	≤0.02	≤0.02
NiO	≤0.01	≤0.01	0.06	0.06	0.08	0.09
MgO	14.00	13.82	17.85	16.80	6.20	6.03
CaO	16.80	16.90	20.27	20.80	12.74	12.86
Na ₂ O	2.63	2.59	0.78	1.29	5.91	5.73
K ₂ O	0.28	0.27	0.02	0.02	0.18	0.19
Oxide Total	99.31	98.67	98.87	98.83	98.91	98.98
P	0.00	0.00	0.00	0.00	0.00	0.00
Si	2.00	2.00	2.01	2.00	1.92	1.94
Ti	0.01	0.01	0.00	0.00	0.00	0.00
Al	0.21	0.21	0.04	0.04	0.73	0.72
Cr	0.00	0.00	0.03	0.03	0.00	0.00
V ³⁺	0.00	0.00	0.00	0.00	0.00	0.00
Fe ²⁺	0.15	0.15	0.06	0.09	0.03	0.04
Mn	0.00	0.00	0.00	0.00	0.00	0.00
Ni	0.00	0.00	0.00	0.00	0.00	0.00
Mg	0.76	0.75	0.97	0.92	0.32	0.32
Ca	0.65	0.66	0.79	0.82	0.48	0.48
Na	0.18	0.18	0.06	0.09	0.40	0.39
K	0.01	0.01	0.00	0.00	0.01	0.01
Cation Total	3.98	3.99	3.97	4.00	3.91	3.90

Table C.6. Electron microprobe analyses of *sulphide* inclusions from A154 South diamonds. Major element compositions (EPMA-analyses) are given as wt%.

Sample	ddmi-2c	ddmi-37a	ddmi-78a	ddmi-93b	ddmi-112a	ddmi-115a	ddmi-127a	ddmi-130b
Assemblage	fper, sulph	3 sulph	2 sulph	sulph	sulph	sulph	sulph	sulph
Suite	E	E	E	E	P	P	E	P
Si	0.04	0.05	0.03	0.03	0.06	0.23	0.03	0.01
Cr	≤0.06	≤0.06	≤0.06	≤0.06	0.35	≤0.06	≤0.06	≤0.06
Fe	45.76	56.47	60.09	53.87	38.10	12.00	56.35	47.61
Mn	≤0.02	≤0.02	≤0.02	≤0.02	≤0.02	≤0.02	≤0.02	≤0.02
Ni	≤0.01	1.10	1.05	0.93	21.93	55.99	1.56	9.97
Mg	≤0.01	≤0.01	≤0.01	≤0.01	≤0.01	0.13	≤0.01	≤0.01
Cu	0.36	2.33	0.49	4.99	0.58	0.07	1.33	0.63
Co	0.05	0.27	0.37	0.29	0.48	1.10	0.34	0.52
Zn	0.05	0.03	0.05	0.06	0.05	0.06	0.05	0.09
S	52.91	38.54	36.28	38.87	36.79	28.71	38.95	40.65
Total	99.18	98.80	98.37	99.03	98.34	98.29	98.60	99.47

Sample	ddmi-150b	ddmi-156a	ddmi-179a	ddmi-196a	ddmi-196b	ddmi-198a	ddmi-199d	ddmi-202b
Assemblage	2 chr, sulph	sulph	ol, sulph	2 sulph	2 sulph	sulph	2 gnt, sulph	2 sulph
Suite	P	P	P	E	E	E	P	P
Si	0.02	0.03	0.02	0.01	0.05	0.02	0.02	0.02
Cr	0.27	0.28	0.68	≤0.06	≤0.06	≤0.06	≤0.06	0.22
Fe	46.84	38.83	39.64	57.89	58.36	58.07	23.89	36.85
Mn	≤0.02	≤0.02	≤0.02	≤0.02	≤0.02	≤0.02	≤0.02	≤0.02
Ni	13.02	22.32	21.19	0.44	0.28	0.59	39.85	22.68
Mg	≤0.01	≤0.01	≤0.01	≤0.01	≤0.01	≤0.01	≤0.01	≤0.01
Cu	0.29	0.57	0.31	1.15	0.83	0.64	0.20	≤0.04
Co	0.45	0.51	0.43	0.22	0.15	0.17	0.96	0.50
Zn	0.05	0.07	0.07	≤0.03	0.06	0.07	0.07	0.04
S	37.13	36.94	36.85	38.30	38.66	38.57	33.75	37.76
Total	98.06	99.54	99.19	98.01	98.39	98.13	98.74	98.07

Table C.7. Electron microprobe analyses of *ferropericlase* and *coesite* inclusions from A154 South diamonds. Major element compositions (EPMA-analyses) are given as wt%.

Sample Assemblage Suite	ddmi-2a fper, s E?	ddmi-114a fper ?	ddmi-153a 3fper ?	ddmi-153b 3fper ?	ddmi-153d 3fper ?	ddmi-173a 2fper ?	ddmi-173b 2fper ?	ddmi-193 coe E
P ₂ O ₅	≤0.01	≤0.01	≤0.01	≤0.01	≤0.01	≤0.01	≤0.01	≤0.01
SiO ₂	0.10	0.02	0.08	0.09	0.13	0.22	0.10	99.95
TiO ₂	≤0.02	≤0.02	≤0.02	≤0.02	≤0.02	≤0.02	≤0.02	≤0.02
Al ₂ O ₃	≤0.02	≤0.02	≤0.02	≤0.02	≤0.02	≤0.02	≤0.02	≤0.02
Cr ₂ O ₃	0.60	0.36	0.44	0.42	0.46	0.47	0.45	≤0.02
V ₂ O ₅	≤0.01	≤0.01	≤0.01	≤0.01	≤0.01	≤0.01	≤0.01	≤0.01
FeO	21.56	28.53	27.17	26.63	26.41	20.78	20.79	≤0.01
MnO	0.15	0.16	0.22	0.22	0.20	0.15	0.15	≤0.02
NiO	1.09	2.03	1.05	0.98	1.02	1.12	1.11	≤0.01
MgO	77.22	69.44	70.18	72.38	71.47	78.25	78.26	≤0.01
CaO	≤0.01	≤0.01	≤0.01	≤0.01	≤0.01	≤0.01	≤0.01	≤0.01
Na ₂ O	0.33	0.34	0.13	0.26	0.22	0.23	0.22	≤0.01
K ₂ O	≤0.01	≤0.01	≤0.01	≤0.01	≤0.01	≤0.01	≤0.01	≤0.01
Oxide Total	101.13	100.96	99.33	101.05	99.99	101.31	101.17	101.11

C.2. Ion Probe Data

Table C.8. Concentrations of major (wt%) elements (EMPA) and trace (wt% ppm) elements (SIMS) from A154 South garnet inclusions in diamond.

Sample	ddmi-008a	ddmi-133a	ddmi-133b	ddmi-154a	ddmi-166a	ddmi-167a
Assemblage Suite	gnt P	2gnt P	2gnt P	gnt, 2ol P	10gnt E	gnt, 2ol P
P ₂ O ₅	0.03	0.03	0.02	0.03	0.06	0.02
SiO ₂	41.33	42.33	41.95	41.04	41.17	42.07
TiO ₂	0.12	0.11	0.12	0.08	0.36	≤0.02
Al ₂ O ₃	14.17	15.00	14.75	11.53	22.77	18.47
Cr ₂ O ₃	10.85	10.87	10.83	15.68	0.08	6.97
V ₂ O ₃	0.05	0.06	0.06	0.05	0.02	0.04
FeO	5.85	6.07	6.31	5.82	9.75	5.50
MnO	0.23	0.24	0.27	0.26	0.21	0.21
NiO	≤0.01	≤0.01	≤0.01	≤0.01	≤0.01	≤0.01
MgO	22.91	23.44	23.28	19.88	11.94	22.70
CaO	2.89	2.64	2.66	5.91	14.08	3.73
Na ₂ O	≤0.01	≤0.01	≤0.01	0.02	0.14	0.02
K ₂ O	≤0.01	≤0.01	≤0.01	≤0.01	≤0.01	≤0.01
Oxide Total	98.44	100.84	100.28	100.30	100.58	99.78
Ti (ppm)	988	858	1059	680	2034	210
Sr (ppm)	4.18	6.26	4.39	10.79	6.15	3.77
Y (ppm)	2.25	1.98	2.23	2.04	12.78	1.14
Zr (ppm)	29.02	15.77	26.76	49.88	27.05	4.59
La (ppm)	0.26	0.32	0.14	1.19	0.12	0.71
Ce (ppm)	4.40	3.98	2.79	9.81	0.91	3.62
Nd (ppm)	3.43	2.64	5.10	7.82	1.74	3.27
Sm (ppm)	0.70	0.24	0.84	1.44	1.10	0.34
Eu (ppm)	0.19	0.10	0.15	0.34	0.50	0.17
Dy (ppm)	0.44	0.12	0.47	0.40	1.68	0.13
Er (ppm)	0.22	0.04	0.25	0.31	1.19	0.07
Yb (ppm)	0.18	0.06	0.10	0.27	1.22	0.30

Table C.8. (cont.)

Sample Assemblage Suite	ddmi-175b 6gnt P	ddmi-199a 2gnt, s P	ddmi-205b 2gnt E	ddmi-208c 12gnt E	ddmi-216a 2gnt P	ddmi-216c 2gnt P
P ₂ O ₅	0.02	≤0.01	0.08	0.05	≤0.04	≤0.04
SiO ₂	41.67	41.45	39.72	40.31	41.32	41.61
TiO ₂	≤0.02	0.06	0.36	0.31	≤0.05	≤0.05
Al ₂ O ₃	16.10	17.69	22.17	22.02	17.50	16.24
Cr ₂ O ₃	10.25	7.15	0.05	0.07	7.99	8.00
V ₂ O ₅	0.04	0.05	0.02	≤0.02	0.05	0.05
FeO	6.19	6.95	11.20	9.48	5.94	6.33
MnO	0.31	0.29	0.19	0.18	0.25	0.25
NiO	≤0.01	≤0.01	≤0.01	≤0.03	≤0.03	≤0.03
MgO	21.69	19.52	10.79	12.11	21.80	21.86
CaO	3.65	6.03	13.63	13.83	4.34	4.30
Na ₂ O	≤0.01	0.02	0.12	0.14	0.02	0.03
K ₂ O	≤0.01	≤0.01	≤0.01	≤0.02	≤0.02	≤0.02
Oxide Total	99.97	99.24	98.33	98.33	98.77	99.28
Ti (ppm)	153	473	1568	2159	311	175
Sr (ppm)	2.79	0.86	2.63	5.60	1.87	0.76
Y (ppm)	3.34	1.36	11.32	11.45	6.70	5.40
Zr (ppm)	39.43	8.52	8.41	25.52	65.54	62.15
La (ppm)	0.11	0.22	0.10	0.15	0.04	0.04
Ce (ppm)	1.58	0.81	0.83	1.12	0.24	0.27
Nd (ppm)	3.08	0.49	1.61	1.72	0.67	0.41
Sm (ppm)	0.61	0.15	1.05	0.77	0.44	0.66
Eu (ppm)	0.21	0.02	0.31	0.50	0.32	0.31
Dy (ppm)	0.34	0.09	1.15	1.38	0.98	0.74
Er (ppm)	0.18	0.07	0.99	1.05	0.43	0.39
Yb (ppm)	0.18	0.20	0.85	0.81	0.35	0.38

C.3. Diamond Characteristics

Table C.9. Results of a random population survey of 200.29 carats (850 diamonds) from the +9 size range from the Diavik Product Sorting Facility (PSF) in Yellowknife.

	Frequency	Percentage (%)
Morphology		
Octahedra	123	14.47
Dodecahedroids	257	30.24
Cube	105	12.35
Twinned	247	29.06
Irregular/Fragments	91	10.71
Aggregates	27	3.18
Colour		
Colourless	533	62.71
Faint Brown	127	14.94
Intermediate Brown	56	6.59
Strong Brown	12	1.41
Faint Yellow	3	0.35
Intermediate Yellow	2	0.24
Strong Yellow	0	0.00
Grey	84	9.88
Pink	33	3.88
Coats		
Uncoated	786	92.47
Coated	64	7.53
Inclusions		
	10	1.18

Figure C.1. The colour distribution of 100 inclusion-bearing diamonds (a) and a random population sample (b) of 850 diamonds from the Diavik Product Sorting Facility (PSF) in Yellowknife.

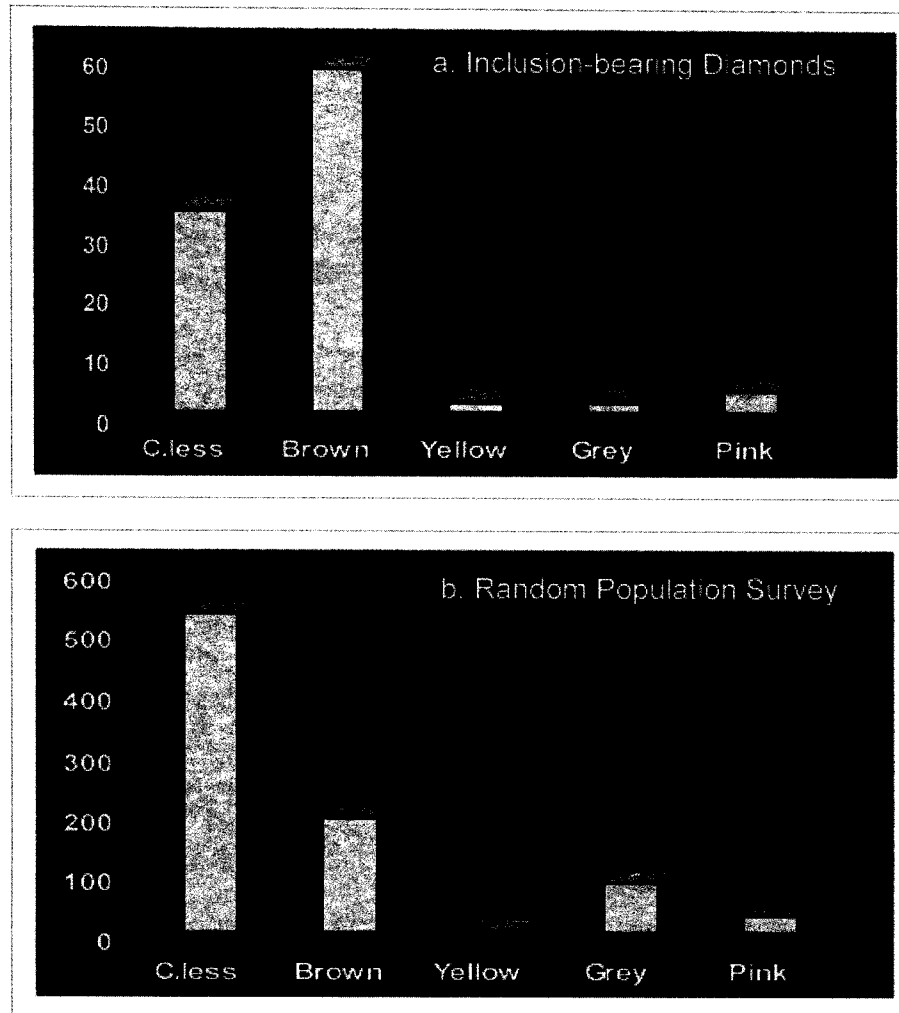
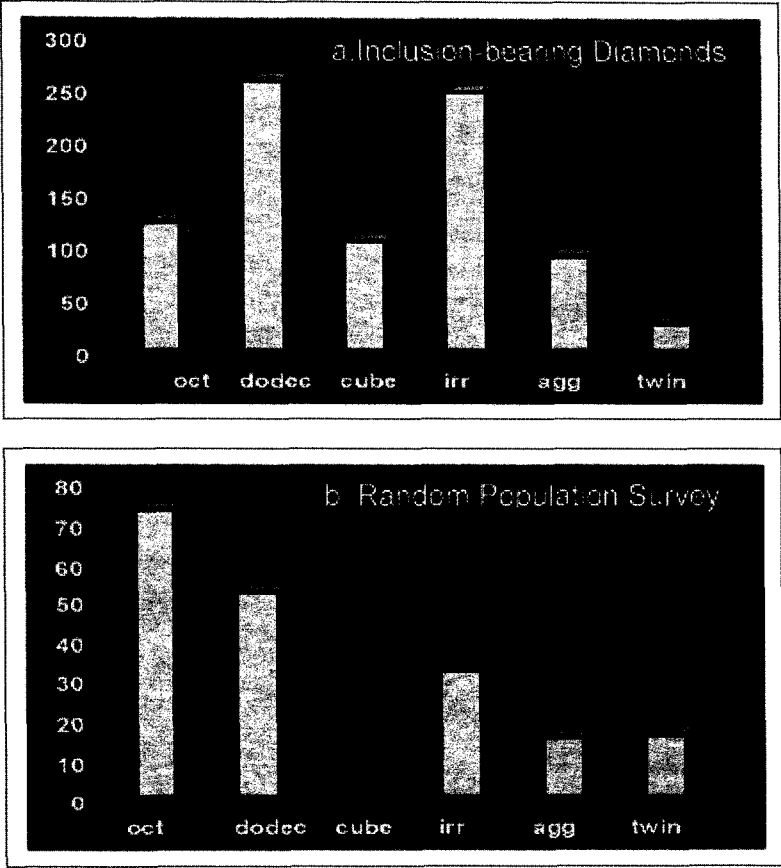


Figure C.2. The morphological distribution of 100 inclusion-bearing diamonds (a) and a random population sample (b) of 850 diamonds from the Diavik Product Sorting Facility (PSF) in Yellowknife.



C.4. Carbon Isotope Data

Table C.10. Carbon isotopic composition of A154 South diamonds, reported in per mille (‰).

Sample	$\delta^{13}\text{C}$	Sample	$\delta^{13}\text{C}$	Sample	$\delta^{13}\text{C}$	Sample	$\delta^{13}\text{C}$
ddmi-001	-4.535	ddmi-101	-5.980	ddmi-147	-5.182	ddmi-180	-6.311
ddmi-002	0.686	ddmi-103	-5.129	ddmi-148	-6.120	ddmi-182	-5.137
ddmi-003	-5.462	ddmi-108	-5.279	ddmi-150	-4.790	ddmi-183	-5.264
ddmi-004	-4.963	ddmi-110	-4.803	ddmi-151	-6.330	ddmi-184	-5.443
ddmi-005	-5.299	ddmi-111	-6.264	ddmi-152	-5.044	ddmi-186	-4.876
ddmi-006	-4.950	ddmi-112	-5.431	ddmi-153	-4.223	ddmi-187	-4.579
ddmi-008	-5.660	ddmi-114	-2.929	ddmi-154	-4.823	ddmi-188	-5.145
ddmi-013	-3.889	ddmi-115	-5.474	ddmi-155	-5.256	ddmi-190	-5.634
ddmi-014	-4.552	ddmi-119	-4.929	ddmi-156	-4.901	ddmi-193	-5.074
ddmi-025	-5.071	ddmi-120	-4.526	ddmi-159	-5.096	ddmi-195	-6.068
ddmi-034	-4.457	ddmi-123	-6.251	ddmi-161	-6.107	ddmi-196	-5.074
ddmi-036	-4.487	ddmi-124	-5.458	ddmi-162	-8.623	ddmi-198	-5.273
ddmi-037	-8.578	ddmi-126	-4.958	ddmi-165	-5.241	ddmi-199	-5.174
ddmi-040	-4.276	ddmi-127	-5.288	ddmi-166	-4.772	ddmi-200	-4.577
ddmi-043	-4.830	ddmi-129	-5.808	ddmi-167	-4.777	ddmi-202	-5.037
ddmi-044	-4.982	ddmi-130	-5.367	ddmi-168	-5.611	ddmi-203	-4.318
ddmi-046	-4.028	ddmi-133	-5.350	ddmi-169	-5.205	ddmi-205	-4.786
ddmi-047	-4.644	ddmi-135	-4.402	ddmi-170	-5.364	ddmi-206	-5.151
ddmi-048	-10.521	ddmi-139	-6.218	ddmi-172	-4.995	ddmi-207	-5.511
ddmi-049	-4.200	ddmi-140	-4.590	ddmi-173	-4.809	ddmi-208	-5.022
ddmi-058	-5.058	ddmi-141	-5.107	ddmi-174	-4.304	ddmi-210	-5.351
ddmi-078	-5.238	ddmi-142	-4.577	ddmi-175	-4.435	ddmi-213	-5.178
ddmi-093	-5.060	ddmi-144	-4.549	ddmi-176	-5.204	ddmi-214	-5.019
ddmi-098	-4.341	ddmi-145	-5.203	ddmi-177	-5.165	ddmi-215	-5.042
ddmi-100	-4.427	ddmi-146	-4.368	ddmi-179	-5.642	ddmi-216	-5.690

C.5. Nitrogen Data

Table C.11. Summary of the nitrogen concentration and aggregation states of the A154 South diamonds.

Paragenesis	Number of Diamonds	Average Nitrogen Concentration (ppm)
Peridotitic		
Type II	2	-
Type IaA	56	355
Type IaAB	20	213
Type IaB	5	450
Eclogitic		
Type II	1	-
Type IaA	8	685
Type IaAB	3	1929
Type IaB	0	-
Uncertain		
Type II	2	-
Type IaA	1	863
Type IaAB	2	83
Type IaB	0	-

Type II= nitrogen free; Type IaA <10 %B; Type IaB >10 %B

Table C.12. Nitrogen concentration and aggregation states for the A154 South diamonds.

Sample	Type	Na	Nb	N_T	%B
ddmi-001	1aAB	445	82	526	15
ddmi-002	1aAB	38	87	125	69
ddmi-003	1aA	47	2	49	4
ddmi-004	1aAB	333	44	377	12
ddmi-005	1aAB	31	56	86	65
ddmi-006	1aAB	83	261	344	76
ddmi-008	1aA	241	9	250	4
ddmi-013	1aA	44	0	44	0
ddmi-014	1aAB	34	21	55	38
ddmi-025	1aA	232	0	232	0
ddmi-034	1aA	322	11	333	3
ddmi-036	1aA	247	0	247	0
ddmi-037	1aA	247	24	270	9
ddmi-040	1aAB	29	113	142	80
ddmi-043	1aAB	139	40	179	22
ddmi-044	1aA	245	0	245	0
ddmi-046	1aAB	135	250	385	65
ddmi-047	1aA	426	9	435	2
ddmi-048	1aAB	32	133	165	81
ddmi-049	1aB	4	115	118	97
ddmi-058	1aA	502	9	511	2
ddmi-078	1aA	560	0	560	0
ddmi-093	1aA	724	0	724	0
ddmi-098	1aA	318	0	318	0
ddmi-100	1aA	20	0	20	0

Table C.12. (cont.)

Sample	Type	NA	Na	Nt	%B
ddmi-101	laB	9	401	410	98
ddmi-103	laAB	93	86	178	48
ddmi-108	laA	416	17	432	4
ddmi-110	laA	466	16	481	3
ddmi-111	laA	179	17	195	8
ddmi-112	laA	366	0	366	0
ddmi-114	ll	-	-	-	-
ddmi-115	laA	48	0	48	0
ddmi-119	laA	257	0	257	0
ddmi-120	laA	542	15	557	3
ddmi-123	laAB	60	39	99	39
ddmi-124	laA	661	0	661	0
ddmi-126	laA	191	2	193	1
ddmi-127	laA	711	0	711	0
ddmi-129	laB	0	1051	1051	100
ddmi-130	laA	1873	0	1873	0
ddmi-133	laA	418	0	418	0
ddmi-135	laA	529	21	549	4
ddmi-139	laA	447	11	458	2
ddmi-140	laA	21	0	21	0
ddmi-141	laA	29	0	29	0
ddmi-142	laA	424	0	424	0
ddmi-144	laA	149	0	149	0
ddmi-145	laA	185	0	185	0
ddmi-146	laA	66	0	66	0

Table C.12. (cont.)

Sample	Type	NA	Nb	NT	%B
ddmi-147	laA	182	0	182	0
ddmi-148	laA	83	6	89	6
ddmi-150	laB	7	287	294	98
ddmi-151	laAB	312	72	384	19
ddmi-152	laA	119	0	119	0
ddmi-153	laAB	25	33	58	57
ddmi-154	laAB	46	63	109	58
ddmi-155	laAB	356	84	440	19
ddmi-156	laA	105	0	105	0
ddmi-159	laA	1225	0	1225	0
ddmi-161	laA	296	20	315	6
ddmi-162	laA	41	0	41	0
ddmi-165	laA	232	0	232	0
ddmi-166	laAB	2469	1364	3833	36
ddmi-167	laA	17	0	17	0
ddmi-168	laA	97	11	109	10
ddmi-169	laA	63	0	63	0
ddmi-170	laA	36	3	38	7
ddmi-172	laA	77.7	0	78	0
ddmi-173	II	-	-	-	-
ddmi-174	laA	76	0	76	0
ddmi-175	laA	294	0	294	0
ddmi-176	laA	63	0	63	0
ddmi-177	II	-	-	-	-
ddmi-179	laAB	142	18	159	11

Table C.12. (cont.)

Sample	Type	Na	Nb	Nt	%B
ddmi-180	laAB	89	37.3	126	30
ddmi-182	ll	-	-	-	-
ddmi-183	laB	33	351	384	91
ddmi-184	laA	388	26	414	6
ddmi-186	laA	822	0	822	0
ddmi-187	laA	373	0	373	0
ddmi-188	laA	321	0	321	0
ddmi-190	laAB	164	21	185	11
ddmi-193	ll	-	-	-	-
ddmi-195	laAB	9.5	51	61	84
ddmi-196	laA	904	0	904	0
ddmi-198	laA	629	0	629	0
ddmi-199	laA	959	35	994	4
ddmi-200	laA	848	15	863	2
ddmi-202	laA	483	19	502	4
ddmi-203	laA	519	38	557	7
ddmi-205	laA	860	0	860	0
ddmi-206	laA	803	59	862	7
ddmi-207	laA	334	10	344	3
ddmi-208	laAB	1189	601	1791	34
ddmi-210	laAB	68	66	134	49
ddmi-213	laAB	96	176	272	65
ddmi-214	laA	617	52	669	8
ddmi-215	laA	2631	4.5	2636	0
ddmi-216	laAB	138	81	219	37

C.6. Inventory

Table C.13. Inventory of all diamonds selected for this study from the Product Splitting Facility in Yellowknife.

Sample #	Size	Lot #	Seal #	Sorter	Sample #	Size	Lot #	Seal #	Sorter
ddmi-1	+9	23666	2004003013	TS	ddmi-26	+9	23664	2004003013	TS
ddmi-2	+9	23666	2004003013	TS	ddmi-27	+9	23664	2004003013	TS
ddmi-3	+9	23666	2004003013	TS	ddmi-28	+9	23664	2004003013	TS
ddmi-4	+9	23666	2004003013	TS	ddmi-29	+9	23664	2004003013	TS
ddmi-5	+9	23666	2004003013	TS	ddmi-30	+9	23664	2004003013	TS
ddmi-6	+9	23666	2004003013	TS	ddmi-31	+9	23669	2004003013	CD
ddmi-7	+9	23666	2004003013	TS	ddmi-32	+9	23669	2004003013	CD
ddmi-8	+9	23666	2004003013	TS	ddmi-33	+9	23669	2004003013	CD
ddmi-9	+9	23666	2004003013	TS	ddmi-34	+9	23669	2004003013	CD
ddmi-10	+9	23666	2004003013	TS	ddmi-35	+9	23669	2004003013	CD
ddmi-11	+9	23666	2004003013	TS	ddmi-36	+9	23669	2004003013	CD
ddmi-12	+9	23666	2004003013	TS	ddmi-37	+9	23669	2004003013	CD
ddmi-13	+9	23666	2004003013	TS	ddmi-38	+9	23669	2004003013	CD
ddmi-14	+9	23666	2004003013	TS	ddmi-39	+9	23669	2004003013	CD
ddmi-15	+9	23666	2004003013	TS	ddmi-40	+9	23669	2004003013	CD
ddmi-16	+9	23666	2004003013	TS	ddmi-41	+9	23669	2004003013	CD
ddmi-17	+9	23666	2004003013	TS	ddmi-42	+9	23669	2004003013	CD
ddmi-18	+9	23666	2004003013	TS	ddmi-43	+9	23669	2004003013	CD
ddmi-19	+9	23666	2004003013	TS	ddmi-44	+9	23669	2004003013	CD
ddmi-20	+9	23666	2004003013	TS	ddmi-45	+9	23669	2004003013	CD
ddmi-21	+9	23670	2004003013	CD	ddmi-46	+9	23669	2004003013	CD
ddmi-22	+9	23670	2004003013	CD	ddmi-47	+9	23669	2004003013	CD
ddmi-23	+9	23664	2004003013	TS	ddmi-48	+9	23669	2004003013	CD
ddmi-24	+9	23664	2004003013	TS	ddmi-49	+9	23669	2004003013	CD
ddmi-25	+9	23670	2004003013	CD	ddmi-50	+9	23669	2004003013	CD

TS: Thomas Stachel; CD: Cara Donnelly; AB: Anetta Banas; PSF: Product Splitting Facility.

Table C.13. (cont.)

Sample #	Size	Lot #	Seal #	Sorter
ddmi-51	+9	23669	2004003013	CD
ddmi-52	+9	23669	2004003013	CD
ddmi-53	+9	23669	2004003013	CD
ddmi-54	+9	23669	2004003013	CD
ddmi-55	+9	23669	2004003013	CD
ddmi-56	+9	23669	2004003013	CD
ddmi-57	+9	23669	2004003013	CD
ddmi-58	+9	23669	2004003013	CD
ddmi-59	+9	23669	2004003013	CD
ddmi-60	+9	23669	2004003013	CD
ddmi-61	+9	23669	2004003013	CD
ddmi-62	+9	23664	2004003013	TS
ddmi-63	+9	23664	2004003013	TS
ddmi-64	+9	23664	2004003013	TS
ddmi-65	+9	23669	2004003013	CD
ddmi-66	+9	23669	2004003013	CD
ddmi-67	+9	23669	2004003013	CD
ddmi-68	+9	23669	2004003013	CD
ddmi-69	+9	23669	2004003013	CD
ddmi-70	+9	23669	2004003013	CD
ddmi-71	+9	23669	2004003013	CD
ddmi-72	+9	23669	2004003013	CD
ddmi-73	+9	23669	2004003013	CD
ddmi-74	+9	23669	2004003013	CD
ddmi-75	+9	23669	2004003013	CD

Sample #	Size	Lot #	Seal #	Sorter
ddmi-76	+9	23669	2004003013	CD
ddmi-77	+9	23669	2004003013	CD
ddmi-78	+9	23669	2004003013	CD
ddmi-79	+9	23669	2004003013	CD
ddmi-80	+9	23669	2004003013	CD
ddmi-81	+9	23669	2004003013	CD
ddmi-82	+9	23668	2004003013	CD
ddmi-83	+9	23668	2004003013	CD
ddmi-84	+9	23668	2004003013	CD
ddmi-85	+9	23668	2004003013	CD
ddmi-86	+9	23668	2004003013	CD
ddmi-87	+9	23668	2004003013	CD
ddmi-88	+9	23668	2004003013	CD
ddmi-89	+9	23668	2004003013	CD
ddmi-90	+9	23668	2004003013	CD
ddmi-91	+9	23668	2004003013	CD
ddmi-92	+9	23668	2004003013	CD
ddmi-93	+9	19049	2004001029	PSF
ddmi-94	+9	19049	2004001029	PSF
ddmi-95	+9	19049	2004001029	PSF
ddmi-96	+9	28120	2004005069	CD/AB
ddmi-97	+11	28125	2004005069	CD/AB
ddmi-98	+11	28125	2004005069	CD/AB
ddmi-99	+11	28125	2004005069	CD/AB
ddmi-100	+9	28120	2004005069	CD/AB

Table C.13. (cont.)

Sample #	Size	Lot #	Seal #	Sorter
ddmi-101	+9	28120	2004005069	CD/AB
ddmi-102	+9	28120	2004005069	CD/AB
ddmi-103	+9	28120	2004005069	CD/AB
ddmi-104	+9	28120	2004005069	CD/AB
ddmi-105	+9	28120	2004005069	CD/AB
ddmi-106	+9	28120	2004005069	CD/AB
ddmi-107	+9	28120	2004005069	CD/AB
ddmi-108	+9	28120	2004005069	CD/AB
ddmi-109	+9	28120	2004005069	CD/AB
ddmi-110	+9	28120	2004005069	CD/AB
ddmi-111	+9	28120	2004005069	CD/AB
ddmi-112	+9	28120	2004005069	CD/AB
ddmi-113	+9	28120	2004005069	CD/AB
ddmi-114	+9	28120	2004005069	CD/AB
ddmi-115	+9	28120	2004005069	CD/AB
ddmi-116	+9	28120	2004005069	CD/AB
ddmi-117	+9	28120	2004005069	CD/AB
ddmi-118	+9	28120	2004005069	CD/AB
ddmi-119	+9	28120	2004005069	CD/AB
ddmi-120	+9	28120	2004005069	CD/AB
ddmi-121	+9	28120	2004005069	CD/AB
ddmi-122	+9	28120	2004005069	CD/AB
ddmi-123	+9	28120	2004005069	CD/AB
ddmi-124	+9	28120	2004005069	CD/AB
ddmi-125	+9	28120	2004005069	CD/AB

Sample #	Size	Lot #	Seal #	Sorter
ddmi-126	+9	28120	2004005069	CD/AB
ddmi-127	+9	28120	2004005069	CD/AB
ddmi-128	+9	28120	2004005069	CD/AB
ddmi-129	+9	28120	2004005069	CD/AB
ddmi-130	+9	28120	2004005069	CD/AB
ddmi-131	+9	28120	2004005069	CD/AB
ddmi-132	+9	28120	2004005069	CD/AB
ddmi-133	+9	28120	2004005069	CD/AB
ddmi-134	+9	28120	2004005069	CD/AB
ddmi-135	+9	28120	2004005069	CD/AB
ddmi-136	+9	28120	2004005069	CD/AB
ddmi-137	+9	28120	2004005069	CD/AB
ddmi-138	+9	28120	2004005069	CD/AB
ddmi-139	+9	28120	2004005069	CD/AB
ddmi-140	+9	28120	2004005069	CD/AB
ddmi-141	+9	28120	2004005069	CD/AB
ddmi-142	+9	28120	2004005069	CD/AB
ddmi-143	+9	28120	2004005069	CD/AB
ddmi-144	+9	28120	2004005069	CD/AB
ddmi-145	+9	28120	2004005069	CD/AB
ddmi-146	+9	28120	2004005069	CD/AB
ddmi-147	+9	28120	2004005069	CD/AB
ddmi-148	+9	28120	2004005069	CD/AB
ddmi-149	+9	28120	2004005069	CD/AB
ddmi-150	+9	28120	2004005069	CD/AB

Table C.13. (cont.)

Sample #	Size	Lot #	Seal #	Sorter
ddmi-151	+9	28120	2004005069	CD/AB
ddmi-152	+9	28120	2004005069	CD/AB
ddmi-153	+9	28120	2004005069	CD/AB
ddmi-154	+9	28120	2004005069	CD/AB
ddmi-155	+9	28120	2004005069	CD/AB
ddmi-156	+9	28120	2004005069	CD/AB
ddmi-157	+9	28120	2004005069	CD/AB
ddmi-158	+9	28120	2004005069	CD/AB
ddmi-159	+9	28120	2004005069	CD/AB
ddmi-160	+9	28120	2004005069	CD/AB
ddmi-161	+9	28120	2004005069	CD/AB
ddmi-162	+9	28120	2004005069	CD/AB
ddmi-163	+9	28120	2004005069	CD/AB
ddmi-164	+9	28120	2004005069	CD/AB
ddmi-165	+9	28120	2004005069	CD/AB
ddmi-166	+9	28120	2004005069	CD/AB
ddmi-167	+9	28120	2004005069	CD/AB
ddmi-168	+9	28120	2004005069	CD/AB
ddmi-169	+9	28120	2004005069	CD/AB
ddmi-170	+9	28120	2004005069	CD/AB
ddmi-171	+9	28120	2004005069	CD/AB
ddmi-172	+9	28120	2004005069	CD/AB
ddmi-173	+9	28120	2004005069	CD/AB
ddmi-174	+9	28120	2004005069	CD/AB
ddmi-175	+9	28120	2004005069	CD/AB

Sample #	Size	Lot #	Seal #	Sorter
ddmi-176	+9	28120	2004005069	CD/AB
ddmi-177	+9	28120	2004005069	CD/AB
ddmi-178	+9	28120	2004005069	CD/AB
ddmi-179	+9	28120	2004005069	CD/AB
ddmi-180	+9	28120	2004005069	CD/AB
ddmi-181	+9	28120	2004005069	CD/AB
ddmi-182	+9	28120	2004005069	CD/AB
ddmi-183	+9	28120	2004005069	CD/AB
ddmi-184	+9	28120	2004005069	CD/AB
ddmi-185	+9	28120	2004005069	CD/AB
ddmi-186	+9	28120	2004005069	CD/AB
ddmi-187	+9	28120	2004005069	CD/AB
ddmi-188	+9	28120	2004005069	CD/AB
ddmi-189	+9	28120	2004005069	CD/AB
ddmi-190	+9	28120	2004005069	CD/AB
ddmi-191	+9	28120	2004005069	CD/AB
ddmi-192	+9	28120	2004005069	CD/AB
ddmi-193	+9	28120	2004005069	CD/AB
ddmi-194	+9	28120	2004005069	CD/AB
ddmi-195	+9	28120	2004005069	CD/AB
ddmi-196	+9	28120	2004005069	CD/AB
ddmi-197	+9	28120	2004005069	CD/AB
ddmi-198	+9	28120	2004005069	CD/AB
ddmi-199	+9	28120	2004005069	CD/AB
ddmi-200	+11	28125	2004005069	CD/AB

Table C.13. (cont.)

Sample #	Size	Lot #	Seal #	Sorter
ddmi-201	+11	28125	2004005069	CD/AB
ddmi-202	+11	28125	2004005069	CD/AB
ddmi-203	+11	28125	2004005069	CD/AB
ddmi-204	+11	28125	2004005069	CD/AB
ddmi-205	+11	28125	2004005069	CD/AB
ddmi-206	+11	28125	2004005069	CD/AB
ddmi-207	+11	28125	2004005069	CD/AB
ddmi-208	+11	28125	2004005069	CD/AB
ddmi-209	+11	28125	2004005069	CD/AB
ddmi-210	+11	28125	2004005069	CD/AB
ddmi-211	+11	28125	2004005069	CD/AB
ddmi-212	+11	28125	2004005069	CD/AB
ddmi-213	+11	28125	2004005069	CD/AB
ddmi-214	+11	28125	2004005069	CD/AB
ddmi-215	+11	28125	2004005069	CD/AB
ddmi-216	+11	28125	2004005069	CD/AB
ddmi-217	+11	28126	2004005069	CD/AB
ddmi-218	+11	28126	2004005069	CD/AB
ddmi-219	+11	28126	2004005069	CD/AB
ddmi-220	+11	28126	2004005069	CD/AB
ddmi-221	+11	28126	2004005069	CD/AB
ddmi-222	+11	28126	2004005069	CD/AB
ddmi-223	+11	28126	2004005069	CD/AB
ddmi-224	+11	28126	2004005069	CD/AB
ddmi-225	+9	23667	2004003013	TS

Sample #	Size	Lot #	Seal #	Sorter
ddmi-226	+9	23667	2004003013	TS
ddmi-227	+9	23667	2004003013	TS
ddmi-228	+9	23667	2004003013	TS
ddmi-229	+9	28121	2004005069	CD/AB
ddmi-230	+9	28121	2004005069	CD/AB
ddmi-231	+9	28121	2004005069	CD/AB
ddmi-232	+9	28121	2004005069	CD/AB
ddmi-233	+9	28121	2004005069	CD/AB
ddmi-234	+9	28121	2004005069	CD/AB
ddmi-235	+9	28121	2004005069	CD/AB
ddmi-236	+9	28121	2004005069	CD/AB
ddmi-237	+9	28121	2004005069	CD/AB
ddmi-238	+9	28121	2004005069	CD/AB
ddmi-239	+9	28121	2004005069	CD/AB
ddmi-240	+9	28121	2004005069	CD/AB
ddmi-241	+9	28121	2004005069	CD/AB
ddmi-242	+9	28121	2004005069	CD/AB
ddmi-243	+9	28121	2004005069	CD/AB
ddmi-244	+9	28121	2004005069	CD/AB
ddmi-245	+9	28121	2004005069	CD/AB
ddmi-246	+9	28121	2004005069	CD/AB
ddmi-247	+9	28121	2004005069	CD/AB
ddmi-248	+9	28121	2004005069	CD/AB
ddmi-249	+9	28121	2004005069	CD/AB
ddmi-250	+9	28121	2004005069	CD/AB

Table C.13. (cont.)

Sample #	Size	Lot #	Seal #	Sorter
ddmi-251	+9	28121	2004005069	CD/AB
ddmi-252	+9	28121	2004005069	CD/AB
ddmi-253	+9	28121	2004005069	CD/AB
ddmi-254	+9	28121	2004005069	CD/AB
ddmi-255	+9	23667	2004003013	TS
ddmi-256	+9	23667	2004003013	TS
ddmi-257	+9	23667	2004003013	TS
ddmi-258	+9	23667	2004003013	TS
ddmi-259	+9	23667	2004003013	TS
ddmi-260	+9	23667	2004003013	TS
ddmi-261	+9	23667	2004003013	TS
ddmi-262	+9	23667	2004003013	TS
ddmi-263	+9	23667	2004003013	TS
ddmi-264	+9	23667	2004003013	TS
ddmi-265	+9	23667	2004003013	TS
ddmi-266	+9	23667	2004003013	TS
ddmi-267	+9	23667	2004003013	TS
ddmi-268	+9	23667	2004003013	TS
ddmi-269	+9	23667	2004003013	TS
ddmi-270	+9	23667	2004003013	TS
ddmi-271	+9	23667	2004003013	TS
ddmi-272	+9	23667	2004003013	TS
ddmi-273	+9	23667	2004003013	TS
ddmi-274	+9	23667	2004003013	TS
ddmi-275	+9	23667	2004003013	TS

Sample #	Size	Lot #	Seal #	Sorter
ddmi-276	+9	23667	2004003013	TS
ddmi-277	+9	23667	2004003013	TS
ddmi-278	+9	23667	2004003013	TS
ddmi-279	+9	23667	2004003013	TS
ddmi-280	+9	23667	2004003013	TS
ddmi-281	+9	23667	2004003013	TS
ddmi-282	+9	23667	2004003013	TS
ddmi-283	+9	23667	2004003013	TS
ddmi-284	+9	23667	2004003013	TS
ddmi-285	+9	23667	2004003013	TS
ddmi-286	+9	23667	2004003013	TS
ddmi-287	+9	23667	2004003013	TS
ddmi-288	+9	23667	2004003013	TS
ddmi-289	+9	23667	2004003013	TS
ddmi-290	+9	23667	2004003013	TS
ddmi-291	+9	23667	2004003013	TS
ddmi-292	+9	23667	2004003013	TS
ddmi-293	+9	23667	2004003013	TS
ddmi-294	+9	19049	2004001029	PSF